Mechanistic Insights into Host Cell Interaction and Cytotoxicity of the RTX Toxin MbxA from *Moraxella bovis*

Inaugural-Dissertation

for the attainment of the title of doctor
in the Faculty of Mathematics and Natural Sciences
at the Heinrich Heine University Düsseldorf

by
Feby Mariam Chacko
Kottayam, India

Düsseldorf, September 2025

From the Institute of Biochemistry at
Heinrich Heine University Düsseldorf

Published by permission of the
Faculty of Mathematics and Natural Sciences
at Heinrich Heine University Düsseldorf

Supervisor: Prof. Dr. Lutz Schmitt
Co-supervisor: Prof. Dr. Johannes Hegemann
Date of the oral examination: 27/10/2025

“Great things are done by a series of small things brought together.”

Vincent van Gogh

Abstract

RTX (Repeats-in-ToXin) family proteins are secreted by Gram-negative bacteria via the type I secretion system (T1SS) and play key roles in host-pathogen interactions. Their activity typically depends on post-translational acylation, Ca^{2+}-induced folding, and membrane interactions mediated by specific lipids or receptors. This thesis presents the detailed characterization of MbxA, an RTX toxin produced by *Moraxella bovis*, focusing on its biochemical activation, structural features, membrane-binding properties, and cytotoxic effects.

A recombinant *Escherichia coli* expression system was optimized to purify both the acylated, active form of MbxA and its non-acylated precursor, proMbxA, using the HlyA secretion components. Cell-based assays in human epithelial (HEp-2) cells demonstrated that acylation is essential for cytotoxicity, with MbxA inducing rapid, non-apoptotic cell death accompanied by intracellular Ca^{2+} modulation and mitochondrial depolarization. At subcytolytic concentrations, MbxA was internalized by cells, although the mechanism of uptake and the role of specific receptors remain unknown.

Biophysical assays with liposomes and giant unilamellar vesicles (GUVs) showed that MbxA efficiently disrupts cholesterol-containing membranes, while cholesterol-free membranes are largely resistant. Membrane binding occurred even in the absence of cholesterol or acylation, suggesting that binding and pore formation are distinct steps governed by lipid composition and acylation status. Leakage kinetics indicated graded, dynamic pore activity. Sequence analysis identified 25 cholesterol-recognition motifs (CRAC/CARC), several of which were clustered near the acylation sites and within a predicted hydrophobic domain. Mapping onto a SAXS-refined AlphaFold2 model supported their spatial proximity to membrane-interacting regions. SEC-MALS analysis confirmed that acylation promotes stable oligomer formation, consistent with pore assembly, whereas proMbxA remains monomeric or dimeric.

When compared with other RTX toxins such as HlyA and LtxA, MbxA shares the requirement for acylation and cholesterol but does not display clear receptor dependence in vitro. This work provides new insights into RTX toxin diversity, defines a lipid-driven mechanism of MbxA cytotoxicity, and establishes a foundation for future studies on its structure, host specificity, and role in *M. bovis* pathogenesis

Table of Contents

1. Introduction

1.1. Pathogenic Bacteria and Host Interaction Mechanisms

Bacterial pathogens have evolved a wide range of strategies to colonize hosts, evade the immune system, and extract nutrients from their environment. Central to many of these strategies are virulence factors that directly interfere with host cell integrity or signaling pathways. These include surface adhesins, secretion systems, effector proteins, and exotoxins, many of which act in a coordinated fashion to subvert host defenses and promote bacterial survival [1-3].

Among these, toxins play a particularly prominent role in host-pathogen interactions. Bacterial toxins can be broadly classified into endotoxins, such as lipopolysaccharide (LPS), and exotoxins, which are secreted proteins that target specific host processes. Exotoxins may act enzymatically, modifying intracellular targets, or function non-enzymatically by forming pores in host membranes [4]. Pore-forming toxins (PFTs) are especially potent, as they can compromise membrane integrity, disrupt ion homeostasis, and induce various forms of cell death [5, 6].

PFTs are found across diverse bacterial genera and contribute to pathogenesis in multiple disease contexts. For example, *Staphylococcus aureus* α-toxin and *Listeria monocytogenes* listeriolysin O form transmembrane pores that lyse host cells or facilitate intracellular escape [5, 6]. Gram-negative bacteria also secrete PFTs, including members of the RTX (Repeats-in-ToXin) family, which insert into target membranes following Ca^{2+}-induced folding and acylation [7].

PFTs can target a variety of host cell types and trigger outcomes ranging from lysis and necrosis to immune modulation and inflammation. The mechanism of action typically begins with binding to the plasma membrane, either through specific protein receptors or via lipid interactions, followed by oligomerization and pore formation. The host response to pore formation can vary depending on cell type, toxin dose, and whether compensatory repair mechanisms are activated. In epithelial barriers and immune cells, this disruption of membrane integrity can result in rapid necrotic cell death and cytokine release, contributing to both tissue damage and pathogen dissemination [4-6].

RTX toxins represent one group of PFTs in Gram-negative bacteria. They are secreted in an unfolded state and undergo Ca^{2+}-dependent refolding upon exposure to extracellular conditions. Many of them require additional post-translational modifications, such as internal lysine acylation, to achieve full cytotoxic activity [7].

1.2. RTX Toxins: Secretion System, Structure, and Diversity

RTX (Repeats-in-ToXin) proteins form a large and functionally diverse family of secreted virulence factors found across numerous Gram-negative bacteria. A common secretion mechanism unifies them, the type I secretion system (T1SS), and this is achieved through conserved structural motifs, notably glycine- and aspartate-rich

ion-binding repeats in their C-terminal regions. Despite these shared features, RTX proteins span a wide functional spectrum, including cytolysins, enzymes, adhesins, and multifunctional effectors, adapted to a variety of pathogenic strategies [7-10].

1.2.1. Secretion via the Type I Secretion System (T1SS)

All RTX proteins are secreted through a dedicated T1SS, a tripartite protein complex that spans both the inner and outer bacterial membranes (Figure 1). The system consists of an inner membrane ATP-binding cassette (ABC) transporter (e.g., HlyB), a membrane fusion protein (MFP; e.g., HlyD), and an outer membrane channel protein (e.g., TolC). These components typically form a continuous channel from the cytoplasm to the extracellular space in the presence of the substrate, allowing substrates to be secreted in a single step without a periplasmic intermediate. However, exceptions exist, such as RTX adhesins (e.g., LapA, ice-binding adhesins), which transiently accumulate in the periplasm before surface localization [11-15].

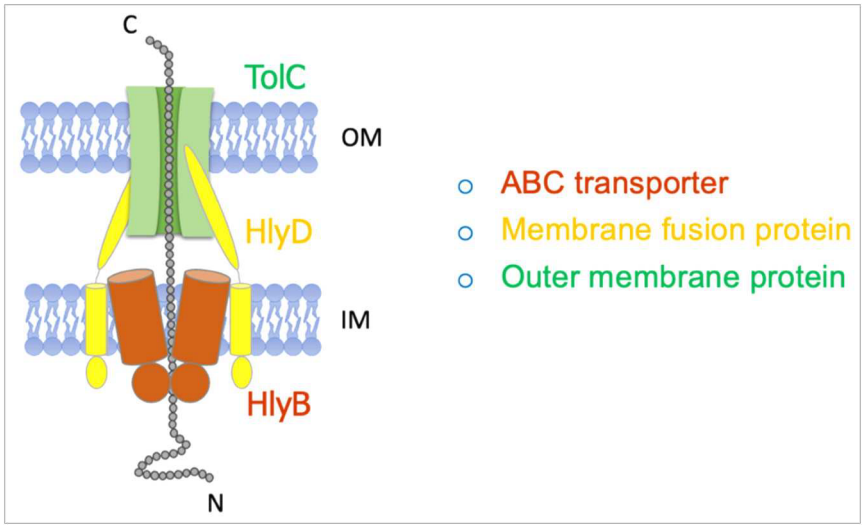

Figure 1. *Schematic representation of a Type I Secretion System used by Gram-negative bacteria to export RTX toxins. The T1SS comprises an inner membrane ATP-binding cassette (ABC) transporter (e.g., HlyB), a membrane fusion protein (e.g., HlyD), and an outer membrane channel (TolC). Substrate proteins are transported directly from the cytoplasm to the extracellular environment in an energy-dependent, one-step process.*

Secretion is energized by ATP hydrolysis through the cytosolic nucleotide-binding domains of the ABC transporter. The secretion signal is located at the extreme C-terminus of RTX proteins and is recognized by the secretion machinery without being cleaved. Because the channel accommodates only unfolded substrates, secretion is subsequently coupled with protein folding in the extracellular region [16].

1.2.2. Defining Structural Features of RTX Proteins

The hallmark of RTX proteins is the presence of C-terminal Ca^{2+}-binding nonapeptide repeats, typically conforming to the motif GGxGxDxUx, where "U" is a large, hydrophobic residue and x can be any amino acid. These GG repeats bind Ca^{2+} in the extracellular environment and fold into a parallel β-roll structure. This folding event not only stabilizes the protein but also contributes to its functional activation [17-19].

Additional common features of some common RTX toxins (eg, pore-forming cytotoxins) include a hydrophobic domain (often N-terminal), potential acylation sites, and a low isoelectric point. Cysteine residues are rarely present. These traits are thought to support stability in the extracellular environment and contribute to target membrane interaction or enzymatic function [7, 20, 21].

1.2.3. Diversity of RTX Protein Subfamilies

Despite their shared mode of secretion and conserved C-terminal elements, RTX proteins are functionally and structurally diverse. They can be grouped into several subfamilies based on domain architecture and biological role (Figure 2) [7].

a) Pore-forming cytotoxins

This group includes classical toxins such as:

- **HlyA** from *E. coli*: a hemolysin that disrupts membranes of erythrocytes and other cells [22].
- **LtxA** from *A. actinomycetemcomitans*: targets leukocytes via β2 integrins [10]
- **LktA** from *M. haemolytica*: specific to bovine immune cells [23]

These toxins typically contain an N-terminal hydrophobic region implicated in membrane binding and pore formation, two conserved internal lysines for acylation, and a C-terminal RTX domain (Figure 2).

b) Enzymatic toxins

CyaA from *B. pertussis* represents a hybrid RTX toxin. In addition to its RTX hemolysin domain, CyaA contains an N-terminal adenylate cyclase domain, which is translocated into host cells. There, it disrupts intracellular signaling by increasing cAMP levels. This dual function, enzymatic activity plus membrane disruption, makes CyaA a unique example of RTX adaptability [24, 25].

c) Multifunctional autoprocessing RTX (MARTX) toxins

MARTX proteins, such as MARTX_Vc from *V. cholerae*, are exceptionally large (e.g., >4500 amino acids) and contain multiple effector domains. These domains are delivered to the host cytosol via an internal autoprocessing mechanism. MARTX toxins are involved in actin modulation, apoptosis, and vesicle trafficking interference [26].

d) RTX adhesins

RTX adhesins are large, multidomain proteins involved in biofilm formation and host cell attachment. Examples include LapA from *Pseudomonas fluorescens*, SiiE from *Salmonella*

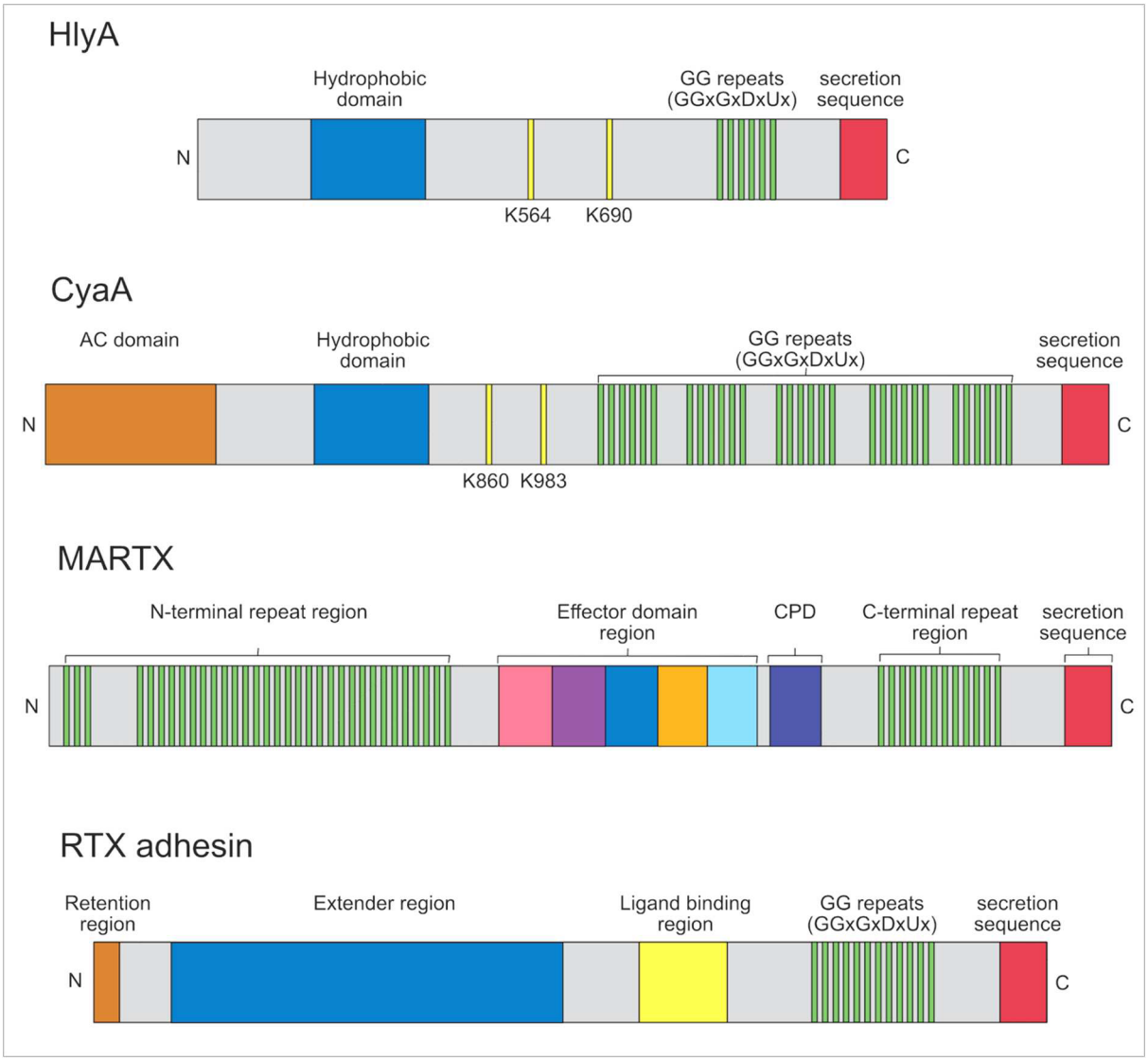

Figure 2: Schematic representation of representative RTX protein architectures. *Domain organization of four functionally distinct RTX protein classes: HlyA (E. coli), CyaA (Bordetella pertussis), a MARTX toxin, and an RTX adhesin. All proteins contain a conserved C-terminal RTX domain composed of GGxGxDxUx repeats (green bars) followed by a secretion signal (red), recognized by the Type I Secretion System (T1SS).*

HlyA and CyaA are pore-forming toxins that harbor an N-terminal hydrophobic domain (blue) required for membrane interaction. Internal lysine residues (yellow lines) are acylated post-translationally by dedicated acyltransferases (e.g., HlyC), essential for full cytotoxic activity. CyaA additionally contains an N-terminal adenylate cyclase (AC) domain (orange) translocated into host cells [7, 27, 28].

MARTX proteins contain extended N- and C-terminal repeat regions flanking a variable central effector region composed of multiple cytosolic effector modules (varied colors), and a conserved cysteine protease domain (CPD, cyan) responsible for autocleavage and release of effectors [29].

RTX adhesins, such as LapA and MpIBP, feature an N-terminal retention domain (brown), a Ca^{2+}-stabilized extender region (dark blue), a ligand-binding domain (yellow), and a C-terminal RTX domain. Unlike cytolysins, MARTX toxins and adhesins are not acylated and primarily mediate adhesion or cytosolic signaling rather than membrane pore formation [30].

This schematic highlights the conserved RTX repeat-containing domain common to the family, while illustrating the functional and structural diversity that underlies the classification of RTX proteins into distinct subfamilies.

enterica, and an ice-binding protein from *Marinomonas primoryensis*. These proteins remain tethered to the T1SS and are released by accessory factors [7, 31].

e) Other RTX proteins and enzymes

Some smaller RTX proteins function as secreted enzymes, such as alkaline protease from *P. aeruginosa* or serralysin-type metalloproteases from *S. marcescens*. Additionally, certain RTX proteins like FrpC from *N. meningitidis* have unusual features, including self-processing modules and potential protein cross-linking activity [7].

This structural and functional diversity reflects the evolutionary flexibility of RTX proteins. While secretion via T1SS and Ca^{2+}-mediated folding are conserved features, their variable N-terminal domains and host interactions give rise to a broad spectrum of biological activities, ranging from membrane permeabilization to enzymatic manipulation of host signaling pathways.

1.3. Ca^{2+}-Dependent Folding and Activation of RTX Proteins

A central feature of RTX toxin biology is the role of calcium ions (Ca^{2+}) in driving protein folding and functional activation. RTX toxins are secreted in an unfolded state from the bacterial cytosol and undergo folding only after encountering the Ca^{2+}-rich extracellular environment. This dependency is directly linked to the structure and function of their C-terminal RTX domain [7].

1.3.1. Folding Triggered by Extracellular Ca^{2+}

The Ca^{2+}-binding GG repeats of the RTX domain form a distinctive parallel β-roll structure upon Ca^{2+} coordination. This structure is stabilized by Ca^{2+} binding between the glycine and aspartate residues of adjacent repeats. Typically, each Ca^{2+} is chelated between two turns of the β-roll, resulting in a repetitive and rigid conformation that promotes overall protein stability (Figure 3) [17, 32].

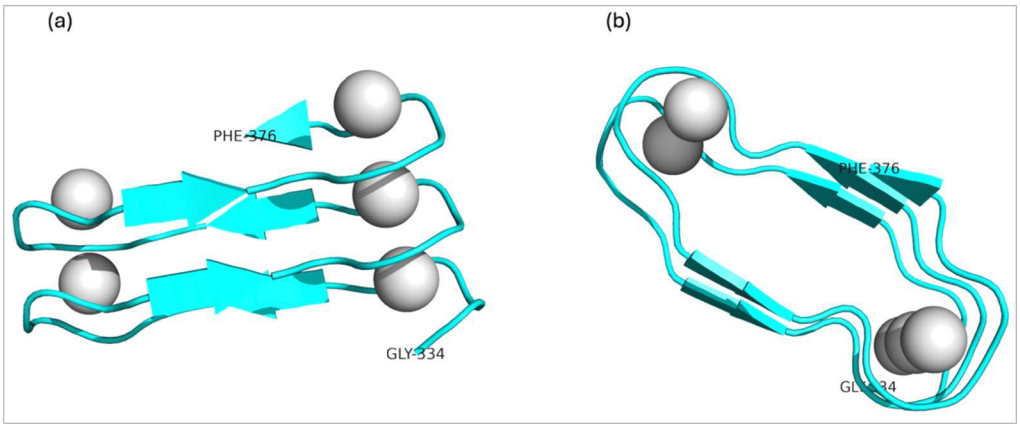

Figure 3. *β-roll structure formed by GG repeats in the RTX domain of alkaline protease from P. aeruginosa [32]. (a) and (b) represents views from different orientations. Gray spheres represent coordinated* Ca^{2+} *ions.*

The number of GG repeats in RTX proteins can vary widely, from a few to more than 40, and this number does not strictly correlate with protein size. For example, *E. coli* HlyA (1,024 residues) contains six highly conserved GGxGxDxUx motifs, but a total of up to 13 nonapeptides have been reported when less conserved variants are included [7, 28, 33, 34].

The RTX domain's folding is Ca^{2+}-dependent. In the bacterial cytosol, free Ca^{2+} concentrations are maintained in the nanomolar range, too low for stable RTX repeat folding [33]. As a result, RTX proteins remain largely disordered before secretion. This unfolded conformation facilitates their passage through the narrow secretion channel of the T1SS [35].

Once translocated, the low millimolar Ca^{2+} concentration in the extracellular space rapidly drives RTX domain folding. This transition from an intrinsically disordered to a structured state is a hallmark of RTX protein activation and is thought to be irreversible under physiological conditions. It also contributes to preventing retro-translocation into the secretion channel, functioning as a folding-based ratchet mechanism [36-39].

1.3.2. Influence on Global Protein Structure and Activity

Ca^{2+}-induced folding of the RTX domain has been shown to influence the structure and function of the entire protein. In HlyA, Ca^{2+} binding not only stabilizes the C-terminal domain but also promotes conformational maturation of upstream domains required for membrane interaction and toxicity. Similar Ca^{2+}-dependency has been demonstrated for the alkaline protease of *P. aeruginosa* and other RTX proteins [40, 41].

The dependence on Ca^{2+} for structural activation represents a unique adaptation that aligns protein folding with environmental transition. It ensures that RTX proteins remain inactive and non-toxic within the bacterial cytosol while rapidly acquiring functional structure only after secretion into the host environment [36-39].

1.4. HlyA - A Prototypical RTX Toxin

Among the RTX family members, hemolysin A (HlyA) from uropathogenic *Escherichia coli* (UPEC) serves as a well-characterized prototype. First identified for its ability to lyse red blood cells, HlyA has since been recognized as a multifunctional cytotoxin capable of targeting a wide range of host cell types [22, 42-46]. Its structural domains, secretion mechanism, and post-translational activation exemplify the defining features of RTX toxins and make it a valuable model for understanding RTX biology [9].

1.4.1. Genetic and Structural Features

HlyA is encoded in an operon that contains genes for its secretion and activation: *hlyB*, *hlyD*, and *hlyC*. The *hlyB* and *hlyD* genes encode components of the inner membrane secretion machinery (an ABC transporter and a membrane fusion protein, respectively), while *tolC*, which encodes the outer membrane channel, is located elsewhere in the genome. *hlyC* encodes a dedicated cytosolic acyltransferase required for HlyA activation [7, 47].

Structurally, HlyA consists of three major regions (Figure 2):

- An N-terminal hydrophobic domain, essential for membrane interaction and pore formation [48]
- Two internal conserved lysine residues (K564 and K690) that are acylated [49, 50]
- A C-terminal RTX domain, composed of GG repeats, followed by a non-cleavable secretion signal [7]

The full-length protein is approximately 110 kDa and is secreted as an unfolded monomer via the T1SS [12].

1.4.2. Post-Translational Activation by Acylation

Cytolytic activity of HlyA depends on the covalent attachment of fatty acids to its internal lysines [49, 51]. This acylation is catalyzed by HlyC, which uses fatty acid-loaded acyl carrier protein (ACP) as a donor [51, 52]. HlyC predominantly transfers myristoyl (C14) groups but

can accommodate longer or shorter fatty acids depending on availability [53-55]. Both lysine residues must be acylated for full activity [50], although recent studies suggest partial activity may be retained with single-site modification [55]. Acylation is thought to promote irreversible membrane insertion, enable oligomerization, and stabilize the toxin in its active conformation [56-59].

1.4.3. Secretion through the T1SS

A proposed HlyA secretion model is illustrated in Figure 4.

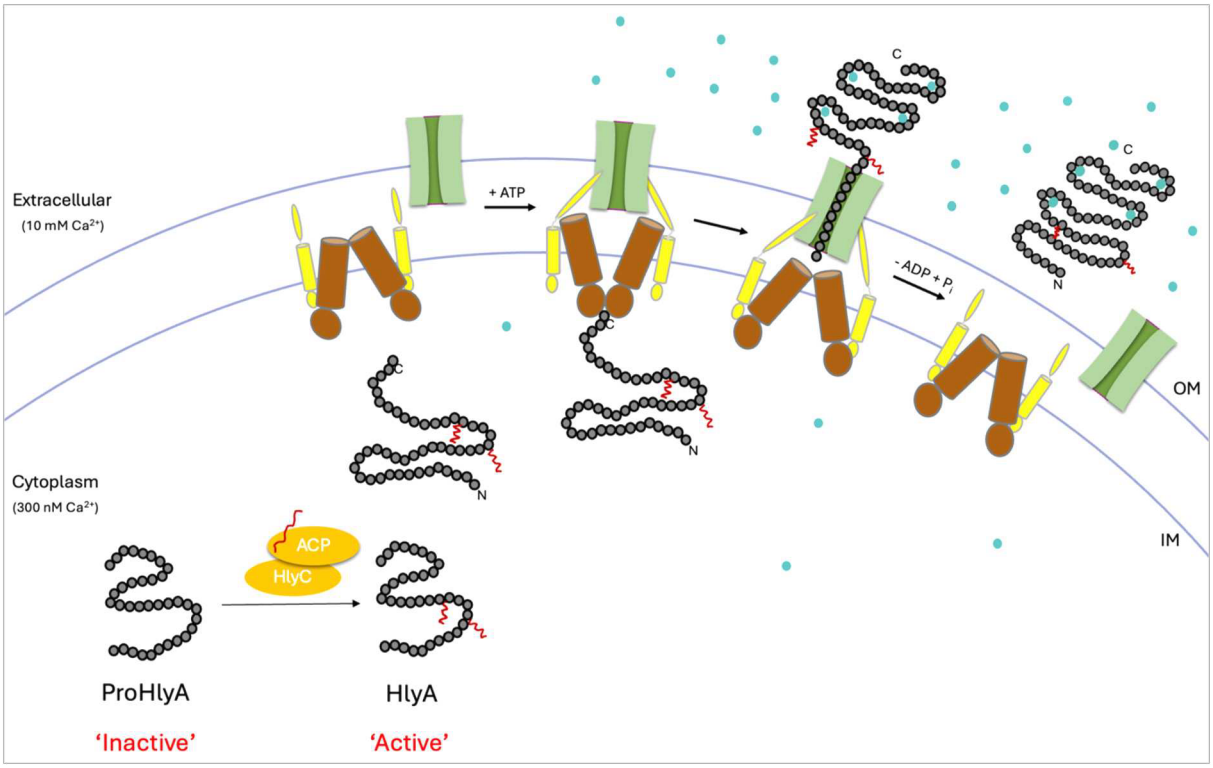

Figure 4. *Stepwise model of HlyA activation and secretion via the Type I Secretion System. In the cytoplasm, HlyA remains unfolded due to low Ca^{2+} concentrations and is post-translationally modified by the acyltransferase HlyC using acyl carrier protein (ACP) as a fatty acid donor. The modified HlyA interacts with the inner membrane complex comprising HlyB (ABC transporter, red) and HlyD (membrane fusion protein, yellow), which together recruit the outer membrane channel TolC (green). The scheme does not take the actual stoichiometry of the complex into account. ATP binding and hydrolysis by HlyB drive substrate engagement and secretion through the assembled trans-envelope complex. The unfolded toxin is translocated in a single step from the cytoplasm to the extracellular environment, where the elevated Ca^{2+} concentration induces folding of the RTX domain into its active conformation. Adapted from [16]. OM: outer membrane, IM: inner membrane.*

HlyA secretion is initiated when the C-terminal secretion signal is recognized by HlyB and HlyD in the inner membrane. Upon substrate engagement, TolC is recruited to form a

continuous channel across both membranes [60, 61]. ATP hydrolysis by HlyB powers the translocation of the unfolded toxin, which proceeds with the C-terminus first [62]. The secretion rate has been estimated at ~16 amino acids per second per channel, although the exact energy requirements remain incompletely understood [63]. Secretion is tightly coupled to Ca^{2+}-dependent folding, which begins at the extracellular face of the channel and prevents backsliding of the protein into the cytoplasm [40, 64, 65]. After secretion, TolC dissociates from the complex, and the folded HlyA becomes functionally active in the host environment [60].

1.4.4. Biological Activities of HlyA

Hemolysin A (HlyA) from uropathogenic *Escherichia coli* (UPEC) is a pore-forming toxin that functions as a potent virulence factor with both cytolytic and subtle modulatory effects on a wide range of host cell types. Recent research has greatly expanded our understanding of its multifaceted interactions with host tissues [42-46].

1.4.4.1. Hemolytic and Pore-Forming Activity

HlyA induces classical hemolysis by forming small cation-selective pores (~3 nm) in erythrocyte membranes [22]. These pores lead to osmotic imbalance, K^+ efflux, Ca^{2+} influx, and eventual cell lysis [22]. Although high concentrations drive immediate lysis, sublytic concentrations can trigger signaling events and metabolic perturbations without immediate cell death [42, 45, 46].

Extensive studies show HlyA is a highly potent leukotoxin, particularly towards polymorphonuclear neutrophils (PMNs), with nanogram-per-milliliter concentrations inducing membrane permeability defects [66].

1.4.4.2. Sublytic Effects and Host Cell Signaling

At sublytic doses, HlyA influences host cell adhesion, inflammation, and survival pathways:

- Proteolysis of cytoskeletal proteins: HlyA triggers cleavage of paxillin, talin, and other cytoskeletal scaffolds in epithelial and immune cells, resulting in impaired adhesion and cell detachment, effects linked to bacterial dissemination [67].

- Ca^{2+} signaling: In renal epithelial cells, HlyA evokes sustained intracellular Ca^{2+} oscillations, activating downstream transcription of cytokines like GM-CSF and promoting inflammatory responses [68, 69].

1.4.4.3. Host Cell Entry and Intracellular Action

A recently described mechanism shows that HlyA is internalized via LDL receptor-mediated, clathrin-dependent endocytosis in renal epithelial cells. Following uptake, HlyA localizes to lysosomes, induces lysosomal membrane permeabilization, triggers mitochondrial dysfunction, and leads to rapid cell death, distinct from the extracellular pore formation traditionally associated with toxin-induced cytotoxicity [70].

1.4.4.4. Inflammasome Activation and Immune Modulation

HlyA has profound effects on immune cells:

- In macrophages, HlyA activates the NLRP3 inflammasome, leading to caspase-1-mediated IL-1β release, mitochondrial damage, and pyroptotic cell death, a proinflammatory outcome that can amplify host tissue damage during infection [71].
- HlyA disrupts Akt signaling pathways and apoptotic regulators in epithelial cells, compromising cell survival and contributing to tissue injury [72].

1.4.4.5. Effects on Neutrophil Recruitment and Barrier Disruption

Evidence indicates HlyA promotes neutrophil migration across the urothelial barrier by inducing ICAM-1 expression on uroepithelial cells, thus facilitating transuroepithelial recruitment of inflammatory cells and exacerbating tissue damage. In vivo studies in mouse models demonstrate that dysregulation of HlyA expression alters both acute and chronic outcomes of urinary tract infection [73].

1.5. Membrane Interactions and Lipid Dependence of RTX Toxins

RTX toxins typically exert their cytolytic activity by disrupting the integrity of host plasma membranes [7, 22, 74]. This interaction can occur via specific protein receptors such as β_2 integrins [23, 75-85], other non-specific cell surface structures such as glycosylated proteins, gangliosides, or cholesterol-enriched microdomains [81, 86-96], or a combination of both [88, 97-99]. The molecular mechanisms of membrane binding and pore formation vary among RTX family members but frequently involve a cholesterol-dependent or lipid raft-associated process

[88, 97, 98]. Understanding these mechanisms is essential for unraveling the host specificity, tissue targeting, and functional diversity of RTX toxins.

1.5.1. β₂-Integrin-Mediated Binding to Leukocytes

Several RTX toxins, including LtxA and CyaA, specifically recognize β₂ integrin receptors (e.g., CD11a/CD18 in leukocytes), enabling targeted attachment to immune cells and efficient delivery of cytotoxic effects [76, 78]. Binding is often carbohydrate-dependent and occurs at nanomolar toxin concentrations [81]. This receptor engagement facilitates non-lytic cellular responses such as cytokine modulation, apoptotic signaling, or immune suppression, aside from direct killing [100].

However, this receptor dependence is not universal across all RTX toxins. For example, RtxA from *Kingella kingae* does not require β₂ integrins but rather binds broadly to glycosylated surfaces, including erythrocytes and epithelial cells, via cell-surface oligosaccharides [93].

The versatility of RTX toxins is thus reflected in their ability to bind receptor-dependently when available, but also receptor-independently in contexts where target membranes lack β₂ integrins.

1.5.2. Receptor-Independent Membrane Association and the Role of Lipids

At higher toxin concentrations, even integrin-binding RTX toxins can induce cytolysis in β₂-deficient cells, such as erythrocytes or liposomes [94, 100, 101]. This occurs via lipid-mediated interactions involving cholesterol, gangliosides, and glycophorins.

- Cholesterol is a central determinant across multiple toxins such as HlyA, CyaA, LtxA, and RtxA, which enhance membrane insertion, oligomerization, and pore formation. Cholesterol recognition motifs (CRAC/CARC) have recently been identified in many RTX proteins, supporting a specific protein-lipid interaction [57, 88, 92, 95, 102, 103].

- Gangliosides (e.g., GM1) contribute to binding and internalization, particularly for toxin subtypes that localize to lipid raft microdomains. For example, CyaA associates with lipid rafts via gangliosides, promoting efficient delivery of its adenylate cyclase domain [90, 98, 104].

- Glycophorins have been shown to modulate HlyA activity. Treatment of erythrocytes with trypsin reduced the sensitivity of RBCs against HlyA to the level of liposome lysis by HlyA, while HlyA preincubated with purified glycophorin was unable to lyse both red blood cells (RBCs) and liposomes [87].

Thus, RTX toxins deploy a dual targeting mechanism: integrin engagement when available, and lipid-dependent membrane recruitment in broader contexts. These complementary modes support both targeted and generalizable host cell interaction.

1.5.3. Binding Versus Insertion: A Two-Step Mechanistic Model

Classic work on HlyA (Bakás et al., 1996) showed that toxin-membrane interaction is a two-stage process: initial reversible adsorption followed by irreversible insertion into the lipid bilayer under favorable biophysical conditions. Reversible adsorption allows the toxin to remain loosely associated with lipid membranes, often without inducing permeabilization. In contrast, irreversible insertion reflects the structural commitment of the toxin into the bilayer, a step influenced by membrane fluidity, lipid packing, and cholesterol content. Importantly, insertion does not always result in pore formation, highlighting the need for additional activation steps beyond membrane anchoring [105].

This distinction emphasizes that membrane binding is necessary but not sufficient for RTX toxin function. Efficient cytolytic activity depends on both proper structural activation (e.g., acylation and Ca^{2+}-dependent folding) and a permissive membrane environment.

1.5.4. Implications for Host Specificity and Therapeutic Targeting

The dependence of RTX toxins on specific lipid compositions and receptors helps explain their varying host specificity. Toxins targeting β_2 integrins affect leukocytes, while those relying on cholesterol-rich or other membrane structures display broader cell specificity. This lipid selectivity has therapeutic implications, as cholesterol-depleting agents or lipid analogues may disrupt toxin function. Additionally, understanding the lipid dependence of RTX toxins can aid in the design of toxin-neutralizing agents or modified vaccine candidates [103].

In summary, membrane interactions of RTX toxins are finely tuned by a combination of receptor presence, lipid environment, and post-translational modification. This layered

mechanism ensures that toxin activity is both potent and spatially regulated, allowing for effective manipulation of host cell membranes in a context-dependent manner.

1.6. MbxA - A Predicted RTX Toxin from *Moraxella bovis*

1.6.1. *Moraxella bovis* and Infectious Bovine Keratoconjunctivitis

Moraxella bovis is a Gram-negative bacterium recognized as the principal causative agent of infectious bovine keratoconjunctivitis (IBK), a highly contagious ocular disease in cattle [106]. IBK leads to inflammation, ulceration, corneal opacity, and, in severe cases, blindness [107]. The economic impact of IBK is substantial, owing to treatment costs, decreased weight gain, and reduced animal welfare [107].

The disease was first associated with *M. bovis* in 1960 by Henson and Grumbles, who described its ability to induce keratoconjunctival lesions upon experimental infection [106]. Since then, *M. bovis* has been extensively studied for its pathogenic mechanisms, which include fimbrial adhesins, iron acquisition systems, and secreted cytotoxins [108-116].

1.6.2. Hemolytic and Cytolytic Activities of *M. bovis*

A key virulence determinant of *M. bovis* is its ability to exert hemolytic and leukotoxic activity, believed to contribute to both tissue damage and immune evasion. Early studies demonstrated the cytopathic effects of whole bacteria and culture supernatants on bovine neutrophils and corneal epithelial cells. The hemolytic factor appeared to be heat-labile, proteinaceous, and capable of damaging erythrocytes and leukocytes *in vitro* [113-117].

Subsequent studies confirmed that cell-free culture filtrates of *M. bovis* exhibit strong cytotoxic effects on bovine immune cells and epithelial tissue. Hoien-Dalen et al. characterized this activity as both leukocidic and hemolytic, suggesting the presence of a secreted toxin with dual cytolytic potential. Beard and Moor further showed that a purified hemolytic and cytotoxic fraction could reproduce IBK lesions when instilled into the bovine conjunctival sac, strongly implicating this factor in disease pathogenesis [112, 114].

1.6.3. Evidence Suggesting an RTX-Type Toxin

The biochemical properties of the cytotoxin described in these studies, its secretion into the extracellular environment, heat-lability, and activity against both erythrocytes and leukocytes,

resemble known features of RTX (Repeats-in-Toxins) family toxins, particularly those from other mucosal pathogens [111, 118]. Clinkenbeard and Thiessen specifically examined the mechanism of action of the hemolysin and reported Ca^{2+}-dependent activity, further aligning it with classical RTX toxin profiles [113].

Although the toxin was not genetically identified in early studies, the presence of RTX-like cytotoxicity suggested that *M. bovis* encodes an RTX toxin functionally analogous to HlyA from *E. coli* or LktA from *Mannheimia haemolytica*. This led to the hypothesis that *M. bovis* may possess an RTX operon encoding a hemolysin-like protein and the associated type I secretion components [114].

1.6.4. Genetic context and Need for Molecular Characterization

Comparative analysis of RTX operons in *Moraxella bovis* and *Escherichia coli* has provided valuable insight into the genetic basis of RTX toxin expression and secretion. In both organisms, the operon encodes a secreted RTX cytotoxin, MbxA in *M. bovis* and HlyA in uropathogenic *E. coli* (UPEC), along with its associated acyltransferase, secretion machinery, and regulatory elements (Figure 5) [114, 117-119].

In *M. bovis*, the *mbxA* gene is flanked upstream by *mbxC*, encoding the presumed acyltransferase, and downstream by the transporter genes *mbxB* and *mbxD*, which are homologous to *hlyB* and *hlyD* of *E. coli*. Importantly, *M. bovis* also harbors an open reading frame encoding a TolC-like outer membrane protein within the same operon. This suggests that all three components of the Type I Secretion System (T1SS), the ABC transporter (MbxB), the membrane fusion protein (MbxD), and the outer membrane protein (TolC), may be co-transcribed as a single locus in *M. bovis* [111].

This organization differs significantly from the RTX operon in UPEC, where the *tolC* gene is located elsewhere in the genome and is shared among multiple efflux and secretion systems [7, 47]. The consolidated operon structure in *M. bovis* may reflect a tighter functional linkage between toxin synthesis and export, potentially enabling more efficient coordination of toxin production and secretion under infection-relevant conditions.

Sequence analysis reveals that MbxA shares ~42% identity with HlyA and contains hallmark features of RTX toxins, including multiple glycine- and aspartate-rich RTX repeats and two predicted acylation sites, similar to those modified by HlyC in *E. coli* [120]. Despite these

conserved features, MbxA remained biochemically uncharacterized for many years, and its activity outside bovine systems had not been investigated. However, a first *in vitro* characterization was recently reported by Erenburg et al. [28], who demonstrated that both proMbxA and MbxA can be heterologously expressed in *E. coli* using the HlyA secretion system. This study provided initial biochemical insights, but a detailed analysis of MbxA structure, lipid interactions, and cytotoxic mechanism remained lacking, and it posed a barrier to understanding the role of MbxA in cytotoxicity and host-pathogen interaction.

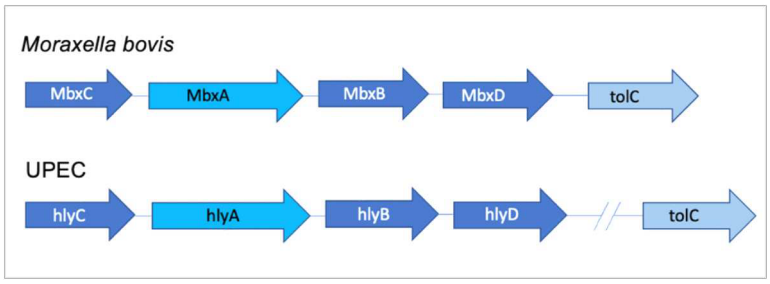

Figure 5. *Genetic organization of the RTX operons in Moraxella bovis and uropathogenic Escherichia coli (UPEC). Both operons encode a secreted RTX toxin, MbxA in M. bovis and HlyA in UPEC, and their respective acyltransferases (MbxC, HlyC) upstream. Downstream of the toxin gene, the inner membrane components of the Type I Secretion System (T1SS) are encoded: HlyB and HlyD in UPEC, and MbxB and MbxD in M. bovis. In M. bovis, the gene encoding the TolC outer membrane protein is also present in the same operon, while in UPEC, tolC is located elsewhere in the genome. This illustrates conserved gene organization in RTX operons and differences in TolC genomic localization.*

2. Aims of the Thesis

RTX (Repeats-in-ToXin) family proteins are a diverse group of virulence factors secreted via the type I secretion system (T1SS) in Gram-negative bacteria. Their function is tightly regulated by post-translational acylation and Ca^{2+}-dependent folding, and many exhibit strong interactions with host cell membranes. While several RTX toxins have been studied in depth, MbxA, a putative RTX toxin encoded by *Moraxella bovis*, has not been characterized at the molecular level. The genomic context of *mbxA* suggests structural and functional similarity to *Escherichia coli* HlyA; however, its biological activity, activation mechanism, and membrane interaction remain unknown.

This thesis aims at the functional, biochemical, and structural characterization of MbxA, using a combination of heterologous expression systems, cytotoxicity assays, lipid model systems, and structural biology approaches. The ultimate goal is to gain mechanistic insight into how MbxA disrupts host membranes and to compare its activity to other RTX toxins.

The specific objectives of this thesis are:

1. **To optimize the heterologous expression system for the production of (pro)MbxA.**
   (pro)MbxA will be expressed in *E. coli* using the well-established HlyA secretion machinery. Co-expression or its absence with the hemolysin acyltransferase HlyC will allow the production of both the acylated (mature) and non-acylated (pro) forms of MbxA. This provides the biochemical basis for isolating and comparing active versus inactive variants.
2. **To characterize the cytotoxic effects of MbxA in mammalian cells.**
   The effect of acylated and non-acylated MbxA will be tested on human epithelial cells to determine membrane-disruptive capacity, Ca^{2+}modulation, and cell death. Imaging and biochemical assays will be used to distinguish necrotic from apoptotic pathways.
3. **To investigate the β_2 integrin-independent interaction of MbxA with host membranes using artificial lipid systems.**
   This objective aims to determine whether MbxA can interact with and disrupt membranes in the absence of protein receptors, such as β_2 integrins, which are used by other RTX toxins like LtxA and CyaA. By employing synthetic liposomes of defined composition, the role of specific membrane constituents, such as cholesterol, gangliosides, and lipid head group charge, will be examined. These experiments are

designed to reveal how lipid composition modulates MbxA binding and pore-forming activity, and to establish whether lipid cues alone are sufficient for cytolytic function.

4. **To analyze the structural properties of MbxA and proMbxA.**
   This aim focuses on determining the oligomeric state and solution conformation of MbxA and proMbxA using techniques such as SEC-MALS and SAXS. In addition, the cytolytic dose (CD_{50}) of MbxA on red blood cells will be measured to quantify its lytic potency in a controlled system. Attempts to visualize MbxA by cryo-electron microscopy will also be made in order to gain insights into its membrane-bound or pore-forming state of the toxin.

By addressing these aims, this thesis seeks to uncover how MbxA functions as a cytotoxic RTX toxin and how lipid composition and acylation regulate its membrane-targeting behavior.

3. Publications

3.1 Chapter 1

Interaction of RTX toxins with the host cell plasma membrane

Authors:	Feby Mariam Chacko and Lutz Schmitt
Published in:	Biological Chemistry (De Gruyter) Impact factor: 2.4
Own work:	90%
Contribution:	Literature search Analysis Writing of the manuscript

DE GRUYTER Biol. Chem. 2023; aop

Review

Feby M. Chacko and Lutz Schmitt*

Interaction of RTX toxins with the host cell plasma membrane

https://doi.org/10.1515/hsz-2022-0336
Received November 28, 2022; accepted February 27, 2023;
published online March 14, 2023

Abstract: **R**epeats in **To**x**in**s (RTX) protein family is a group of exoproteins secreted by Type 1 secretion system (T1SS) of several Gram-negative bacteria. The term RTX is derived from the characteristic nonapeptide sequence (GGxGxDxUx) present at the C-terminus of the protein. This RTX domain binds to calcium ions in the extracellular medium after being secreted out of the bacterial cells, and this facilitates folding of the entire protein. The secreted protein then binds to the host cell membrane and forms pores via a complex pathway, which eventually leads to the cell lysis. In this review, we summarize two different pathways in which RTX toxins interact with host cell membrane and discuss the possible reasons for specific and unspecific activity of RTX toxins to different types of host cells.

Keywords: β_2 integrins; cholesterol; CyaA; gangliosides; HlyA; pore forming.

1 Introduction

RTX toxins were initially classified as hemolysins or leukotoxins depending on the type of cells which they show cytotoxicity towards (Linhartová et al. 2010). While hemolysins target various cell types through different cell surface structures such as glycoproteins, glycolipids, and cholesterol, which are extensively expressed in almost all mammalian cells, leukotoxins exhibit cell type specificity towards leukocytes by recognizing β_2-integrins which are solely expressed on leukocytes. However, in later studies, some RTX toxins which were initially classified as leukotoxins such as LtxA or LktA showed cytotoxicity against β_2 integrin-negative cells (Balashova et al. 2006; Linhartová et al. 2010) and similarly some hemolysins such as HlyA or CyaA displayed specific affinity towards β_2 integrins (Guermonprez et al. 2001; Lally et al. 1997). Importantly, binding of RTX toxins towards β_2 integrin expressing cells occurred with higher affinity and in a saturable manner, while binding towards β_2 integrin-deficient cells appeared to be of lower affinity and occurred in a non-saturable manner (Guermonprez et al. 2001; Osicka et al. 2015; Valeva et al. 2005). These observations resulted in two different mechanisms or pathways for RTX toxins interacting with the host cell plasma membrane:

(1) Receptor-dependent (β_2 integrin protein receptors) interactions,
(2) Receptor-independent interactions.

2 Interaction of RTX toxins with specific β_2-integrin receptors of the host cell

Five RTX toxins were so far investigated with respect to a potential interaction with the β_2 integrin receptor expressed on the surface of host cell membranes. These RTX toxins are hemolysin A (HlyA) from *Escherichia coli*, LtxA from *Aggregatibacter actinomycetemcomitans*, CyaA from *Bordetella pertussis*, LktA from *Mannheimia haemolytica* and ApxIIIA from *Actinobacillus pleuropneumoniae* (Table 1).

HlyA is a prototypic RTX toxin and its mechanism of action is the paradigm for the whole family of RTX toxins and HlyA is shown schematically in Figure 1. This common architecture is shared by most of the RTX toxins, i.e. the functional domain (pore formation) is located at the N-terminus followed by the RTX domain and the secretion signal which is located at the extreme C-terminus of the protein (exceptions: CyaA and MARTX RTX proteins have a different architecture). The RTX domain contains the characteristic nonapeptide repeats with consensus sequence GGxGxDxUx that binds to Ca^{2+} ions which facilitate the complete folding of the protein (Boehm et al. 1990). A model for the structure of HlyA was obtained by AlphaFold2 (Figure 2; Jumper et al. 2021; Spitz et al.

***Corresponding author: Lutz Schmitt**, Institute of Biochemistry, Heinrich-Heine-University Düsseldorf, Universitätsstr. 1, D-40225 Düsseldorf, Germany, E-mail: lutz.schmitt@hhu.de. https://orcid.org/0000-0002-1167-9819
Feby M. Chacko, Institute of Biochemistry, Heinrich-Heine-University Düsseldorf, Universitätsstr. 1, D-40225 Düsseldorf, Germany

Table 1: Different host cell interaction partners of RTX toxins.

RTX toxin	β_2 integrin subunits involved in RTX toxin interaction	Reference	Other cell surface structures involved in RTX toxin interaction	Reference
HlyA	CD18	Lally et al. (1997), Ristow et al. (2019)	– Glycophorin – Cholesterol	Cortajarena et al. (2001, 2003), Vazquez et al. (2014)
LtxA	CD18 & CD11a	Dileepan et al. (2007), Lally et al. (1997), Reinholdt et al. (2013), Ristow et al. (2019)	– Gangliosides/Sialic acids – Cholesterol	Brown et al. (2013, 2016), Forman et al. (2010), Munksgaard et al. (2014)
CyaA	CD11b	Guermonprez et al. (2001), Osicka et al. (2015)	– Gangliosides – Cell surface oligosaccharides – Sphingomyelin – Cholesterol	Gable et al. (1985), González Bullón et al. (2021), Gordon et al. (1989), Martín et al. (2004), Morova et al. (2008), Vojtová et al. (2006), Mrówczyńska et al. (2011)
LktA	CD18	Wang et al. (1998), Dassanayake et al. (2007), Deshpande et al. (2002), Dileepan et al. (2005, 2007), Jeyaseelan et al. (2000), Li et al. (1999)	Unknown	
ApxIIIA	CD18	Vanden Bergh et al. (2009)	Unknown	
RtxA	None	Rahman et al. (2020)	– Cell surface oligosaccharides – Cholesterol	Osickova et al. (2018), Rahman et al. (2020)

2021). Here the functional pore forming domain at the N-terminus is shown in orange and the C-terminal secretion signal in red. Importantly, two internal lysine residues highlighted as spheres in Figure 2 must be acylated to convert HlyA from the inactive (non-acylated) pro-HlyA form into the active pore forming HlyA. This acylation is performed in the cytosol prior to secretion by the acyl transferase HlyC, a protein also encoded in the *hlyA* operon (Stanley et al. 1994; Thomas et al. 2014).

β_2 integrins belongs to the integrin superfamily of proteins composed of 24 αβ heterodimers that mediate the attachment of cells to the extracellular matrix, specialized cell-cell interactions and act as signaling receptors that bind

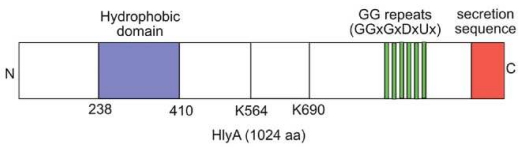

Figure 1: Schematic view of the primary structure of the RTX toxin HlyA. Six conserved GG repeats with consensus sequence GGxGxDxUx are shown in green which constitute the RTX domain that binds to Ca^{2+} ions. Membrane interacting hydrophobic domain that facilitate pore formation is shown in blue and it is located towards the N-terminus of the protein. T1SS recognizing secretion signal of approximately 60 amino acids is located at the C-terminus of the protein which is shown in red. Acylation at two lysine residues K564 and K690 are important for the lytic activity of the toxin and these lysine locations are depicted in the figure.

various soluble, extracellular matrix and cell surface ligands (Arnaout 1990; Barczyk et al. 2010; Fagerholm et al. 2019). There are four α-subunit binding partners for β_2 integrins and together they form: $\alpha_L\beta_2$ (CD11a/CD18 or LFA-1), $\alpha_M\beta_2$ (CD11b/CD18 or Mac1 or complement receptor 3 (CR3)), $\alpha_X\beta_2$ (CD11c/CD18 or CR3) and $\alpha_D\beta_2$(CD11d/CD18) (Arnaout 1990; Barczyk et al. 2010; Fagerholm et al. 2019).

In 1997, Lally and coworkers showed for the first time that a RTX toxin binds to the host cell surface through β_2 integrins (Lally et al. 1997). They employed a monoclonal antibody against a cell surface molecule present on HL60 cells that inhibited cytolysis of these cells by the RTX toxins LtxA from *A. actinomycetemcomitans* and HlyA from *E. coli*. In the absence of this monoclonal antibody, HL60 cells were sensitive to both toxins. Microsequencing of the two polypeptides obtained from immunopurification of detergent-solubilized membranes revealed that the purified proteins corresponded to the alpha and beta subunit of the β_2 integrin CD11a/CD18 receptor (Lally et al. 1997). K562 cell lines lacks CD11a/CD18 integrin proteins in its plasma membrane and are insensitive to both RTX toxins. However, sensitivity towards both toxins was induced when the cells were transfected with the genes encoding the CD11a/CD18 integrin (Lally et al. 1997). Further studies conducted on the LtxA toxin revealed that it is the CD18 subunit that is necessary and sufficient for the cytotoxicity of LtxA, but none of the α-subunit binding partners of the β_2 integrin was involved in toxin-integrin receptor interaction (Dileepan et al. 2007;

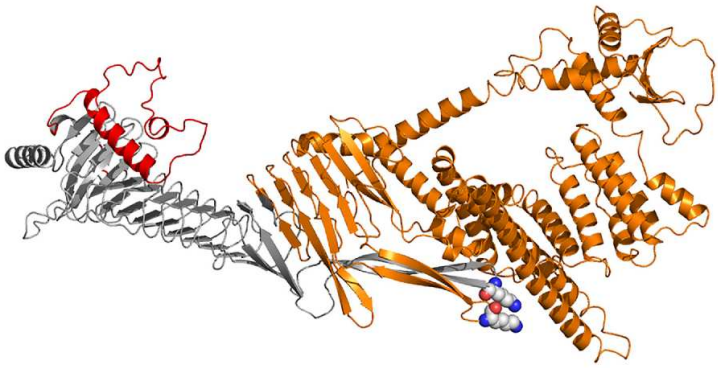

Figure 2: Cartoon representation of the AlphaFold2 model of HlyA (Jumper et al. 2021; Spitz et al. 2021). The N-terminal pore forming domain is shown in orange, the RTX domain in grey, and the C-terminal secretion signal in red. The two lysine residues that are acylated are highlighted as spheres.

Reinholdt et al. 2013; Ristow et al. 2019). Ectopic expression of human β_2 integrins CD11b/CD18 and CD11c/CD18 showed a similar sensitivity to LtxA as that of CD11a/CD18 ectopic expression (Reinholdt et al. 2013), which indicated the insignificance of the alpha subunits in LtxA recognition. By ectopic expression of heterodimers of human and bovine CD11a and CD18, BoLFA-1, HuCD11a/BoCD18, or BoCD11a/HuCD18 in HL-60, K562, KL-4 or P75 cell lines, it was demonstrated that human CD18 acts as the receptor for LtxA, but none of the bovine CD18a, which also explained the species-specific cytotoxicity of LtxA (Dileepan et al. 2007). However, later studies on HlyA showed that HlyA does not require CD11a/CD18 integrins as receptors in the host cell membranes and HlyA binds non-specifically and in a non-saturable manner to erythrocytes and granulocytes (Valeva et al. 2005). In stark contrast to the findings of Lally et al. (1997), Munksgaard and colleagues showed that both, the unmodified and $\alpha_L\beta_2$-integrin-transfected K562 cell line, were similarly susceptible to lysis by HlyA (Munksgaard et al. 2014). To resolve this contradiction, Ristow et al. performed an unbiased forward genetic screen in a mutant library of human monocyte cells, U-937, for host factors involved in HlyA cytotoxicity and cytotoxicity of the related RTX toxin LtxA (Ristow et al. 2019). This unbiased approach finally revealed that the β subunit of β_2 integrin is sufficient, and none of the α subunit is required for the cytotoxic activity of both HlyA and LtxA. This was also confirmed by a far-western blot analysis. $\Delta\beta_2$ cell lines are around 100-fold more resistant to HlyA than wildtype U-937 cells and even larger than 1000-fold more resistant to LtxA toxin, but $\Delta\beta_2$ cell lines remained sensitive to HlyA at higher concentrations (Ristow et al. 2019).

Binding of LktA toxin from *M. haemolytica* to β_2 integrin was first reported by Wang et al. (1998). Preincubation of BL3 bovine leukemia cells with anti-β_2 integrin antibodies inhibited LktA induced apoptosis (Wang et al. 1998). This observation was confirmed in later investigations (Jeyaseelan et al. 2000; Li et al. 1999) where preincubation of LktA-susceptible BL3 bovine lymphoma cells with bovine anti-CD18 or anti-CD11a/CD18 antibodies caused partial inhibition of LktA-induced leukolysis (Li et al. 1999), and LktA-induced cytolysis in neutrophils and bovine alveolar macrophages (BAM) was inhibited by anti-CD11a or anti-CD18 antibodies in a concentration dependent manner (Jeyaseelan et al. 2000). Two investigations (Deshpande et al. 2002; Dileepan et al. 2005) further provided the evidence that bovine CD11a/CD18 is necessary and sufficient to mediate LktA-induced cytolysis of target cells by showing that, ectopic expression of CD18 or CD11a/CD18 in LktA-non-susceptible cell lines showed cytotoxicity against LktA toxin. cDNA transfection of bovine CD18 in a murine cell line non-susceptible to LktA (Deshpande et al. 2002) and recombinant expression of CD11a/CD18 on the cell surface of CD11a/CD18-negative human K562 cell line (Dileepan et al. 2005) showed susceptibility to LktA and induced cytotoxicity, when the cells were subjected to LktA treatment. Finally, by ectopic expression of monomeric bovine CD18 and CD11a and heterodimeric CD11a/CD18 in transfected HEK-293 cells, Dassanayake et al. (2007) demonstrated that all three transfectant effectively bound to LktA. However, LktA-induced cytolysis was observed only with transfectants expressing monomeric bovine CD18 or CD11a/CD18 (Dassanayake et al. 2007).

Vanden Bergh et al. (2009) showed that species specific toxicity of ApxIIIA from *A. pleuropneumoniae* was mediated by porcine CD18 (Vanden Bergh et al. 2009). A β_2-integrin-deficient and ApxIIIA-resistant human K562 cell line was transfected with cDNA coding for either homologous or heterologous CD11a/CD18 heterodimers of human (ApxIIIA-resistant), bovine (ApxIIIA-resistant) or porcine (ApxIIIA-susceptible) CD11a and CD18 subunits. Cell lines that rendered only porcine CD18 subunit within the LFA1

subunits showed susceptibility towards ApxIIIA exposure, which indicates that porcine CD18 is necessary to mediate ApxIIIA-induced leukolysis (Vanden Bergh et al. 2009).

Different from other RTX toxins, CyaA is the only known RTX toxin that showed binding affinity towards the CD11b subunit of the CD11b/CD18 integrin of the host cell instead of CD18 subunit of beta integrins (Guermonprez et al. 2001). Guermonprez et al. demonstrated that binding of CyaA and the resultant increase in intracellular cAMP levels and subsequent cell death in murine cell lines and human neutrophils were blocked by anti-CD11b monoclonal antibodies (Guermonprez et al. 2001). Ectopic expression of CD11b/CD18 integrin on CyaA-non-susceptible Chinese hamster ovary (CHO) cells made these cells susceptible to CyaA binding and subsequent cAMP increase and cell death, but not cells transfected with CD11c/CD18 (Guermonprez et al. 2001). Later investigations confirmed this finding and showed that acylation of CyaA is required for the tight interaction of CyaA with CD11b of the integrin receptor (El-Azami-El-Idrissi et al. 2003). Further analysis by Morova et al. (2008) revealed that the promiscuous initial interaction of CyaA with CD11b/CD18 integrin receptors is mediated via N-linked oligosaccharides (Morova et al. 2008). De-glycosylation of the plasma membrane proteins by glycosidase treatment or inhibition of N-glycosylation of proteins by tunicamycin treatment inhibited the interaction of CyaA with CD11b expressing host cells (Morova et al. 2008). The initial interaction of CyaA with the integrin receptor via N-linked glycans further facilitate highly selective interaction of the receptor binding domain in the RTX region of CyaA with the specific positively charged loop in the thigh region of CD11b to which CyaA binds with high affinity (Osicka et al. 2015). Interaction with N-linked oligosaccharides was also examined for other RTX toxins, LtxA from *A. actinomycetemcomitans* and HlyA from *E. coli*, that binds to CD11a/CD18 integrins, and confirmed that glycosylation is necessary for the interaction of these RTX toxins with the β_2 integrin receptor (Morova et al. 2008). The same laboratory later reported that N-glycans located in the C terminus of the CD11b subunit are involved in the interaction of CyaA with the integrin receptor of the host cell membrane (Hasan et al. 2015). In a subsequent study, they examined that CD11b interacts with CyaA using a domain (residues 614–682) outside the I-domain, which is the usual ligand-binding site of the integrin (Osicka et al. 2015). Based on these results they proposed that the protein segment containing residues 614–682 together with the N-linked glycans of CD11b forms a specialized structure in the protein that facilitate strong binding of CyaA to CD11b/CD18 integrin (Osicka et al. 2015). Most recent study of Goldsmith et al. (2022) provided structural evidence for the non-canonical engagement of CyaA with CD11b/CD18 integrin using cryo-electron microscopy (Goldsmith et al. 2022). This finding also explains the specific affinity of CyaA to the bent conformation of CD11b/CD18 integrin by interacting with both headpiece and tailpiece, which separate during extension (Goldsmith et al. 2022).

Recently, Rahman et al. (2020) have shown that RtxA does not interacts with β_2 integrins (Rahman et al. 2020). They investigated the binding and cytotoxicity of RtxA on CHO cells that ectopically expressed three different human β_2 integrins, CD11a/CD18, CD11b/CD18, or CD11c/CD18. They showed that CHO cells expressing the β_2 integrins bound similar amounts of RtxA as CHO cells not expressing any β_2 integrin. Also, β_2 integrin-expressing CHO cells were killed in a same time-dependent manner as CHO cells lacking β_2 integrins. Analyses of the binding of RtxA to primary mouse macrophages differentiated from bone marrow cells isolated from CD11a knockout (KO), CD11b KO, and control (WT) mice showed that RtxA bound to CD11a KO and CD11b KO macrophages with the same efficacy as to WT macrophages expressing both CD11a/CD18 and CD11b/CD18. Similarly, CD11a KO and CD11b KO macrophages were killed in a same time-dependent manner as that of the WT macrophages when treated with RtxA toxin (Rahman et al. 2020).

3 β_2 integrin receptor-independent interaction of RTX toxins with the host cell

Cortajarena et al. (2001) reported that glycophorin acts as a receptor for HlyA in erythrocytes. Treatment of erythrocytes with trypsin reduced the sensitivity of RBCs against HlyA to the level of liposome lysis by HlyA (Cortajarena et al. 2001), while HlyA preincubated with purified glycophorin was unable to lyse both red blood cells (RBCs) and liposomes (Cortajarena et al. 2001). Later, the same group showed that amino acid residues 914–936 serve as the glycophorin binding region in HlyA (Cortajarena et al. 2003) as a 10,000-fold reduction in hemolytic activity was observed in a mutant of HlyA lacking this sequence. Furthermore, this deletion mutant was unable to bind to human and horse RBCs as well as purified glycophorin (Cortajarena et al. 2003). One reason for this behavior is likely that the deletion mutant in this case results in a poorly folded repeat region because the mutation removes much of the hydrophobic capping structure important for efficient secretion and folding (Bumba et al. 2016). On the other hand, glycophorin does not serve as a receptor for LtxA in RBCs; Instead, gangliosides act as receptor for LtxA in RBCs (Forman et al. 2010). Herlax et al. (2009) showed a

correlation between cholesterol containing microdomains in the host cell membrane and HlyA hemolytic activity (Herlax et al. 2009). This correlation was further proven by biochemical experiments, in which HlyA insertion process using monolayer technique was studied. This demonstrated that the insertion is favored in cholesterol and sphingomyelin containing membranes (Vazquez et al. 2014). These results favor the proposal that the interaction between HlyA and cholesterol induces a conformational change in the protein that facilitates membrane insertion and oligomerization to form the protein pore (Vazquez et al. 2014). Furthermore, so-called cholesterol recognition amino acid consensus sequence (Li and Papadopoulos 1998) (CRAC) motifs with the pattern L/V-(X)(1–5)-Y-(X)(1–5)-R/K (where (X)(1–5) represents one to five residues of any amino acid) were identified in the HlyA sequence (Vazquez et al. 2014). But the cholesterol recognition motif of HlyA is with an opposite orientation along the polypeptide chain: CARC motif K/R(X_{1-5})Y/F(X_{1-5})L/V from the N- to C-terminus and this CARC motif lies between the residues 336 and 353 of HlyA protein sequence (Vazquez et al. 2014).

Initially, LtxA was assumed to be specific only for human and primate white blood cells (Balashova et al. 2006). In 2006, however, Balashova and colleagues reported hemolytic activity of this leukotoxin (Balashova et al. 2006). Nevertheless, the amount of LtxA required for hemolysis is much higher compared to the lysis of β_2 integrin expressing cells, which suggested the presence of low affinity receptors of the toxin in the host cell membrane (Balashova et al. 2006). Forman et al. (2010) showed that gangliosides serve as an interaction partner of LtxA in erythrocytes (Forman et al. 2010). But gangliosides do not serve as a functional receptor for β_2 integrin expressing cells, because ganglioside expressing but β_2 integrin-negative leukocyte cell lines are completely resistant to LtxA induced cytotoxicity (Forman et al. 2010; Kachlany et al. 2010; Kiguchi et al. 1990; Lally et al. 1997). Sialic acid residues present in the glycosylated proteins (including β_2 integrins) or other glycosylated cell surface structures have been shown to be the binding partner responsible for LtxA interaction on host cell membranes and the removal of sialic acids by neuraminidase reduced the cytotoxicity of the LtxA toxin against these cells (Munksgaard et al. 2014). In summary, sialic acid residues in gangliosides and other glycosylated structures could serve as a functional receptor of LtxA in β_2 integrin-negative host cells, but only as a co-receptor *or* binding partner along with other receptors in β_2 integrin expressing host cells.

Lally et al. (1997) showed that LtxA binds to the host cell and elevates intracellular calcium ion levels, which leads to the activation of calpain and subsequent talin cleavage (Fong et al. 2006). Talin bridges β_2 integrin proteins with the cytoskeleton and its cleavage results in the mobilization of β_2 integrins to the cell surface especially to cholesterol and sphingolipid-rich regions of the plasma membrane known as lipid rafts (Figure 3). Events of LtxA binding and calcium ion elevation in host T-cells is independent of the presence of β_2 integrin, but LtxA interaction with β_2 integrin in the lipid rafts is important because only β_2 integrin positive T-cells were killed by the toxin. Thus, initial binding of LtxA is a receptor independent mechanism and subsequently receptor mediated cell lysis occurs with the involvement of cholesterol and sphingolipid rich lipid rafts (Fong et al. 2006). Binding of LtxA to cholesterol was also demonstrated through other biochemical experiments by the same laboratory using surface plasmon resonance and differential scanning calorimetry to quantitatively determine the interaction of LtxA and cholesterol (Brown et al. 2013). Binding of LtxA to phospholipids containing 40% cholesterol is 4 times higher than in the absence of cholesterol (Brown et al. 2013). As of HlyA, CRAC motifs are also present in the LtxA sequence (Brown et al. 2013). Consequently, removal of cholesterol or mutation in CRAC motifs blocks LtxA cytotoxicity against host cell (Brown et al. 2013, 2016).

Ganglioside aided interaction of CyaA with the host cell membrane was first reported by Gable et al. (1985). They showed that a reduction in CyaA-induced cAMP accumulation in human neutrophils occurred when the toxins were pretreated with bovine brain gangliosides or when cells were pretreated with neuraminidase (Gable et al. 1985). Later studies of other laboratories obtained consistent results (Gordon et al. 1989). Further studies addressed the question of how CyaA interacts with host cell membranes that lack β_2 integrin. Mrówczyńska et al. (2011) demonstrated that CyaA interacts with the ganglioside GM1. Cholera toxin subunit B (CTB) is a ligand of GM1, and pretreatment of erythrocytes and K562 cells that lacks β_2 integrin with CTB reduced the binding capability of CyaA to these host cells. This indicated that CyaA binds to ganglioside GM1, apparently by recognizing galactose and sialic acid residues in GM1. These results were in accordance with the findings of Morova et al. (2008) that showed that binding and killing of target cells by RTX toxins occurs via recognition of N-linked oligosaccharide chains of β_2 integrin receptors present in the host cell (Morova et al. 2008).

Apart from binding to ganglioside, (Martín et al. 2004) showed that CyaA has an affinity towards cholesterol. CyaA induced an enhanced release of liposomal content of liposomes containing cholesterol compared to liposomes containing only phospholipids (Martín et al. 2004). Later, (Vojtová et al. 2006) further demonstrated the cholesterol dependency of CyaA binding to sheep erythrocytes. They observed a clustered distribution of CyaA molecules in

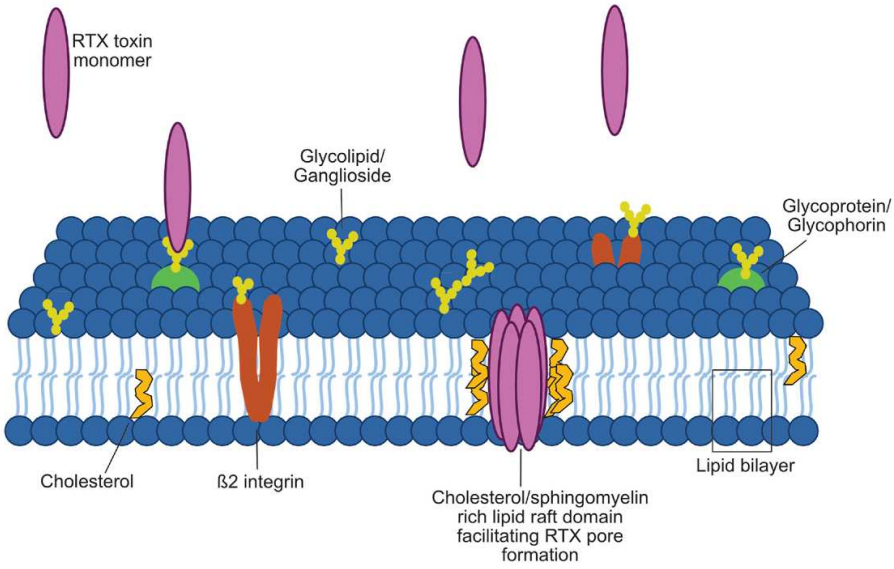

Figure 3: Simplified representation of different interacting partners of RTX toxins with host cell plasma membrane in general. Secreted RTX toxins can be recruited to the membrane by glycolipid/ganglioside or glycoprotein/glycophorin and/or by β_2 integrins. Cholesterol facilitates the protein oligomerization and pore formation in the lipid raft domain in the plasma membrane after the toxin monomers being recruited to the cell membrane via above mentioned cell surface structures.

erythrocyte membrane using confocal microscopy or immunolabeling of inserted CyaA-232/FLAG molecules with specific anti-FLAG antibodies and IgG-gold particles, which suggests that CyaA binds to specific domains of the erythrocyte membrane (Vojtová et al. 2006). Cholesterol depletion in erythrocyte resulted in decreased binding of CyaA to the cells. This implies that the toxin targets and binds to membrane microdomains (lipid rafts made of cholesterol) of erythrocytes (Vojtová et al. 2006).

Recently Rahman et al. (2020) demonstrated that binding of RtxA toxin from *Kingella kingae* on host cell membrane also depends on oligosaccharides present on the host cell surface (Rahman et al. 2020). Removal of sialic acid residues by neuraminidase treatment significantly reduced the binding and cytotoxicity of RtxA to host cells. Hence, the interaction between RtxA and target cells was proposed to be mediated by positively charged lysine and arginine residues of the RTX domain of RtxA and the negatively charged sialic acid residues linked to cell surface structures. In addition, de-glycosylation of cell surface structures by glycosidase treatment, or inhibition of protein N- and O-glycosylation considerably reduced RtxA binding to host cell membranes and de-glycosylated cells were more resistant to cytotoxic activity of RtxA (Rahman et al. 2020). Hence, RtxA not only recognizes the sialic acid residues but also other saccharide units of the cell surface glycoproteins on the surface of target cells (Rahman et al. 2020). Using various biochemical and biophysical approaches, Osickova et al. (2018) demonstrated that cholesterol facilitates the interaction of RtxA with artificial and cell membranes (Osickova et al. 2018). Furthermore, two CRAC/CARC motifs CARC340-348 and CRAC349-354 of RtxA located between residues 340–354 were required for maximal cytolytic activity of RtxA. Since both of these motifs are adjacent to each other in the predicted membrane-interacting and pore-forming domain of RtxA, this CARC/CRAC domain might be involved in the interaction of the toxin with membrane cholesterol (Osickova et al. 2018).

4 Conclusions

Interaction of RTX toxins with host cell plasma membrane and the subsequent pore formation and cell death is a complex process that includes different cell surface structures present in the host cell plasma membrane. Even though the initial binding of RTX toxins with the plasma membrane and the subsequent calcium ion elevation is an event independent of β_2 integrins, interaction of RTX toxin with β_2 integrin is important for the cytotoxicity of RTX toxins against β_2 integrin expressing cells. But what is the exact role played by β_2 integrin in the RTX pore formation or RTX cytotoxicity? Also, the exact pathways by which the

toxin creates pores and results in cytotoxicity in β_2 integrin-positive and β_2 integrin-negative cells and how do they differ remains to be answered in the future.

Acknowledgements: We thank all current and former members of the Institute of Biochemistry, the Center of Advanced Imaging (CAi), and the Center for Structural Studies (CSS), Heinrich Heine University Düsseldorf for support and stimulating discussions. Research on RTX toxins is supported by the Jürgen Manchot Graduate School "Molecules of Infections" (to L.S.).
Author contributions: All the authors have accepted responsibility for the entire content of this submitted manuscript and approved submission.
Research funding: This work was financially supported by the Jürgen Manchot Stiftung (MOI IV).
Conflict of interest statement: The authors declare no conflicts of interest regarding this article.

References

Arnaout, M.A. (1990). Structure and function of the leukocyte adhesion molecules CD11/CD18. Blood 75: 1037–1050.

Balashova, N.V., Crosby, J.A., Al Ghofaily, L., and Kachlany, S.C. (2006). Leukotoxin confers β-hemolytic activity to *Actinobacillus actinomycetemcomitans*. Infect. Immun. 74: 2015–2021.

Barczyk, M., Carracedo, S., and Gullberg, D. (2010). Integrins. Cell Tissue Res. 339: 269–280.

Boehm, D.F., Welch, R.A., and Snyder, I.S. (1990). Domains of *Escherichia coli* hemolysin (HlyA) involved in binding of calcium and erythrocyte membranes. Infect. Immun. 58: 1959–1964.

Brown, A.C., Balashova, N.V., Epand, R.M., Epand, R.F., Bragin, A., Kachlany, S.C., Walters, M.J., Du, Y., Boesze-Battaglia, K., and Lally, E.T. (2013). *Aggregatibacter actinomycetemcomitans* leukotoxin utilizes a cholesterol recognition/amino acid consensus site for membrane association. J. Biol. Chem. 288: 23607–23621.

Brown, A.C., Koufos, E., Balashova, N.V., Boesze-Battaglia, K., and Lally, E.T. (2016). Inhibition of LtxA toxicity by blocking cholesterol binding with peptides. Mol Oral Microbiol 31: 94–105.

Bumba, L., Masin, J., Macek, P., Wald, T., Motlova, L., Bibova, I., Klimova, N., Bednarova, L., Veverka, V., and Kachala, M. (2016). Calcium-driven folding of RTX domain β-rolls ratchets translocation of RTX proteins through type I secretion ducts. Mol. Cell 62: 47–62.

Cortajarena, A.L., Goni, F.M., and Ostolaza, H. (2003). A receptor-binding region in *Escherichia coli* α-haemolysin. J. Biol. Chem. 278: 19159–19163.

Cortajarena, A.L., Goñi, F.M., and Ostolaza, H. (2001). Glycophorin as a receptor for *Escherichia coli* α-hemolysin in erythrocytes. J. Biol. Chem. 276: 12513–12519.

Dassanayake, R.P., Maheswaran, S.K. and Srikumaran, S. (2007). Monomeric expression of bovine beta2-integrin subunits reveals their role in *Mannheimia haemolytica* leukotoxin-induced biological effects. Infect. Immun. 75: 5004–5010.

Deshpande, M.S., Ambagala, T.C., Ambagala, A.P., Kehrli, M.E., Jr., and Srikumaran, S. (2002). Bovine CD18 is necessary and sufficient to mediate *Mannheimia (Pasteurella) haemolytica* leukotoxin-induced cytolysis. Infect. Immun. 70: 5058–5064.

Dileepan, T., Kachlany, S.C., Balashova, N.V., Patel, J., and Maheswaran, S.K. (2007). Human CD18 is the functional receptor for *Aggregatibacter actinomycetemcomitans* leukotoxin. Infect. Immun. 75: 4851–4856.

Dileepan, T., Thumbikat, P., Walcheck, B., Kannan, M.S., and Maheswaran, S.K. (2005). Recombinant expression of bovine LFA-1 and characterization of its role as a receptor for *Mannheimia haemolytica* leukotoxin. Microb. Pathog. 38: 249–257.

El-Azami-El-Idrissi, M., Bauche, C., Loucka, J., Osicka, R., Sebo, P., Ladant, D. and Leclerc, C. (2003). Interaction of *Bordetella pertussis* adenylate cyclase with CD11b/CD18: role of toxin acylation and identification of the main integrin interaction domain. J. Biol. Chem. 278: 38514–38521.

Fagerholm, S.C., Guenther, C., Llort Asens, M., Savinko, T., and Uotila, L.M. (2019). Beta2-integrins and interacting proteins in leukocyte trafficking, immune suppression, and immunodeficiency disease. Front. Immunol. 10: 254.

Fong, K.P., Pacheco, C.M., Otis, L.L., Baranwal, S., Kieba, I.R., Harrison, G., Hersh, E.V., Boesze-Battaglia, K., and Lally, E.T. (2006). *Actinobacillus actinomycetemcomitans* leukotoxin requires lipid microdomains for target cell cytotoxicity. Cell Microbiol. 8: 1753–1767.

Forman, M.S., Nishikubo, J.B., Han, R.K., Le, A., Balashova, N.V., and Kachlany, S.C. (2010). Gangliosides block *Aggregatibacter actinomycetemcomitans* leukotoxin (LtxA)-mediated hemolysis. Toxins 2: 2824–2836.

Gable, P., Eaton, J., and Confer, D. (1985). Intoxication of human phagocytes by bordetella adenylate-cyclase toxin-implication of a ganglioside receptor. Clin. Res. 33: A844.

Goldsmith, J.A., Divenere, A.M., Maynard, J.A., and Mclellan, J.S. (2022). Structural basis for non-canonical integrin engagement by *Bordetella* adenylate cyclase toxin. Cell Rep. 40: 111196.

González Bullón, D., Uribe, K.B., Amuategi, J., Martín, C., and Ostolaza, H. (2021). Cholesterol stimulates the lytic activity of adenylate cyclase toxin on lipid membranes by promoting toxin oligomerization and formation of pores with a greater effective size. FEBS J., https://doi.org/10.1111/febs.16107.

Gordon, V.M., Young, W.W., Jr., Lechler, S.M., Gray, M.C., Leppla, S.H., and Hewlett, E.L. (1989). Adenylate cyclase toxins from *Bacillus anthracis* and *Bordetella pertussis*. Different processes for interaction with and entry into target cells. J. Biol. Chem. 264: 14792–14796.

Guermonprez, P., Khelef, N., Blouin, E., Rieu, P., Ricciardi-Castagnoli, P., Guiso, N., Ladant, D., and Leclerc, C. (2001). The adenylate cyclase toxin of *Bordetella pertussis* binds to target cells via the αMβ2 integrin (CD11b/CD18). J. Exp. Med. 193: 1035–1044.

Hasan, S., Osickova, A., Bumba, L., Novák, P., Sebo, P., and Osicka, R. (2015). Interaction of *Bordetella* adenylate cyclase toxin with complement receptor 3 involves multivalent glycan binding. FEBS Lett. 589: 374–379.

Herlax, V., Maté, S., Rimoldi, O., and Bakás, L. (2009). Relevance of fatty acid covalently bound to *Escherichia coli* α-hemolysin and membrane microdomains in the oligomerization process. J. Biol. Chem. 284: 25199–25210.

Jeyaseelan, S., Hsuan, S.L., Kannan, M.S., Walcheck, B., Wang, J.F., Kehrli, M.E., Lally, E.T., Sieck, G.C., and Maheswaran, S.K. (2000). Lymphocyte function-associated antigen 1 is a receptor for *Pasteurella haemolytica* leukotoxin in bovine leukocytes. Infect. Immun. 68: 72–79.

Jumper, J., Evans, R., Pritzel, A., Green, T., Figurnov, M., Ronneberger, O., Tunyasuvunakool, K., Bates, R., Žídek, A., and Potapenko, A. (2021). Highly accurate protein structure prediction with AlphaFold. Nature 596: 583–589.

Kachlany, S.C., Schwartz, A.B., Balashova, N.V., Hioe, C.E., Tuen, M., Le, A., Kaur, M., Mei, Y., and Rao, J. (2010). Anti-leukemia activity of a bacterial toxin with natural specificity for LFA-1 on white blood cells. Leuk. Res. 34: 777–785.

Kiguchi, K., Henning-Chubb, C.B., and Huberman, E. (1990). Glycosphingolipid patterns of peripheral blood lymphocytes, monocytes, and granulocytes are cell specific. J. Biochem. 107: 8–14.

Lally, E.T., Kieba, I.R., Sato, A., Green, C.L., Rosenbloom, J., Korostoff, J., Wang, J.F., Shenker, B.J., Ortlepp, S., Robinson, M.K., et al. (1997). RTX toxins recognize a β2 integrin on the surface of human target cells. J. Biol. Chem., 272, 30463–30469.

Li, H. and Papadopoulos, V. (1998). Peripheral-type benzodiazepine receptor function in cholesterol transport. Identification of a putative cholesterol recognition/interaction amino acid sequence and consensus pattern. Endocrinology 139: 4991–4997.

Li, J., Clinkenbeard, K.D., and Ritchey, J.W. (1999). Bovine CD18 identified as a species specific receptor for *Pasteurella haemolytica* leukotoxin. Vet. Microbiol. 67: 91–97.

Linhartová, I., Bumba, L., Mašín, J., Basler, M., Osička, R., Kamanová, J., Procházková, K., Adkins, I., Hejnová-Holubová, J., Sadílková, L., et al. (2010). RTX proteins: a highly diverse family secreted by a common mechanism. FEMS Microbiol. Rev. 34: 1076–1112.

Martín, C., Requero, M.A., Masin, J., Konopasek, I., Goñi, F.M., Sebo, P., and Ostolaza, H. (2004). Membrane restructuring by *Bordetella pertussis* adenylate cyclase toxin, a member of the RTX toxin family. J. Bacteriol. 186: 3760–3765.

Morova, J., Osicka, R., Masin, J., and Sebo, P. (2008). RTX cytotoxins recognize β2 integrin receptors through N-linked oligosaccharides. Proc. Natl. Acad. Sci. U. S. A. 105: 5355–5360.

Mrówczyńska, L., Bobrowska-Hägerstrand, M., Lindqvist, C., and Hägerstrand, H. (2011). *Bordetella* adenylate cyclase toxin can bind ganglioside GM1. Bio 1: 67–71.

Munksgaard, P.S., Skals, M., Reinholdt, J., Poulsen, K., Jensen, M.R., Yang, C., Leipziger, J., Vorup-Jensen, T., and Praetorius, H.A. (2014). Sialic acid residues are essential for cell lysis mediated by leukotoxin from *Aggregatibacter actinomycetemcomitans*. Infect. Immun. 82: 2219–2228.

Osicka, R., Osickova, A., Hasan, S., Bumba, L., Cerny, J., and Sebo, P. (2015). *Bordetella* adenylate cyclase toxin is a unique ligand of the integrin complement receptor 3. Elife 4: e10766.

Osickova, A., Balashova, N., Masin, J., Sulc, M., Roderova, J., Wald, T., Brown, A.C., Koufos, E., Chang, E.H., Giannakakis, A., et al. (2018). Cytotoxic activity of *Kingella kingae* RtxA toxin depends on post-translational acylation of lysine residues and cholesterol binding. Emerg. Microb. Infect. 7: 178.

Rahman, W.U., Osickova, A., Klimova, N., Lora, J., Balashova, N., and Osicka, R. (2020). Binding of *Kingella kingae* RtxA toxin depends on cell surface oligosaccharides, but not on β(2) integrins. Int. J. Mol. Sci. 21: 9092.

Reinholdt, J., Poulsen, K., Brinkmann, C.R., Hoffmann, S.V., Stapulionis, R., Enghild, J.J., Jensen, U.B., Boesen, T., and Vorup-Jensen, T. (2013). Monodisperse and LPS-free *Aggregatibacter actinomycetemcomitans* leukotoxin: interactions with human β2 integrins and erythrocytes. Biochim. Biophys. Acta, 1834, 546–558.

Ristow, L.C., Tran, V., Schwartz, K.J., Pankratz, L., Mehle, A., Sauer, J.D., and Welch, R.A. (2019). The extracellular domain of the β(2) integrin β subunit (CD18) is sufficient for *Escherichia coli* hemolysin and *Aggregatibacter actinomycetemcomitans* leukotoxin cytotoxic activity. mBio 10: e01459–19.

Spitz, O., Erenburg, I.N., Kanonenberg, K., Peherstorfer, S., Lenders, M.H.H., Reiners, J., Ma, M., Luisi, B.F., Smits, S.H.J., and Schmitt, L. (2021). Identity determinants of the translocation signal for a type 1 secretion system. Front. Physiol. 12: 804646.

Stanley, P., Packman, L.C., Koronakis, V., and Hughes, C. (1994). Fatty acylation of two internal lysine residues required for the toxic activity of *Escherichia coli* hemolysin. Science 266: 1992–1996.

Thomas, S., Smits, S.H., and Schmitt, L. (2014). A simple *in vitro* acylation assay based on optimized HlyA and HlyC purification. Anal. Biochem. 464: 17–23.

Valeva, A., Walev, I., Kemmer, H., Weis, S., Siegel, I., Boukhallouk, F., Wassenaar, T.M., Chavakis, T., and Bhakdi, S. (2005). Binding of *Escherichia coli* hemolysin and activation of the target cells is not receptor-dependent. J. Biol. Chem. 280: 36657–36663.

Vanden Bergh, P.G., Zecchinon, L.L., Fett, T., and Desmecht, D. (2009). Porcine CD18 mediates *Actinobacillus pleuropneumoniae* ApxIII species-specific toxicity. Vet. Res. 40: 33.

Vazquez, R.F., Maté, S.M., Bakás, L.S., Fernández, M.M., Malchiodi, E.L., and Herlax, V.S. (2014). Novel evidence for the specific interaction between cholesterol and α-haemolysin of *Escherichia coli*. Biochem. J. 458: 481–489.

Vojtová, J., Kofronová, O., Sebo, P., and Benada, O. (2006). *Bordetella* adenylate cyclase toxin induces a cascade of morphological changes of sheep erythrocytes and localizes into clusters in erythrocyte membranes. Microsc. Res. Tech. 69: 119–129.

Wang, J.F., Kieba, I.R., Korostoff, J., Guo, T.L., Yamaguchi, N., Rozmiarek, H., Billings, P.C., Shenker, B.J., and Lally, E.T. (1998). Molecular and biochemical mechanisms of *Pasteurella haemolytica* leukotoxin-induced cell death. Microb. Pathog. 25: 317–331.

Bionotes

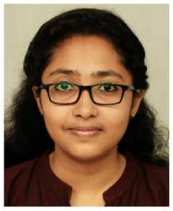

Feby M. Chacko
Institute of Biochemistry, Heinrich-Heine-University Düsseldorf, Universitätsstr. 1, D-40225 Düsseldorf, Germany

Feby M. Chacko did her integrated bachelor's and master's degree in Biology and Chemistry from Indian Institute of Science Education and Research, Thiruvananthapuram. For her master's thesis, she screened for membrane fission catalysts in bacterial cells using Supported Membrane Tube (SMrT) assay system. After her graduation in 2019 from India, she moved to Germany in 2020 and started pursuing her PhD in Institute of Biochemistry, Heinrich Heine University Düsseldorf. Her work focused on the mechanism of RTX toxins.

Lutz Schmitt
Institute of Biochemistry, Heinrich-Heine-University Düsseldorf, Universitätsstr. 1, D-40225 Düsseldorf, Germany
lutz.schmitt@hhu.de
https://orcid.org/0000-0002-1167-9819

Lutz Schmitt did his master's in Chemistry at the University of Freiburg and obtained his PhD from the Technical University Munich. After a Post Doc at Stanford University, he moved as a DFG-funded Emmy Noether fellow to the University of Marburg and University of Frankfurt. In 2005 he was appointed as Professor of Biochemistry at Heinrich Heine University Düsseldorf. His research interest are recognition processes at membranes and transport across membranes with an emphasis on ABC transporters.

3.2 Chapter 2

Heterologously secreted MbxA from *Moraxella bovis* induces a membrane blebbing response of the human host cell

Authors: Isabelle N. Erenburg, Sebastian Hänsch, Feby M. Chacko, Anna Hamacher, Sebastian Wintgens, Fabian Stuhldreier, Gereon Poschmann, Olivia Spitz, Kai Stühler, Sebastian Wesselborg, Johannes H. Hegemann, Sander H. J. Smits, Stefanie Weidtkamp-Peters and Lutz Schmitt.

Published in: Scientific Reports
Impact factor: 3.9

Own work: 25%

Contribution:
Optimization of protein expression and secretion
Protein purification
Site-directed mutagenesis
Atto-488 labelling of MbxA
Cytotoxicity assay (Hb Release)
Assisted in microscopy image optimization
Preparation of microscopy figures
Writing of part of the manuscript

www.nature.com/scientificreports

scientific reports

Check for updates

OPEN

Heterologously secreted MbxA from *Moraxella bovis* induces a membrane blebbing response of the human host cell

Isabelle N. Erenburg[1], Sebastian Hänsch[2], Feby M. Chacko[1], Anna Hamacher[2], Sebastian Wintgens[3], Fabian Stuhldreier[4], Gereon Poschmann[5], Olivia Spitz[1], Kai Stühler[5,6], Sebastian Wesselborg[4], Johannes H. Hegemann[3], Sander H. J. Smits[1], Stefanie Weidtkamp-Peters[2] & Lutz Schmitt[1]✉

Many proteins of the Repeats in Toxins (RTX) protein family are toxins of Gram-negative pathogens including hemolysin A (HlyA) of uropathogenic *E. coli*. RTX proteins are secreted via Type I secretion systems (T1SS) and adopt their native conformation in the Ca^{2+}-rich extracellular environment. Here we employed the *E. coli* HlyA T1SS as a heterologous surrogate system for the RTX toxin MbxA from the bovine pathogen *Moraxella bovis*. In *E. coli* the HlyA system successfully activates the heterologous MbxA substrate by acylation and secretes the precursor proMbxA and active MbxA allowing purification of both species in quantities sufficient for a variety of investigations. The activating *E. coli* acyltransferase HlyC recognizes the acylation sites in MbxA, but unexpectedly in a different acylation pattern as for its endogenous substrate HlyA. HlyC-activated MbxA shows host species-independent activity including a so-far unknown toxicity against human lymphocytes and epithelial cells. Using live-cell imaging, we show an immediate MbxA-mediated permeabilization and a rapidly developing blebbing of the plasma membrane in epithelial cells, which is associated with immediate cell death.

In light of a growing frequency of antibiotic resistance observed in human pathogenic bacteria, characterization of virulence factors, their posttranslational modifications and their secretion machineries are key factors for the development of novel anti-virulence strategies against bacterial infections. Targeting for example bacterial toxins is a promising approach for future therapeutics that need to be tailored to specific pathogens and pathogenicity factors[1,2].

Proteins of the Repeats in Toxins (RTX) family are secreted to the extracellular space by many Gram-negative bacteria employing Type 1 Secretion Systems (T1SS). The growing number of sequenced bacterial genomes revealed novel members of this RTX family[3]. Many RTX proteins are virulence factors of important pathogens such as the toxins CyaA from *Bordetella pertussis* or hemolysin A (HlyA) from uropathogenic *E. coli* (UPEC). RTX proteins are characterized by glycine rich nonapeptide repeats with the consensus sequence GGxGxDxU (x—any amino acid, U—large hydrophobic amino acid), which represent the so-called GG-repeats[3,4].

Repetitions of this repeat close to the C-terminus form the RTX domain[5], while the variability of the N-terminus between different RTX proteins allows diverse functions (for a review see[3]). One of the best-characterized T1SS is the HlyA secretion system from *E. coli*, which consists of the ABC transporter hemolysin B (HlyB), the membrane fusion protein hemolysin D (HlyD) and the outer membrane protein TolC[6–8]. Here, the C-terminal, non-cleavable secretion sequence of 50–60 amino acids of HlyA (Fig. 1) conveys specific interaction with the inner membrane components HlyB and HlyD of this T1SS[9–12]. Prior to and during transport, which occurs in a

[1]Institute of Biochemistry, Heinrich-Heine-University Düsseldorf, Universitätsstr. 1, 40225 Düsseldorf, Germany. [2]Center for Advanced Imaging, Heinrich Heine University Düsseldorf, Düsseldorf, Germany. [3]Institute of Functional Microbial Genomics, Heinrich Heine University Düsseldorf, Düsseldorf, Germany. [4]Institute of Molecular Medicine I, Medical Faculty and University Hospital Düsseldorf, Heinrich Heine University Düsseldorf, Düsseldorf, Germany. [5]Institute of Molecular Medicine, Protein Research, University Hospital and Medical Faculty, Heinrich Heine University Düsseldorf, Düsseldorf, Germany. [6]Molecular Proteomics Laboratory, BMFZ, Heinrich Heine University Düsseldorf, Düsseldorf, Germany. ✉email: lutz.schmitt@hhu.de

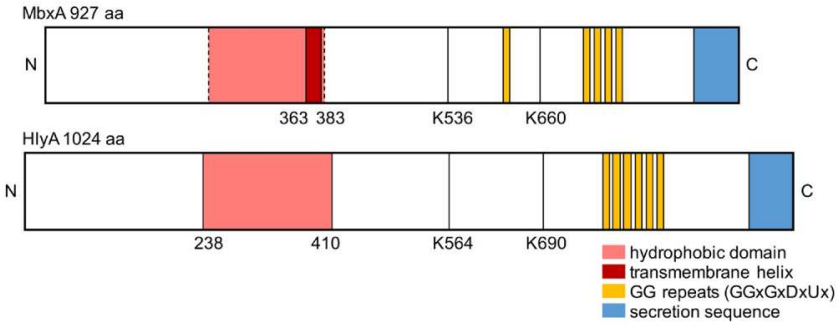

Figure 1. Schematic view of the primary structure of MbxA and HlyA. Five conserved GG repeats with the consensus sequence GGxGxDxUx are present in MbxA, while HlyA carries six conserved GG repeats (yellow boxes). They together form the Ca^{2+} binding RTX domain. As a RTX protein, HlyA characteristically possesses a C-terminal secretion signal of approximately 60 amino acids[10–12], which is shown in blue. For MbxA the length of the secretion sequence is unknown and drawn not to scale. In the N-terminal part of HlyA, a hydrophobic domain is involved in pore formation[53] and marked in red. Depending on the prediction algorithm (see Materials and Methods) for MbxA either (1) a single membrane spanning helix is predicted from residue 363 to 383, (2) a set of transmembrane helices forming an ambiguous hydrophobic domain from residue 210 to 383, or (3) even from residue 120 to 383 (dashed lines) are predicted[52]. The position of the acylated lysine residues K564 and K690 of HlyA and the homologous residues predicted on sequence comparisons to become acylated in MbxA, K536 and K660, are indicated and served as anker point for the scheme.

one-step mechanism across both membranes of the Gram-negative bacterium[9,11,12], HlyA remains unfolded and only achieves its native conformation upon secretion into the extracellular fluid, where binding of Ca^{2+} ions to the RTX domain induces folding of the protein[5,13–15].

HlyA belongs to the classic pore-forming RTX toxins and is active against a variety of cells including erythrocytes, leukocytes, epithelial and endothelial cells of different species[16–18]. For the cytotoxic activity, but not for secretion, a posttranslational fatty acid acylation of two internal lysine residues (Lys 564 and Lys 690), catalyzed by the intracellular acyltransferase HlyC, is required prior to secretion (Fig. 1)[19,20]. Such an acylase is required for other RTX toxins such as CyaA from *Bordetella pertussis* or LktA from *Mannheimia haemolytica* as well and the gene encoding for the transferase is present in the operon coding for the T1SS. The structure of the acylase from *Actinobacillus pleuropneumoniae*[21] might serve as a blue print and provides first insights into how the acyltransferase transfers two fatty acids to the RTX toxin, a process for which acyl carrier protein (ACP) is required. For HlyA, the fatty acids transferred are predominantly C_{14} and to a minor extent C_{15} and C_{17}[22]. Most importantly, both lysine residues can be acylated independent of each other in vivo, but the acylation of both lysine residues is strictly required for toxic activity of HlyA[20]. The latter observation has been recently challenged[23].

Despite being studied for decades, the mechanism of pore-formation by RTX toxins remains elusive. Fatty acid acylation is required for cell lysis, but the architecture of the pore or the exact number of HlyA protomers forming the pore is unknown. Currently, two models are discussed. First, a pure proteinaceous pore, in which the pore lumen is formed exclusively by protein segments, and second a proteo-lipidic or toroidal pore, in which the pore lumen is formed by both, lipid and protein segments[24]. The latter one is supported by recent data obtained for CyaA[25], while the first one was initially described by electrophysiological studies demonstrating that HlyA forms a water filled, cation-specific ion channel with a diameter of approximately 2 nm[26]. Next to pore formation[4], Ca^{2+} oscillations at sub-lytic concentrations of the toxin[27], inflammasome activation[28], and cell death based on apoptotic, necrotic or pyroptotic processes[29,30] have been described.

The nature of the HlyA receptor in the host's plasma membrane has also not been fully resolved. In principle, two major pathways might exist, which both are supported by experimental data. First, a receptor-independent mode of action. This proposal is based on studies using artificial membranes [31,32] and the observation that HlyA displays a non-saturable binding to rabbit erythrocytes[33]. The identification of the heterodimeric integrin LFA-1 ($\alpha_L ß_2$) as a receptor represented the starting point of a receptor-dependent mode of action. The receptor was later narrowed down to the $ß_2$ subunit (CD18)[34,35]. A similar result was obtained for CyaA[36,37], which recognized the integrin $\alpha_M ß_2$ (CD11b/CD18). Interestingly, binding occurred to N-linked carbohydrates of the integrin[36]. This would also explain why CyaA or HlyA can bind erythrocytes that lack LFA-1, but contain glycosylated proteins such as glycophorin, which was shown to function as a receptor for HlyA as well[38] and likely possesses a similar or identical glycosylation pattern.

In general, the primary structure of the secretion signal is not conserved among RTX proteins. This is illustrated by the fact that the HlyA secretion system seems to tolerate some non-native RTX toxins as substrates such as for example CyaA from *Bordetella pertussis*, FrpA from *Neisseria meningitidis*, PaxA from *Pasteurella aerogenes* or LktA from *Mannheimia haemolytica*[39–42]. However, the secretion of these heterologous RTX proteins was not quantified or demonstrated to be efficient in terms of amounts of secreted protein. Furthermore, different experiments showed that the HlyA T1SS could secrete fusion proteins. The exchange of the HlyA secretion sequence

with the C-terminus of LktA still facilitates secretion of HlyA[43]. At the same time non-related, but slow-folding proteins carrying the HlyA secretion sequence are recognized and transported[13].

MbxA from *Moraxella bovis* shares a sequence identity of 42% with HlyA and is a key factor in the pathogenicity of *Moraxella bovis*[44,45]. This animal pathogen is the cause of the most prevalent ocular disease in cattle, the infectious bovine keratoconjunctivitis (IBK)[46,47]. Studies with supernatants of pathogenic *M. bovis* cultures revealed a cytotoxicity against bovine neutrophils, erythrocytes and corneal epithelial cells attributed to a possibly secreted cytotoxin[48–51]. A classic RTX operon that comprises MbxA together with the putative acyltransferase MbxC along with the transporter components was later identified only in pathogenic, hemolytic *M. bovis* strains but not in non-hemolytic strains. With a length of 927 amino acids, MbxA is approximately 10% smaller than HlyA. Like for HlyA, sequence alignment and topology predictions revealed two potential acylation sites as well as an ambiguous membrane interaction domain at the N-terminal part of MbxA[44,52,53], while the GG-repeats are located closer to the C-terminus of MbxA compared to the setting in HlyA. Altogether, MbxA has a putative domain organization that is typical for pore-forming RTX toxins (Fig. 1).

A functional characterization of MbxA requires purified and active protein. So far, MbxA has only been produced for vaccination purposes as precipitated or partially solubilized protein[54] or as C-terminal fragments[55,56].

Here, we established a complete surrogate T1SS in an *E. coli* laboratory strain by a combination of the UPEC HlyA T1SS with the heterologous substrate MbxA that secretes active MbxA or its precursor proMbxA. The heterologous *E. coli* system allows to induce expression of large amounts of RTX protein and with the help of stable expression of the T1SS achieve efficient secretion. Recombinant production yields protein quantities sufficient for functional in vitro characterization. This reliable and inducible recombinant protein production system is independent of potential environmental stimuli needed for the production of the toxin by *M. bovis* and avoids cultivation of the pathogen altogether.

Based on this result, we developed a rapid and efficient purification procedure for both MbxA species from the supernatant of secreting *E. coli* cells. This approach is different from the cytosolic production and isolation of active RTX toxins from inclusion bodies such as for example CyaA from *Bordetella pertussis*[57] or LtxA from *Aggregatibacter actinomycetencomitans*[58]. In our set-up, recombinant MbxA was efficiently activated by HlyC, but with an unexpected acylation pattern compared to HlyA. In contrast to the previously shown activity against bovine and ovine cells, we further observed that MbxA displays a host species independent cytotoxic activity against human epithelial cells and leukocytes. Using live-cell imaging, we finally demonstrate a rapid and distinct membrane blebbing phenotype in human epithelial cells in response to permeabilization by MbxA. RTX toxin induced plasma membrane blebbing has been so far only described for the multifunctional-autoprocessing RTX (MARTX) toxin RtxA1 from *Vibrio vulnificus*[59]. This multidomain protein, composed of approximately 5200 amino acids, contains six putative effector domains including a pore-forming domain. Our results thus demonstrate that the ability of MbxA to induce membrane blebs is encoded in the pore-forming domain of this ´classic´ RTX toxin and might be a general feature of this family of membrane damaging proteins.

Results

MbxA is secreted and activated by the HlyA system. The HlyA T1SS has been shown to possess a certain degree of promiscuity[39–42]. Therefore, we rationalized that producing MbxA might be possible by employing the UPEC-derived HlyA T1SS secretion system in *E. coli* BL21(DE3). The *mbxA* gene containing a hexa-histidine tag (*6H*-mbxA) for ease of purification was therefore introduced into the pSU2726 vector[60] resulting in the plasmid pSU-*6H-mbxA*. The UPEC-derived HlyA T1SS inner membrane components HlyB and HlyD were expressed from the pK184-*hlyBD* vector, while endogenous BL21(DE3) TolC is chromosomally encoded[13]. In a two-plasmid-system comprised of pK184-*hlyBD* together with pSU-*6H-mbxA* or pSU-*hlyC/6H-mbxA*, *mbxA* could either be expressed in the presence of the transporter components or additionally in the presence of the activating acyltransferase HlyC. *E. coli* BL21(DE3) that carry both, pK184-*hlyBD* and pSU-*hlyC/6H-mbxA*, showed hemolytic activity when grown on sheep blood agar, while in the absence of HlyC no halo formation occurred. Colonies harboring only pSU-*hlyC/6H-mbxA* did not cause hemolysis indicating that secretion via the T1SS and not cell lysis is not the reason for toxic activity of MbxA. This indicates that the secretion of active MbxA was indeed mediated by heterologous *E. coli* HlyBD-TolC (Fig. 2).

The IPTG-induced expression of HlyBD together with MbxA only or MbxA with HlyC in liquid cultures led to an accumulation of an approximately 100 kDa protein, proMbxA or MbxA as verified by MS analysis (see below), respectively, in the medium (Fig. 3). In the absence of the HlyC protein, secretion levels of proMbxA were higher during 5 h of expression. While proMbxA was stable in the supernatant, MbxA tended to accumulate in the foam floating on the medium.

Purification of proMbxA and MbxA from the supernatants of *E. coli* cultures. From the *E. coli* BL21(DE3) pK184-*hlyBD*, pSU-*6H-mbxA* system approximately 6 mg/L of precursor protein proMbxA was recovered from the supernatant using Ni^{2+} affinity chromatography. A subsequent size exclusion chromatography (SEC) and SDS PAGE analysis revealed that two separable species of proMbxA were present (Fig. 4).

Determination of the molecular weight (MW) by multi angle light scattering (MALS) analysis confirmed that the first peak with an experimentally determined molecular weight (MW) of 201.5 ± 1.1 kDa corresponded to proMbxA dimers (theoretical MW 201.2 kDa). The second peak contained monomeric proMbxA as the determined MW of 93.9 ± 0.3 kDa fitted to the theoretical mass of 100.6 kDa (Fig. 5). The plasmid combination pK184-*hlyBD* and pSU-*hlyC/6H-mbxA* allowed the isolation of activated MbxA that was solubilized with 6 M urea from the foam of the expression culture and was afterwards refolded in the presence of Ca^{2+}. It was equally purified via IMAC and subsequent SEC. MbxA eluted from the Superose 6 Increase column earlier (elution volume 13.6 ml) and in a broader peak than the proMbxA dimer (elution volume 14.9 ml), which is due

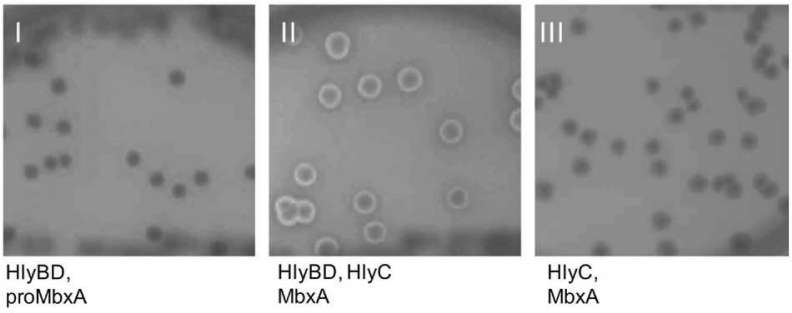

Figure 2. *E. coli* BL21(DE3) grown on Columbia agar with 5% sheep blood harboring the plasmids pK184-*hlyBD* with pSU-*6H-mbxA* (I), pK184-*hlyBD* with pSU-*hlyC/6H-mbxA* (II) or pSU-*hlyC/6H-mbxA* alone (III). Halo formation around colonies that expressed MbxA and HlyC together with the transporter components HlyBD (II) and absence of hemolysis around colonies that express only MbxA and HlyC (III) indicates functional secretion of active and acylated MbxA. Thus functional MbxA is not released from *E. coli* without additional expression of the HlyBD secretion system.

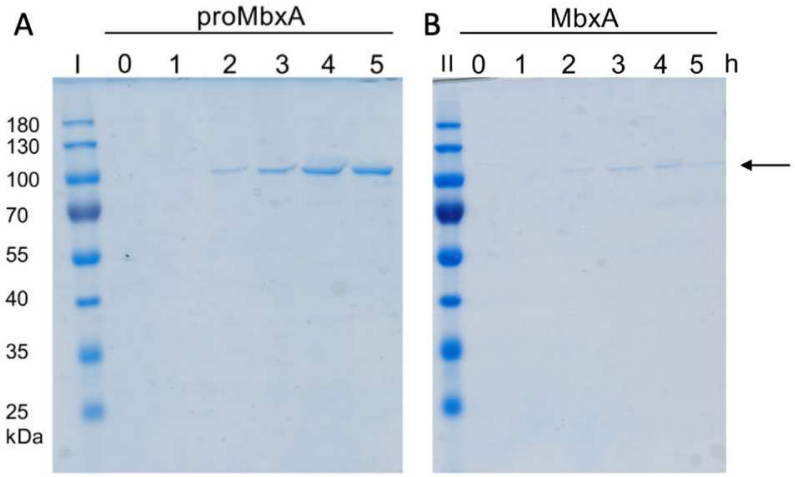

Figure 3. Heterologous secretion of proMbxA and MbxA via the HlyBD system. The Coomassie Brilliant Blue (CBB) SDS PAGE of culture supernatants of *E. coli* BL21(DE3) co-expressing HlyBD and MbxA (proMbxA, (**A**)) or HlyBD, HlyC and MbxA (MbxA, (**B**)) show accumulation of proMbxA or MbxA during a period of 0–5 h of expression (indicated by the numbers above the gel) after induction with IPTG. Samples of the supernatant were applied to the SDS gel without additional concentration by TCA precipitation. Molecular weight markers in kDa are shown in lanes I and II. An arrow indicates proMbxA and MbxA.

to acylation and eventually indicates the presence of a higher oligomeric species of MbxA, probably including MbxA dimers and a small fraction of monomers (elution volume 17.1 ml) (Fig. 4). CBB staining confirmed the purity of proMbxA and activated MbxA already after IMAC (Fig. 4b).

Active MbxA is acylated by HlyC at two conserved acylation sites. Besides HlyA, several other pore-forming RTX toxins are known to require a post-translational acylation at two or, as in the example of CyaA, at least one conserved internal lysine residue to confer toxic activity[20,61–65]. For HlyA, acylation of both acylation sites was shown to be required for toxicity[20]. The amide linked fatty-acylation is facilitated by an acyltransferase encoded upstream of the RTX gene and an acyl carrier protein[66]. The presence of the *mbxC* gene in the *M. bovis* operon indicates that expressed MbxA is likely acylated[44]. The lysine residues K536 and K660 of MbxA correspond to the acylation sites at K564 and K690 of HlyA (Fig. S1)[20,44]. The areas around the two acylation sites, residues H516-G566 and K640-Q680, share a sequence identity of approximately 46% with those of HlyA. This identity is comparable to the overall identity of both proteins. To analyze a possible acylation status of proMbxA expressed in the absence of HlyC and MbxA co-expressed with HlyC, we used mass spectrometry. No acylation was detected for proMbxA in the absence of HlyC. In contrast, in the presence of HlyC MbxA

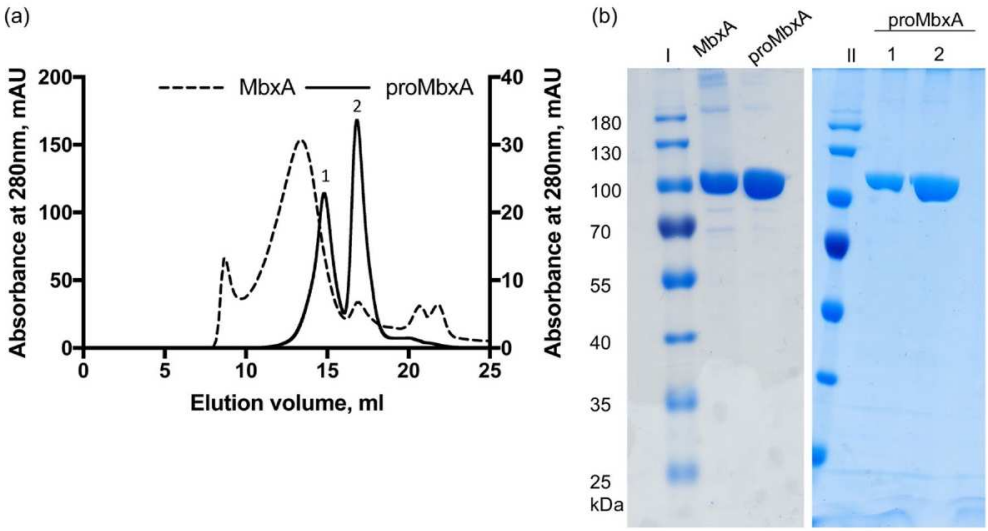

Figure 4. (**a**) SEC chromatographs of samples of active MbxA (dashed line) and proMbxA (solid line), respectively, applied to a Superose 6 Increase 6/30 column (GE Healthcare). The absorbance at 280 nm of the elution profile of proMbxA was plotted on the left Y axis, the elution profile of active MbxA on the right Y axis. proMbxA eluted in two separate main peaks, marked 1 and 2 in the chromatogram. (**b**) CBB stained SDS PAGE gels of pooled fractions of active MbxA and proMbxA obtained from IMAC purification (left panel) and used for SEC. The entire gels are shown in Figure S9. proMbxA was separated in two species, peak 1 and peak 2, during SEC and evaluated by SDS PAGE (right panel). Molecular weight markers in kDa are shown in lanes I and II.

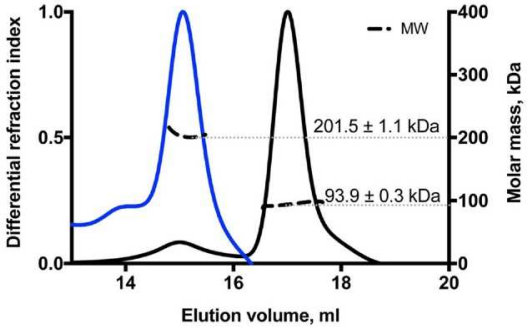

Figure 5. MALS coupled to SEC analysis of the two proMbxA species separated via SEC (blue line peak 1 of Fig. 4, black line peak 2 of Fig. 4). The calculated molecular weight of 201.5 ± 1.1 kDa of the first peak (blue) corresponds to a dimer of proMbxA (theoretical MW (6H-MbxA)$_2$ = 201.2 kDa). The molecular weight of 93.9 ± 0.3 kDa of the second peak (black) confirms a monomeric species of proMbxA (theoretical MW 6H-MbxA = 100.6 kDa).

peptides containing acylated lysine residues were identified at the predicted sites, K536 and K660, respectively. No peptide with non-acylated K536 or K660 was detected in the acylated MbxA variant. Myristoylation (C_{14} acylation) as well as hydroxy myristoylation (C_{14}-OH*) were determined for all three detected peptides that covered the first acylation site K536 (ERLTNG**K**YSYINK, LTNG**K**YSYINK and LTNG**K**YSYINKLK) (Fig. 6 and Tab. S1). Each of those peptides was identified by more than one fragment spectrum recorded by the mass spectrometer resulting in a total of 24 informative spectra for C_{14} modification with additional 5 informative spectra for C_{14}-OH* modifications of these three peptides. Those peptide spectrum matches (PSM) can be used as semi-quantitative measure for the occurrence of peptides and peptide modifications. The peptide LTNG**K**YSYINK was additionally found to be modified with C_{13}, C_{15} and C_{16} acylations as well as a C_{12} hydroxy acylation. These modifications with C_{13}, C_{15}, C_{16} and C_{12}-OH* fatty acids are probably less frequent as they were detected only with 2, 4, 1 and 1 PSM, respectively. The second acylation site, K660, was only found to be acylated at a low level

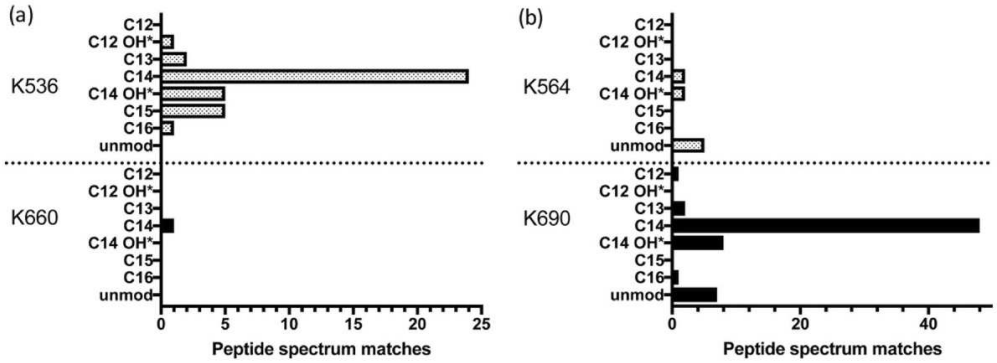

Figure 6. MS analysis of MbxA acylation (**a**) and HlyA acylation (**b**). MbxA and HlyA were in vivo acylated by co-expressing HlyC[67]. For both acylation sites in MbxA and HlyA, K536 and K660 or K564 and K690 respectively, all detected acyl modifications ranging from C_{12} to C_{16} fatty acids including hydroxy fatty acids are shown with the corresponding number of recorded PSM. Mass shifts contributing to hydroxy fatty acids could possibly originate from the oxidation of tyrosine residues in the peptide fragment and PSM of supposed hydroxy acylations are therefore marked (*). For proMbxA and proHlyA, both expressed in the absence of HlyC, only unmodified peptides were detected. Acyl modifications were detected only in peptides covering the predicted lysine residues K536 and K660 of MbxA. The PSM of C_{14} modified sequences suggest that the predominant modification is myristoylation.

with C_{14} fatty acids (Fig. 6a). As no other fatty-acylated lysine residues were observed, we conclude that modification of MbxA with the non-native, but promiscuous acyltransferase HlyC, here referred to as cross-acylation, targets only the predicted acylation sites albeit to different degrees (Tab S1).

To test whether HlyC confers the same modifications to MbxA as to HlyA in the *E. coli* BL21(DE3) background, proHlyA (absence of HlyC) and HlyA (presence of HlyC) were analyzed for their acylation status. For HlyA, peptides acetylated at both known acylation sites[20] could be identified (Tab S1). At K564 peptides modified with C_{14} acylation and C_{14}-OH* acylation contributed both with 2 PSM. The second acylation site, K690, was predominantly found acylated with C_{14} fatty acids (48 PSM) but also hydroxy acylated with C_{14}-OH* modifications (8 PSM). Moreover, and in contrast to the second acylation site of MbxA, also less frequent modifications, namely C_{12}, C_{13} and C_{16} acylations were detected at the K690 acylation site of HlyA with 1, 2 and 1 PSM, respectively. Additionally, unmodified peptides containing K564 and K690 were detected for HlyA (5 and 7 PSM, respectively) (Fig. 6b). Based on the PSM data, we assume that the vast majority of HlyA proteins are acylated, as in proHlyA no acylated peptides were determined, but unmodified peptide variants including K564 and K690 with 114 and 68 PSM, respectively. Interestingly, the ratio of acylation of the two sites is invers. While in MbxA the first site is more efficiently acylated, the second site showed a more efficient acylation in HlyA, although the same acyltransferase catalyzed the reaction in the context of the laboratory strain BL21(DE3). The presence of peptides resulting from cleavage directly after the less frequently detected second acylation site of MbxA and the first acylation site of HlyA further indicates that these sites were not fully acylated as a modification would have masked the cleavage site (Tab. S1).

The analysis of the in vivo acylation of HlyA by HlyC confirms the acylation of the K564 and K690 acylation sites. Similar to K536 in MbxA, C_{14} and C_{14}-OH* acylations account for the majority of PSM of acyl modified peptides at K690 in HlyA.

MbxA is cytotoxic to human epithelial cells and T cells. As acylated MbxA displayed hemolytic activity on sheep blood agar, human epithelial cells (HEp-2) and human T lymphocytes (Jurkat) were tested for their susceptibility to MbxA with a lactate dehydrogenase (LDH) release assay[68]. Both cell lines were susceptible to MbxA-induced LDH release, which implies cell membrane damage, and showed a sigmoidal dose–response curve with increasing MbxA concentrations (Fig. 7). This is indeed a novel finding since so far only bovine cells were reported to be targeted by MbxA. The half-maximal effect (cytotoxic dose 50, CD_{50}) of MbxA against HEp-2 cells occurred at a concentration of 28.1 ± 4.7 nM. For Jurkat cells 50% cytotoxicity was reached at a lower concentration of MbxA resulting in a CD_{50} of 17.7 ± 3.9 nM. Importantly, proMbxA displayed no cytotoxic effect after 1 h. The calculation of the CD_{50} values was performed under the assumption that the entire pool of MbxA is active. Thus, the values reported likely correspond to a upper limit for the CD_{50} values. These data demonstrate that MbxA is toxic to both, human epithelial and immune cells, in a similar concentration range, but strictly requires activation by acylation to confer membrane-damaging activity.

proMbxA cannot protect human cells from MbxA-induced membrane damage. As proMbxA did not display any cytotoxicity against epithelial cells or T cells we further proceeded to assess if proMbxA can protect any potential MbxA binding sites by binding and shielding the recognition site on the surface of human cells. To test this, we treated cells with 250 nM proMbxA, a concentration that gives maximal effects when active MbxA is used. In case proMbxA is able to recognize and bind specific structures this pre-treatment should pro-

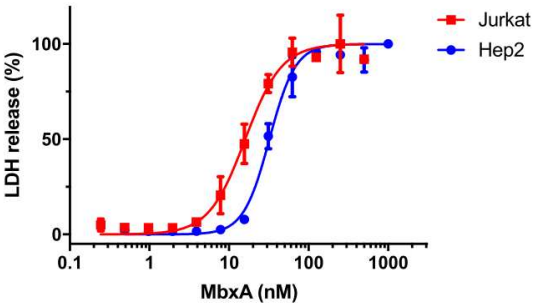

Figure 7. MbxA induces LDH release in human epithelial cells (HEp-2, blue filled circle) and human T cells (Jurkat, red filled square), respectively. The cytotoxicity mediated by MbxA-induced membrane damage was measured using an LDH release assay. LDH release into the supernatant was measured after 1 h of incubation with MbxA. For the CD_{50} determination the MbxA cytotoxicity was plotted against the MbxA concentration and fitted with GraphPad Prism 7 according to Eq. (2) (see materials and methods). For each cell type, the highest LDH release was set to 100%. For simplicity, measurements with proMbxA were not included as no LDH release, even at concentrations of 1 µM, was detected.

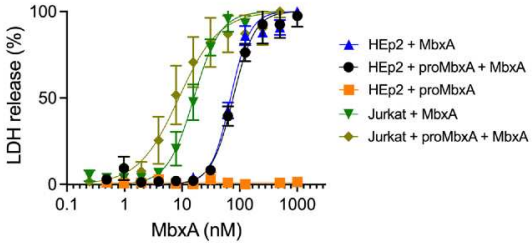

Figure 8. proMbxA does not protect epithelial cells (HEp-2) from MbxA-induced membrane damage. Preincubation with 250 nM of proMbxA for 30 min at 37 °C resulted in a nearly identical dose–response curve to MbxA (black) compared to treatment with MbxA alone (37 °C for 30 min, blue). proMbxA was not cytotoxic (orange). A similar effect was observed for Jurkat cells. Preincubation with 250 nM of proMbxA for 30 min at 37 °C resulted in a not significant different dose–response curve to MbxA (light green) compared to treatment with MbxA alone (37 °C for 30 min, green). The cytotoxicity mediated by MbxA-induced membrane damage was measured using an LDH release assay. LDH release into the supernatant was measured after 1 h of incubation with MbxA. The relative LDH release was calculated from the maximal LDH release reached in each measurement, which was set to 100%. For the CD_{50} determination the MbxA cytotoxicity was plotted against the MbxA concentration and fitted with GraphPad Prism 7 according to Eq. (2) (see material and methods).

tect the cells from active MbxA that was applied in a second step. Based on a previously established protocol[69], preincubation with 250 nM of proMbxA for 30 min at 37 °C before addition of a serial dilution of active MbxA to HEp-2 cells and Jurkat cells had no effect on the dose–response curve and the CD_{50} value compared to MbxA alone (Fig. 8). The presence of proMbxA did not decrease the sensitivity of any of the two cell lines indicating that proMbxA cannot interfere with the cytotoxic action of MbxA.

MbxA induces membrane permeabilization and membrane blebbing in HEp-2 cells. To study the dynamics and the appearance of the changes in the membrane morphology of HEp-2 cells, which occurred upon incubation with MbxA in more detail, we used confocal live-cell imaging. Therefore, the plasma membrane of HEp-2 cells was stained by CellMask Deep Red prior to incubation with MbxA. In parallel, the membrane impermeable high affinity DNA dye Sytox Green was supplied in the surrounding medium of the HEp-2 cells, to monitor the permeabilization of the HEp-2 cells indicated by an increasing Sytox Green signal. Different final concentrations of MbxA (250 nM, 30 nM and 10 nM) and 250 nM of proMbxA were provided to the HEp-2 cells and confocal micrographs were acquired every 15 s for a total of 20 min. When HEp-2 cells were treated with 250 nM MbxA (Fig. 9), Sytox Green entered the nuclei rapidly within the first minutes and stained the DNA with increasing intensity during the observation period of 20 min. Immediate alteration of the plasma membrane morphology could be observed as deformation and blebbing on the cell boundaries (second row) and prominent occurrence of large membrane blebs was seen above the HEp-2 cell layer (third row). To further verify and observe the dose-dependent effect of MbxA in live-cell experiments, Sytox Green influx was analyzed when HEp-2 cells were challenged with 30 nM of MbxA (a concentration around the CD_{50} determined by the LDH release assay) and 10 nM (a concentration that resulted in minimal effects; Fig. 7).

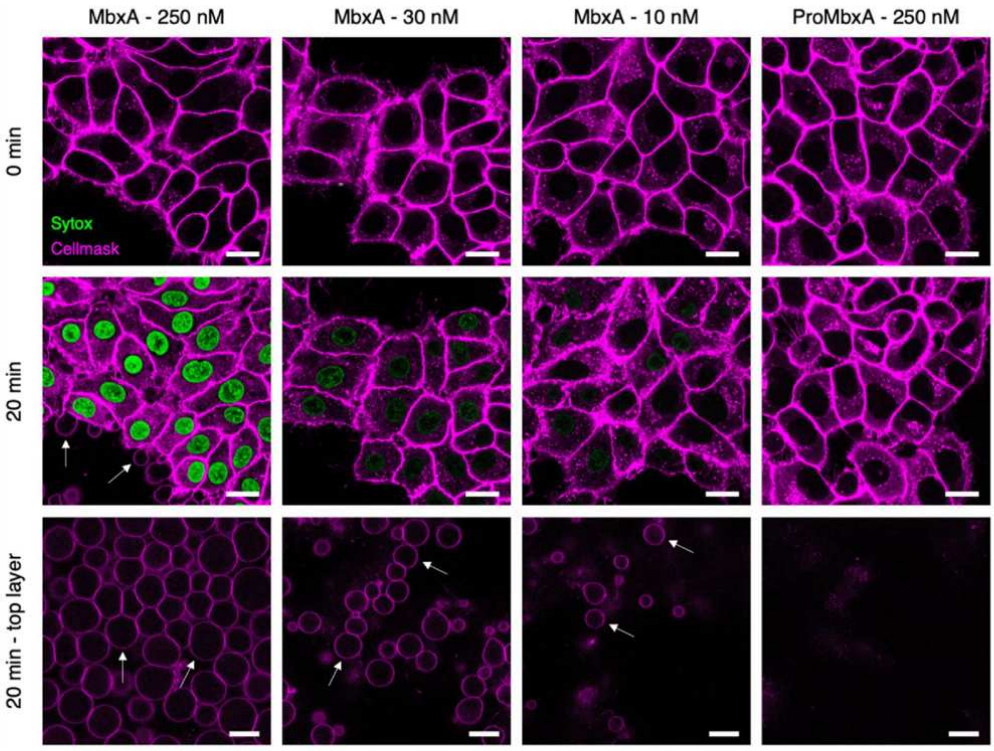

Figure 9. Confocal microscopy images of MbxA-induced membrane permeabilization and membrane blebbing in HEp-2 cells. HEp-2 cells were incubated with MbxA (250 nM, 30 nM and 10 nM at 37 °C) or proMbxA (250 nM) and analyzed at time point zero (first row) and after 20 min (second row). Plasma membrane was stained by CellMask Deep Red and membrane permeabilization was monitored using Sytox Green staining of the nuclear DNA. Incubation of HEp-2 cells with 250 nM, 30 nM and 10 nM MbxA resulted in DNA staining with Sytox Green cells in decreasing intensity corresponding to the decreasing concentration of MbxA and hence in membrane permeabilization. DNA staining was not observed when HEp-2 cells were incubated with 250 nM proMbxA. Membrane blebs were observed in the same focus layer as the HEp-2 cells (second row; white arrows) and above the HEp-2 cells (third row; white arrows). While incubation with 250 nM and 30 nM MbxA led to severe appearance of membrane blebbing, incubation with 10 nM of MbxA was less noticeable and 250 nM proMbxA incubation did not lead to any formation of blebs. Please see Fig. S4 for the entire images. Scale bar: 20 µm.

To understand the correlation between membrane permeabilization and cell death using different MbxA concentrations, quantification of Sytox Green signal was performed per nucleus over time (Fig. 10). Incubating HEp-2 cells with 30 nM MbxA also resulted in a detectable Sytox Green staining of the DNA, but the slope of the intensity per nucleus over time was notably lower compared to the Sytox Green staining observed with 250 nM MbxA (Fig. 9 and 10). Additionally, membrane blebbing of HEp-2 cells with 30 nM MbxA occurred slower and formation of blebs was less pronounced compared to 250 nM MbxA. Using only 10 nM MbxA during the measurement, even less or occasionally no Sytox Green intensity per nucleus was detected, and a few membrane blebbing events were observed at the cells and above the cell layer (Fig. 9 and Fig. S4). While MbxA incubation of HEp-2 cells leads to membrane permeabilization and membrane blebbing, incubation of HEp-2 cells with 250 nM proMbxA resulted in neither Sytox Green staining of the DNA nor observable changes in membrane morphology such as blebbing, which is indicative of a preserved plasma membrane integrity (Fig. 9 and 10). Similar results were observed using AlexaFluor488-labeled Wheat Germ Agglutinin (WGA-488) as membrane marker and propidium iodide (PI) staining for nuclear DNA as measure for permeabilization (Fig. S5 & S6).

Together, this data imply that HEp-2 cells were almost immediately permeable for Sytox Green after contact with MbxA in a dose-dependent manner and underwent changes in membrane morphology like blebbing caused or accompanied by cell death. Moreover, these observed effects must be a functional trait of active MbxA, since the inactive precursor proMbxA did not induce permeabilization, morphological changes or cell death.

Labeled MbxA localizes to the plasma membrane of HEp-2 cells. In order to visualize the localization of MbxA, MbxA was purified and labeled using Atto-488 at the N-terminus. The toxicity of Atto488-MbxA^{S9C} was verified using a hemoglobin release assay (materials and methods) which demonstrated that the

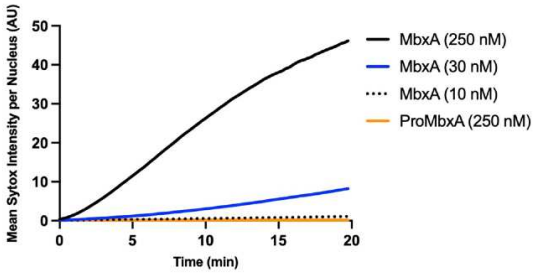

Figure 10. Quantification of MbxA-induced permeabilization of HEp-2 cells. Mean Sytox Green intensity per nucleus of HEp-2 cells (y-axis) was continuously measured over a period of 20 min at 37 °C (see mateirals and methods for details) and is plotted against time (x-axis) for different MbxA concentrations (250 nM, 30 nM and 10 nM) and 250 nM. Sytox Green staining of the HEp-2 cells´ DNA is faster and more intense when 250 nM MbxA were used and is reduced at lower MbxA concentrations (30 nM and 10 nM). In contrast to that, no significant Sytox Green staining of the nuclear DNA was observed with 250 nM proMbxA (number of nuclei used for quantification: 250 nM MbxA—71, 30 nM MbxA—74, 10 nM MbxA—79, 250 nM proMbxA—62). Nuclei have been analyzed from two independent experiments with two biological replicates each. The original images at different time points are provided in Fig. S7.

introduction of the fluorophore reduced the activity by approximately 10% (Fig. S8). HEp-2 cells were incubated with 250 nM Atto488-MbxA^{S9C} for 30 min. Before a washing step with fresh medium, Atto488-MbxA^{S9C} was clearly detectable in the medium (Fig. 11a), while induced morphological changes of the plasma membrane were observed as membrane blebs (Fig. 11b). The strong fluorescence dots in Fig. 11a likely represent aggregated protein as they were hardly detectable after the washing step. To analyze the localization of Atto488-MbxA^{S9C} after unbound protein in the cell supernatant was removed and replaced by fresh media, cells were imaged again (Fig. 11d). A zoom in is provided in Fig. 11g. Accumulations of Atto488-MbxA^{S9C} tracing the shape of the HEp-2 cells were clearly visible when the unbound Atto488-MbxA^{S9C} was removed as shown in the overview images (Fig. 11d) and in the super–resolution micrographs acquired using the Airyscan technique (Fig. 11e). This visualizes the localization of MbxA to the plasma membrane of HEp2 cells, which goes together with permeabilization, potential pore formation and subsequent cell death. Incubation with free Atto488 as a control did not lead to accumulation of the dye in the membrane (Fig. 11c before washing and Fig. 11f after washing) underlining the specific insertion of MbxA into the membrane.

Discussion

MbxA is a cytotoxin of the bovine pathogen *M. bovis* and belongs to the RTX protein family[44]. As an RTX toxin, MbxA is characterized by five conserved Ca^{2+} binding repeats that form the RTX domain and is likely secreted via a cognate T1SS. The necessary tripartite secretion system secreting MbxA is encoded together with an activating acyltransferase and the toxin gene on a pathogenicity island in the *M. bovis* genome[70]. The presence of an intact RTX operon and cytotoxicity of *M. bovis* culture supernatant allows the conclusion that the MbxA secretion system and the MbxA toxin itself are functional[48,49,71]. However, a detailed molecular analysis is still lacking.

Here we employed the secretion system of HlyA from the uropathogenic *E. coli* strain UTI89, considered as a prototype of RTX proteins, to secrete MbxA, thus creating a heterologous T1SS in *E. coli* BL21(DE3). In our recombinantly assembled secretion system the inner membrane components HlyB and HlyD (from UPEC *E. coli*) successfully recognize and interact with the secretion signal of MbxA (from *M. bovis*). The C-terminal secretion signals of RTX proteins do not harbor a conserved sequence, which can be identified in the primary structure, but are likely recognized by a secondary structure element, presumably an amphipathic helix motif[72]. This suggests that MbxA carries the required information within its native C-terminus as it is efficiently transported by the HlyA system. As a putative pore-forming toxin of the RTX family MbxA requires a post-translational activation by acylation of two internal lysine residues. Therefore, we completed the recombinant secretion system by expression of *E. coli* UTI89 HlyC instead of the putative *M. bovis* acyltransferase MbxC resulting in an hemolytically active *E. coli* BL21(DE3) strain (Fig. 2). Both, acylated MbxA and the precursor proMbxA, although in higher amounts, were secreted and facilitated purification from culture supernatants (Fig. 3). The difference in secretion efficiency is similar to proHlyA which is more efficiently secreted than its acylated version, HlyA[67]. Our SEC analysis revealed that proMbxA exists as a dimer and a monomer, while the acylated MbxA forms higher oligomeric species, which presumably include dimers (Fig. 4). Similarly, proHlyA forms dimers when purified, but active HlyA is prone to aggregation[67]. On the contrary, acylation of proCyaA results in formation of the active, monomeric CyaA species[57].

Mass spectrometric analysis of HlyC-acylated MbxA demonstrated that HlyC acylates the proposed lysine residues, K536 and K660, that correspond to the two acylation sites of HlyA (K564, K690)[20,44]. HlyC displays a clear preference for myristic acid (C_{14} fatty acids) and only small amounts of C_{13}, C_{15} or C_{16} fatty acids appear at the first acylation site. Additionally potential C_{12}-OH* and C_{14}-OH* hydroxy acylations were detected at the first acylation site. The second acylation site is only found to be myristoylated (Fig. 6). We observed a similar

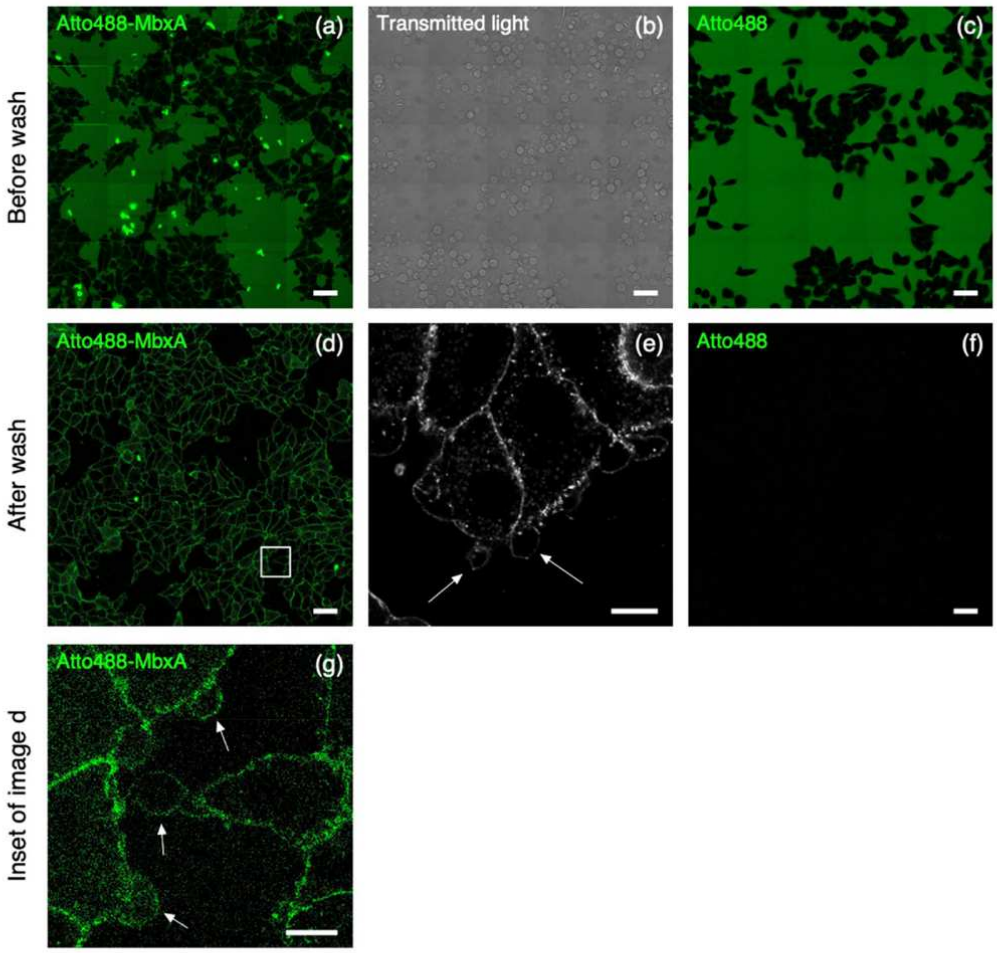

Figure 11. Incubation experiment of Atto488-MbxA^{S9C} with HEp-2 cells. HEp-2 cells after 30 min of incubation with 250 nM Atto488-MbxA^{S9C}, before (**a** and **b**) and after (**d** and **e**) removing excess unbound Atto488-MbxA^{S9C}. Confocal overview images of fluorescent signal are shown in (**a**) and (**d**), transmitted light showing formation of blebbing process in (**b**) and super-resolution Airyscan micrograph in (**e**). Accumulations of Atto488-MbxA^{S9C} tracing the outline of HEp-2 cells are clearly visible after removing the unbound Atto488-MbxA^{S9C} (**d**). Control experiment with Atto488 (dye used to label MbxA) is shown in (**c**) and (**f**). HEp-2 cells after 30 min of incubation with Atto488, before (**c**) and after (**f**) washing off the unbound Atto488 from surrounding medium. The control experiment confirmed that accumulations tracing the outline of HEp-2 cells in (**d**) and (**e**) are Atto488-MbxA^{S9C}, not the free dye. White arrows indicate the position of membrane blebs. (**g**) Zoom into white square in panel (**d**). Scale bars: **a**, **b**, **c**, **d**, **f**: 50 µm; **e**: 10 µm.

preference for myristoylation and a similar variety of fatty acids utilized for modification of HlyA including C_{12}, C_{13}, C_{14}, C_{14}-OH* and C_{16} acyl chains. In contrast to MbxA, where preferentially the first acylation site is modified with different fatty acids, in the case of HlyA variable modifications are detected mainly at the second acylation site. Previous studies already showed that HlyA is predominantly myristoylated but reported a substantial percentage of C_{15} and C_{17} modifications of up to 32%[22], which we did not observe in HlyA expressed and acylated *E. coli* BL21(DE3). Another recent study underlined the preference of HlyC for C_{14} and C_{14}-OH fatty acids and reported that the acylation pattern and choice of acylation sites is inherent to the acyltransferase in the case of non-secreted substrates[23]. At the same time, our study shows that the acylation is not solely controlled by the acyltransferase as we observed that HlyC acylates the first acylation site with a variety of fatty acids in MbxA, while for HlyA more variation of the modification is found at the second site. This illustrates that the same acyltransferase, HlyC, displays different acylation patterns depending on the substrate protein. Interestingly, Osickova et al.[23] reported that mono-acylation of the second acylation site was also observed for the active species, while our study and the study of Stanley et al.[20] demonstrated that the double acylated version represents the active species. Assuming that the relative efficiency of acylation partially depends on the amount of the RTX protein present in the bacterial cytosol prior to secretion, the unmodified peptide fragments of HlyA detected in our

system reflect its higher expression levels compared to MbxA. A very high level expression of the RTX protein that results in inclusion body formation as given in the study of Osickova et al.[23] may explain the incomplete modification of the first acylation site. Altogether, the HlyA system can successfully replace the complete T1SS of another RTX substrate and facilitate its recombinant activation and secretion in *E. coli*. This acylation is obviously the prerequisite for the toxic activity of MbxA.

In contrast to previous studies focusing on the activity of MbxA against bovine cells[49–51,73] we demonstrated cytotoxicity of MbxA outside of its known target species. Besides the hemolytic activity towards sheep erythrocytes, MbxA exhibited cytotoxic activity against human epithelial cells (HEp-2) and human T cells (Jurkat) as demonstrated by LDH release assays (Fig. 7) suggesting that MbxA might act species-independent. Importantly, proMbxA did no induce any LDH release indicating that acylation of MbxA was strictly required for its cytotoxicity. Additionally, preincubation with unmodified proMbxA was not able to block interaction of active MbxA with epithelial cells and T cells or hamper MbxA-induced membrane damage (Fig. 8). This suggests that without the fatty acid-acylation proMbxA cannot successfully bind potential receptors or surface structures on the human cells. This confirms that MbxA as a representative of RTX pore-forming toxins relies on posttranslational acylation. The necessity of acylation for cytotoxicity was previously shown for different RTX toxins and is linked to oligomerization, irreversible insertion into the membrane and / or an effective binding to a host cell receptor[64,65,74–76]. At the same time, acylation is not required for binding to and insertion into membranes or pore-formation, at least for HlyA[60,77,78].

The cytotoxicity of MbxA, a toxin from a bovine pathogen, against human epithelial cell or leukocytes was, with a CD_{50} value of 28.1 ± 4.7 nM or 17.7 ± 3.9 nM (Fig. 7), similar to the activity reported for RTX toxins of human pathogens underlining that its activity is not confined to specific structures of bovine cells. HlyA for example is active at CD_{50} values ranging from approximately 0.2 nM to 30 nM depending on the cell line[79]. The pore-forming activity of MbxA was previously described for bovine erythrocytes, in which MbxA induces leakage of K^+ ions, cell swelling and finally lysis by forming pores of an estimated size of 0.9 nm[48]. We performed live-cell imaging and super-resolution microscopy of HEp-2 cells challenged with MbxA and observed specific localization of MbxA to the plasma membrane and a distinct change in the membrane morphology. Besides permeabilization of the membrane indicated by PI and Sytox Green uptake, large spherical membrane protrusions of up to 20 µm diameter were induced by MbxA at concentrations ranging from 10 to 250 nM, but importantly not by proMbxA (Fig. 9). The formation of these protrusions is reminiscent of membrane blebbing, a phenomenon that is a part of apoptosis and necrosis[80,81], but is also observed in healthy cells during cell division, spreading and migration[82–84]. To the best of our knowledge, RTX toxin-induced formation of membrane blebs was only described for contact-dependent RtxA1 from *V. vulnificus*[59]. In other words, the cytotoxic action of RtxA1 requires a physical contact of the bacterial cell with the host cell. Only then, a time-dependent expression of the protein was detected. In addition, RtxA1 is a multidomain protein and belongs the sub-family of MARTX toxins[85]. Next to membrane blebbing, RtxA1 induced also cell rounding as a consequence of a re-arrangement of the actin cytoskeleton[59]. In contrast to MbxA, RtxA1 contains not only a pore-forming domain but also four additional functional domains, one or more of which are responsible for the changes in cell rounding. For MbxA, which lacks this multidomain architecture, such cell rounding was hardly observed in our image analysis. This clearly suggests that the formation of membrane blebs is an intrinsic function of the pore-forming unit of MbxA and does not require any cofactor or cell–cell contact as in the case of RtxA1.

Membrane blebs form either when an increased intracellular pressure leads to tearing of the membrane from the cytoskeleton or when the actin cortex itself breaks and the excess membrane subsequently inflates[86–88]. The lesions induced by MbxA probably might lead to an increase in the cell pressure by influx of medium components such as Ca^{2+} along the concentration gradient, which than leads to inflation of the excess membrane forming the bleb-like structure. In contrast to blebbing in healthy cells, the blebs observed in this study did not retract and were stable during an imaging time of 90 min (Fig. S8). The nearly linear increase of Sytox Green staining of nuclei upon MbxA treatment was steeper if higher toxin concentrations were applied (Fig. 10). This indicates that the cell membrane is immediately permeabilized after contact with MbxA and possibly the number of pores increases with increasing toxin concentrations. This is also in clear contrast to RtxA1, which displays a cytotoxicity that depends on contact between the bacterium and the host cell[59]. Additionally, accumulation of labeled Atto488-$MbxA^{S9C}$ on HEp-2 cell membranes is an indication of the presence of potential receptors for MbxA binding on human epithelial cells, which might be involved in pore formation in HEp-2 cells. The CD18 (or ß2 integren) subunit of the intern heterodimer was found to be the receptor for RTX toxins such as *Actinobacillus actinomycetemcomitans* leukotoxin and *E. coli* HlyA, promoting cytotoxicity against human immune cells[34,35]. The presence of integren receptors on HEp-2 cells[89], together with our observation of accumulation of Atto488-$MbxA^{S9C}$ on HEp-2 cell membranes further enhances the possibility of a potential receptor for MbxA on HEp-2 cells as well.

In summary, we demonstrated that the *M. bovis* cytotoxin MbxA is secreted and acylated by the heterologous UPEC HlyA system in an *E. coli* lab strain, which allowed purification of proMbxA and MbxA from *E. coli* culture supernatants. *E. coli* UTI89 HlyC efficiently acylated MbxA at the two predicted lysine residues with predominantly C_{14} fatty acids. The acylation of MbxA is strictly necessary for activity against sheep RBC, human epithelial and human T cells, as proMbxA did not exert any cytotoxicity. The cytotoxicity studies showed that MbxA is not species- or cell type-specific and active against human cells in a nanomolar range. Live-cell imaging revealed localization of MbxA at the plasma membrane of human epithelial cells, an immediate permeabilization and membrane blebbing upon contact with MbxA.

Methods

Sequence alignment and topology prediction. Alignment was carried out using EMBOSS Needle pairwise sequence alignment[90]. For the prediction of membrane spanning regions the Constrained Consensus TOPology prediction server (CCTOP) with different implemented algorithms was used[52].

Cloning of the mbxA gene. The *mbxA* gene (Uniprot Q93GI2) was amplified from *M. bovis* DSM 6328 genomic DNA with the primer pair mbxA-for 5′-AACCTTTTCTAACACAACGAGGAGAGAC-3′ and mbxA-rev 5′-AAATCACTAAACACTTGGAGCCAAAATTC-3′ and cloned into the pJET1.2 vector (Thermo Scientific). Subsequently the *mbxA* gene was cloned into the pSU2726 *hlyA* vector[60] replacing the *hlyA* gene. An N-terminal His_6-Tag site was introduced, resulting in plasmid pSU-*6H-mbxA*. To produce acylated MbxA, *6H-mbxA* was cloned into the pSU-*hlyC-6H/hlyA* plasmid[67] replacing the *hlyA* gene. To restore the *hlyA* enhancer region[91] the His_6-Tag of *hlyC* was deleted, creating pSU-*hlyC/6H-mbxA*. In this vector, both genes, *hlyC* and *mbxA*, form a bicistronic operon and are under the control of one LacZ promoter[67].

Expression and secretion of proMbxA and MbxA. Secretion of MbxA in *E. coli* BL21(DE3) was facilitated by co-expression of the transporter components HlyB and HlyD of the *E. coli* UIT89 HlyA system. For expression of recombinant proMbxA, ten 300 ml flasks containing 50 ml LB with 100 µg/ml ampicillin and 30 µg/ml kanamycin per flask were inoculated with an *E. coli* BL21(DE3) overnight culture harboring plasmids pK184-*hlyBD*[13] and pSU 6H-*mbxA* to obtain a starting OD_{600} of 0.05. The culture was grown at 37 °C and 180 rpm until OD_{600} reached 0.4–0.6. Subsequently, the culture was supplemented with 10 mM $CaCl_2$ and expression was induced with 1 mM IPTG. After 5 h of expression at 37 °C and 180 rpm the cells were removed by centrifugation at 13500 g for 45 min. The supernatant was filtered with a 0.45 µm filter and stored on ice for purification.

For the secretion of active MbxA, *E. coli* BL21(DE3) transformed with the plasmids pK184-*hlyBD* and pSU-*hlyC/6H-mbxA* were grown in 2 L LB medium with 100 µg/ml ampicillin and 30 µg/ml kanamycin in baffled 5 L flasks at 37 °C and 160 rpm and induced at the same conditions as pSU-*6H-mbxA*. Secreted MbxA accumulated in the foam of the culture. After the culture reached an OD_{600} between 3.5 to 4.0, the foam was collected and centrifuged at 4000 g for 10 min. The condensed foam was solubilized in solubilization buffer (6 M urea, 100 mM NaCl, 50 mM TRIS pH 8.0) by stirring at room temperature overnight. Aggregate was collected by centrifugation at 160.000 g for 30 min and the solubilized protein stored at − 80 °C.

Purification of MbxA. Solubilized MbxA was refolded by dropwise dilution from 6 M to 400 mM urea with IMAC buffer (50 mM Tris pH 7.8, 400 mM NaCl, 10 mM $CaCl_2$) with constant stirring at room temperature. All subsequent steps were performed at 4 °C. Refolded MbxA was loaded on a 5 ml Ni^{2+} loaded HiTrap IMAC HP column (GE Healthcare) and eluted with a linear 0–75 mM histidine gradient with elution buffer (50 mM Tris pH 7.8, 400 mM NaCl, 10 mM $CaCl_2$, 75 mM histidine). Elution fractions containing MbxA were pooled and concentrated with Amicon Ultra-15 Centrifugal Filter Units (50 kDa NMWL, Merck Millipore). Histidine was removed with a PD10 desalting column (GE Healthcare) at room temperature and the protein eluted with cold IMAC buffer. Activity of MbxA was tested on Columbia agar with 5% sheep blood (Oxoid).

Purification of proMbxA. The culture supernatant containing proMbxA was concentrated with Amicon Ultra-15 Centrifugal Filter Units (50 kDa NMWL, Merck Millipore) to 1/10 of the starting volume and loaded on a 5 ml Ni^{2+} HiTrap IMAC HP column (GE Healthcare). A linear 0–75 mM histidine gradient with elution buffer was used to elute proMbxA. Elution fractions containing proMbxA were pooled and concentrated. Histidine was removed with a PD10 desalting column (GE Healthcare) and the protein eluted with IMAC buffer.

Size exclusion chromatography (SEC) and multi angle light scattering (MALS). For SEC, proMbxA or MbxA containing IMAC fractions were pooled, concentrated to 0.5 ml and after centrifugation at 21,700 g for 20 min directly applied to a Superose 6 Increase 10/300 GL column (GE Healthcare) in SEC buffer (50 mM TRIS pH 7.8, 100 mM NaCl, 10 mM $CaCl_2$). The chromatography was performed on an ÄKTA Purifier system (GE Healthcare).

proMbxA peaks resulting from the SEC were pooled separately and stored with 20% glycerol at − 80 °C. A subsequent SEC-MALS analysis was carried out to investigate the oligomeric state of the proMbxA species. The separated species were concentrated to 1.3–2.5 mg/ml and 200 µl of each were applied to a Superose 6 Increase 10/300 GL column (GE Healthcare) equilibrated with SEC buffer and connected to a miniDAWN TREOS II triple-angle light scattering detector (Wyatt Technologies) and an Optilab T-rEX differential refractive index detector (Wyatt Technologies). The set up was performed using an Agilent 1260 HPLC system with a flowrate of 0.6 ml/min and the data was analyzed with the ASTRA 7.1.2.5 software (Wyatt Technologies).

Expression and purification of proHlyA and HlyA. proHlyA was expressed in *E. coli* BL21(DE3) carrying pSU2726-*hlyA*[60] without transporter components to produce inclusion bodies. 2 L of 2xYT medium with 100 µg/ml ampicillin in baffled 5 L flasks were inoculated with an overnight culture to OD_{600} 0.1 and incubated at 37 °C and 160 rpm. At an OD_{600} of 0.6 expression was induced with 1 mM IPTG, and expression continued for 4 h at 37 °C and 160 rpm. Afterwards cells were collected by centrifugation for 15 min at 13900 g and inclusion bodies purified according to[92]. proHlyA solubilized in 6 M urea was refolded by dropwise dilution to 400 mM urea with 100 mM HEPES pH 8.0, 250 mM NaCl, 10 mM $CaCl_2$. The refolded protein was concentrated with Amicon Ultra-15 Centrifugal Filter Units (100 kDa NMWL, Merck Millipore) and remaining urea removed

with a PD10 desalting column (GE Healthcare). The eluted protein was concentrated and applied to a Superose 6 Increase 10/300 GL column (GE Healthcare) in the same buffer.

Active HlyA was purified from secreting *E. coli* BL21(DE3) harboring pK184-*hlyBD* and pSU-6H-*hlyC/hlyA*. 2 L 2xYT medium with 100 µg/ml ampicillin and 30 µg/ml kanamycin in baffled 5 L flasks were inoculated with an overnight culture to OD_{600} 0.1 and grown at 37 °C and 160 rpm. At OD_{600} 0.4–0.6 the culture was supplemented with 10 mM $CaCl_2$ and expression induced with 1 mM IPTG. After 4 h of expression the foam of the culture was collected, HlyA solubilized in 6 M urea and refolded by dropwise dilution as described for MbxA. Refolded HlyA was concentrated (Amicon Ultra-15 Centrifugal Filter Units, 100 kDa NMWL, Merck Millipore) and remaining urea removed with PD10 desalting column (GE Healthcare).

MS analysis. MbxA, proMbxA as well as HlyA and proHlyA were separated in a polyacrylamide gel, stained with Coomassie Brilliant Blue (CBB), the corresponding bands of the proteins were cut out from the gel and processed for mass spectrometric analysis as described[93]. Briefly, proteins were reduced with dithiothreitol, alkylated with iodoacetamide, and digested with trypsin. Resulting peptides were separated during a 1 h gradient on C18 material using an Ultimate3000 rapid separation liquid chromatography system (Thermo Fisher Scientific) and subsequently injected in an online-coupled QExactive plus mass spectrometer (Thermo Fisher Scientific) via a nano-electrospray interface (described in[93]). Briefly, survey scans were recorded at a resolution of 70000 and subsequently up to 10 precursors were selected by the build-in quadrupole, fragmented via higher energy collisional dissociation, and analyzed at a resolution of 17500.

Recorded spectra were further analyzed by MaxQuant version 1.6.10.43 (MPI for Biochemistry, Planegg, Germany) using standard parameters if not stated otherwise. Searches for MbxA and proMbxA were carried out in a dataset containing 2734 *Moraxella bovis* sequences (UP000254133, downloaded on 27th February from the UniProt KB) as well as an entry for MbxA. For HlyA and proHlyA, a data set was used containing 4156 *Escherichia coli* BL21(DE3) sequences (UP000002032, downloaded on 29th April 2019 from the UniProt KB) and an additional entry for HlyA. Carbamidomethylation at cysteines was considered as fixed and methionine oxidation, n-terminal acetylation, and acylation with C_{12}, C_{13}, C_{14}, C_{15}, C_{16}, C_{17} and C_{18} chains at lysines as variable modifications. In a second search, additionally the hydroxylated variants of the acyl chains were considered. The minimal peptide length was set to five, and two variable modifications were allowed per peptide. Identified proteins and peptides were reported at a false discovery rate of 1%.

Cell culture. Human epithelial cells, HEp-2 (epithelial larynx carcinoma, American Culture Collection (ATCC-CCL-23)) were routinely cultured in Dulbecco´s modified Eagle´s medium (DMEM GlutaMAX; Thermo Fisher) supplemented with 10% fetal calf serum (FCS), MEM vitamins, non-essential amino acids, amphotericin B (2.5 µg/ml) and gentamicin (50 µg/ml) (all Thermo Fisher Scientific) and human T lymphocytes, Jurkat J16 (Adult lymphoblastic leukemia ACC-282, DSMZ) were cultured in RPMI-1640 (Thermo Fisher) supplemented with 10% FCS, 100 U/ml penicillin, 100 µg/ml streptomycin and 10 mM HEPES at 37 °C under 5% CO_2.

Lactate dehydrogenase (LDH) release assay. To monitor the cytotoxicity of MbxA the release of cytosolic LDH was measured as an indicator of membrane damage using the LDH Cytox Assay Kit (Biolegend).

For HEp-2 cells, 10000 cells per well were seeded in a 96 well plate and grown over night. Prior to the assay, the medium was exchanged to DMEM supplemented with 5% FCS. For Jurkat cells, 100 µl with a density of 6×10^5 cells/ml in RPMI with 5% FCS were seeded in 96 well plates and for both cell lines all following incubations were carried out in the appropriate cell culture medium supplemented with 5% FCS. HEp-2 cells and Jurkat cells were incubated with a serial dilution of MbxA in DMEM respectively RPMI for 1 h at 37 °C under 5% CO_2. To assess if preincubation with proMbxA influences MbxA cytotoxicity purified proMbxA was added to the HEp-2 cells together with fresh DMEM and incubated for 30 min at 37 °C under 5% CO_2 before addition of the serial dilution of MbxA. For Jurkat cells proMbxA was added to the cell suspension immediately before seeding and the cells were likewise incubated for 30 min at 37 °C under 5% CO_2 before the addition of MbxA. To monitor the basal release and activity of LDH, HEp-2 and Jurkat cells were incubated with cell culture medium with IMAC buffer (basal LDH). Plates were centrifuged (3 min, 1000 g) and supernatants of HEp-2 and Jurkat cells were collected. For the quantification of the LDH release, the assay was carried out according to manufacturer´s manual (Biolegend) and absorbance measured at 490 nm. The assay was conducted in biological and technical triplicates. For the calculation of the cytotoxicity absorbance of the background control was subtracted from all other values and the average absorption of triplicates was calculated. The relative cytotoxicity was normalized to the maximal LDH release (maximal absorption after MbxA treatment, Max Abs (MbxA treated)) of each experiment and calculated with the following equation:

Equation (1).

$$Cytotoxicity(\%) = \frac{Abs\ (MbxA\ treated) - Abs\ (basal\ LDH)}{Max\ Abs\ (MbxA\ treated) - Abs\ (basal\ LDH)} \times 100 \quad (1)$$

The concentration of the half-maximal effect of MbxA (cytotoxic dose 50, CD_{50}) was calculated from three biological replicates with GraphPad Prism 7 with the following equation:

Equation (2).

$$Cytotoxicity(\%) = \frac{100}{1 + 10^{log(CD50 - conc(MbxA)) \times Hillslope}} \quad (2)$$

Labelling of MbxA with Atto-488 maleimide. Since MbxA does not have any intrinsic cysteine, a serine to cysteine point mutation (StoC) in the N-terminal region of MbxA at the 9th amino acid position was introduced. Site directed mutagenesis of the plasmid pSU-hlyC/6H-mbxA was performed by PCR using the primer pairs mbxAStoC-for 5'-GTAATTAAATGTAATATTCAAGCAGG-3' and mbxAStoC-rev 5'-ATTTATATTGGA CATACGAC-3'. Serine to cysteine point mutation was confirmed by sequencing and the lytic activity of the mutated MbxA was tested on Columbia agar with 5% sheep blood (Oxoid). For the quantitative comparison of MbxA activity, hemoglobin release assay was performed (protocol given below).

Secretion and purification of MbxA^{S9C} was performed using the protocol for wild type MbxA as described above. Labeling reaction with Atto-488 was performed based on manufacturer's instructions for thiol-reactive fluorescent dyes. 6 ml of purified MbxA^{S9C} with a concentration of 0.5 mg/ml was used for labeling reactions. MbxA^{S9C} was incubated with tenfold molar excess of TCEP (0.5 M TCEP stock solution) for 6 h on ice. The solution was concentrated to 2.5 ml using a 50 kDa MWCO filter concentrator, buffer was exchanged to DPBS buffer (Solution C—see below) using a PD10 column and the solution was again concentrated to 4 mg/ml (540 µL) using a 50 kDa MWCO filter concentrator. Subsequently, reduced MbxA^{S9C} was incubated with a 15-fold molar excess of Atto-488 (5 mM stock solution in DMSO) for 24 h on ice. The reaction was quenched using a fivefold molar excess of GSH (6 mM stock solution in DPBS + + buffer (Solution A—see below)) compared to the dye and incubated for 10 min on ice. Unbound dye and GSH were removed using a PD10 column buffered with DPBS + + buffer (Solution A—see below). Furthermore, the in-gel fluorescence of the labeled protein was detected by a Bio-Rad gel documentation system (Fig.S3).

[DPBS + + buffer (Solution A): 0.90 mM $CaCl_2.2H_2O$, 0.5 mM $MgCl_2.6H_2O$, 2.67 mM KCl, 1.47 mM KH_2PO_4, 137.9 mM NaCl, 8.06 mM Na_2HPO4, pH 7.4. Solution B: 0.2 M sodium bicarbonate solution, adjusted to pH 9.0 with 2 M sodium hydroxide. Labeling buffer (Solution C) – > To 20 parts of Solution A add 1 part of Solution B to obtain a labeling buffer of pH 8.3.

Calculation of degree of labeling (DOL). The degree of labeling (DOL, dye-to-protein ratio) was determined by absorption spectroscopy (Table S2: Absorbance (A) = extinction coefficient (ε) × molar concentration (c) × path length (d).

Labeling efficiency/DOL = Concentration of the dye/Concentration of the protein.

$$\mathrm{DOL} = \frac{A_{max}/\varepsilon_{max}}{A_{prot}/\varepsilon_{prot}} = \frac{A_{max} \times \varepsilon_{prot}}{(A_{280} - A_{max} \times CF) \times \varepsilon_{max}}$$

Absorbance of the labeled dye at 494 nm and 280 nm were measured using a NanoDrop. As all dyes show some absorption at 280 nm, the measured absorbance A_{280} must be corrected for the contribution of the dye. This is given by Amax × CF_{280}.

Hemoglobin release assay. Defibrinated sheep blood was obtained from Oxoid. 1 ml of cells were transferred into 1.5 ml reaction tubes and centrifuged for 1 min at 14000 g. The supernatant was removed, and cells were resuspended in buffer containing 10 mM Tris–HCl pH 7.5, 155 mM NaCl, 20 mM $CaCl_2$, 5 mM KCl and 2 mM $MgSO_4$ by 5–10 s vortexing intervals. This process was repeated until the supernatant remained colorless. The resuspended cells were transferred into a 50 ml falcon tube to guarantee equal cell distribution and immediately used for the in vitro assay. All steps were performed at room temperature. 250 nM concentrations of Atto-488 labeled MbxA^{S9C}, MbxA^{S9C}, MbxA or HlyA were added to 500 µl washed sheep blood cells each. 16% SDS was used as the positive control and set arbitrarily as 100% and IMAC buffer was used as the negative control. The cells were incubated for 30 min at 37 °C with the proteins. Subsequently, the cells were removed by centrifugation (1 min at 14000 × g) and 200 µl of 1/10 diluted fraction of the supernatant transferred to a 96-well plate. The hemoglobin amount in the supernatant was determined on a FLUOstar OPTIMA microplate reader (BMG Labtech) with an absorption wavelength of 544 nm.

Live-cell imaging. HEp-2 cells were cultivated and passaged in DMEM (Pan Biotech) supplemented with 10% FCS, MEM vitamins, non-essential amino acids, amphotericin B (2.5 µg/ml) and gentamicin (50 µg/ml) (all Thermo Fisher Scientific). Two days prior to use, HEp-2 cells were seeded in 2 ml DMEM in 35 mm µ-Dish 1,5H glass bottom dishes (Ibidi) and grown for 39–48 h at 37 °C under 5% CO_2.

In case of the incubation experiment with unlabeled MbxA, cells were washed twice with 1 ml of prewarmed DMEM supplemented with 20 mM HEPES as live cell medium (Pan Biotech) and preincubated with 250 µl of 20 µM of Hoechst 33342 (Invitrogen) in live cell medium for 22 min at 37 °C and 5% CO_2. After this, 750 µl of live cell medium containing 1 µl of 5 mg/ml Hoechst 33342 (Invitrogen), resulting in a 5 µM concentration of Hoechst 33342 and 5 µg/ml CellMask Deep Red and were incubated for another 8 min at 37 °C and 5% CO_2 (total incubation of 30 min). The cells were washed once gently with 1 ml of pre-warmed live cell medium and 1 ml of live cell medium with a 5 µM concentration of Sytox Green was added. The cells were transferred to a Zeiss LSM880 Airyscan microscope system (Carl Zeiss Microscopy GmbH). A region of interest was preset for the incubation experiment. 1 ml of a fresh solution of MbxA or proMbxA protein was prepared at the twofold of the indicated final concentration in 1 ml of live cell medium containing a 5 µM concentration of Sytox Green. The MbxA solution at twice the concentration was added to the cells and gently mixed by pipetting three times without touching the live cell dish to keep the region of interest in focus. This resulted in total in 2 ml live cell medium containing the indicated final concentration of MbxA supplemented with 5 µg/ml of Sytox Green during the acquisition of the time series. The measurement was started immediately.

In the case of incubation experiment with Atto488-labeled MbxA^{S9C}, cells were washed with 1 ml of DMEM supplemented with 20 mM HEPES as live cell medium (Pan Biotech, Germany), incubated in 1 ml of pre-warmed live cell medium and transferred to the LSM880 (Carl Zeiss Microscopy GmbH) focusing a region of interest. 1 ml of a fresh solution of Atto488-labeled MbxA^{S9C} at twice the final concentration was prepared in live cell medium, added and again gently mixed by pipetting three times without touching the live cell dish to keep the region of interest in focus. The measurement was started immediately. After 30 min the supernatant containing the Atto488-labeled MbxA^{S9C} was carefully replaced by fresh pre-warmed live cell medium and analyzed for protein localization again.

The imaging conditions were set up as follows. Confocal and Airyscan micrographs were recorded using a Zeiss LSM880 Airyscan microscope system (Carl Zeiss Microscopy GmbH) equipped with a Plan-Apochromat 63x/1.4 oil immersion objective lens. For excitation a 405 nm Laser was used for Hoechst 33342, a 488 nm Argon laser for excitation of Sytox Green and Atto488-labeled MbxA^{S9C} and a 633 nm laser for excitation of CellMask Deep Red.

In confocal microscopy of unlabeled MbxA a pixel dwell time of 1 µs was used without averaging at a frame rate of 15 s/frame to reduce phototoxicity to a minimum. Excitation and detection of different dyes was set up in a frame wise switch to reduce crosstalk and detection ranges were set for Hoechst 33342 at 415–460 nm, for Sytox Green at 495–550 nm and for CellMask Deep Red at 648–700 nm. Focus was maintained during the time series using the hardware based autofocus system Definite Focus 2 (Carl Zeiss Microscopy GmbH).

In confocal microscopy of Atto488-labeled MbxA^{S9C} tiles can experiments of 25 single images were acquired at a pixel dwell time of 0.77 µs and the detection range for ^{Atto488}MbxA was set at 495–550 nm. Additional super-resolution Airyscan micrographs were acquired at a pixel dwell time of 2 µs and a fourfold averaging in Airyscan super-resolution mode after alignment on detector elements was established. To limit the detection range a BP 495–535 + LP 555 filter was used. The final Airyscan image was generated by using the Zeiss Airyscan processing at 2D automatic settings.

Image quantification. Confocal images of unlabeled MbxA were analyzed using Cellprofiler image analysis software version 4[94]. The nuclei area were determined by merging the Hoechst 33342 and Sytox Green signal and applying adaptive Sauvola thresholding. Tracking of nuclei across the time series was performed by the TrackObjects module with overlap tracking and a maximum pixel distance of 40 to consider matches. Extracted image data were processed to consider only nuclei that have been successfully tracked during the whole time series of 20 min (80 frames). The Cellprofiler pipeline and Jupyter notebook for data processing are available publicly at github (https://github.com/abhamacher/timelapseMic_MbxA).

Data availability

All fluorescence data have been deposited at BioImage Archive (https://www.ebi.ac.uk/biostudies/studies/S-BIAD295). The mass spectrometry proteomics data have been deposited to the ProteomeXchange Consortium via the PRIDE [95] partner repository with the dataset identifier PXD030929.

Received: 24 May 2022; Accepted: 14 October 2022
Published online: 24 October 2022

References

1. Rasko, D. A. & Sperandio, V. Anti-virulence strategies to combat bacteria-mediated disease. *Nat. Rev. Drug. Discov.* **9**, 117–128. https://doi.org/10.1038/nrd3013 (2010).
2. Krueger, E. & Brown, A. C. Inhibition of bacterial toxin recognition of membrane components as an anti-virulence strategy. *J. Biol. Eng.* **13**, 4. https://doi.org/10.1186/s13036-018-0138-z (2019).
3. Linhartova, I. *et al.* RTX proteins: A highly diverse family secreted by a common mechanism. *FEMS Microbiol. Rev.* **34**, 1076–1112. https://doi.org/10.1111/j.1574-6976.2010.00231.x (2010).
4. Welch, R. A. Pore-forming cytolysins of gram-negative bacteria. *Mol. Microbiol.* **5**, 521–528. https://doi.org/10.1111/j.1365-2958.1991.tb00723.x (1991).
5. Baumann, U., Wu, S., Flaherty, K. M. & McKay, D. B. Three-dimensional structure of the alkaline protease of Pseudomonas aeruginosa: A two-domain protein with a calcium binding parallel beta roll motif. *EMBO J.* **12**, 3357–3364 (1993).
6. Mackman, N., Nicaud, J. M., Gray, L. & Holland, I. B. Identification of polypeptides required for the export of haemolysin 2001 from *E. coli*. *Mol. Gen. Genet.* **201**, 529–536. https://doi.org/10.1007/bf00331351 (1985).
7. Mackman, N., Nicaud, J. M., Gray, L. & Holland, I. B. Genetical and functional organisation of the *Escherichia coli* haemolysin determinant 2001. *Mol. Gen. Genet.* **201**, 282–288. https://doi.org/10.1007/bf00425672 (1985).
8. Wandersman, C. & Delepelaire, P. TolC, an *Escherichia coli* outer membrane protein required for hemolysin secretion. *Proc. Natl. Acad. Sci. USA* **87**, 4776–4780. https://doi.org/10.1073/pnas.87.12.4776 (1990).
9. Felmlee, T. & Welch, R. A. Alterations of amino acid repeats in the *Escherichia coli* hemolysin affect cytolytic activity and secretion. *Proc. Natl. Acad. Sci. USA* **85**, 5269–5273. https://doi.org/10.1073/pnas.85.14.5269 (1988).
10. Gray, L. *et al.* A novel C-terminal signal sequence targets *Escherichia-coli* hemolysin directly to the medium. *J. Cell Sci.* **1989**, 45–57 (1989).
11. Gray, L., Mackman, N., Nicaud, J. M. & Holland, I. B. The carboxy-terminal region of hemolysin 2001 is required for secretion of the toxin from *Escherichia-coli*. *Mol. Gen. Genet.* **205**, 127–133. https://doi.org/10.1007/Bf02428042 (1986).
12. Koronakis, V., Koronakis, E. & Hughes, C. Isolation and analysis of the c-terminal signal directing export of *Escherichia-coli* hemolysin protein across both bacterial-membranes. *EMBO J.* **8**, 595–605. https://doi.org/10.1002/j.1460-2075.1989.tb03414.x (1989).
13. Bakkes, P. J., Jenewein, S., Smits, S. H. J., Holland, I. B. & Schmitt, L. The rate of folding dictates substrate secretion by the *Escherichia coli* hemolysin type 1 secretion system. *J. Biol. Chem.* **285**, 40573–40580. https://doi.org/10.1074/jbc.M110.173658 (2010).
14. Ostolaza, H., Soloaga, A. & Goni, F. M. The binding of divalent-cations to *Escherichia-coli* alpha-hemolysin. *Eur. J. Biochem.* **228**, 39–44. https://doi.org/10.1111/j.1432-1033.1995.tb20225.x (1995).
15. Thomas, S., Bakkes, P. J., Smits, S. H. & Schmitt, L. Equilibrium folding of pro-HlyA from *Escherichia coli* reveals a stable calcium ion dependent folding intermediate. *Biochim. Biophys. Acta* **1500–1510**, 2014. https://doi.org/10.1016/j.bbapap.2014.05.006 (1844).

16. Bhakdi, S. *et al.* Potent leukocidal action of Escherichia coli hemolysin mediated by permeabilization of target cell membranes. *J. Exp. Med.* **169**, 737–754. https://doi.org/10.1084/jem.169.3.737 (1989).
17. Keane, W. F., Welch, R., Gekker, G. & Peterson, P. K. Mechanism of *Escherichia coli* alpha-hemolysin-induced injury to isolated renal tubular cells. *Am. J. Pathol.* **126**, 350–357 (1987).
18. Suttorp, N., Floer, B., Schnittler, H., Seeger, W. & Bhakdi, S. Effects of *Escherichia coli* hemolysin on endothelial cell function. *Infect. Immun.* **58**, 3796–3801 (1990).
19. Nicaud, J. M., Mackman, N., Gray, L. & Holland, I. B. Characterisation of HlyC and mechanism of activation and secretion of haemolysin from *E. coli* 2001. *FEBS Lett.* **187**, 339–344 (1985).
20. Stanley, P., Packman, L. C., Koronakis, V. & Hughes, C. Fatty acylation of two internal lysine residues required for the toxic activity of *Escherichia coli* hemolysin. *Science* **266**, 1992–1996. https://doi.org/10.1126/science.7801126 (1994).
21. Greene, N. P., Crow, A., Hughes, C. & Koronakis, V. Structure of a bacterial toxin-activating acyltransferase. *Proc. Natl. Acad. Sci. USA* https://doi.org/10.1073/pnas.1503832112 (2015).
22. Lim, K. B. *et al.* Escherichia coli alpha-hemolysin (HlyA) is heterogeneously acylated in vivo with 14-, 15-, and 17-carbon fatty acids. *J. Biol. Chem.* **275**, 36698–36702. https://doi.org/10.1074/jbc.C000544200 (2000).
23. Osickova, A. *et al.* Acyltransferase-mediated selection of the length of the fatty acyl chain and of the acylation site governs activation of bacterial RTX toxins. *J. Biol. Chem.* https://doi.org/10.1074/jbc.RA120.014122 (2020).
24. Ostolaza, H. *et al.* Membrane permeabilization by pore-forming RTX toxins: What kind of lesions do these toxins Form?. *Toxins (Basel)* https://doi.org/10.3390/toxins11060354 (2019).
25. Gonzalez-Bullon, D. *et al.* Membrane permeabilization by bordetella adenylate cyclase toxin involves pores of tunable size. *Biomolecules* https://doi.org/10.3390/biom9050183 (2019).
26. Menestrina, G., Mackman, N., Holland, I. B. & Bhakdi, S. Escherichia coli haemolysin forms voltage-dependent ion channels in lipid membranes. *Biochim. Biophys. Acta* **905**, 109–117 (1987).
27. Uhlen, P. *et al.* Alpha-haemolysin of uropathogenic *E. coli* induces Ca2+ oscillations in renal epithelial cells. *Nature* **405**, 694–697 (2000).
28. Murthy, A. M. V. *et al.* Regulation of hemolysin in uropathogenic *Escherichia coli* fine-tunes killing of human macrophages. *Virulence* https://doi.org/10.1080/21505594.2018.1465786 (2018).
29. Gu, H. *et al.* A previously uncharacterized two-component signaling system in uropathogenic *Escherichia coli* coordinates protection against host-derived oxidative stress with activation of hemolysin-mediated host cell pyroptosis. *PLoS Pathog.* **17**, e1010005. https://doi.org/10.1371/journal.ppat.1010005 (2021).
30. Russo, T. A. *et al. E. coli* virulence factor hemolysin induces neutrophil apoptosis and necrosis/lysis in vitro and necrosis/lysis and lung injury in a rat pneumonia model. *Am. J. Physiol. Lung Cell Mol. Physiol.* **289**, L207-216 (2005).
31. Menestrina, G., Moser, C., Pellet, S. & Welch, R. Pore-formation by *Escherichia coli* hemolysin (HlyA) and other members of the RTX toxins family. *Toxicology* **87**, 249–267 (1994).
32. Ostolaza, H., Bartolome, B., Ortiz de Zarate, I., de la Cruz, F. & Goni, F. M. Release of lipid vesicle contents by the bacterial protein toxin alpha-haemolysin. *Biochem. Biophys. Acta.* **1147**, 81–88 (1993).
33. Valeva, A. *et al.* Binding of *Escherichia coli* hemolysin and activation of the target cells is not receptor-dependent. *J. Biol. Chem.* **280**, 36657–36663. https://doi.org/10.1074/jbc.M507690200 (2005).
34. Lally, E. T. *et al.* RTX toxins recognize a beta2 integrin on the surface of human target cells. *J. Biol. Chem.* **272**, 30463–30469. https://doi.org/10.1074/jbc.272.48.30463 (1997).
35. Ristow, L. C. *et al.* The Extracellular Domain of the β(2) Integrin β Subunit (CD18) Is Sufficient for *Escherichia coli* Hemolysin and Aggregatibacter actinomycetemcomitans Leukotoxin Cytotoxic Activity. *MBio* https://doi.org/10.1128/mBio.01459-19 (2019).
36. Morova, J., Osicka, R., Masin, J. & Sebo, P. RTX cytotoxins recognize beta2 integrin receptors through N-linked oligosaccharides. *P. Natl. Acad. Sci. USA* **105**, 5355–5360. https://doi.org/10.1073/pnas.0711400105 (2008).
37. Bumba, L., Masin, J., Fiser, R. & Sebo, P. Bordetella adenylate cyclase toxin mobilizes its beta2 integrin receptor into lipid rafts to accomplish translocation across target cell membrane in two steps. *PLoS Pathog.* **6**, e1000901. https://doi.org/10.1371/journal.ppat.1000901 (2010).
38. Cortajarena, A. L., Goni, F. M. & Ostolaza, H. Glycophorin as a receptor for *Escherichia coli* alpha-hemolysin in erythrocytes. *J. Biol. Chem.* **276**, 12513–12519. https://doi.org/10.1074/jbc.M006792200 (2001).
39. Highlander, S. K., Engler, M. J. & Weinstock, G. M. Secretion and expression of the Pasteurella haemolytica Leukotoxin. *J. Bacteriol.* **172**, 2343–2350 (1990).
40. Kuhnert, P., Heyberger-Meyer, B., Nicolet, J. & Frey, J. Characterization of PaxA and its operon: A cohemolytic RTX toxin determinant from pathogenic Pasteurella aerogenes. *Infect. Immun.* **68**, 6–12 (2000).
41. Sebo, P. & Ladant, D. Repeat sequences in the Bordetella pertussis adenylate cyclase toxin can be recognized as alternative carboxy-proximal secretion signals by the *Escherichia coli* alpha-haemolysin translocator. *Mol. Microbiol.* **9**, 999–1009. https://doi.org/10.1111/j.1365-2958.1993.tb01229.x (1993).
42. Thompson, S. A. & Sparling, P. F. The RTX cytotoxin-related FrpA protein of Neisseria meningitidis is secreted extracellularly by meningococci and by HlyBD+ Escherichia coli. *Infect. Immun.* **61**, 2906–2911 (1993).
43. Zhang, F., Greig, D. I. & Ling, V. Functional replacement of the hemolysin A transport signal by a different primary sequence. *Proc. Natl. Acad. Sci. U S A* **90**, 4211–4215 (1993).
44. Angelos, J. A., Hess, J. F. & George, L. W. Cloning and characterization of a moraxella bovis cytotoxin gene. *Am. J. Vet. Res.* **62**, 1222–1228 (2001).
45. Beard, M. K. & Moore, L. J. Reproduction of bovine keratoconjunctivitis with a purified haemolytic and cytotoxic fraction of Moraxella bovis. *Vet. Microbiol.* **42**, 15–33 (1994).
46. Baptista, P. J. Infectious bovine keratoconjunctivitis: A review. *Br. Vet. J.* **135**, 225–242. https://doi.org/10.1016/s0007-1935(17)32882-8 (1979).
47. Henson, J. B. & Grumbles, L. C. Infectious Bovine Keratoconjunctivitis. 1 Etiology. *Am. J. Vet. Res.* **21**, 761–766 (1960).
48. Clinkenbeard, K. D. & Thiessen, A. E. Mechanism of action of Moraxella bovis hemolysin. *Infect. Immun.* **59**, 1148–1152 (1991).
49. Hoien-Dalen, P. S., Rosenbusch, R. F. & Roth, J. A. Comparative characterization of the leukocidic and hemolytic activity of Moraxella bovis. *Am. J. Vet. Res.* **51**, 191–196 (1990).
50. Kagonyera, G. M., George, L. & Miller, M. Effects of Moraxella bovis and culture filtrates on 51Cr-labeled bovine neutrophils. *Am. J. Vet. Res.* **50**, 18–21 (1989).
51. Kagonyera, G. M., George, L. W. & Munn, R. Cytopathic effects of Moraxella bovis on cultured bovine neutrophils and corneal epithelial cells. *Am. J. Vet. Res.* **50**, 10–17 (1989).
52. Dobson, L., Remenyi, I. & Tusnady, G. E. CCTOP: A Consensus Constrained TOPology prediction web server. *Nucleic Acids Res.* **43**, W408-412. https://doi.org/10.1093/nar/gkv451 (2015).
53. Ludwig, A., Schmid, A., Benz, R. & Goebel, W. Mutations affecting pore formation by haemolysin from *Escherichia coli*. *Mol. Gen. Genet.* **226**, 198–208. https://doi.org/10.1007/bf00273604 (1991).
54. Angelos, J. A., Chigerwe, M., Edman, J. M. & Hess, J. F. Systemic and ocular immune responses in cattle following intranasal vaccination with precipitated or partially solubilized recombinant Moraxella bovis cytotoxin adjuvanted with polyacrylic acid. *Am. J. Vet. Res.* **77**, 1411–1418. https://doi.org/10.2460/ajvr.77.12.1411 (2016).

55. Angelos, J. A. & Ball, L. M. Relatedness of cytotoxins from geographically diverse isolates of Moraxella bovis. *Vet. Microbiol.* **124**, 382–386. https://doi.org/10.1016/j.vetmic.2007.04.042 (2007).
56. Angelos, J. A., Bonifacio, R. G., Ball, L. M. & Hess, J. F. Prevention of naturally occurring infectious bovine keratoconjunctivitis with a recombinant Moraxella bovis pilin-Moraxella bovis cytotoxin-ISCOM matrix adjuvanted vaccine. *Vet. Microbiol.* **125**, 274–283. https://doi.org/10.1016/j.vetmic.2007.05.028 (2007).
57. Karst, J. C. *et al.* Calcium, acylation, and molecular confinement favor folding of Bordetella pertussis adenylate cyclase CyaA toxin into a monomeric and cytotoxic form. *J. Biol. Chem.* **289**, 30702–30716. https://doi.org/10.1074/jbc.M114.580852 (2014).
58. Balashova, N. *et al.* Generation of a recombinant Aggregatibacter actinomycetemcomitans RTX toxin in *Escherichia coli*. *Gene* **672**, 106–114. https://doi.org/10.1016/j.gene.2018.06.003 (2018).
59. Kim, Y. R. *et al.* Vibrio vulnificus RTX toxin kills host cells only after contact of the bacteria with host cells. *Cell Microbiol.* **10**, 848–862. https://doi.org/10.1111/j.1462-5822.2007.01088.x (2008).
60. Soloaga, A., Ostolaza, H., Goni, F. M. & de la Cruz, F. Purification of *Escherichia coli* pro-haemolysin, and a comparison with the properties of mature alpha-haemolysin. *Eur. J. Biochem.* **238**, 418–422. https://doi.org/10.1111/j.1432-1033.1996.0418z.x (1996).
61. Basar, T., Havlicek, V., Bezouskova, S., Hackett, M. & Sebo, P. Acylation of lysine 983 is sufficient for toxin activity of Bordetella pertussis adenylate cyclase. Substitutions of alanine 140 modulate acylation site selectivity of the toxin acyltransferase CyaC. *J. Biol. Chem.* **276**, 348–354. https://doi.org/10.1074/jbc.M006463200 (2001).
62. Fong, K. P. *et al.* Aggregatibacter actinomycetemcomitans leukotoxin is post-translationally modified by addition of either saturated or hydroxylated fatty acyl chains. *Mol. Oral Microbiol.* **26**, 262–276. https://doi.org/10.1111/j.2041-1014.2011.00617.x (2011).
63. Hormozi, K., Parton, R. & Coote, J. Target cell specificity of the Pasteurella haemolytica leukotoxin is unaffected by the nature of the fatty-acyl group used to activate the toxin in vitro. *Fems Microbiol. Lett.* **169**, 139–145 (1998).
64. Masin, J. *et al.* Acylation of lysine 860 allows tight binding and cytotoxicity of bordetella adenylate cyclase on CD11b-expressing cells. *Biochemistry* **44**, 12759–12766. https://doi.org/10.1021/bi050459b (2005).
65. Osickova, A. *et al.* Cytotoxic activity of Kingella kingae RtxA toxin depends on post-translational acylation of lysine residues and cholesterol binding. *Emerg. Microbes Infect.* **7**, 178. https://doi.org/10.1038/s41426-018-0179-x (2018).
66. Issartel, J. P., Koronakis, V. & Hughes, C. Activation of *Escherichia coli* prohaemolysin to the mature toxin by acyl carrier protein-dependent fatty acylation. *Nature* **351**, 759–761. https://doi.org/10.1038/351759a0 (1991).
67. Thomas, S., Smits, S. H. J. & Schmitt, L. A simple in vitro acylation assay based on optimized HlyA and HlyC purification. *Anal. Biochem.* **464**, 17–23. https://doi.org/10.1016/j.ab.2014.07.001 (2014).
68. Kumar, P., Nagarajan, A. & Uchil, P. D. Analysis of cell viability by the lactate dehydrogenase assay. *Cold Spring Harb. Protoc.* https://doi.org/10.1101/pdb.prot095497 (2018).
69. Moelleken, K. & Hegemann, J. H. The chlamydia outer membrane protein OmcB is required for adhesion and exhibits biovar-specific differences in glycosaminoglycan binding. *Mol. Microbiol.* **67**, 403–419. https://doi.org/10.1111/j.1365-2958.2007.06050.x (2008).
70. Hess, J. F. & Angelos, J. A. The Moraxella bovis RTX toxin locus mbx defines a pathogenicity island. *J. Med. Microbiol.* **55**, 443–449. https://doi.org/10.1099/jmm.0.46366-0 (2006).
71. Angelos, J. A., Hess, J. F. & George, L. W. An RTX operon in hemolytic moraxella bovis is absent from nonhemolytic strains. *Vet. Microbiol.* **92**, 363–377. https://doi.org/10.1016/s0378-1135(02)00410-8 (2003).
72. Hui, D., Morden, C., Zhang, F. & Ling, V. Combinatorial analysis of the structural requirements of the *Escherichia coli* hemolysin signal sequence. *J. Biol. Chem.* **275**, 2713–2720 (2000).
73. Gray, J. T., Fedorka-Cray, P. J. & Rogers, D. G. Partial characterization of a Moraxella bovis cytolysin. *Vet. Microbiol.* **43**, 183–196 (1995).
74. El-Azami-El-Idrissi, M. *et al.* Interaction of Bordetella pertussis adenylate cyclase with CD11b/CD18: Role of toxin acylation and identification of the main integrin interaction domain. *J. Biol. Chem.* **278**, 38514–38521. https://doi.org/10.1074/jbc.M304387200 (2003).
75. Herlax, V. & Bakas, L. Acyl chains are responsible for the irreversibility in the *Escherichia coli* alpha-hemolysin binding to membranes. *Chem. Phys. Lipids* **122**, 185–190. https://doi.org/10.1016/s0009-3084(02)00191-3 (2003).
76. Herlax, V., Mate, S., Rimoldi, O. & Bakas, L. Relevance of fatty acid covalently bound to *Escherichia coli* alpha-hemolysin and membrane microdomains in the oligomerization process. *J. Biol. Chem.* **284**, 25199–25210. https://doi.org/10.1074/jbc.M109.009365 (2009).
77. Benz, R., Maier, E., Ladant, D., Ullmann, A. & Sebo, P. Adenylate-cyclase toxin (Cyaa) of bordetella-pertussis–evidence for the formation of small ion-permeable channels and comparison with hlya of *Escherichia-coli*. *J. Biol. Chem.* **269**, 27231–27239 (1994).
78. Ludwig, A. *et al.* Analysis of the in vivo activation of hemolysin (HlyA) from *Escherichia coli*. *J. Bacteriol.* **178**, 5422–5430. https://doi.org/10.1128/jb.178.18.5422-5430.1996 (1996).
79. Ristow, L. C. *et al.* The extracellular domain of the beta2 integrin beta subunit (CD18) is sufficient for *Escherichia coli* hemolysin and aggregatibacter actinomycetemcomitans leukotoxin cytotoxic activity. *MBio* https://doi.org/10.1128/mBio.01459-19 (2019).
80. Barros, L. F. *et al.* Apoptotic and necrotic blebs in epithelial cells display similar neck diameters but different kinase dependency. *Cell Death Differ.* **10**, 687–697. https://doi.org/10.1038/sj.cdd.4401236 (2003).
81. Mills, J. C., Stone, N. L., Erhardt, J. & Pittman, R. N. Apoptotic membrane blebbing is regulated by myosin light chain phosphorylation. *J. Cell Biol.* **140**, 627–636. https://doi.org/10.1083/jcb.140.3.627 (1998).
82. Fishkind, D. J., Cao, L. G. & Wang, Y. L. Microinjection of the catalytic fragment of myosin light chain kinase into dividing cells: Effects on mitosis and cytokinesis. *J. Cell Biol.* **114**, 967–975. https://doi.org/10.1083/jcb.114.5.967 (1991).
83. Norman, L. L., Brugues, J., Sengupta, K., Sens, P. & Aranda-Espinoza, H. Cell blebbing and membrane area homeostasis in spreading and retracting cells. *Biophys. J.* **99**, 1726–1733. https://doi.org/10.1016/j.bpj.2010.07.031 (2010).
84. Trinkaus, J. P. Surface activity and locomotion of Fundulus deep cells during blastula and gastrula stages. *Dev. Biol.* **30**, 69–103. https://doi.org/10.1016/0012-1606(73)90049-3 (1973).
85. Kwak, J. S., Jeong, H. G. & Satchell, K. J. Vibrio vulnificus rtxA1 gene recombination generates toxin variants with altered potency during intestinal infection. *Proc. Natl. Acad. Sci. USA* **108**, 1645–1650. https://doi.org/10.1073/pnas.1014339108 (2011).
86. Charras, G. T. A short history of blebbing. *J. Microsc.* **231**, 466–478. https://doi.org/10.1111/j.1365-2818.2008.02059.x (2008).
87. Charras, G. T., Yarrow, J. C., Horton, M. A., Mahadevan, L. & Mitchison, T. J. Non-equilibration of hydrostatic pressure in blebbing cells. *Nature* **435**, 365–369. https://doi.org/10.1038/nature03550 (2005).
88. Paluch, E., Piel, M., Prost, J., Bornens, M. & Sykes, C. Cortical actomyosin breakage triggers shape oscillations in cells and cell fragments. *Biophys. J.* **89**, 724–733. https://doi.org/10.1529/biophysj.105.060590 (2005).
89. El Ahmer, O. R., Raza, M. W., Ogilvie, M. M., Weir, D. M. & Blackwell, C. C. Binding of bacteria to HEp-2 cells infected with influenza A virus. *FEMS Immunol. Med. Microbiol.* **23**, 331–341. https://doi.org/10.1111/j.1574-695X.1999.tb01255.x (1999).
90. Madeira, F. *et al.* The EMBL-EBI search and sequence analysis tools APIs in 2019. *Nucleic Acids Res.* **47**, W636–W641. https://doi.org/10.1093/nar/gkz268 (2019).
91. Khosa, S. *et al.* An A/U-rich enhancer region is required for high-level protein secretion through the HlyA Type I secretion system. *Appl. Environ. Microbiol.* https://doi.org/10.1128/AEM.01163-17 (2018).
92. Kanonenberg, K., Smits, S. H. J. & Schmitt, L. Functional Reconstitution of HlyB, a type I secretion ABC transporter, in saposin-A nanoparticles. *Sci. Rep.* **9**, 8436. https://doi.org/10.1038/s41598-019-44812-0 (2019).

93. Grube, L. *et al.* Mining the secretome of C2C12 muscle cells: Data dependent experimental approach to analyze protein secretion using label-free quantification and peptide based analysis. *J. Proteome Res.* **17**, 879–890. https://doi.org/10.1021/acs.jproteome.7b00684 (2018).
94. McQuin, C. *et al.* Cell profiler 3.0: Next-generation image processing for biology. *PLoS Biol.* **16**, e2005970. https://doi.org/10.1371/journal.pbio.2005970 (2018).
95. Perez-Riverol, Y. T. *et al.* The PRIDE database resources in 2022: A hub for mass spectrometry-based proteomics evidences. *Nucleic Acids Res.* https://doi.org/10.1093/nar/gkab1038 (2021).

Acknowledgements
We thank Diana Kleinschrodt for valuable support and all members of the Institute of Biochemistry for fruitful discussions. We would also like to thank former students Nicole Jasny and Fabian Adamek. This study was funded by the Jürgen Manchot Graduate School "Molecules of Infection III & IV" (to J.H.H. and L.S.), by the RTG 2158 (to S.W.) and the RTG 2578 (to S.W.) and CRC 1208 (project INF to S.W.-P.) of the Deutsche Forschungsgemeinschaft.

Author contributions
I.N.E., S.H., F.M.C., A.H., S.W., F.S., G.P., O.S. performed the experiments; I.N.E., S.H., F.M.C., AH, G.P., K.S., S.W., J.H.H., S.H.J.S, S.W.P.: analyzed and evaluated the data; I.N.E., S.H., F.M.C., A.H., J.H.H., S.H.J.S., S.W.P., L.S.: wrote the manuscript.

Funding
Open Access funding enabled and organized by Projekt DEAL.

Competing interests
The authors declare no competing interests.

Additional information
Supplementary Information The online version contains supplementary material available at https://doi.org/10.1038/s41598-022-22480-x.

Correspondence and requests for materials should be addressed to L.S.

Reprints and permissions information is available at www.nature.com/reprints.

Publisher's note Springer Nature remains neutral with regard to jurisdictional claims in published maps and institutional affiliations.

Supplementary information

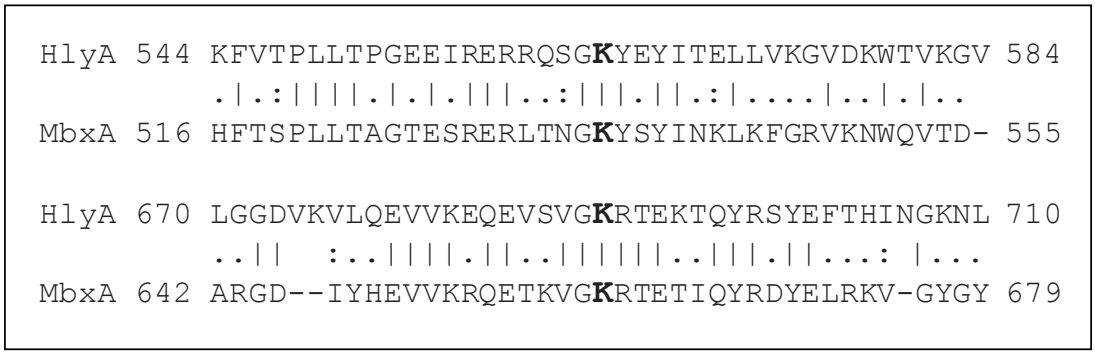

Fig. S1 *Sequence alignment [1] of the acylation sites of HlyA sites at lysine residues K564 and K690, which are highlighted in bold [2]. The homologous residues K536 and K660 predicted to be acylated in MbxA [3] are likewise shown in bold.*

Table S1: *MS analysis of MbxA acylation. MbxA was in vivo cross-acylated by co-expressing HlyC[4]. Modified peptides are listed with their detected fatty acid and hydroxy fatty acid modifications (C_{12}-C_{16}) and the corresponding number of peptide spectrum matches. Mass shifts contributing to hydroxy fatty acids could possibly originate from the oxidation of tyrosine residues in the peptide fragment and PSM of supposed hydroxy acylations are therefore marked (*). The acylated lysine residues are shown in bold in row 'Sequence'. Furthermore, the charge states are given with which the respective peptides were detected in the mass spectrometer as well as the score from search engine MaxQuant.*

Acyl modifications were detected only in peptides covering the predicted lysine residues K536 and K660, respectively. Only a low number of PSM were detected for K536 and no K660 lysine containing peptides in proMbxA. This is probably due to a higher specific cleavage of the respective peptides resulting in quite small fragments which have not been considered in the search. Here, the cleavage behind K536 and K660 might not be masked by acylation of the respective residues. The analysis of the in vitro acylation of HlyA by HlyC confirms the acylation of the K564 and K690 acylation sites.

Sequence	Site	Modifications	Charges	Score	PSM
MbxA					
ERLTNGKYSYINK	K536	C14	2	209.19	5
ERLTNGKYSYINK	K536	C14 - OH*	2	103.22	2
ERLTNGKYSYINK	K536	C15	3	61.423	1
LTNGKYSYINK	K536	C12 -OH*	2	50.909	1
LTNGKYSYINK	K536	C13	2	93.649	2
LTNGKYSYINK	K536	C14	2	150.66	17
LTNGKYSYINK	K536	C14 - OH*	2	63.159	1
LTNGKYSYINK	K536	C15	2	139.98	4
LTNGKYSYINK	K536	C16	2	56.258	1
LTNGKYSYINKLK	K536	C14	2	146.11	2
LTNGKYSYINKLK	K536	C14 - OH*	2;3	69.815	2
VGKRTETIQYR	K660	C14	3	69.721	1
proMbxA					
LTNGKYSYINKLK	K536	Unmodified	2;3;4	299.29	6
HlyA					
QSGKYEYITELLVK	K564	C14	2	92.19	1
QSGKYEYITELLVK	K564	C14 - OH*	2	74.611	1
QSGKYEYITELLVK	K564	Unmodified	3	83.633	4
RQSGKYEYITELLVK	K564	C14	3	90.754	1
RQSGKYEYITELLVK	K564	C14 - OH*	3	93.909	1
RQSGKYEYITELLVK	K564	Unmodified	3	71.545	1
EQEVSVGKR	K690	C12	2	49.813	1
EQEVSVGKR	K690	C14	2;3	190.08	3
EQEVSVGKR	K690	C14 - OH*	2	159.04	3
VLQEVVKEQEVSVGKR	K690	C13	3	76.85	2
VLQEVVKEQEVSVGKR	K690	C14	2;3	314.04	45
VLQEVVKEQEVSVGKR	K690	C14 - OH*	2;3	173.11	5
VLQEVVKEQEVSVGKR	K690	C16	3	97.836	1
VLQEVVKEQEVSVGKR	K690	Unmodified	2	75.479	2
VLGGDVKVLQEVVKEQEVSVGK	K690	Unmodified	3	19.975	1
VLQEVVKEQEVSVGK	K690	Unmodified	2;3	126.83	4
proHlyA					
QSGKYEYITELLVK	K564	Unmodified	2;3	287.76	36

RQSGKYEYITELLVK	K564	Unmodified	2;3	158.11	32
EQEVSVGKRTEK	K690	Unmodified	2;3	122.51	4
VLGGDVKVLQEVVKEQEVSVGK	K690	Unmodified	2;3;4	241.13	5
VLQEVVKEQEVSVGK	K690	Unmodified	2;3	283.47	69
VLQEVVKEQEVSVGKR	K690	Unmodified	2;3;4	334.04	36

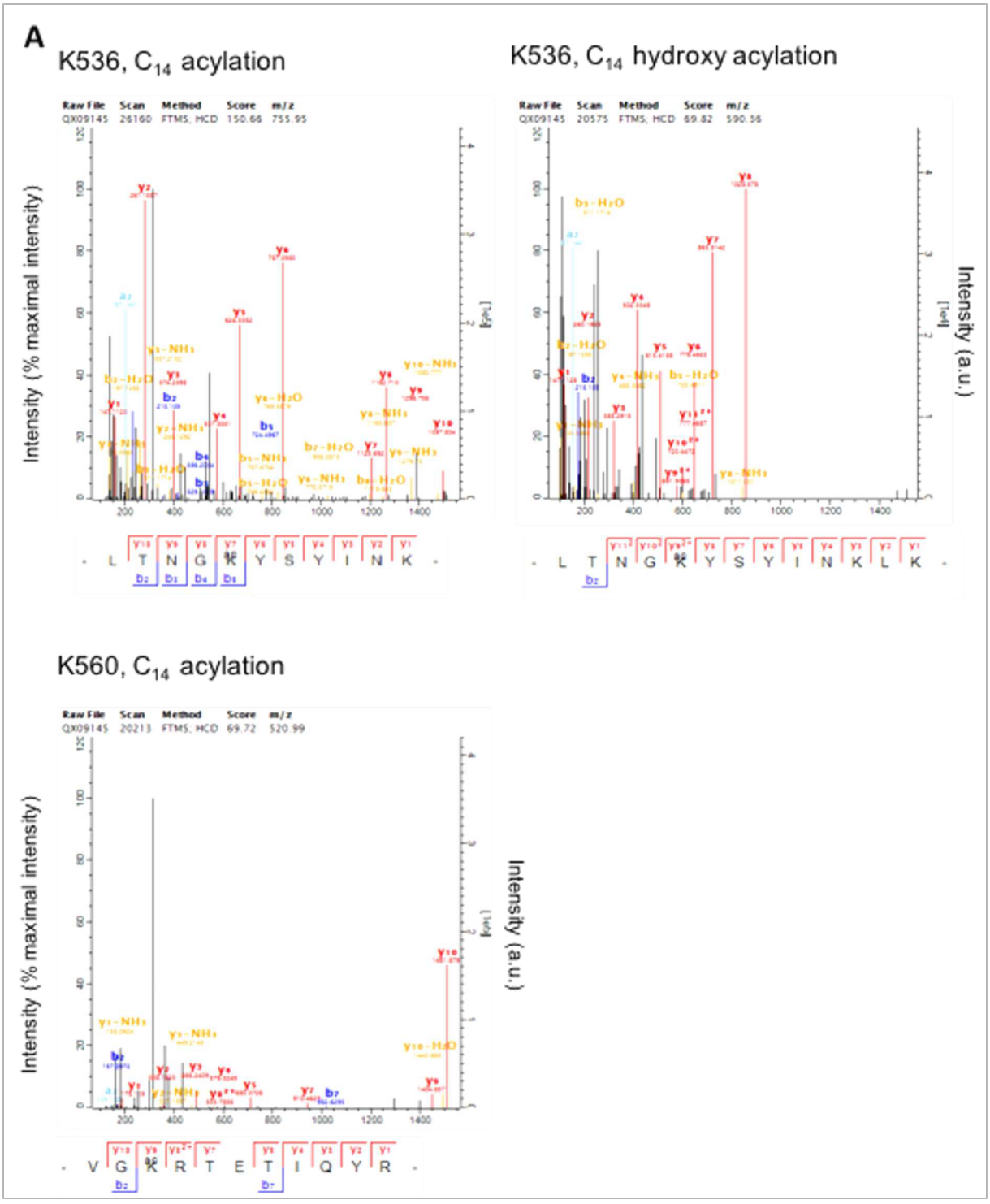
A
K536, C14 acylation
K536, C14 hydroxy acylation
K560, C14 acylation
Intensity (% maximal intensity)
Intensity (a.u.)
Raw File Scan Method Score m/z
QX09145 26160 FTMS, HCD 150.66 755.95
QX09145 20575 FTMS, HCD 69.82 590.36
QX09145 20213 FTMS, HCD 69.72 520.99
- L T N G K Y S Y I N K -
- L T N G K Y S Y I N K L K -
- V G K R T E T I Q Y R -

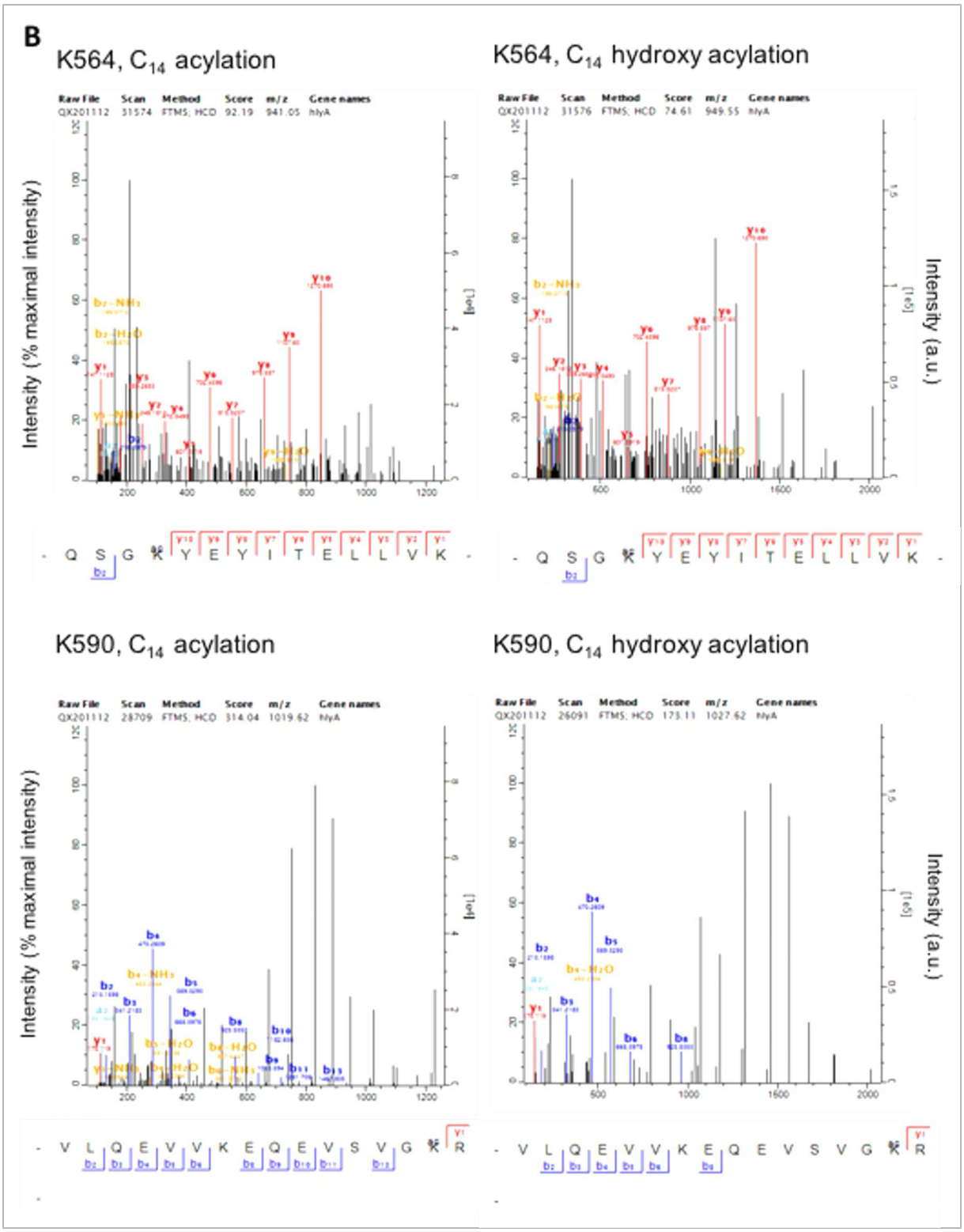

Fig. S2 *Exemplary MS spectra of the peptides that cover the first, K536, and second acylation site, K660, of MbxA (A) and of the two acylation sites K564 and K690 of HlyA (B) modified with C_{14} or C_{14}-OH* acylation.*

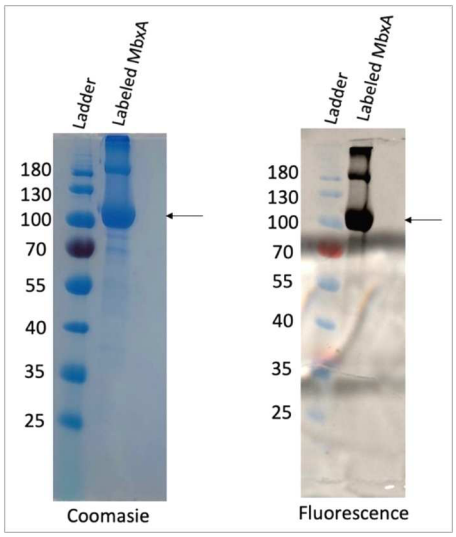

***Fig. S3**. Coomassie staining and Fluorescence of ^{Atto488}MbxA on SDS gel. Labelling of MbxA with Atto-488 was confirmed by SDS PAGE by Coomassie staining and fluorescence. The entire gels are shown in Figure S10. The fluorescence of the ^{Atto488}MbxA was detected after separation in the SDS gel by a BioRad gel documentation system. Arrow mark shows the ^{Atto488}MbxA monomers. The protein dimers near 180 kDa are more prominent due to the introduced Cysteine and subsequent disulfide bond formation.*

Parameters	**Values**
Molecular weight of MbxA (Da)	98,846
Extinction coefficient of MbxA at 280 nm in H_2O ($M^{-1}cm^{-1}$)	58000
Absorbance value at 280 nm	1.34
Absorbance value at 494 nm (Atto-488)	2.3
Specific correction factor for the Atto-488	0.09
Protein concentration (mg/ml)	0.46 (3.4 mL)
Extinction coefficient of Atto-488 at 494 nm ($M^{-1}cm^{-1}$)	90000
Labeling efficiency (fraction)	1.308

***Table S2:** Calculation of Labeling efficiency of MbxA with Atto-488 maleimide. Absorbance values at 280 nm and 494 nm are measured using NanoDrop One. The evaluation gives a protein concentration of 0.46 mg/ml and a labeling efficiency of 130.8% for the protein labeled with Atto-488 maleimide.*

Detailed protocol of imaging procedures

Using epifluorescence / DIC microscopy, experiments were performed using another set of dyes. To visualize the changes in the membrane morphology, the HEp-2 plasma membrane was labeled with Wheat Germ Agglutinin conjugated with Alexa Fluor 488 (WGA-488) and to monitor possible permeabilization of the cells, propidium iodide (PI) fluorescence was measured. As observed in confocal microscopy, membrane blebbing and permeabilization of HEp-2 cells observed in epifluorescence / DIC microscopy as well, when treated with MbxA, but not with proMbxA (Fig. S4). Incubation of HEp-2 cells with proMbxA did not show any visible changes in the membrane morphology over a period of 20 min. Additionally, no increase in PI signal intensity was detected indicating preserved plasma membrane integrity. HEp-2 cells were incubated with different concentrations of MbxA (250 nM, 30 nM and 10 nM) and proMbxA (250 nM), and images were taken in every 10 s over a total time period of 20 min (Fig. S4). Incubation of HEp-2 cells with 250 nM MbxA resulted in membrane bulges in first few minutes itself. At the same time, PI influx and DNA staining also started occurring, and the staining increased with higher incubation time of the same experiment (Fig. S5). As observed in confocal microscopy, 30 nM MbxA incubation of HEp-2 cells also resulted in the membrane blebbing and PI influx, but delayed and showing lower intensity response when compared to 250nM MbxA treatment (Fig. S4 and Fig. S5). In the case of 10 nM MbxA, smaller membrane bulges were visible only after 20 min going in hand with a small slope of PI fluorescence signal increase. After an extended incubation time of 90 min, small bulges as well as large blebs of approximately 10 µm were visible and PI staining could be detected demonstrating the dose dependent effect of cell permeabilization by MbxA again.

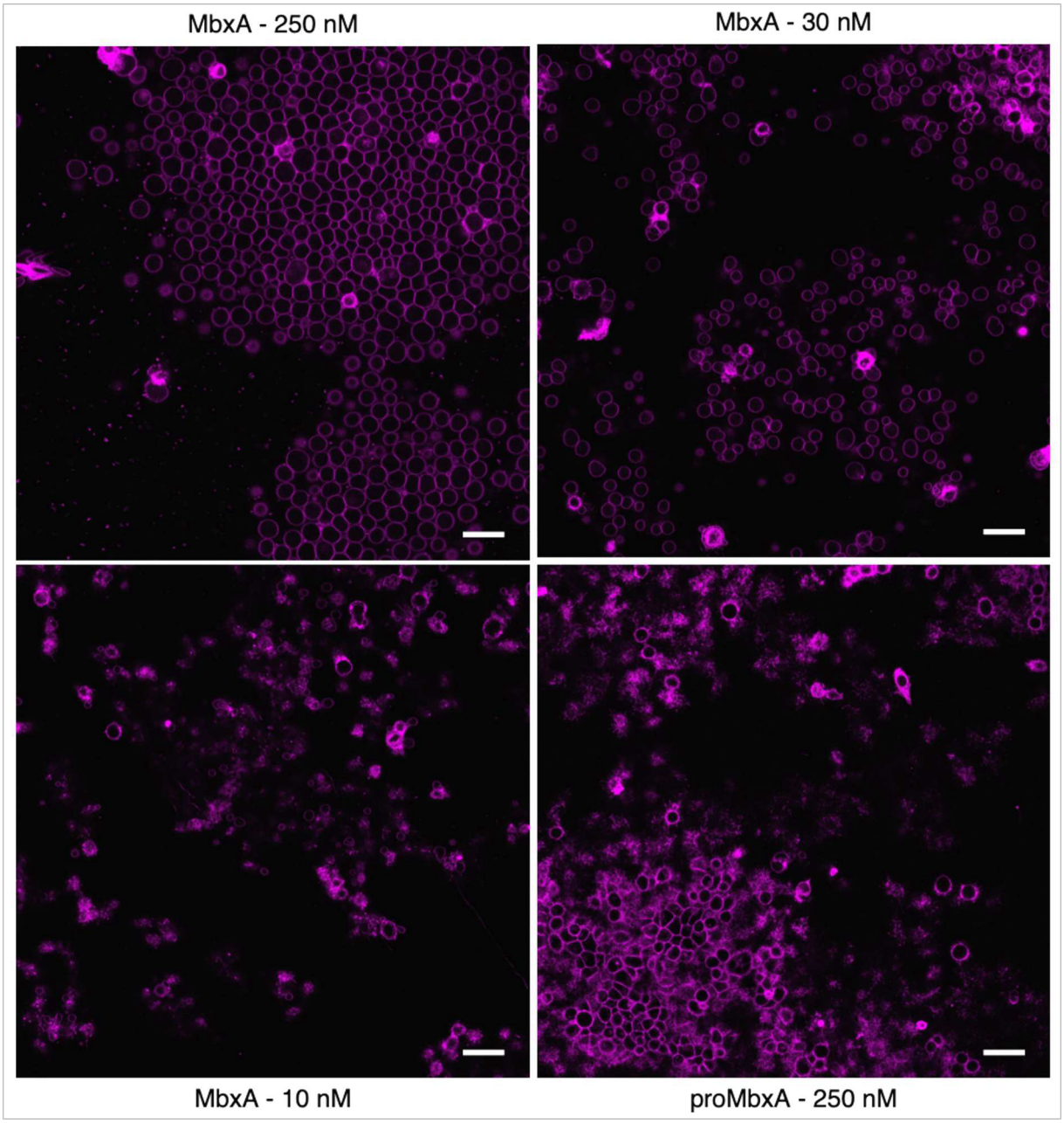

Fig. S4 *Entire images of Figure 9. For further details, please see the main manuscript. Please note that for 250 nM proMbxA, the top cell layer is visible. (Scale bar: 50 µm).*

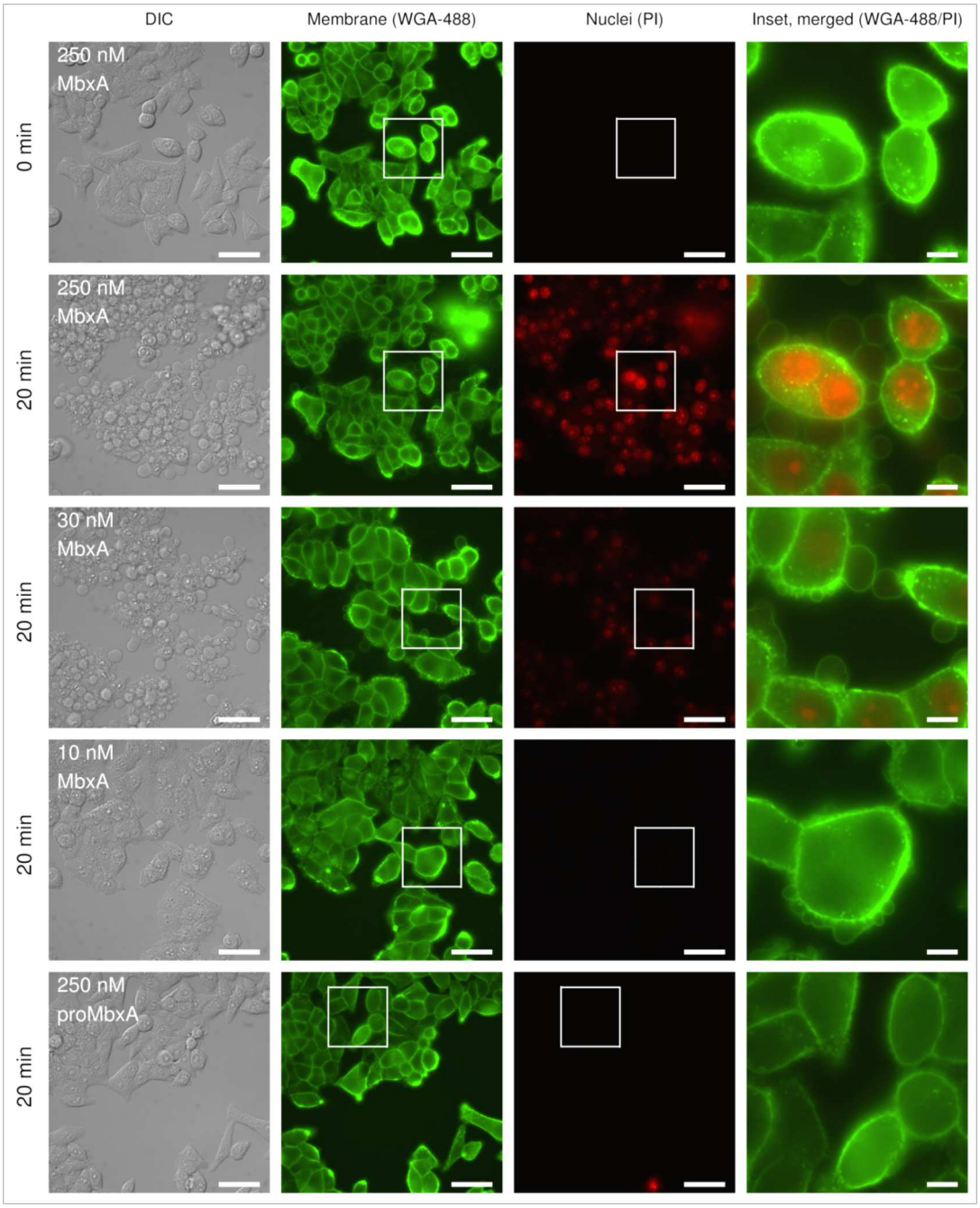

Fig. S5. *Epifluorescence live-cell imaging of HEp-2 cells treated with 250 nM, 30 nM or 10 nM of MbxA and 250 nM of proMbxA for 20 min. HEp-2 cells exposed to 250 nM of MbxA are shown after 0 min and after 20 min of incubation (first and second row). HEp-2 cells treated with 30 nM and 10 nM are shown after 20 min (third and fourth row). Data at later timepoints of the same experiment confirm potential permeabilization at lower concentrations in Fig.S6. HEp-2 cells incubated with 250 nM proMbxA and images after 20 min (fifth row). Membranes were stained with WGA-488 (second column), and membrane permeability was monitored with PI (third column). ProMbxA did not induce membrane damage, while MbxA induced the formation of spherical membrane protrusions and permeabilization. Growth of spherical membrane protrusions and permeabilization are highlighted by the white boxes in the second and third columns and shown in the insets in the right-most column as a merge of WGA-488 (green) and PI (red) fluorescence (Scale bar 50 µm, inset 10 µm).*

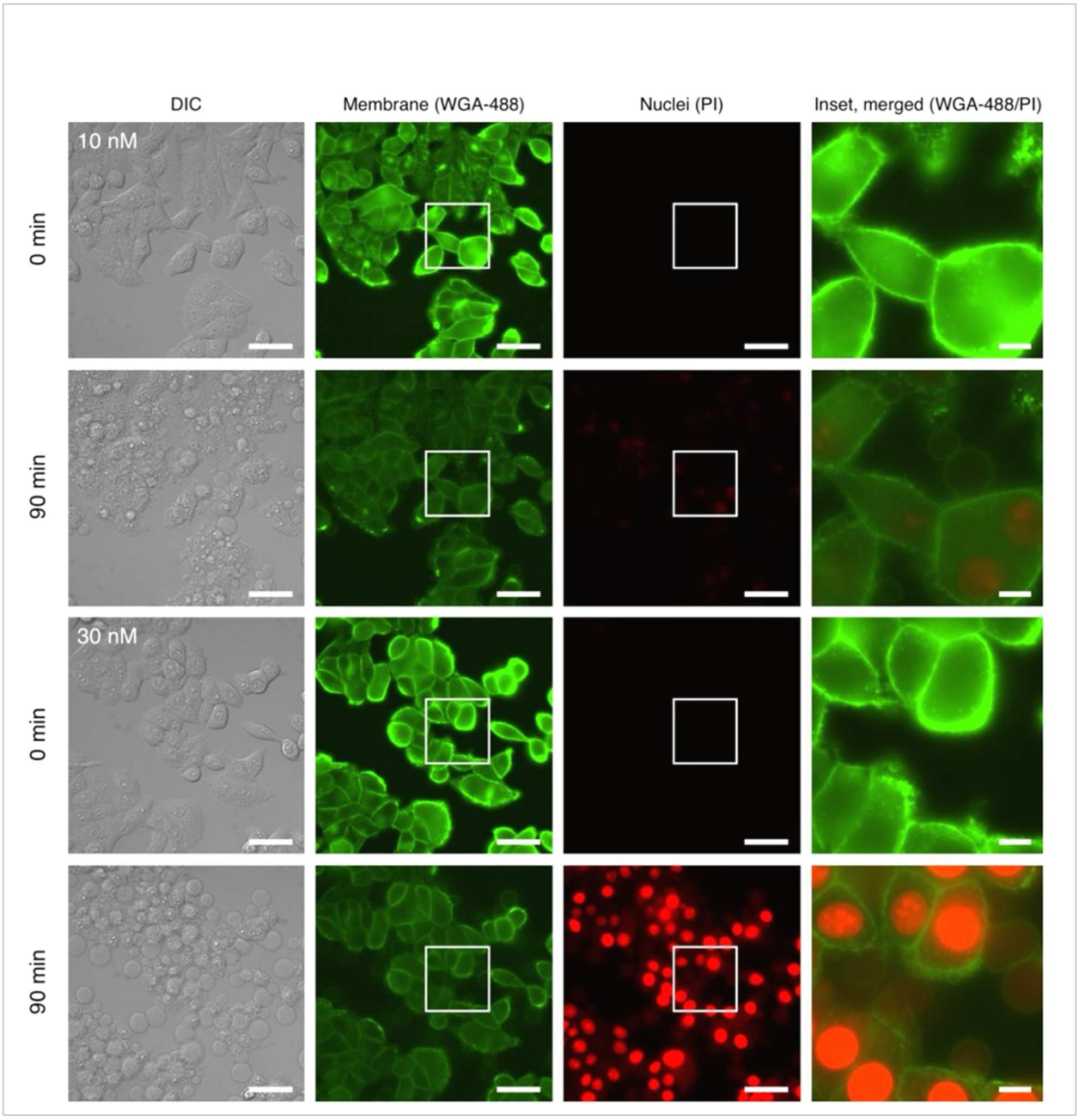

***Fig. S6**. Live-cell imaging of HEp-2 cells treated with 10 nM (first and second row) or 30 nM of MbxA (third and fourth row) over a duration of 90 min. HEp-2 cells of the experiment shown in Fig.S4 after 0 min and 90 min of incubation. Membranes were stained with WGA-488 (second column), and membrane permeability was monitored with PI (third column). Visible staining after an extended period of time verifies the potential permeabilizing effect at lower concentrations of MbxA, but with different strengths. Growth of spherical membrane protrusions and permeabilization are highlighted by the white boxes and shown in the insets on the right as a merge of WGA-488 (green) and PI fluorescence (red) (Scale bar 10 µm).*

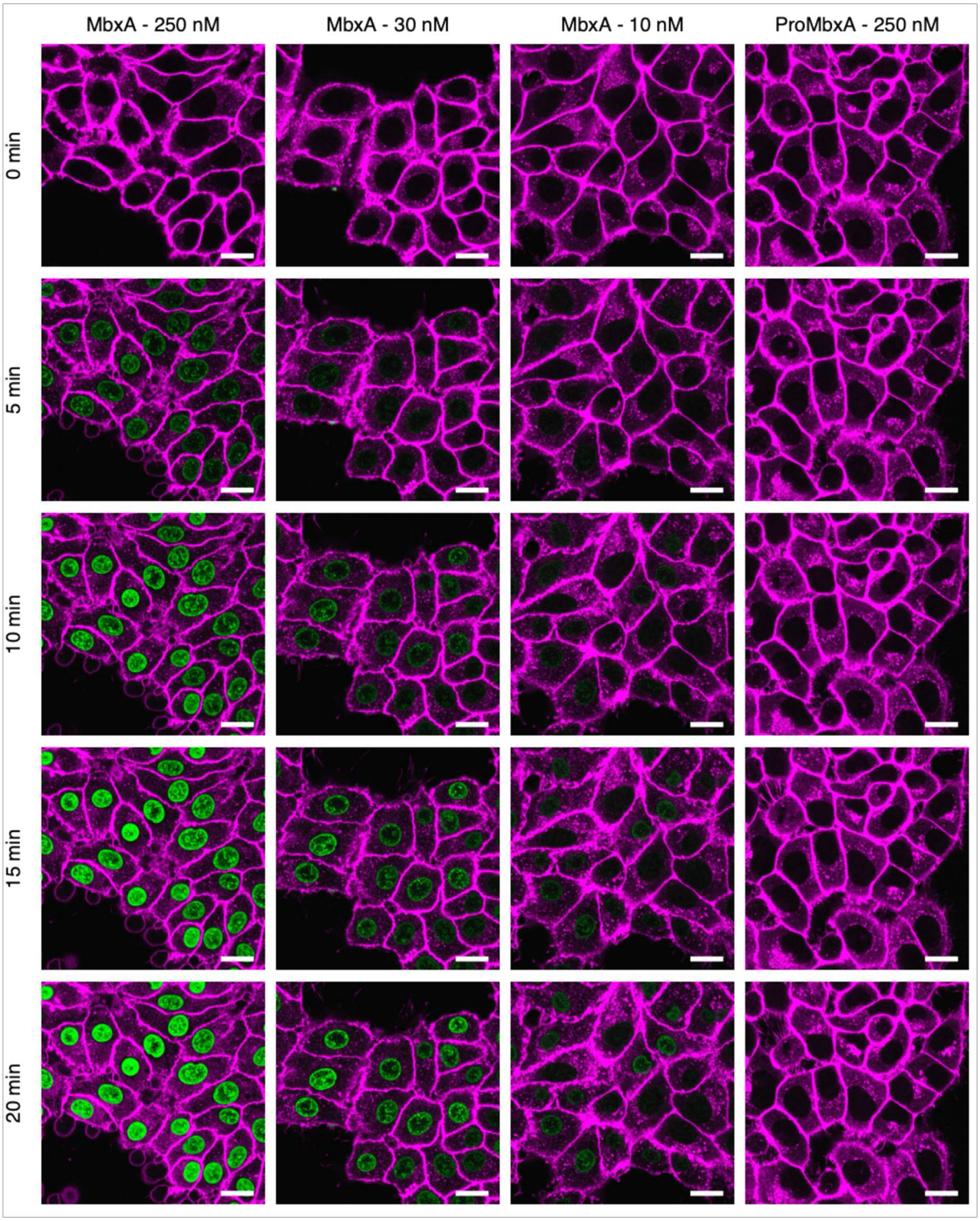

Fig. S7 *Time courses of live-cell imaging of HEp-2 cells treated with different concentrations of MbxA. These time courses were used to calculated the time dependence of cell permeabilization shown in Figure 10. (Scale bar: 20 µm).*

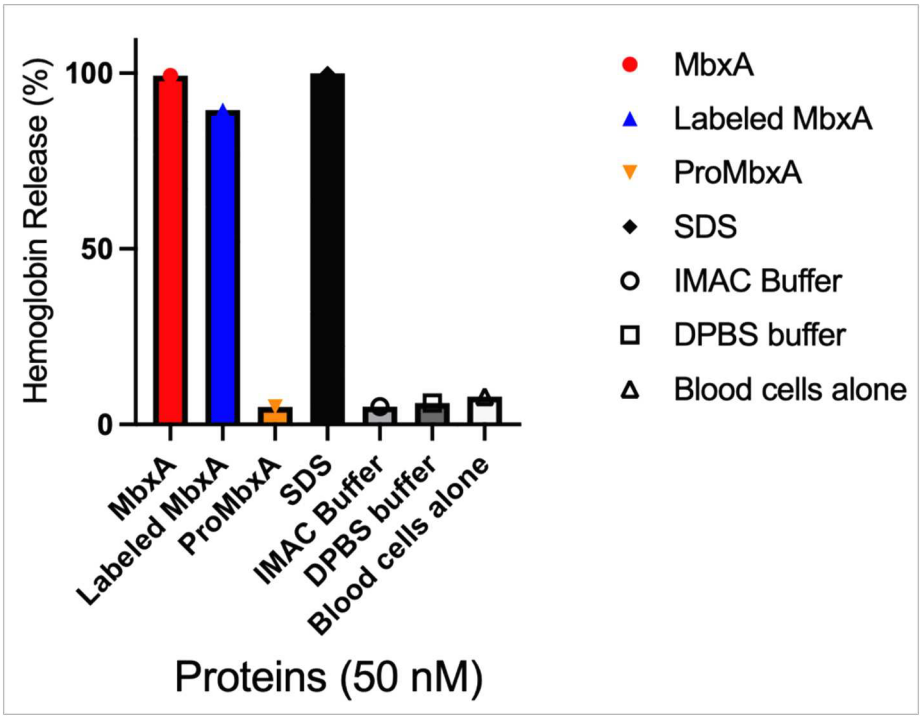

Fig. S8 *Hemoglobin release assay of MbxA (red bar), Atto488-MbxA^{S9C} (blue bar), proMbxA (orange bar), and buffers used in these experiments. All proteins were used at a concentration of 50 nM. The hemoglobin release was normalized to the SDS sample (black bar), which was set arbitrarily to 100%. Data correspond to three independent experiments with the SD reported as error.*

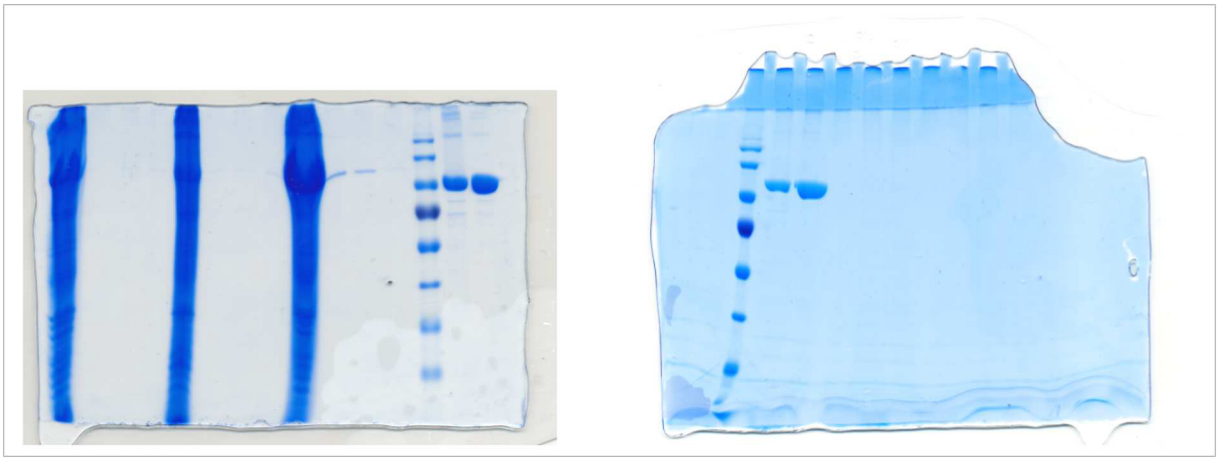

Fig. S9 *Entire CBB-stained SDS PAGE gels shown in Figure 4b.*

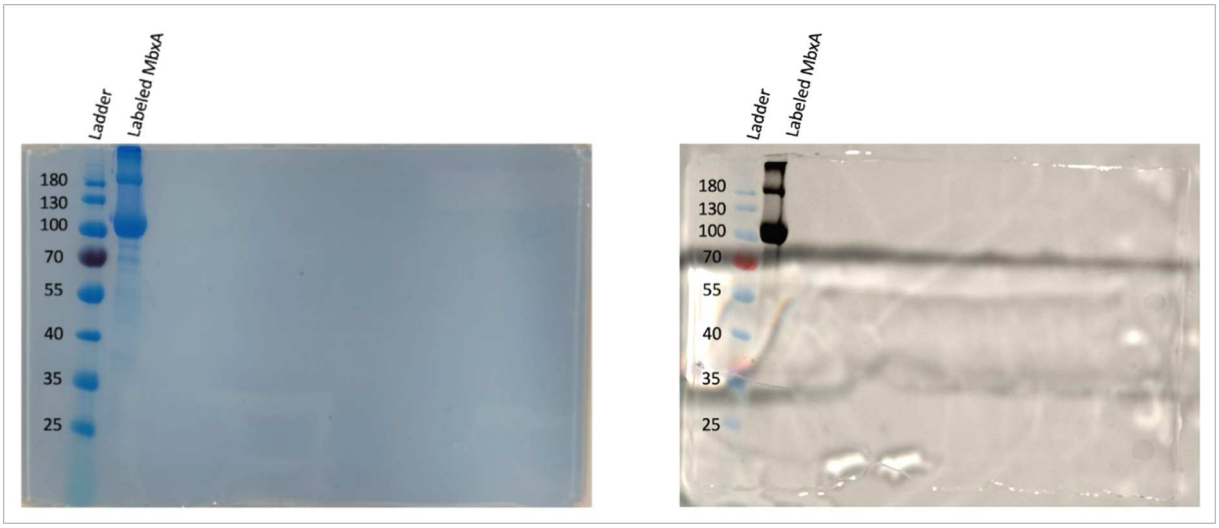

Fig. S10 *SDS PAGE (left) and fluorescence (right) gels of the insets shown in Figure S3.*

References:

1. Madeira F, Park YM, Lee J, Buso N, Gur T, Madhusoodanan N, et al. The EMBL-EBI search and sequence analysis tools APIs in 2019. Nucleic Acids Res. 2019;47(W1):W636-W41.
2. Stanley P, Packman LC, Koronakis V, Hughes C. Fatty acylation of two internal lysine residues required for the toxic activity of Escherichia coli hemolysin. Science. 1994;266(5193):1992-6.
3. Angelos JA, Hess JF, George LW. Cloning and characterization of a Moraxella bovis cytotoxin gene. Am J Vet Res. 2001;62(8):1222-8.
4. Thomas S, Smits SHJ, Schmitt L. A simple in vitro acylation assay based on optimized HlyA and HlyC purification. Anal Biochem. 2014;464:17-23.

Chapter 3

Cytotoxic Mechanism of the RTX Toxin MbxA in Human Epithelial Cells

Authors: Feby M. Chacko, Anna Hamacher, Sebastian Hänsch, Johannes H. Hegemann, Sander H. J. Smits, Stefanie Weidtkamp-Peters and Lutz Schmitt.

Published in: In preparation

Own work: 65%

Contribution:
Optimization of protein expression and secretion
Protein purification
Site-directed mutagenesis
Atto-488 labelling of MbxA
Cytotoxicity assay (Hb Release)
Assisted in microscopy image optimization
Microscopy image analysis
PARP cleavage experiment
Preparation of figures
Writing of the manuscript

Cytotoxic Mechanism of the RTX Toxin MbxA in Human Epithelial Cells

Feby Mariam Chacko[1], Anna Hamacher[2], Sebastian Hänsch[2], Johannes H. Hegemann[3], Stefanie Weidtkamp-Peters[2], Sander H. J. Smits[1] & Lutz Schmitt[1#].

[1] Institute of Biochemistry, Heinrich Heine University Düsseldorf, Universitätsstraße 1, 40225 Düsseldorf, Germany.
[2] Center for Advanced Imaging, Heinrich Heine University Düsseldorf, Universitätsstraße 1, 40225 Düsseldorf, Germany.
[3] Institute of Functional Microbial Genomics, Heinrich Heine University Düsseldorf, Universitätsstraße 1, 40225 Düsseldorf, Germany.

[#]Corresponding author: Lutz.Schmitt@hhu.de

Abstract

RTX (Repeats-in-Toxin) toxins are important virulence factors produced by Gram-negative pathogens, capable of disrupting host cell membranes and triggering diverse cytotoxic responses. MbxA, an RTX toxin from *Moraxella bovis*, was recently shown to induce membrane blebbing in human epithelial (HEp-2) cells, but its cytotoxic mechanism remains unclear. We investigated the cytotoxic effects of MbxA on HEp-2 cells using live-cell imaging, quantitative fluorescence microscopy, and biochemical assays. Membrane integrity, calcium dynamics, mitochondrial function, and cell death pathways were systematically analyzed following MbxA exposure. MbxA triggered rapid plasma membrane permeabilization, mitochondrial depolarization, an increase in cytosolic Ca^{2+} levels, and nuclear shrinkage in a dose-dependent manner. Despite phosphatidylserine externalization, no apoptotic PARP cleavage was detected, indicating non-apoptotic cell death. These findings suggest that MbxA-induced cytotoxicity primarily involves calcium-driven necrotic mechanisms rather than classical apoptosis. At sublytic concentrations, MbxA was internalized into undamaged cells, whereas damaged cells failed to internalize the toxin. This dual behavior - membrane binding at high concentrations and internalization at low concentrations - provides new insights into RTX toxin-host interactions and paves the way for the development of new strategies to counteract bacterial virulence.

Keywords

RTX toxins, MbxA, Acylation, Moraxella bovis, HEp-2 cells, Plasma membrane blebbing, Nuclear shrinkage, Calcium signaling, Live-cell imaging, Confocal microscopy, Cytotoxicity

1. Introduction

RTX toxins are a family of virulence factors produced by Gram-negative bacteria, known to contribute significantly to host-pathogen interactions and disease pathogenesis [1-3]. These toxins typically disrupt host cell physiology by forming pores in plasma membranes, triggering calcium influx, inducing cytoskeletal remodeling, and activating distinct cell death pathways [4-7]. While the cytotoxicity of RTX toxins such as HlyA (*Escherichia coli*) and leukotoxins (*Actinobacillus actinomycetemcomitans*, *Mannheimia haemolytica*) has been extensively studied [5-12], the mechanisms underlying the activity of less-characterized RTX family members remain incompletely understood.

MbxA is an RTX toxin produced by *Moraxella bovis,* the bacterium that causes keratoconjunctivitis in cattle [13-19]. MbxA was recently characterized and shown to elicit a membrane blebbing response in HEp-2 cells [20]. This observation raised important questions about the relevance of MbxA cytotoxicity beyond its natural bovine host and suggested potential mechanistic parallels with well-known RTX toxins. However, the precise cellular pathways involved in MbxA-induced cytotoxicity and the nature of the cell death it triggers remained unexplored.

Previous studies have shown that RTX toxins can disrupt plasma membrane integrity and calcium homeostasis by directly interacting with cholesterol-rich lipid microdomains [5, 8, 9, 21, 22]. Additionally, certain RTX toxins exploit receptor-mediated endocytosis for cellular entry, as demonstrated for HlyA through LDL receptor pathways [23] and adenylate cyclase toxin and other RTX toxins through β2 integrin clustering [8, 9, 22]. While β2 integrins are absent in epithelial cells like HEp-2, other entry pathways involving lipid rafts [8, 9, 22] and low-density lipoprotein receptor (LDLR) [23] family receptors may play a role in facilitating toxin uptake and downstream signaling.

In the present study, we investigated the cytotoxic effects of MbxA on HEp-2 cells, focusing on its impact on membrane integrity, calcium signaling, mitochondrial function, and cell death pathways. Using high-resolution, live-cell imaging and their quantitative analysis, we dissected the sequence of events following MbxA interactions with the plasma membrane of HEp-2 cells and explored whether MbxA induces apoptosis or alternative non-apoptotic cell death mechanisms. Our findings provide mechanistic insights into MbxA-induced cytotoxicity and

highlight key similarities and differences with other RTX toxins, offering a broader perspective on RTX-mediated pathogenesis and host defense strategies.

2. Results

2.1. MbxA-induced membrane-permeabilization and membrane-blebbing in HEp-2 cells.

In our previous study [20], we demonstrated that recombinant, acylated MbxA produced via the heterologous *E. coli* HlyA secretion system rapidly permeabilizes human epithelial cells and induces plasma-membrane blebbing, accompanied by Sytox Green uptake. These effects were dependent on post-translational acylation and occurred across a range of toxin concentrations. The present work builds on those observations to characterize additional cellular responses to MbxA.

2.2. MbxA triggers loss of mitochondrial membrane potential and induces intracellular calcium modulation in a concentration-dependent manner.

Given that several RTX toxins, including HlyA and leukotoxins, are known to disrupt calcium homeostasis [5, 8, 9, 22] and impair mitochondrial function in host cells [24-27], we investigated whether MbxA induces similar calcium elevation and mitochondrial depolarization in HEp-2 cells using Fluo-4 AM and TMRE live-cell imaging, respectively. HEp-2 cells were stained with TMRE to assess mitochondrial membrane potential, Fluo-4 AM to monitor intracellular calcium levels, and Hoechst 33342 to track the nucleus. Prior to protein treatment, cells displayed strong TMRE fluorescence, indicating intact mitochondrial function, and minimal basal Hoechst 33342 and Fluo-4 AM signal across all conditions (Fig. 1a). After 30 minutes of MbxA exposure (Fig. 1b), a concentration-dependent reduction in TMRE signal was observed, consistent with mitochondrial depolarization. At 125 nM and 250 nM MbxA, TMRE fluorescence was nearly abolished, while cells treated with the inactive precursor proMbxA retained TMRE signal. Simultaneously, the Fluo-4 AM signal markedly increased in MbxA-treated cells, indicating elevated cytosolic calcium levels. The increase was most pronounced at higher MbxA concentrations. No calcium modulation or mitochondrial depolarization was observed in proMbxA-treated cells. These findings suggest that MbxA induces mitochondrial dysfunction and robust calcium signaling in HEp-2 cells in a dose-dependent manner. As previously shown, brightfield images once again highlight the

membrane blebbing upon MbxA incubation, especially at higher concentrations, 125 nM and 250 nM.

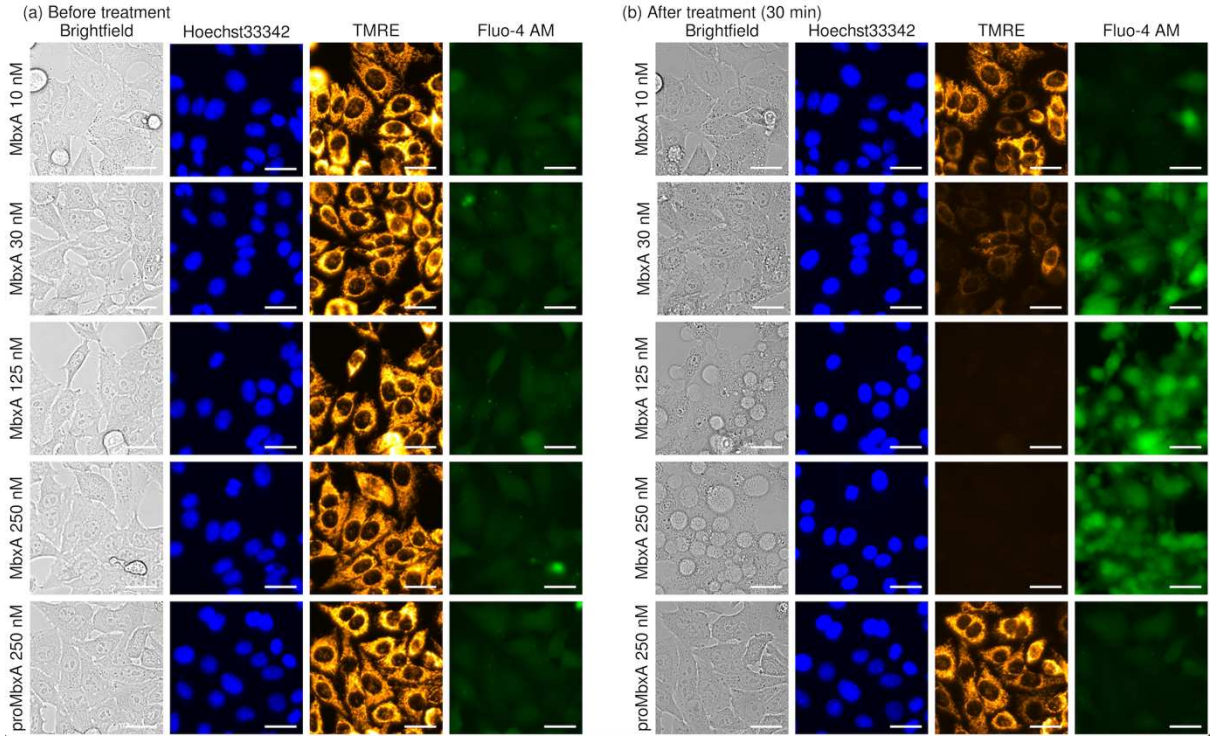

Figure 1: MbxA induces mitochondrial depolarization and calcium influx in HEp-2 cells*. Live-cell imaging of HEp-2 cells stained with Hoechst 33342 (blue), TMRE (orange), and Fluo-4 AM (green) before (a) and 30 minutes after (b) incubation with increasing concentrations of active MbxA or 250 nM of inactive proMbxA.* ***(a)*** *Prior to MbxA treatment, cells under all conditions show intact mitochondrial membrane potential (bright TMRE signal) and low basal calcium levels (dim Fluo-4 AM).* ***(b)*** *After 30 minutes, MbxA induces a concentration-dependent loss of TMRE fluorescence and a strong increase in Fluo-4 AM signal, indicating mitochondrial depolarization and calcium signaling. Brightfield images show a membrane blebbing phenotype in HEp-2 cells upon incubation with higher MbxA concentrations of 125 nM and 250 nM. No such effects were observed with proMbxA. Cells were stained with Hoechst33342 to track the nuclei. Scale bars: 30 µm. Representative images from at least three independent experiments are shown.*

2.3. MbxA induces progressive nuclear shrinkage and intracellular calcium accumulation in a concentration-dependent manner.

To quantitatively assess MbxA-induced morphological and signaling changes in HEp-2 cells, nuclei were tracked over time using Hoechst 33342 staining, and changes in nuclear area and Fluo-4 AM fluorescence were measured. Upon MbxA treatment, a concentration-dependent reduction in nuclear area was observed (Fig. 2a). While low concentrations (10 nM) caused only a slight decline, higher concentrations (≥30 nM; approximately the LC_{50} value [20]) resulted in a progressive shrinkage of the nuclei over the 30-minute observation period. This

effect was most pronounced at 250 nM MbxA. In contrast, the inactive proMbxA control had no significant effect on nuclear area even at 250 nM.

Simultaneously, Fluo-4 AM intensity increased in a dose-dependent manner, reflecting calcium elevation triggered by MbxA (Fig. 2b). Notably, the calcium signal rose rapidly after treatment at 125 nM and 250 nM and plateaued and gradually declined over time. Analysis of the same live-cell imaging dataset revealed that MbxA induces nuclear shrinkage and calcium signaling in the same HEp-2 cells, with both responses increasing in a concentration- and time-dependent manner.

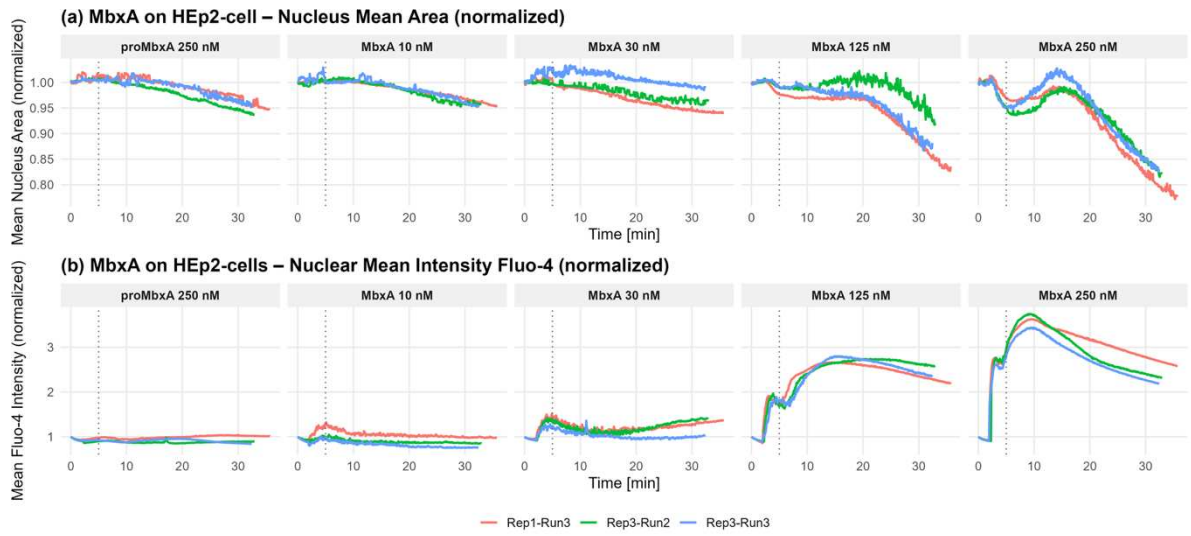

Figure 2. Quantitative analysis of MbxA-induced nuclear shrinkage and calcium elevation in HEp-2 cells. (a) *Time series quantification of nuclei tracked by Hoechst 33342 staining following treatment with increasing concentrations of MbxA or 250 nM proMbxA. Normalized mean nuclear area over 35 minutes. Nuclear shrinkage becomes increasingly apparent at 30 nM, 125 nM, and 250 nM MbxA, while proMbxA and 10 nM MbxA show minimal effect.* ***(b)*** *Normalized mean Fluo-4 AM intensity over time. A clear, concentration-dependent increase in calcium levels is observed after MbxA addition, with the strongest responses at 125 nM and 250 nM. Vertical dashed lines indicate the time of treatment addition. Each line represents an individual imaging run from one of three biological replicates.*

2.4. MbxA incubation leads to Phosphatidylserine externalization in HEp-2 cells.

To examine whether MbxA-induced cell death involves early membrane asymmetry changes typical of apoptosis or necrosis, we assessed the externalization of phosphatidylserine using Annexin V staining, a commonly used marker for early stages of cell death [28]. HEp-2 cells were incubated with 250 nM MbxA and stained with fluorescently labeled Annexin V, which binds to externalized phosphatidylserine (PS) [28]. In untreated control cells incubated with Annexin buffer alone, a weak Annexin V signal was detectable at the cell surface, consistent with unspecific binding, but no distinct membrane staining was observed (Fig. 3a). In clear

contrast, MbxA-treated cells showed strong, uniform Annexin V labeling along the plasma membrane (Fig. 3b), indicating widespread PS exposure. These results demonstrate that MbxA rapidly triggers membrane perturbation consistent with early apoptotic or necrotic events, characterized by loss of lipid bilayer asymmetry.

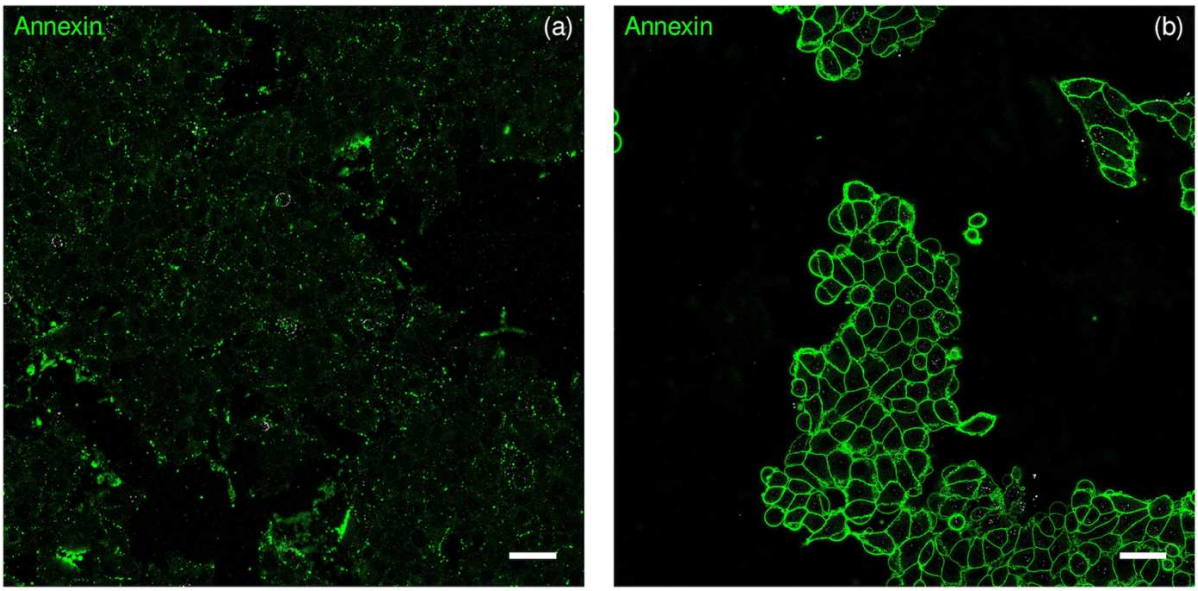

Figure 3. MbxA induces phosphatidylserine externalization in HEp-2 cells. *HEp-2 cells were incubated with Alexa Fluor 488-conjugated Annexin V to detect phosphatidylserine (PS) exposure on the outer leaflet of the plasma membrane.* ***(a)*** *Control samples showed low-intensity Annexin V fluorescence, likely due to unspecific association with the plasma membrane, which was distinguishable from the strong, uniform staining seen after MbxA treatment.* ***(b)*** *Cells treated with 250 nM MbxA for 5 minutes show strong membrane-localized Annexin V staining, indicating PS externalization. Scale bars: 20 µm.*

2.5. MbxA-induced cytotoxicity in HEp-2 cells occurs independently of the canonical apoptotic pathway.

To determine whether MbxA-induced cell death involves apoptosis, we examined cleavage of poly(ADP-ribose) polymerase (PARP), a hallmark of caspase-dependent apoptosis [28, 29]. HEp-2 cells were incubated with 250 nM MbxA for 20 minutes or 2 hours, and lysates were probed for full-length PARP (p113) and its cleaved fragment (p89) by immunoblotting. As expected, apoptotic induction by the positive control led to clear PARP cleavage (p89 band). In contrast, MbxA-treated cells showed no detectable PARP cleavage at either time point, with only full-length PARP present (Fig. 4a). The inactive precursor proMbxA also showed no PARP processing.

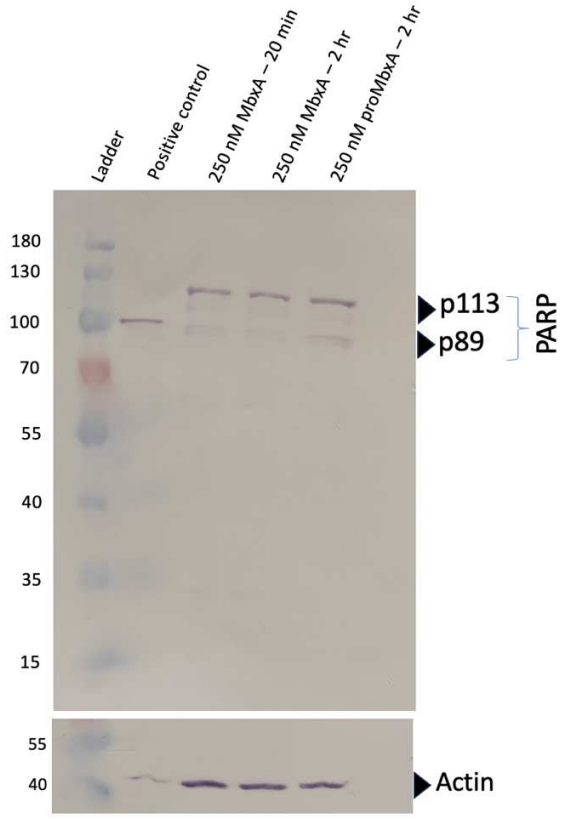

Figure 4. MbxA does not induce PARP cleavage in HEp-2 cells. *Western blot analysis of PARP and Actin in HEp-2 cell lysates following incubation with 250 nM MbxA for 20 minutes or 2 hours. For experimental details see Materials & Methods. Full-length PARP (p113) is present in all lanes. A cleaved PARP fragment (p89), indicative of apoptosis, is seen only in the positive control (staurosporine). No PARP cleavage is observed in MbxA-treated or proMbxA-treated cells. Actin loading control in the lower panel confirms equal protein amounts across samples except the staurosporine lane. Data are representative of three independent experiments.*

Actin was used as a loading control and confirmed equal protein loading across conditions, except for staurosporine (Fig. 4b). These results suggest that MbxA-induced membrane damage and cell death in HEp-2 cells do not proceed through proper apoptotic pathways.

2.6. MbxA exhibits concentration-dependent plasma membrane binding and internalization in HEp-2 cells.

To examine the localization of MbxA in HEp-2 cells, we used Atto488-labeled MbxA ($MbxA^{S9C}$) and performed confocal imaging after 30 minutes of incubation. At a high concentration (250 nM), Atto488-MbxA showed strong labeling along the plasma membrane (Fig. 5a,e; reprinted from Erenburg IN, *et al.*, *Scientific Reports* 2022, under CC BY), with dense clustering and surface accumulation consistent with toxin binding and membrane disruption [20].

In contrast, at a lower concentration (30 nM), Atto488-MbxA displayed a punctate, intracellular distribution pattern, suggesting uptake into cytoplasmic vesicles (Fig. 5b,f). Co-staining with CellMask to visualize plasma membranes confirmed reduced surface association and increased intracellular localization at 30 nM (Fig. 5c,g). In some regions of the field of view, cells with strong CellMask signal also showed strong Atto488-MbxA uptake and no visible membrane blebbing, whereas in other regions, membrane blebbing was widespread and toxin uptake was lower (Fig. 5d,e). These data indicate that MbxA interacts with the plasma membrane at high concentrations, while at sublytic concentrations (30 nM), it is internalized into HEp-2 cells. Importantly, 30 nM was previously calculated to be the IC50 of MbxA on HEp-2 cells [20].

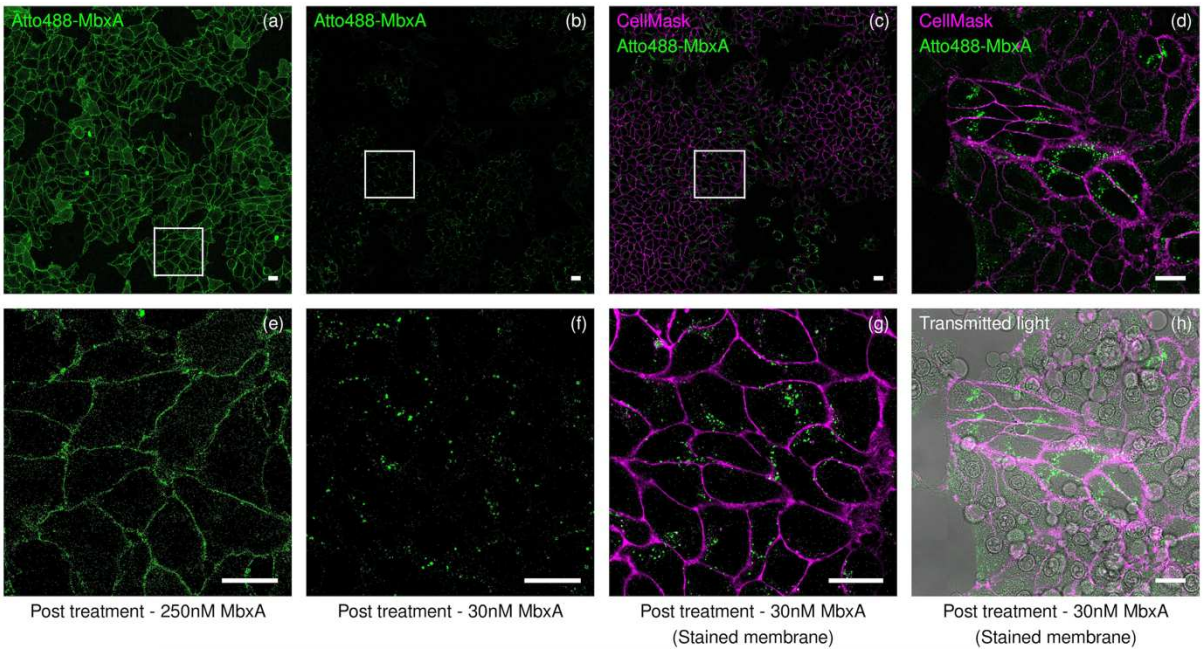

Figure 5. Concentration-dependent localization of Atto488-labeled MbxA in HEp-2 cells. *Representative confocal images showing Atto488-MbxA (green) and CellMask (magenta) staining in HEp-2 cells after MbxA treatment. (a, e) Post-treatment with 250 nM MbxA. Panels are reprinted from Erenburg IN, et al., Scientific Reports (2022) 12:17825, https://doi.org/10.1038/s41598-022-22480-x, under a Creative Commons Attribution (CC BY) license, for direct comparison with the current observations. (b, f) and (c, g) Post-treatment with 30 nM MbxA; within each pair, images are of the same sample acquired at different time points during the same experiment, with the membrane stain added between acquisitions. (d, h) Post-treatment with 30 nM MbxA and membrane staining. In these regions, strong CellMask signal coincided with a strong Atto488-MbxA uptake and the absence of visible membrane blebbing, whereas other areas of the same field showed a lower toxin signal and widespread blebbing. Scale bars: 20 nm. Images representative of two independent experiments.*

3. Discussion

RTX (repeats-in-toxin) toxins are a diverse group of secreted virulence factors widely employed by Gram-negative pathogens to manipulate and disrupt host cell physiology [1-3]. These toxins can act via pore formation, membrane remodeling, calcium dysregulation, or induction of specific death pathways [1-4]. MbxA is an RTX toxin from the bovine pathogen *Moraxella bovis* [13-19], previously shown to induce membrane blebbing and cell damage in two human cell lines, HEp-2 cells and Jurkat T-cells [20]. However, the mechanisms underpinning this cytotoxicity and its potential relevance for cross-species pathogenicity remained unclear.

Here, we systematically investigated the cellular effects of active MbxA on HEp-2 cells using confocal live-cell imaging (Figures 1, 3, and 5), functional readouts (Figures 1 and 4), and quantitative analysis (Figure 2). Our study reveals that MbxA induces rapid, non-apoptotic cell

death through a multifaceted process involving membrane permeabilization, intracellular calcium modulation, mitochondrial depolarization, and nuclear shrinkage. These findings offer new mechanistic insights into MbxA's mode of action and extend the initial observations of Erenburg et al. [20] by dissecting downstream cellular responses in detail.

MbxA exposure in HEp-2 cells resulted in loss of plasma membrane integrity (Sytox Green uptake), mitochondrial depolarization (TMRE loss), membrane blebbing, calcium elevation (Fluo-4 AM), and nuclear shrinkage. These effects were strongly dose-dependent. Importantly, PARP cleavage, a hallmark of apoptosis [29-31], was absent, suggesting that the observed cytotoxicity does not involve caspase activation or classical apoptotic execution.

In the absence of apoptosis, the observed morphological and molecular signatures suggest alternative forms of regulated or lytic cell death. PS externalization and calcium overload are commonly associated with necrosis, pyroptosis, and necroptosis [31-33]. While pyroptosis classically depends on caspase-1 and gasdermin activation in immune cells, recent studies have identified pyroptosis-like features in epithelial cells exposed to pore-forming toxins [5, 7, 31, 34-36]. According to our results, MbxA-induced cytotoxicity in HEp-2 cells is most consistent with a non-apoptotic, calcium-driven necrotic pathway, possibly resembling necroptosis or toxin-triggered necrosis.

This interpretation is further supported by parallels with other RTX toxins. For example, *Actinobacillus actinomycetemcomitans* leukotoxin and *Mannheimia haemolytica* leukotoxin have been shown to induce calcium elevation and cytotoxicity via interactions with lipid rafts in the host plasma membrane [8, 9]. Similarly, the adenylate cyclase toxin from *Bordetella pertussis* mobilizes its β2 integrin receptor into lipid rafts to facilitate membrane translocation and downstream effects [22]. Although HEp-2 epithelial cells are not known to express β2 integrins, the shared reliance on cholesterol-rich membrane microdomains for RTX toxin activity may underlie a conserved mechanism of calcium dysregulation and membrane disruption, as also suggested for MbxA [21].

Comparable cellular perturbations have also been documented for HlyA from uropathogenic *E. coli*, another member of the RTX family. HlyA induces intracellular calcium oscillations in renal epithelial cells through P2 receptor activation [5, 37], a response observed in our Fluo-4 AM calcium imaging data for MbxA. Moreover, HlyA has been shown to trigger NLRP3 inflammasome activation and mitochondrial dysfunction in THP-1 macrophages [26], and to

induce programmed necrosis in epithelial cells by altering mitochondrial dynamics [25]. These studies reinforce a broader pattern among RTX toxins, including MbxA, in which early membrane destabilization and calcium elevation coincide with mitochondrial disruption to promote non-apoptotic forms of cell death.

At the highest toxin concentrations (125 nM and 250 nM), nuclei displayed an initial rapid shrinkage followed by a partial re-expansion in size. This re-expansion is likely not a reversal of the shrinkage process, but instead reflects swelling associated with late-stage loss of membrane integrity and osmotic imbalance, as observed in other forms of necrotic cell death [38-40]. In these conditions, permeabilization of the plasma membrane occurs rapidly, allowing influx of ions and water that can increase nuclear volume after the initial condensation phase.

An important observation was that regions with strong Atto488-MbxA internalization generally lacked visible membrane blebbing, whereas regions with widespread blebbing showed lower internal signal. This pattern suggests that internalization may occur preferentially in cells with preserved membrane morphology and could involve receptor-dependent endocytic processes requiring both functional membrane microdomains and sufficient cellular energy. At higher MbxA concentrations, extensive pore formation likely disrupts membrane integrity, saturates or damages receptor regions, and depletes ATP, thereby precluding active uptake. Such receptor clustering and microdomain disintegration have been observed with other pore-forming toxins, including RTX leukotoxin [8] and anthrax protective antigen [41]. Findings of MbxA internalization mirror recent reports for HlyA, which hijacks LDL receptor-mediated endocytosis to access host cells [23]. LDLR-mediated endocytosis has been reported for other exotoxins [42-47] as well as for viruses [48]. Our results raise the possibility that MbxA utilizes similar receptors, potentially members of the LDLR family or heparan sulfate proteoglycans, to gain entry, and that this process is disrupted upon toxin-induced damage.

From a host-pathogen interaction perspective, our findings highlight the vulnerability of epithelial cells to RTX toxin-mediated attack and emphasize the importance of membrane integrity and calcium homeostasis in cellular defense. The selective internalization of sublytic MbxA by intact cells may represent a host surveillance opportunity to neutralize low-level toxin exposure before catastrophic damage occurs. Alternatively, it may reflect a bacterial strategy to modulate host signaling via controlled delivery of toxins. Understanding how

epithelial cells detect and respond to RTX-mediated damage will be crucial in identifying protective signaling networks, such as membrane repair mechanisms or calcium buffering pathways, that may be targeted for therapeutic intervention.

Despite the mechanistic insights gained here, this study has several limitations. All experiments were conducted in a single epithelial cell line, and future work should assess whether these findings generalize to other cell types, including immune and endothelial cells. Furthermore, while we infer non-apoptotic death based on morphological and molecular markers, further validation using specific pathway inhibitors (e.g., necrostatins or gasdermin blockers) is necessary. Additionally, the presence of PS externalization also opens a potential caution in interpreting Annexin V staining. Under conditions of membrane permeabilization, Annexin V may bind to intracellular PS that becomes accessible from the outside, rather than reporting true apoptotic flipping. Therefore, while Annexin positivity is evident, its mechanistic implication must be interpreted cautiously.

In conclusion, MbxA induces rapid, non-apoptotic cell death in HEp-2 cells through a multifaceted process involving membrane disruption, Ca^{2+} elevation, mitochondrial depolarization, and nuclear shrinkage. Internalization at sublytic concentrations suggests a receptor-mediated entry mechanism, possibly analogous to HlyA. These findings expand our understanding of RTX toxin-host interactions and open new avenues for studying epithelial defense strategies against bacterial virulence factors.

4. Materials & Methods

Cell culture and live-cell imaging.

HEp-2 cells were cultivated and passaged in DMEM (Pan Biotech, P04-03588) supplemented with 10 % FCS (Gibco, A5209501), 1 % MEM vitamins (Gibco, 11120052), 1 % non-essential amino acids (Gibco, 11140050), amphotericin B (2.5 µg/ml, Thermo Fisher, 15290026), and gentamicin (50 µg/ml, Gibco, 1575003). Two days prior to use, HEp-2 cells were seeded in 2 ml DMEM in 35 mm µ-Dish 1,5H glass bottom dishes (Ibidi) and grown for 39 - 48 h at 37 °C under 5 % CO_2.

Incubation experiment with MbxA and Sytox Green, Atto488-labeled MbxA^{S9C}, and Annexin-V staining.

As described before [20], for the incubation experiment with Atto488-labeled MbxA^{S9C}, cells were washed with 1 mL of DMEM supplemented with 20 mM HEPES as live cell medium (Pan Biotech), incubated in 1 mL of pre-warmed live cell medium, and transferred to the LSM880 (Carl Zeiss Microscopy GmbH), focusing on a region of interest. 1 mL of a fresh solution of Atto488-labeled MbxA^{S9C} at twice the final concentration was prepared in live cell medium, added, and again gently mixed by pipetting three times without touching the live cell dish to keep the region of interest in focus. The measurement was started immediately. After 30 min, the supernatant containing the Atto488-labeled MbxA^{S9C} was carefully replaced by fresh pre-warmed live cell medium and analyzed for protein localization again.

For the Annexin V staining experiment, HEp-2 cells were washed with 1 ml of DMEM supplemented with 20 mM HEPES as live cell medium (Pan Biotech) and incubated the cells with 250 nM MbxA for 5 minutes at 37°C and 5% CO_2. Cells were washed twice with prewarmed DPBS, then twice with prewarmed Annexin buffer (10 mM HEPES pH 7.4, 140 mM NaCl, 2.5 mM $CaCl_2$). HEp-2 cells were incubated with Annexin-V (Thermofisher Scientific, Alexa Fluor 488) (2.4 µL Annexin-V in 120 µL Annexin buffer) for 15 minutes in the dark at room temperature. The cells were washed three times with Annexin buffer and imaged in Annexin buffer.

Image acquisition

Confocal and Airyscan micrographs were recorded using a Zeiss LSM880 Airyscan microscope system (Carl Zeiss Microscopy GmbH) equipped with a Plan-Apochromat 63x/1.4 oil immersion objective lens. For excitation a 405 nm Laser was used for Hoechst 33342, a 488 nm Argon laser for excitation of Sytox Green and Atto488-labeled $MbxA^{S9C}$ and a 633 nm laser for excitation of CellMask Deep Red.

In confocal microscopy of unlabeled MbxA, a pixel dwell time of 1 µs was used without averaging at a frame rate of 15 sec/frame to reduce phototoxicity to a minimum. Excitation and detection of different dyes were set up in a frame-wise switch to reduce crosstalk, and detection ranges were set for Hoechst 33342 at 415 – 460 nm, for Sytox Green at 495 – 550 nm, and CellMask Deep Red at 648 - 700 nm. Focus was maintained during the time series using the hardware-based autofocus system Definite Focus 2 (Carl Zeiss Microscopy GmbH).

In confocal microscopy of Atto488-labeled $MbxA^{S9C}$ tilescan experiments, 25 single images were acquired at a pixel dwell time of 0.77 µs, and the detection range for ^{Atto488}MbxA was set at 495 – 550 nm.

In confocal microscopy of Annexin-V staining tilescan experiments, again, 25 single images were acquired at a pixel dwell time of 0.77 µs, and the detection range for Annexin-V (Alexa Fluor-488 conjugate) was set at 495 – 550 nm.

Calcium imaging experiments.

One day prior to use, HEp-2 cells were counted (LUNA counter, L10001) to seed 15000 cells in 100 µl of DMEM per well in a 96-well black flat-bottom microscopy plate (Revvity, PhenoPlate 6055300). After seeding, the plate was placed in a humidified incubator (37 °C, 5 % CO_2) for 24 - 30 h. Groups of five wells were stained, imaged, and treated (different treatment concentrations) together per biological replicate. For staining, first, the medium was aspirated and the cells gently washed with 90 µl per well of prewarmed (37 °C) HBSS (Gibco, 14025092) supplemented with 25 mM HEPES (Gibco, 15630056). Then, the washing solution was aspirated, and 50 µl of staining solution in HBSS with HEPES was added per well (RT). The staining solution contained 2 µM Fluo-4 AM (invitrogen, F14201), an equal volume of 20 % pluronic acid F-127 (Invitrogen, P3000MP), 10 µM Hoechst33342 (invitrogen, 62249)

and 150 nM TMRE (Invitrogen, T669). After dye incubation of 30 min in darkness at RT, the staining solution was aspirated and the cells gently washed once with 90 µl per well of prewarmed (37 °C) HBSS with HEPES. Last, the washing solution was aspirated, and 100 µl per well of fresh prewarmed HBSS with HEPES was added for imaging. Then, the plate was transferred to the microscope, and it was waited 11-15 min at 37 °C before imaging to allow complete de-esterification of intracellular AM esters. Afterwards, imaging was started immediately for baseline recording (24 frames, at least 2 min). For treatment, shortly before applying to the cells, MbxA resp. proMbxA dilutions were prepared in a conical, transparent 96-well micro test plate (Sarstedt, 82.1583.001) with the same HEPES-supplemented HBSS solution. After baseline recording, a programmed imaging break was used to transfer 50 µl of triple-concentrated MbxA resp. proMbxA from the micro test plate to the imaging plate at the same time using an 8-channel pipet (final volume of 150 µl per well). After transferring, the solution was pipet up and down once to mix the MbxA resp. proMbxA solution inside each well. Imaging was resumed as fast as possible for another 360 frames (at least 30 min) to follow intracellular calcium level changes over time. The procedure was done two to four times per plate at three individual days, leading to three technical replicates from different cell passages.

Image acquisition

Images were recorded at an Operetta CLS high-content screening system (Revvity) with environmental control (37 °C, 5 % CO_2). Images were acquired with the software Harmony 5.2 (Revvity, 2024) and saved as TIFF files. All images have been captured with the Zeiss EC Plan-Neofluar 40x air objective (NA 0.75) in widefield mode and binning set to 2. Imaging was done in groups of five wells with one field per well, close to the well center. Two-channel groups were used within the captured time series. First, channel group 1 (Hoechst33342, Fluo-4 AM, TMRE, Brightfield) was acquired as a pre-treatment state. Then, channel group 2 (Hoechst33342, Fluo-4 AM) was acquired as baseline for 24 frames as fast as possible, which means on average one frame every 5 sec and a total time of at least 2 min. A programmed break stopped the imaging for applying MbxA, respectively. proMbxA. On average, the total break took 45 seconds before imaging was resumed. Then, another 360 frames of channel group 2 were acquired again as fast as possible, leading to at least 30 min of observation post-treatment. Last, channel group 1 was acquired once again as a final post-treatment state. Same filters were used in both channel groups, these are ex. 370 nm (+/- 15 nm) and em. 430-500 nm for Hoechst33342, ex. 475 nm (+/- 15 nm) and em. 500-550 nm for Fluo-4 AM, exc. 550 nm (+/- 15 nm) and em. 570-650 nm for TMRE and transmission for Brightfield.

Image quantification

Time series images of MbxA resp. proMbxA treated cells were analyzed using the Harmony 5.2 image analysis module (Revvity, 2024). First, for every timepoint of channel group 2, the nucleus areas were determined based on the Hoechst33342 image using building block "Find Nuclei" with method C. Objects touching the image border were omitted. Tracking of nuclei across the time series was achieved using building block "Track Objects" with active error correction and overlap ≥ 1 %. Morphological and fluorescence intensity parameters were measured per nucleus and exported as individual objects data. This data was processed with KNIME 5.2 (KNIME AG) to consider only nuclei that have been successfully tracked during the whole baseline and post-treatment time series (in total 384 frames, at least 32 min). In addition, KNIME was used to normalize values of each individual nucleus to the initial state in the first frame of the baseline recording.

PARP cleavage experiment

To test for the induction of apoptosis by MbxA, cells were incubated with 250 nM MbxA for up to 2 hours. 250 nM inactive proMbxA was used as the negative control. To induce apoptosis in HEp-2 cells, confluent HEp-2 cells were incubated in serum-free medium containing 2.5 µM staurosporine as the positive control. After the incubation of HEp-2 cells with the proteins, the media was carefully removed and cells were incubated with 100 uL of phospholysis buffer (1% NP-40, 1% Triton-X100, 20 mM Tris/HCl pH 7.4) for 30 minutes at 4°C. The lysed cells were resuspended in a gel loading buffer containing DTT and incubated at 100°C for 15-30 minutes before loading on a 10% gel. The samples in the gel were then transferred to a PVDF membrane (Amersham Hybond P 0.45) by western transfer (using BioRAD semidry western transfer apparatus). Two membranes were immunostained using 1° antibodies of PARP and Actin overnight at 4°C and then with Alkaline phosphatase-conjugated secondary antibody for 1 hour at 4°C. Membranes were finally developed using MBT/BCIP solution in 1:1 ratio in the detection buffer (0.1 M Tris/HCl pH 9.5, 0.1 M NaCl, 50 mM $MgCl_2$).

5. References

1. Linhartová, I., et al., *RTX proteins: a highly diverse family secreted by a common mechanism.* FEMS microbiology reviews, 2010. **34**(6): p. 1076-1112.
2. Chacko, F.M. and L. Schmitt, *Interaction of RTX toxins with the host cell plasma membrane.* Biological Chemistry, 2023. **404**(7): p. 663-671.
3. Filipi, K., et al., *Kingella kingae RtxA cytotoxin in the context of other RTX toxins.* Microorganisms, 2022. **10**(3): p. 518.
4. Benz, R., *Channel formation by RTX-toxins of pathogenic bacteria: Basis of their biological activity.* Biochimica et Biophysica Acta (BBA)-Biomembranes, 2016. **1858**(3): p. 526-537.
5. Uhlen, P., et al., *α-Haemolysin of uropathogenic E. coli induces Ca2+ oscillations in renal epithelial cells.* Nature, 2000. **405**(6787): p. 694-697.
6. Dhakal, B.K. and M.A. Mulvey, *The UPEC pore-forming toxin α-hemolysin triggers proteolysis of host proteins to disrupt cell adhesion, inflammatory, and survival pathways.* Cell host & microbe, 2012. **11**(1): p. 58-69.
7. Gu, H., et al., *A previously uncharacterized two-component signaling system in uropathogenic Escherichia coli coordinates protection against host-derived oxidative stress with activation of hemolysin-mediated host cell pyroptosis.* PLoS Pathogens, 2021. **17**(10): p. e1010005.
8. Fong, K.P., et al., *Actinobacillus actinomycetemcomitans leukotoxin requires lipid microdomains for target cell cytotoxicity.* Cellular Microbiology, 2006. **8**(11): p. 1753-1767.
9. Atapattu, D.N. and C.J. Czuprynski, *Mannheimia haemolytica leukotoxin binds to lipid rafts in bovine lymphoblastoid cells and is internalized in a dynamin-2-and clathrin-dependent manner.* Infection and immunity, 2007. **75**(10): p. 4719-4727.
10. Wang, C., et al., *Alpha-hemolysin of uropathogenic Escherichia coli induces GM-CSF-mediated acute kidney injury.* Mucosal Immunology, 2020. **13**(1): p. 22-33.
11. Nhu, N.T.K., et al., *Complex multilevel control of hemolysin production by uropathogenic Escherichia coli.* MBio, 2019. **10**(5): p. 10.1128/mbio. 02248-19.
12. Welch, R.A., *The Escherichia coli hemolysin.* EcoSal Plus, 2005. **1**(2): p. 10.1128/ecosalplus. 8.7. 2.

13. Angelos, J.A., J.F. Hess, and L.W. George, *Cloning and characterization of a Moraxella bovis cytotoxin gene.* American journal of veterinary research, 2001. **62**(8): p. 1222-1228.
14. Angelos, J.A., J.F. Hess, and L.W. George, *An RTX operon in hemolytic Moraxella bovis is absent from nonhemolytic strains.* Veterinary microbiology, 2003. **92**(4): p. 363-377.
15. Baptista, P., *Infectious bovine keratoconjunctivitis a review.* British Veterinary Journal, 1979. **135**(3): p. 225-242.
16. Beard, M.M. and L. Moore, *Reproduction of bovine keratoconjunctivitis with a purified haemolytic and cytotoxic fraction of Moraxella bovis.* Veterinary microbiology, 1994. **42**(1): p. 15-33.
17. Clinkenbeard, K.D. and A. Thiessen, *Mechanism of action of Moraxella bovis hemolysin.* Infection and immunity, 1991. **59**(3): p. 1148-1152.
18. Henson, J. and L. Grumbles, *Infectious bovine keratoconjunctivitis. I. Etiology.* 1960.
19. Hess, J.F. and J.A. Angelos, *The Moraxella bovis RTX toxin locus mbx defines a pathogenicity island.* Journal of medical microbiology, 2006. **55**(4): p. 443-449.
20. Erenburg, I.N., et al., *Heterologously secreted MbxA from Moraxella bovis induces a membrane blebbing response of the human host cell.* Scientific Reports, 2022. **12**(1): p. 17825.
21. Chacko, F.M., et al., *Acylation of the RTX Toxin MbxA stimulates host membrane disruption through a specific interaction with cholesterol.* bioRxiv, 2025: p. 2025.02. 19.639210.
22. Bumba, L., et al., *Bordetella adenylate cyclase toxin mobilizes its β2 integrin receptor into lipid rafts to accomplish translocation across target cell membrane in two steps.* PLoS pathogens, 2010. **6**(5): p. e1000901.
23. Kuhn, H.W., et al., *LDL receptor-mediated endocytosis of Escherichia coli α-hemolysin mediates renal epithelial toxicity.* bioRxiv, 2025: p. 2025.02. 14.638193.
24. Korostoff, J., et al., *Perturbation of mitochondrial structure and function plays a central role in Actinobacillus actinomycetemcomitans leukotoxin-induced apoptosis.* Microbial pathogenesis, 2000. **29**(5): p. 267-278.
25. Lu, Y., et al., *Uropathogenic Escherichia coli virulence factor hemolysin A causes programmed cell necrosis by altering mitochondrial dynamics.* The FASEB Journal, 2018. **32**(8): p. 4107-4120.

26. Verma, V., et al., *α-Hemolysin of uropathogenic E. coli regulates NLRP3 inflammasome activation and mitochondrial dysfunction in THP-1 macrophages.* Scientific Reports, 2020. **10**(1): p. 12653.
27. Kisiela, D.I., et al., *N-terminal region of Mannheimia haemolytica leukotoxin serves as a mitochondrial targeting signal in mammalian cells.* Cellular Microbiology, 2010. **12**(7): p. 976-987.
28. Galle, J.N., et al., *A Chlamydia pneumoniae adhesin induces phosphatidylserine exposure on host cells.* Nature Communications, 2019. **10**(1): p. 4644.
29. Lawen, A., *Apoptosis—an introduction.* Bioessays, 2003. **25**(9): p. 888-896.
30. Elmore, S., *Apoptosis: a review of programmed cell death.* Toxicologic pathology, 2007. **35**(4): p. 495-516.
31. Tsuchiya, K., *Switching from apoptosis to pyroptosis: gasdermin-elicited inflammation and antitumor immunity.* International journal of molecular sciences, 2021. **22**(1): p. 426.
32. Yu, P., et al., *Pyroptosis: mechanisms and diseases.* Signal transduction and targeted therapy, 2021. **6**(1): p. 128.
33. Ros, U., L. Pedrera, and A.J. Garcia-Saez, *Partners in crime: the interplay of proteins and membranes in regulated necrosis.* International Journal of Molecular Sciences, 2020. **21**(7): p. 2412.
34. He, W.-t., et al., *Gasdermin D is an executor of pyroptosis and required for interleukin-1β secretion.* Cell research, 2015. **25**(12): p. 1285-1298.
35. Zhu, C., et al., *The gasdermin family: emerging therapeutic targets in diseases.* Signal Transduction and Targeted Therapy, 2024. **9**(1): p. 87.
36. Broz, P., *Pyroptosis: molecular mechanisms and roles in disease.* Cell research, 2025: p. 1-11.
37. Christensen, M.G., et al., *[Ca2+] i oscillations and IL-6 release induced by α-hemolysin from Escherichia coli require P2 receptor activation in renal epithelia.* Journal of Biological Chemistry, 2015. **290**(23): p. 14776-14784.
38. Kashyap, B. and P. Reddy, *Physiologic to Pathologic Cellular and Molecular Levels of Elusive Cell Death Programs and Their Manipulative Action.* Clinics in Oncology, 4 (1), 2019. **1674**.
39. Miller, M.A. and J.F. Zachary, *Mechanisms and morphology of cellular injury, adaptation, and death.* Pathologic basis of veterinary disease, 2017: p. 2.

40. Hu, X.-m., et al., *Guidelines for regulated cell death assays: a systematic summary, a categorical comparison, a prospective.* Frontiers in cell and developmental biology, 2021. **9**: p. 634690.
41. Abrami, L., et al., *Anthrax toxin triggers endocytosis of its receptor via a lipid raft–mediated clathrin-dependent process.* The Journal of cell biology, 2003. **160**(3): p. 321-328.
42. Tao, L., et al., *Sulfated glycosaminoglycans and low-density lipoprotein receptor contribute to Clostridium difficile toxin A entry into cells.* Nature microbiology, 2019. **4**(10): p. 1760-1769.
43. Zhou, Y., et al., *Sulfated glycosaminoglycans and low-density lipoprotein receptor mediate the cellular entry of Clostridium novyi alpha-toxin.* Cell Research, 2021. **31**(8): p. 935-938.
44. Zhou, Y., et al., *LDLR, LRP1, and Megalin redundantly participate in the uptake of Clostridium novyi alpha-toxin.* Communications Biology, 2022. **5**(1): p. 906.
45. Kounnas, M., et al., *The alpha 2-macroglobulin receptor/low density lipoprotein receptor-related protein binds and internalizes Pseudomonas exotoxin A.* Journal of Biological Chemistry, 1992. **267**(18): p. 12420-12423.
46. Schoellkopf, J., et al., *Genome wide CRISPR screen for Pasteurella multocida toxin (PMT) binding proteins reveals LDL Receptor Related Protein 1 (LRP1) as crucial cellular receptor.* PLoS Pathogens, 2022. **18**(12): p. e1010781.
47. Wei, W., et al., *The LDL receptor-related protein LRP6 mediates internalization and lethality of anthrax toxin.* Cell, 2006. **124**(6): p. 1141-1154.
48. Li, Y., et al., *Structural basis of Semliki Forest virus entry using the very-low-density lipoprotein receptor.* hLife, 2023. **1**(2): p. 124-136.

Chapter 4

Acylation of the RTX Toxin MbxA stimulates host membrane disruption through a specific interaction with cholesterol.

Authors: Feby Mariam Chacko, Sarah Michelle Ganz, Anne Pfitzer-Bilsing, Sebastian Hänsch, Philipp Westhoff , Stefanie Weidtkamp-Peters, Marten Exterkate, Sander H. J. Smits & Lutz Schmitt

Published in: Submitted to Biochimica et Biophysica Acta - Biomembranes
Impact factor: 2.5

Own work: 80%

Contribution:
Optimization of protein expression and secretion
Protein purification
Biochemical assays – Liposome leakage, GUV, Floatation, GP & Anisotropy
Assistance in AFM
Site-directed mutagenesis of MbxA
Atto-488 labelling of (pro)MbxA
Cytotoxicity assay (Hb Release)
Capturing of microscopy images
Microscopy image analysis
Preparation of figures
Writing of the manuscript

Acylation of the RTX Toxin MbxA stimulates host membrane disruption through a specific interaction with cholesterol.

Feby Mariam Chacko[1], Anna Hamacher[2], Anne Pfitzer-Bilsing[1], Sebastian Hänsch[2], Philipp Westhoff [3], Stefanie Weidtkamp-Peters[2], Marten Exterkate[4], Sander H. J. Smits[1,5] & Lutz Schmitt[1#].

[1] Institute of Biochemistry, Heinrich-Heine-University Düsseldorf, Universitätsstraße 1, 40225 Düsseldorf, Germany.

[2] Center for Advanced Imaging, Heinrich Heine University Düsseldorf, Universitätsstraße 1, 40225 Düsseldorf, Germany.

[3] Metabolomics and Metabolism Laboratory, Cluster of Excellence for Plant Sciences (CEPLAS), Heinrich Heine University Düsseldorf, Germany.

[4] Membrane Biogenesis and Lipidomics group, Heinrich Heine University Düsseldorf, Universitätsstraße 1, 40225 Düsseldorf, Germany.

[5] Center for Structural Studies, Heinrich Heine University Düsseldorf, Universitätsstraße 1, 40225 Düsseldorf, Germany

[#]Corresponding author: Lutz.Schmitt@hhu.de

Abstract

RTX toxins (Repeat in ToXins) are pore-forming toxins secreted by gram-negative bacteria. They are known for their ability to disrupt host cell membranes, among which various human cells. The acylation of specific lysine residues in these toxins is crucial for their hemolytic activity, but the precise mechanisms underlying this enhancement remain unclear. By comparing the lytic activities of acylated MbxA and its non-acylated form, we explored the role of acylation in the pore-forming behaviour of this RTX toxin. Our findings demonstrate that acylation specific interactions of MbxA with cholesterol promote membrane disruption, both *in vitro* and in living cells. More specifically, acylation is not necessary for initial membrane binding, but markedly enhances pore formation. Overall, our results provide detailed insights into the molecular determinants that regulate MbxA toxin activity. We highlight a complex interplay between lipid composition (sterols), acylation, and membrane disruption, thereby advancing our general understanding of RTX toxin pathogenesis.

Keywords

RTX toxins, MbxA, Acylation, Cholesterol, Lipid composition, Membrane disruption, Membrane fluidity.

1. Introduction

RTX (repeats-in-toxin) toxins are a family of exoproteins secreted by Gram-negative bacteria through a Type-1 secretion system (T1SS) [1]. Many bacteria utilize these pore-forming RTX toxins [2] as virulence factors during infection. For instance, the uropathogenic *Escherichia coli* hemolysin A (HlyA) is an RTX toxin linked to urinary tract infections, one of the most common bacterial infections worldwide [3]. Another example is the Adenylate Cyclase Toxin from *Bordetella pertussis*. This bacteria targets the human respiratory tract and causes whooping cough, a highly contagious and recurring disease [4]. Furthermore, the oral bacterium *Aggregatibacter actinomycetemcomitans* (known to cause localized aggressive periodontitis and endocarditis), produces an RTX protein called leukotoxin A (LtxA), which is lethal to human immune cells [5].

RTX proteins are distinguished by the presence of calcium-binding glycine-rich nonapeptide repeats (GGxGxDxUx; where x represents any amino acid and U indicates a large hydrophobic amino acid) located in the C-terminal part of the protein [6]. HlyA serves as the prototype of the RTX toxin family research. In the cytoplasm of *E. coli*, the translated HlyA remains unfolded and inactive prior to secretion [7, 8]. It becomes active through post-translational acylation at two lysine residues, K564 and K690, which is catalyzed by the acyl transferase HlyC [9]. The acylated HlyA is then secreted via the T1SS, composed of the ABC transporter HlyB (the inner membrane protein), HlyD (the membrane fusion protein), and TolC (the outer membrane protein) [10]. Once the entire HlyA protein is outside the cell, it fully folds through binding of calcium and becomes active, ready to form pores in various types of cells.

Secreted RTX toxins generally exhibit a broad range of host cell specificity [6, 11]. Many RTX toxins have been shown to interact with specific β_2 integrin receptors of certain host cells, such as Jurkat cells (human T-lymphocyte cells) [3, 12-21]. However, not all RTX toxins rely on β_2 integrin receptors to interact with host cell membranes. For instance, the RTX toxin RtxA from *Kingella kingae* does not engage with β_2 integrin receptors at all [22]. Likewise, several RTX toxins induce cytotoxicity in red blood cells that lack β_2 integrin receptors [23, 24]. Moreover, pore-forming and lytic properties of RTX toxins have been demonstrated in various artificial membranes [25, 26]. Overall, these findings suggest a β_2 integrin receptor-independent mechanism for RTX toxin interaction with host cell membranes. Indeed, several RTX toxins

have been associated with non-protein structures on host cell membranes, such as the carbohydrate chains of glycophorins, gangliosides, and cholesterol, further supporting the idea of a receptor-independent interaction pathway [4, 22, 27-36]. However, the precise mechanism by which they facilitate RTX toxin pore formation remains poorly understood.

Moraxella bovis is an intracellular parasite that inhabits mucous membranes and causes the ocular disease infectious bovine keratoconjunctivitis in cattle. MbxA is an uncharacterized RTX toxin produced by *M. bovis*. In this study, we employed an established heterologous system to secrete both the acylated, active form of MbxA and the non-acylated, inactive form using the *E. coli* T1SS [37]. MbxA shares 42% sequence identity with HlyA, and alternative to the *hly* operon (*hlyB, hlyD, and tolc*), the RTX operon of *M. bovis* contains all the genes required for activation (*mbxC*) and secretion (*mbxB*, *mbxD*, and *tolC*) of an RTX toxin [37-44] , which helped in the successful heterologous secretion of MbxA using *E. coli* T1SS.

Our previous work demonstrated that MbxA induces cytotoxicity in a wide variety of cells, including sheep red blood cells, suggesting MbxA activity independent of β_2 integrin receptors as well [37]. Here, we further explore the mechanisms underlying MbxA-mediated cytotoxicity, in which we specifically focus on the role of the lipid membrane. By combining *in vitro* and *in vivo* approaches, we reveal a prominent role for cholesterol in the pore-forming activity of MbxA, which is acylation-dependent.

2. Results

2.1. A liposome leakage assay to understand the lipid dependency in the lytic activity of acylated MbxA and non-acylated proMbxA.

To examine the β_2 integrin receptor-independent pore-forming activity of MbxA, we conducted a commonly used liposome leakage assay, based on the fluorophore 8-Aminonaphthalene-1,3,6-Trisulphonic acid (ANTS) and its quencher p-Xylene-Bis-Pyridinium Bromide (DPX) (figure 1a). After establishing baseline fluorescence, 100 nM of either acylated MbxA or non-acylated proMbxA was added to the liposomes, thereby initiating possible pore formation/leakage. After reaching a stable plateau, 0.5% Triton X-100 was introduced,

dissolving all liposomes. As a consequence, the measured fluorescence represents 100% content release (figure 1b).

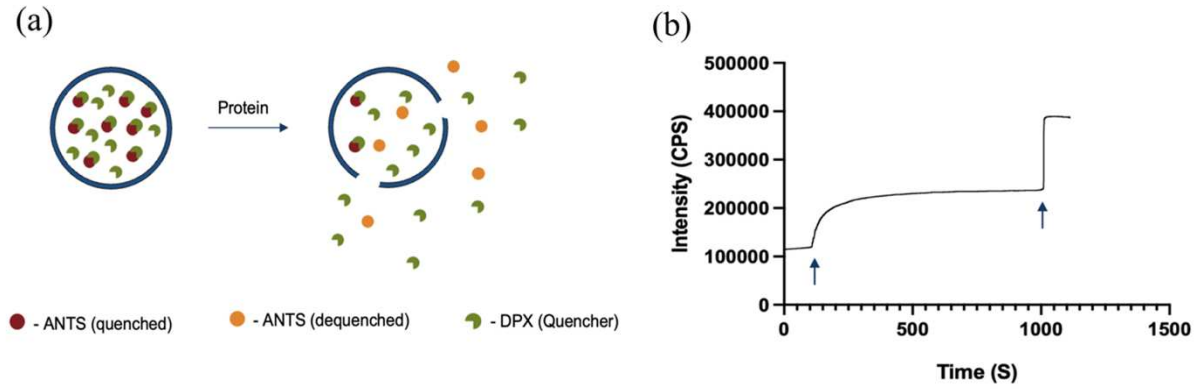

Figure 1: *(a) Liposomes with various lipid compositions were encapsulated with the fluorophore ANTS and the quencher DPX. Upon addition of protein (MbxA or proMbxA), pores might be formed, resulting in leakage and consequently dequenching of ANTS. (b) Fluorescence measurement of DOPC liposomes encapsulated with ANTS/DPX prepared from 12 µM DOPC. After 100 sec, 100 nM MbxA is added (first arrow). Once a plateau is reached, 0.5% Triton X-100 was added (second arrow), resulting in the complete release of the liposomal content.*

2.2. Increased lytic activity of MbxA and proMbxA for liposomes composed of unsaturated fatty acids and negatively charged lipid headgroups.

To investigate the lipid dependency of pore formation by MbxA and proMbxA, we assessed the lytic activity of the proteins on a series of liposomes with varying lipid compositions based on either the saturation of their lipid tails or the charge of the headgroup. Focusing on the acyl chains, three different lipid species were chosen: di-palmitoyl phosphatidylcholine (DPPC), which has two saturated acyl chains, palmitoyl-oleoyl phosphatidylcholine (POPC) containing one unsaturated acyl chain, and di-oleoyl phosphatidylcholine (DOPC), which consists of two unsaturated acyl chains (lipid saturation in the order DPPC>POPC>DOPC). Both MbxA and proMbxA exhibited a higher pore-forming efficiency in the presence of the highly unsaturated DOPC liposomes, while only limited pore formation was observed for the fully saturated DPPC liposomes (fig. 2a) as evident by the lower fluorescence increase after protein addition for DPPC liposomes. Notably, MbxA demonstrated a specific activity in the presence of POPC liposomes compared to proMbxA, illustrating that the acyl moieties of the protein affect the lytic activity under specific membrane conditions (protein activity: MbxA; DOPC>POPC>DPPC, proMbxA; DOPC>POPC=DPPC). Subsequently, the lytic activity of

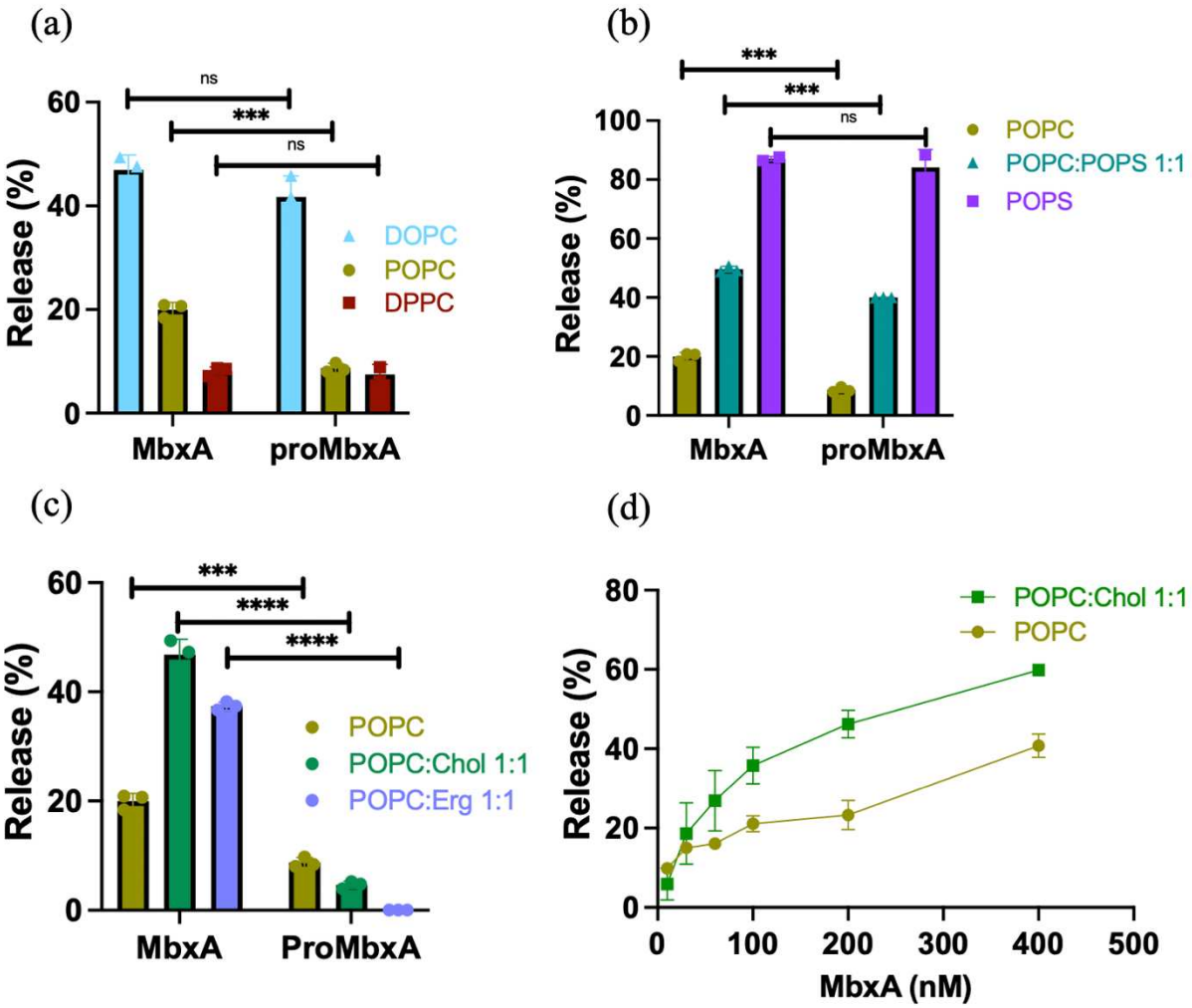

Figure 2: *The percentage release of liposomal content by the lytic activity of MbxA and proMbxA on different sets of liposomes. Lytic activity of MbxA and proMbxA on liposomes based on (a) the acyl chain saturation of the lipid chain, (b) the charge of the lipid head group, and (c) cholesterol and ergosterol incorporation into the liposomes. 100 nM (pro)MbxA was added to 12 uM liposomes (final lipid concentration), and fluorescence release was measured for 15 minutes. (d) Percentage release of liposomal content when different concentrations of MbxA were incubated with 12 uM POPC and POPC:Chol 1:1 liposomes. Statistical analysis was performed using an unpaired t-test, and for each liposomal lipid composition the maximal release values between MbxA and proMbxA were checked to see if they were biologically not significant (ns) or significant (* if $p<0.05$, ** if $p<0.01$; *** if $p<0.001$; **** if $p<0.0001$). Data shown represent technical replicates (n = 3). Similar results were obtained in [3] independent biological replicates.*

MbxA and proMbxA was tested in the presence of different head groups, differing in their overall charge. While POPC possesses a net neutral charge, palmitoyl-oleoyl phosphatidylserine (POPS) has a net negative charge (lipid headgroup charge: POPS>POPC:POPS 1:1>POPC). Both MbxA and proMbxA exhibited increased lytic activity toward the negatively charged liposomes (fig. 2b). Notably, the release of liposomal content

from the POPC:POPS 1:1 mixture was intermediate between that of the POPC and POPS liposomes for both MbxA and proMbxA (protein activity: POPS>POPC:POPS>POPC), indicating no specific interaction between the acyl-chain moieties of the protein and the lipid headgroup.

2.3. MbxA exhibits specific lytic activity towards cholesterol-containing liposomes, while proMbxA does not.

Given that cholesterol is present in mammalian cell membranes but absent in bacterial cell membranes, we assessed whether MbxA and proMbxA exhibit specific lytic activity against cholesterol-containing membranes. Although the highest lytic activity was shown in the presence of POPS liposomes, anionic lipids are predominantly found in the inner leaflet of mammalian plasma membranes [45]. For this reason, we continued with POPC liposomes as they are most representative of the outer leaflet. When cholesterol was added to POPC liposomes at a 1:1 ratio, a 2.5-fold increase in liposome leakage was observed for MbxA compared to POPC liposomes, whereas proMbxA showed no such increase (Fig. 2c).

A specific role of the acylation moieties of MbxA in the lytic activity of the protein was already observed for POPC liposomes, but seems to be further enhanced in the presence of cholesterol. To further elucidate this phenomenon, we tested the lytic activity of POPC vs. POPC:Chol liposomes at varying MbxA concentrations (10 nM, 30 nM, 60 nM, 100 nM, 200 nM, and 400 nM) (Fig. 2d, Supplementary Fig. 2a,b). For both sets of liposomes, we observed a linear increase in the release of liposomal content, but the POPC:Chol liposomes exhibit an overall higher release, thereby confirming the stimulating effect of cholesterol on the lytic activity of MbxA.

Furthermore, we examined the lytic activity of MbxA and proMbxA in the presence of sterols other than cholesterol by incorporating ergosterol into POPC liposomes (POPC:Ergosterol 1:1). Remarkably, similar to cholesterol, ergosterol enhanced the leakage of liposomal content when incubated with MbxA, although it did not have the same effect on proMbxA (Fig. 2c).

Given that gangliosides have been reported as receptors for other RTX toxins [29, 30, 34], we further investigated the effect of gangliosides on the lytic activity of MbxA and proMbxA. However, POPC liposomes containing 30% GM1 gangliosides did not induce any significant

lytic activity for either MbxA or proMbxA; in fact, the lytic activity of MbxA decreased by approximately 5% compared to that observed with POPC liposomes (Supplementary Fig. 2c).

2.4. MbxA, but not proMbxA, causes rupture of POPC:Chol GUVs.

To visualize the different leakage effects of MbxA vs. proMbxA on POPC:Chol liposomes, we prepared Giant Unilamellar Vesicles (GUVs), incubated them with 100 nM of either MbxA or proMbxA and analyzed them by microscope (Evos M5000 imaging system) over time. Upon incubation with MbxA, noticeable changes in the shape of the GUVs were observed within 30 seconds (Fig. 3b), but they returned to their normal round shapes within 3 minutes, shown with colored arrow marks (Fig. 3c). Ultimately, after 10 minutes, the incubation with MbxA resulted in complete destabilization of the GUVs (Fig. 3d). In contrast, the incubation of 100 nM proMbxA with GUVs did not induce any disturbances in the GUV architecture, and they remained stable for 30 minutes (Fig. 3f to j).

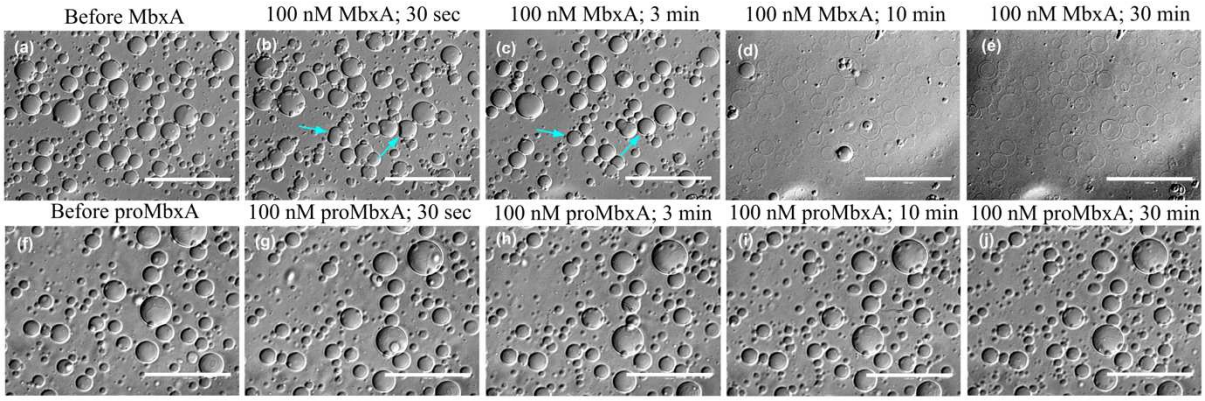

Figure 3: *POPC:Chol 1:1 Giant Unilamellar Vesicles (GUVs) (a) before treatment with MbxA, (b) 30 seconds (c) 3 minutes (d) 10 minutes and (e) 30 minutes after incubating with 100 nM MbxA, (f) before treatment with proMbxA, (g) 30 seconds (h) 3 minutes (i) 10 minutes and (j) 30 minutes after incubating with 100 nM proMbxA. Change in GUV shape upon MbxA incubation and its return back to the original shape is shown with colored arrow marks (b&c). The data shown are representative of two biological replicates. Scale bar: 100 μm.*

2.5. Flotation assay reveals that acyl chains are not essential for toxin binding to the membrane.

Previous experiments (Fig. 2c) indicated that the acyl chains play a crucial role in the lytic activity of the protein within cholesterol-containing membranes. To assess the importance of the acyl chains in the binding of the protein to these membranes, we conducted a flotation assay

using MbxA and proMbxA. In this assay, we established a sucrose gradient ranging from 30% at the bottom to 0% at the top. Initially, liposomes incubated with the proteins reside in the bottom fraction. Following ultracentrifugation, the buoyancy of the liposomes causes them to float to the top fraction. If the protein successfully binds to the liposomes, the liposome-bound proteins will also float to the top fraction alongside the liposomes and can be detected via SDS-PAGE (Fig. 4a).

The flotation assay using POPC:Chol liposomes and MbxA demonstrated the presence of MbxA in all three fractions: bottom, middle, and top (Fig. 4b). Although, most of the protein was found in the bottom fraction, probably aggregated protein, some protein was detected in the middle and top fraction, indicating liposomal binding. Given the definition of the volume for each fraction, it is expected to observe some protein crossover in the middle fraction from the top fraction. Importantly, the control experiment, which included only MbxA protein without any liposomes, revealed no protein in the top and middle fractions (Fig. 4b). Similarly, the flotation assay with POPC:Chol liposomes and proMbxA indicated that proMbxA also binds to these liposomes (Fig. 4c). Please note that potential liposomal rupture by MbxA inhibits the flotation ability of those liposomes, meaning that the level of observed MbxA in the top fraction could be higher. Nevertheless, the presence of ProMbxA in the top fraction clearly indicates that the acyl chains are not essential for the protein its binding to the membrane.

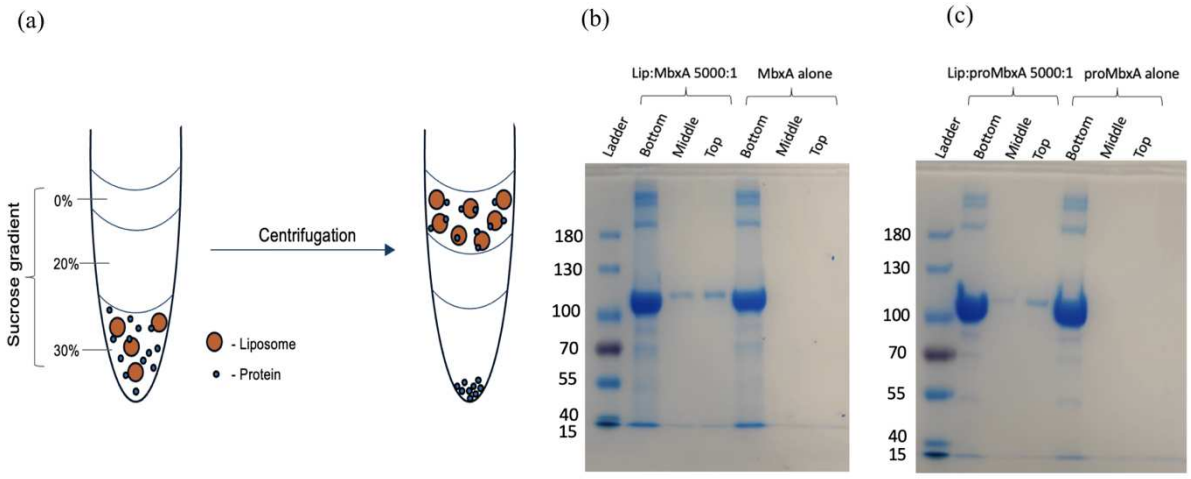

Figure 4: *(a) Schematic representation of the flotation assay. (b) Flotation assay with POPC: Chol 1:1 liposome and MbxA (Lipid: MbxA in 5000:1 ratio). (c) Flotation assay with POPC: Chol 1:1 liposome and proMbxA (Lipid: proMbxA in 5000:1 ratio). Gels are stained using Coomassie brilliant blue. The data shown are representative of two biological replicates.*

2.6. AFM reveals cholesterol-dependent insertion of acylated MbxA.

To investigate the membrane association and coupled pore formation by MbxA in more detail, we conducted Atomic Force Microscopy (AFM) using Supported Lipid Bilayers (SLBs) on a mica surface. AFM images of SLBs composed of POPC or POPC:Chol displayed distinct background stripe pattern before treatment with any proteins (Fig. 5a). Following the incubation of SLBs with 100 nM MbxA or proMbxA, we observed an increase in surface height, indicating binding of the protein to the SLB. Notably, MbxA proteins remained stably bound to the POPC:Chol SLBs even after three rounds of rigorous washing of the preincubated SLBs (Fig. 5b). In contrast, proMbxA proteins were entirely removed from the SLBs upon washing with buffer, resulting in the reappearance of the background signal. (Fig. 5c). These results implicate that the binding of MbxA to the membrane is stronger.

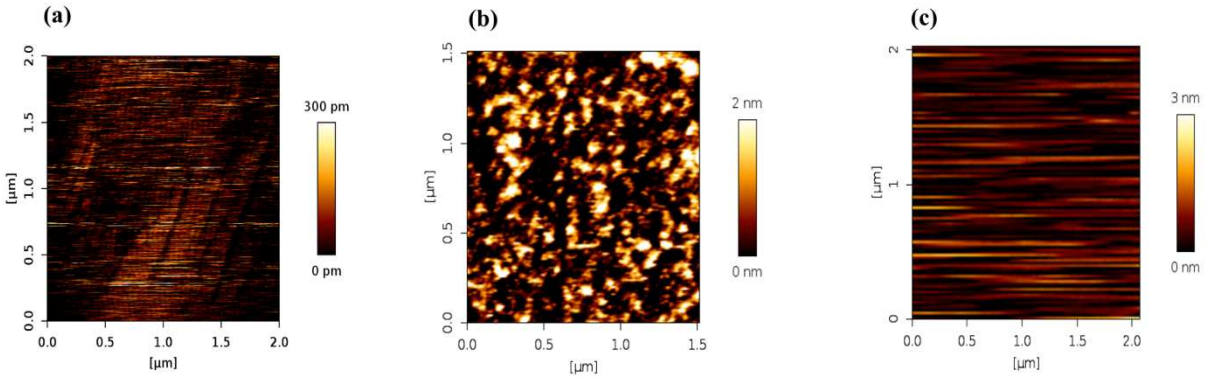

Figure 5: *AFM images of (a) Supported Lipid Bilayer (SLB) before any protein treatment; (b) POPC:Chol 1:1 SLB after three rounds of buffer washes following pre-incubation with 100 nM MbxA; (c) POPC:Chol 1:1 SLB after three rounds of buffer washes following pre-incubation with 100 nM proMbxA. The data shown are representative of two biological replicates.*

2.7. Sterol-induced membrane packing facilitates the insertion of acylated MbxA.

To further elucidate the differences in lytic activity observed between MbxA and proMbxA, we examined the physical properties of membranes containing a variety of lipid compositions. We specifically focused on the fluidity and packing of the membrane, which can be measured by integrating the fluorescent dye Laurdan [46, 47]. Membrane fluidity was assessed by measuring the anisotropy, while membrane packing can be evaluated through general polarization (GP) measurements derived from the Laurdan emission spectrum across different lipid compositions (Sup. Fig 2d). When a sterol such as cholesterol or ergosterol is incorporated

into a membrane in a liquid-disordered state ($T > T_m$; T: working temperature, T_m: melting temperature), it leads to closer packing of the membrane, resulting in a liquid-ordered state (Fig. 6a). Conversely, when a sterol is integrated into a membrane in a gel phase ($T < T_m$), it results in looser packing of the membrane, also yielding a liquid-ordered state (Fig. 6a).

Anisotropy measurements indicate a similar degree of membrane fluidity for DOPC and POPC liposomes, while DPPC exhibits reduced fluidity (Fig. 6b). This is in accordance with previous observations [48], and indicates that the earlier observed difference in lytic activity between MbxA and proMbxA on POPC membranes (fig. 2a) is not a consequence of altered membrane fluidity. Concurrently, GP measurements reveal membrane packing in the order of DOPC < POPC < DPPC (Fig. 6c), which does align with the lytic activity of MbxA, observed in the order of DOPC > POPC > DPPC (Fig. 2a). In other words, MbxA demonstrates greater lytic activity when the packing of the membrane decreases.

Next, the effect of cholesterol on membrane packing and fluidity was examined. Since a POPC lipid membrane is in a liquid disordered state at 20°C (T_m; POPC=-2°C [49]), cholesterol incorporation strongly increased the GP of POPC membranes at 20°C resulting in membrane packing more similar to DPPC membranes (Fig. 6c). Likewise, the membrane fluidity of POPC liposomes decreased in the presence of cholesterol, indicated by an increased anisotropy (Fig. 6b). Based on the packing/fluidity results observed for membranes containing only PC lipids, a decrease in lytic activity of MbxA would be in accordance. However, the contrary is observed, as instead, cholesterol increases the lytic activity to levels comparable with DOPC membranes (Fig. 6d). As no such effect was observed for proMbxA, the specific role of the acyl-moieties in the lytic activity of this protein with cholesterol is highlighted once again.

To further specify the impact of cholesterol on membrane fluidity and packing, liposomes containing DOPC:Chol 1:1, and DPPC:Chol 1:1, were tested for anisotropy and GP (Fig. 6e,f) while assessing the lytic activity of MbxA and proMbxA on these formulations (Fig. 6g). In all cases, cholesterol incorporation stimulated the lytic activity of MbxA, although no such increase was observed for proMbxA (Fig. 6g). DOPC lipid membrane is in a liquid disordered state while DPPC membrane is in a gel phase at 20°C (T_m; DOPC=-17°C [50], DPPC=41°C [51]). Anisotropy measurements showed that cholesterol reduces the fluidity of DOPC liposomes, similar to POPC liposomes, while increasing the fluidity of DPPC liposomes (Fig. 6e). GP values for DOPC:Chol liposomes strongly increased, as observed for POPC:Chol

liposomes, while the membrane fluidity of DPPC and DPPC:Chol 1:1 liposomes were similar, possibly caused by saturation of the signal (Fig. 6f). Altogether, these results clearly show the specific impact of cholesterol on the lytic activity of MbxA. Nevertheless, a secondary effect can be attributed to the membrane packing as an increase in GP coincides with reduced lytic activity both in the presence and absence of cholesterol.

Interestingly, while cholesterol incorporation into DOPC liposomes increased membrane packing (as indicated by GP measurements; Fig. 6d) and reduced membrane fluidity (as shown by anisotropy measurements; Fig. 6e) compared to DOPC liposomes, proMbxA was capable of inducing lytic activity toward DOPC:Chol 1:1 liposomes. This finding is in contrast with the results from POPC:Chol 1:1 and DPPC:chol 1:1 liposomes, where MbxA exhibited lytic activity, but proMbxA did not. This result indicates that the positive effect of cholesterol on the lytic activity of MbxA is not entirely dependent on the acyl-moieties of the protein. Previous studies have reported that incorporating cholesterol into DOPC membranes (but not for POPC or DPPC membranes) can lead to phase separation within the membrane [52-54].

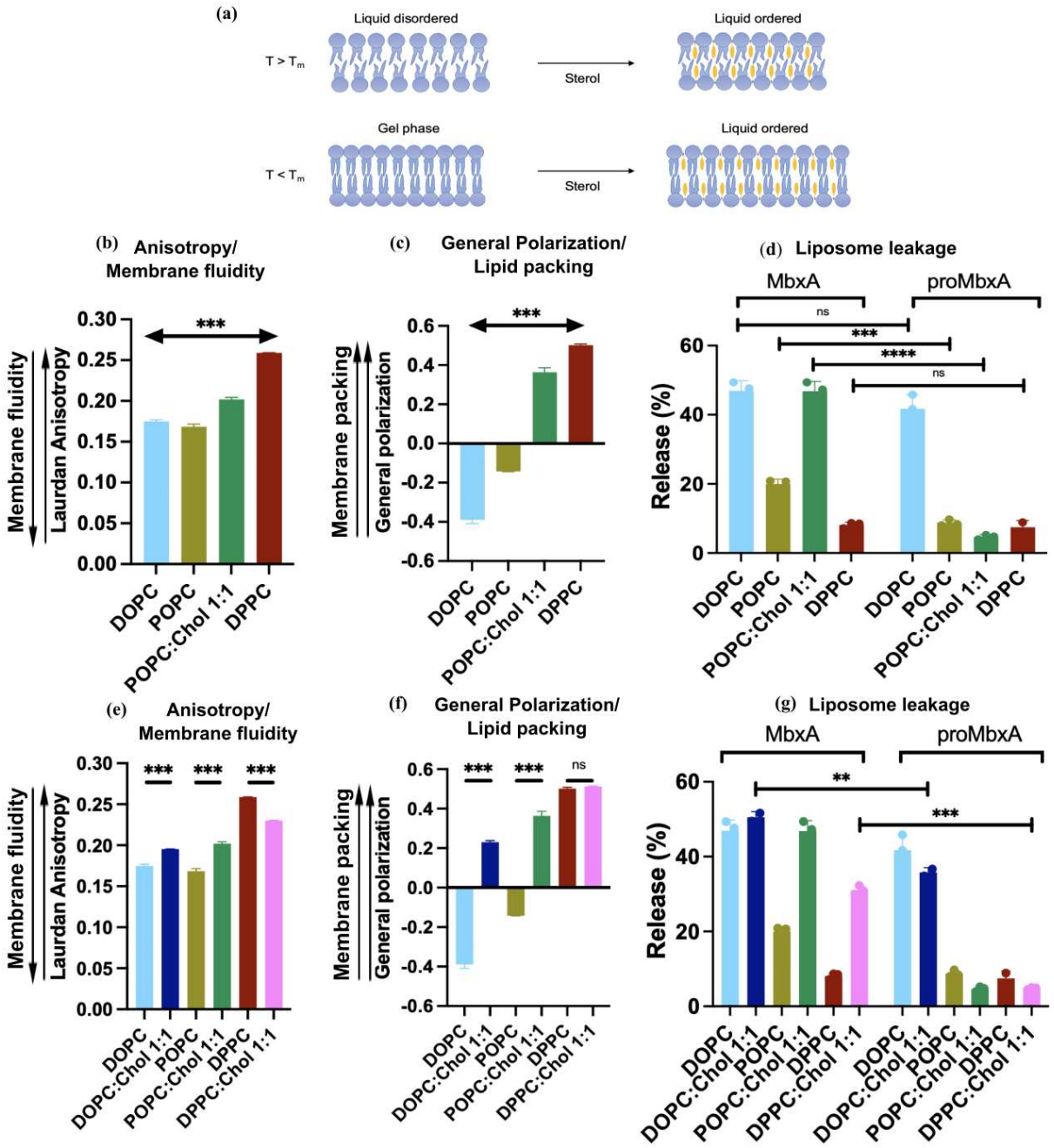

Figure 6: *(a) Theory of lipid packing when sterol is introduced into a membrane in the liquid-disordered state and in the gel phase. (b, e) Anisotropy values of liposomes of different lipid compositions are calculated using the equation* $r = (I_{vv} - GI_{vh})/(I_{vv} + 2GI_{vh})$ *where I is the fluorescence intensity; v and h are vertical and horizontal settings for the excitation and emission polarizers, respectively; G is the instrumental correction factor provided by the instrument for each instrument (further details are mentioned in the materials and methods section). A higher anisotropy measurement indicates less fluidic membranes and a lower anisotropy measurement indicates highly fluidic membranes. (c, f) General Polarization (GP) values calculated from the Laurdan emission spectrum using the equation* $(I_{435} - I_{500})/(I_{435} + I_{500})$*, where I is the fluorescence intensity at the respective wavelengths mentioned. A higher GP value (more positive) indicates more closely packed membranes and a lower GP value (more negative) indicates loosely packed membranes. (d, g) Liposome leakage assay of MbxA and proMbxA on*

*liposomes of different lipid compositions. (d) is a combined data of Fig. 2a and 2c. All the measurements are performed at 20°C. Lipid compositions with colour codes: **DOPC**, **DOPC:Chol 1:1**, **POPC**, **POPC:Chol 1:1**, **DPPC**, **DPPC:Chol 1:1**. Statistical analysis for Anisotropy and GP measurements was performed using a one-way ANOVA test for overall significance between different lipids, and Turkey's post hoc test for pairwise significance. The significance of maximal liposomal release values between MbxA and proMbxA of DOPC:Chol and DPPC:Chol was checked using an unpaired t-test. ns (not significant) if $p>0.05$; * if $p<0.05$, ** if $p<0.01$; *** if $p<0.001$. One-way ANOVA test for Anisotropy: $p=3.80\times10^{-8}$(significant); for GP: $p=2.67\times10^{-7}$(significant).* The data shown (three technical replicates) are representative of two biological replicates.

2.8. MbxA is unable to induce cytotoxicity when cholesterol is removed from human epithelial (HEp-2) cells.

Although the above *in vitro* results clearly demonstrate the effect of cholesterol on the activity of MbxA, they hardly represent an *in vivo* membrane. Cellular membranes contain a wide variety of different lipids that vary in headgroup and lipid tail configuration. To investigate the *in vivo* effects of cholesterol on the cytotoxicity of MbxA and proMbxA, their lytic activity was tested on HEp-2 cells with and without cholesterol. HEp-2 cells contain 24.5% cholesterol [55]. Cytotoxicity was assessed by observing plasma membrane permeabilization and membrane blebbing, which serve as indicators of MbxA-induced cytotoxicity, as described previously [37]. HEp-2 cells were stained with CellMask™ Deep Red to visualize the plasma membrane and suspended in a medium containing Sytox Green, a nuclear staining dye. Following incubation with MbxA, the plasma membrane of the HEp-2 cells became permeabilized, allowing Sytox Green to stain the nuclei (Fig. 7; first row). Additionally, MbxA cytotoxicity led to a membrane blebbing phenotype, with noticeable blebbing observed just 5 minutes after MbxA treatment (Fig. 7b, arrowheads). The size of the bleb and intensity of the nuclear staining slowly increases in the subsequent time points, which can be visualized in the 10-minute, 15-minute, and 20-minute images of MbxA treatment on cholesterol-intact HEp-2 cells (Fig. 7; first row). A quantification of time-dependent nuclear staining was performed in the previous work [37]. After 20 minutes of incubation, more pronounced nuclear staining by Sytox Green and an increase in the number of membrane blebs were evident. Supplementary Fig. 3b illustrates a broader area of HEp-2 cells subjected to MbxA, highlighting the Sytox Green permeabilization and membrane blebbing, while supplementary Fig. 3c shows the top layer of HEp-2 cells where membrane blebs are prominently visible. To deplete cholesterol, varying concentrations of methyl beta-cyclodextrin (m-βCD) were used, after which the cholesterol content was assessed by GC-MS (Supplementary Fig. 3a). As the viability of the

cells decreased above 10 mM m-βCD, a concentration of 7mM was chosen for the experiment. This reduces the total cholesterol content, leaving 2.2 - 3.9% of the total content of 24.5%. When cholesterol was removed from HEp-2 cells using 7 mM m-βCD, MbxA failed to induce cytotoxicity. No nuclear staining by Sytox Green or membrane blebbing was observed, even after 20 minutes of incubation with 100 nM MbxA (Fig. 7; second row). Notably, whether cholesterol was present or absent, proMbxA did not induce cytotoxicity in HEp-2 cells, consistent with previous observations [37] (Supplementary Fig. 3d).

2.9. MbxA & proMbxA bind to HEp-2 cell membranes with and without cholesterol.

The flotation assay indicated that both MbxA and proMbxA can associate with POPC:Chol membranes, suggesting that the acyl chains are not required for membrane binding. To validate this finding *in vivo*, both MbxA and proMbxA were labeled with Atto-488, allowing for visualization of their binding to the HEp-2 cell membrane.

HEp-2 cells were treated with 100 nM Atto488-MbxA^{S9C}(Fig. 8b), and any unbound protein was subsequently washed away to highlight the membrane-bound protein (Fig. 8c). As previously reported [37], with a lytic activity of 97% of the wild-type protein, Atto488-MbxA^{S9C} effectively bound to the plasma membrane of HEp-2 cells (Fig. 8c). To investigate whether cholesterol in the host cell membrane is essential for the binding process of the toxin, Atto 488-labeled MbxA was incubated with cholesterol-removed HEp-2 cells (Fig. 8e) and subsequently washed away (Fig. 8f). Atto488-MbxA^{S9C} was able to bind to the cholesterol-removed plasma membrane of HEp-2 cells, similarly to the binding observed in cholesterol-intact HEp-2 cells (Fig. 8f), indicating that cholesterol is not involved in the initial binding process of the protein to the membrane.

To examine if the acyl chain is necessary for the binding of MbxA to the HEp-2 cell plasma membrane, atto 488-labeled proMbxA was added to both cholesterol-intact (Fig. 8g, h, i) and cholesterol-removed HEp-2 cells (Fig. 8j, k, l). Similar to MbxA, proMbxA was also observed to bind clearly to the plasma membrane of both cholesterol-intact (Fig. 8i) and cholesterol-removed HEp-2 cells (Fig. 8l). This experiment demonstrates that the acyl chain is not necessary for the initial binding of MbxA to the HEp-2 cell membrane.

A control experiment with 100 nM Atto-488 dye showed no binding to the HEp-2 cell membrane, further confirming that the binding of Atto488-MbxA^{S9C} and Atto488-proMbxA^{S9C} is due to the proteins themselves rather than free dye (Sup. Fig. 4). Additionally, a control experiment involving wheat germ agglutinin (WGA) binding to the HEp-2 cell membrane exhibited a binding pattern similar to that of Atto488-MbxA^{S9C} and Atto488-proMbxA^{S9C}, reinforcing the conclusion that these proteins are indeed binding to the plasma membrane of the HEp-2 cells (Sup. Fig. 4). The stability and activity of the labelled proteins were confirmed using an SDS gel and hemoglobin release assay (Sup. Fig. 5)

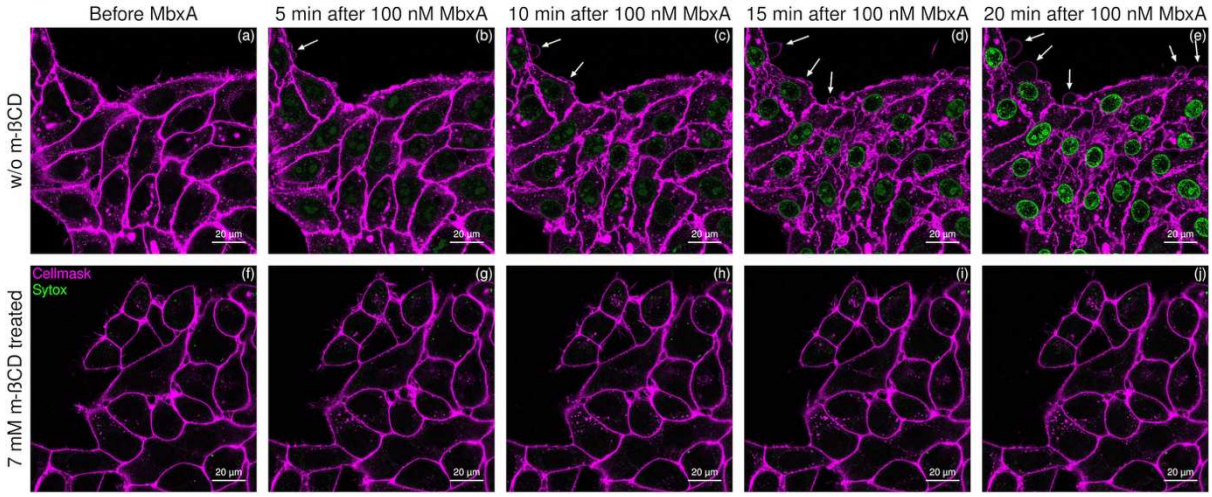

***Figure** 7: Confocal microscopy images of CellMask™ Deep Red-stained HEp-2 cells. First row (a,b,c,d,e): Nuclear staining of HEp-2 cells by Sytox green from the surrounding media due to the plasma membrane permeabilization and membrane blebbing (white arrowheads) resulting from the MbxA cytotoxicity in cholesterol-intact membranes of the HEp-2 cells. Second row (f,g,h,i,j): No nuclear staining nor membrane blebbing phenotype has been observed in HEp-2 cells when cholesterol-removed HEp-2 cells are incubated with 100 nM MbxA. The data shown are representative of two biological replicates.*

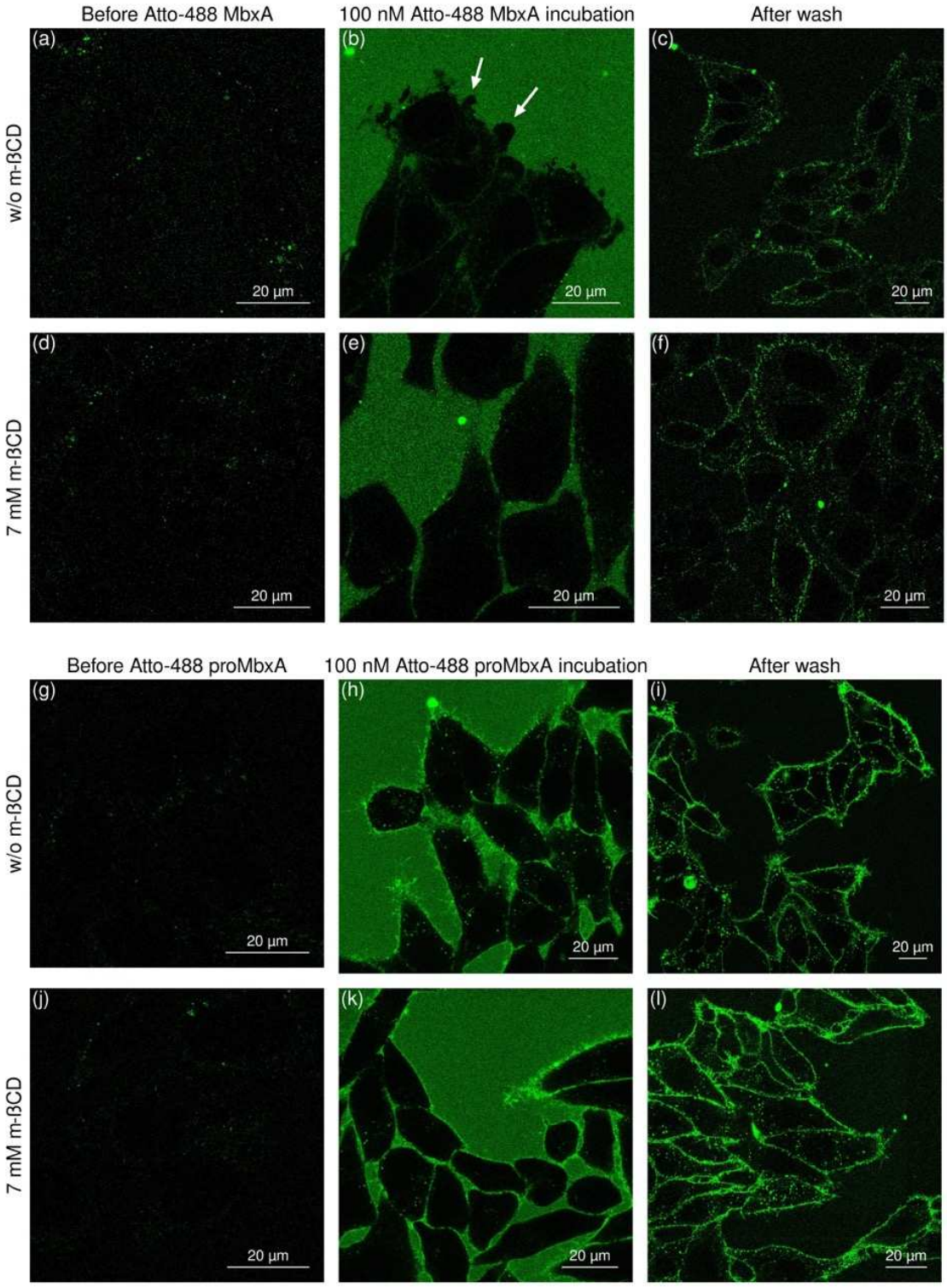

Figure 8: *Confocal microscopy images of (a,b,c) cholesterol intact HEp-2 cells; (a) before incubating with Atto488-MbxA^{S9C}, (b) incubation of HEp-2 cells with Atto488-MbxA^{S9C} which results in membrane blebbing, (c) HEp-2 cells after the excessive unbound protein being washed away. (d,e,f) Cholesterol removed HEp-2 cells using 7 mM m- βCD; (d) before incubating with Atto488-MbxA^{S9C}, (e) incubation of HEp-2 cells with Atto488-MbxA^{S9C} which doesn't show any membrane blebbing, (f) HEp-2 cells after the excessive unbound protein being washed away. (g,h,i) cholesterol intact HEp-2 cells; (g) before incubating with Atto488-proMbxA^{S9C}, (h) incubation of HEp-2 cells with Atto488-proMbxA^{S9C} which doesn't show any membrane blebbing, (i) HEp-2 cells*

after the excessive unbound protein being washed away. (j,k,l) Cholesterol removed HEp-2 cells using 7 mM m-βCD; (j) before incubating with Atto488-proMbxA^{S9C}, (k) incubation of HEp-2 cells with Atto488-proMbxA^{S9C} which doesn't show any membrane blebbing, (l) HEp-2 cells after the excessive unbound protein being washed away. The data shown are representative of two biological replicates.

3. Discussion

RTX toxins, such as MbxA from *M. bovis,* display virulence by disrupting the host cell membranes. Besides the β_2 integrin receptor-dependent activity, RTX toxins can exhibit lytic activity via a receptor-independent interaction pathway, which is suggested to rely on specific interactions between the two acyl-moieties of the RTX toxin with the membrane [4, 22, 27-36]. Here, we systematically characterized the role of the lipid membrane in the binding and lytic activity of MbxA (acylated at lysine residues K536 and K660 [37]), and its non-acylated counterpart proMbxA.

Introducing negatively charged lipids, exemplified by POPS (Fig. 2b), into neutral liposomes enhances the lytic activity of both MbxA and ProMbxA, illustrating this effect is independent on the acyl-moieties of the protein. This stimulating effect may be explained by a net positive surface charge density of the pore-forming hydrophobic domain at the N-terminus, as indicated by a model of proMbxA predicted by AlphaFold, which was verified by the SAXS (Sup. Fig. 1). Putting this into context, negatively charged lipids are predominantly located in the inner leaflet of host cell membranes and therefore not accessible for RTX toxins [45]. However, during cell signaling or apoptosis, these lipids could be transiently exposed, potentially allowing the toxins to exploit these conditions for binding.

Similarly, introduction of unsaturated acyl chains in the liposomal lipids also increases the lytic activity of MbxA and Pro-MbxA (fig. 2a). This can be directly linked to changes in the biophysical properties of the membrane *i.e.*, decreased membrane packing and to a lesser extent increased fluidity (Fig. 6b,c), thereby facilitating the membrane its accessibility. Noteworthy, the lytic activity of proMbxA compared to MbxA is severely lower in POPC membranes, possibly highlighting a specific role for the acyl-chain moieties of the protein while interacting with the membrane. Although POPC membranes most closely resemble the acyl-chain configuration of native membranes [45], membrane packing and fluidity are also greatly influenced by sterols. Indeed, incorporating cholesterol (or ergosterol) into POPC liposomes

significantly increased liposome leakage induced by MbxA, with leakage rising from 20% in POPC liposomes to 45% in POPC:Chol liposomes (fig. 2c). On the contrary, a (small) decrease in lytic activity has been observed for proMbxA, clearly showing the importance of the protein its acyl-chain moieties. Remarkably, the presence of cholesterol deteriorated the earlier described favorable biophysical properties of the membrane. The membrane fluidity decreased, whereas membrane packing drastically increased to levels observed with DPPC liposomes. In other words, the enhanced lytic activity is caused by a specific interaction of acylated MbxA with cholesterol, and not a result of an overall more accessible membrane. A possible explanation for this could be that MbxA accumulates cholesterol into microdomains, thereby creating a favorable local environment for the protein. However, additional experiments would be required to confirm the presence of actual microdomains. To that respect, phase separation has not been reported for POPC:Chol 1:1 liposomes, but is observed in DOPC:Chol 1:1 liposomes, which may explain the observed lytic activity of the non-acylated proMbxA [52-54]. Noteworthy, enhanced lytic activity was observed for ergosterol as well, indicating that this phenomenon could be general for sterols.

Overall, the *in vitro* setup provides a systematic overview, displaying several factors (*e.g.,* lipid charge, membrane packing, sterols, etc.) that play a role in (pro)MbxA activity. Nevertheless, liposomes are simplified model membranes and do not necessarily represent the *in vivo* situation. Using HEp-2 cells as a model system, we tested (pro)MbxA activity in presence and absence of cholesterol. In short, MbxA only showed pore forming activity in normal cholesterol containing membranes, allowing the membrane impermeable Sytox Green to stain the nucleus. On the contrary, depleting the cholesterol content resulted in inactive MbxA. In the case of proMbxA, no lytic activity was observed, regardless of the cholesterol content, thereby confirming the earlier observed difference in the *in vitro* setup. Altogether, the *in vivo* experiments provide critical insights into the combined role of cholesterol and acylation in MbxA's cytotoxic activity within a physiological context. The complete abrogation of lysis in cholesterol-depleted HEp-2 cells underscores its necessity for MbxA's functional conformation and pore formation. This finding aligns with previous studies implicating the presence of cholesterol-rich regions in the activity of pore-forming toxins, further cementing cholesterol as a key lipid component for RTX toxin-mediated cytotoxicity [26, 32, 36, 56, 57].

A possible explanation for the cholesterol-dependent lytic activity of MbxA is that the presence of cholesterol results in the formation of more (stable) pores. To determine whether the acyl

chains are essential for the binding of MbxA to cholesterol membranes, *in vivo* experiments using confocal microscopy were performed, showing both Atto-488-labeled $MbxA^{S9C}$ and $proMbxA^{S9C}$ were bound to the plasma membrane of HEp-2 cells, regardless of cholesterol presence (Fig. 8). Moreover, an *in vitro* flotation assay with liposomes revealed that after centrifugation both acylated MbxA and non-acylated proMbxA were present in the liposome fraction, although with slightly lower levels of proMbxA. These observations highlight that the initial membrane binding of MbxA is not dependent on its acyl-chains or on cholesterol. On the other hand, by AFM, it was observed that MbxA stayed tightly bound to the membrane, whereas proMbxA was removed upon washing, suggesting cholesterol may act as a stabilizer, enhancing pore stability and persistence in the lipid bilayer, likely through the protein's acylation. The stabilizing role of cholesterol is consistent with findings from for example Herlax et al. (2009), who showed through FRET experiments that cholesterol enhances the oligomerization of HlyA in the host membrane [32].

Overall, these results highlight the intricate interplay between lipid composition and protein acylation on the pore-forming behavior of MbxA. However, the specific MbxA-membrane/cholesterol interactions at the molecular level remain unknown. There are several potential interpretations:

1. **Cholesterol-Mediated Membrane Organization**: Cholesterol may (re-)organize the local lipid environment, such that the insertion and possible oligomerization of acylated MbxA is favored. Such membrane restructuring could further potentiate the toxin's lytic activity.
2. **Direct Acyl Chain-Cholesterol Interactions**: Alternatively, the acyl chains of MbxA might interact directly with cholesterol, aiding in the stabilization and clustering of the protein within cholesterol-enriched microdomains [28, 58, 59].
3. **Acylation-Induced Conformational Changes**: Finally, acylation may trigger conformational changes that expose specific cholesterol-binding motifs. In theory, exposure of these domains could stabilize membrane interactions and/or promote pore formation within the membrane, possibly by stimulating MbxA oligomerization. Sequence analysis of MbxA reveals the presence of 25 so-called CRAC/CARC motifs [60]. In fact, various other RTX proteins are known to possess these specific cholesterol recognition motifs, of which some are located within, or near, the pore-forming domain and found to directly interact with membrane cholesterol [26, 36, 56, 61].

To integrate our experimental results with previous findings on RTX toxin behavior, we propose a model (Figure 9) illustrating how acylated MbxA, but not proMbxA, interacts with cholesterol-containing membranes to form transmembrane pores, consistent with the cholesterol-dependent oligomerization observed for acylated HlyA [32].

In summary, our *in vitro* and *in vivo* studies elucidate the complex relationships between lipid composition, acylation, and the pore-forming mechanisms of MbxA. The findings highlight cholesterol's essential role in enhancing MbxA's lytic activity facilitated through protein's acylation, even though the acyl chains and cholesterol are not needed for initial membrane binding. The varying effects of different lipid compositions show that secondary factors like membrane fluidity, packing, and surface charge also impact MbxA's function, further emphasizing the complex interplay between protein and membrane. The specific interactions at the molecular level between acylated MbxA and cholesterol remain unknown, but could involve conformational changes that promote pore formation, possibly by activating cholesterol recognition motifs such as CRAC/CARC. The recognition of alternative sterols, like ergosterol, suggests some flexibility of MbxA in adapting to different lipid environments, thereby expanding its range of targets. Overall, these findings deepen our understanding of the molecular factors underlying RTX toxin activity and their role in membrane disruption and cytotoxicity.

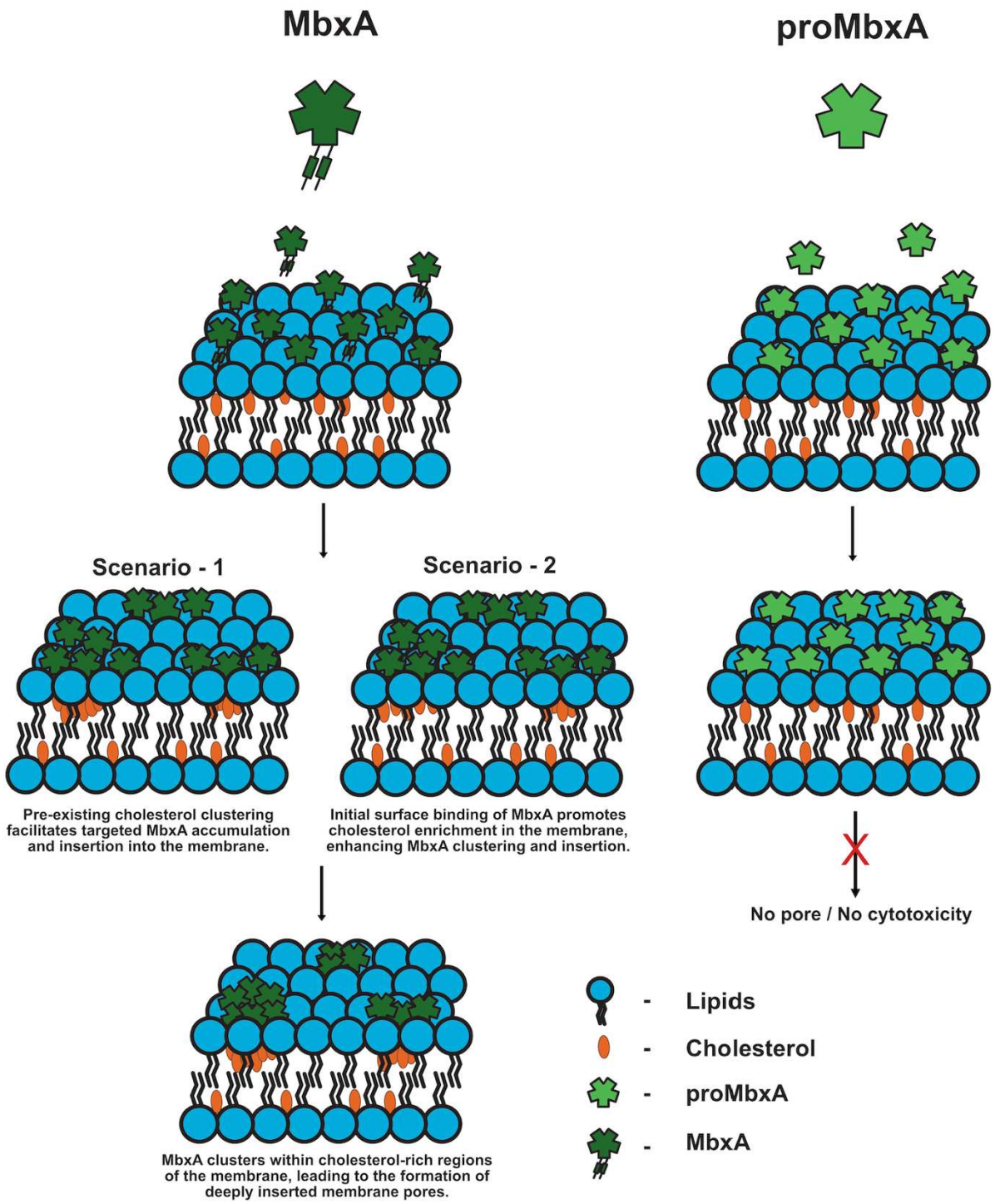

Figure 9: Proposed membrane interaction model of acylated MbxA versus non-acylated proMbxA in cholesterol-containing membranes. *Both acylated MbxA and non-acylated proMbxA bind to cholesterol-containing membranes; however, only MbxA leads to pore formation and cytotoxicity. The schematic illustrates two potential scenarios for MbxA action:* ***(Scenario 1)*** *cholesterol clustering occurs first, facilitating MbxA recruitment and deep insertion; and* ***(Scenario 2)*** *initial MbxA binding promotes local cholesterol accumulation, which further stabilizes and deepens MbxA insertion. In both cases, MbxA forms clusters in cholesterol-rich domains, promoting the formation of deeply penetrating transmembrane pores. In contrast, proMbxA, though capable of membrane binding, does not cause cholesterol clustering or membrane disruption, and therefore*

remains functionally inactive. This functional difference aligns with prior findings on the RTX toxin HlyA, where acylated HlyA was shown to oligomerize on cholesterol-containing membranes, while proHlyA did not [32], supporting the notion that acylation is critical for cholesterol-dependent oligomerization and cytolytic activity.

4. Materials and Methods

4.1. Protein expression & purification

Expression, secretion, and purification of (pro)MbxA were performed as described before [37]. (pro)MbxA was expressed in BL21 (DE3) *E. coli* strains. The proteins were expressed in a two-plasmid system in which one plasmid carries the ABC transporter *hlyBD* gene, and the second carries either the *hlyC-mbxA gene* (for acylated MbxA) or *mbxA* gene (for proMbxA). The expressed proteins were secreted via HlyBD, culture supernatants were pooled, and purified by Immobilised Metal Affinity Chromatography (IMAC).

4.2. Hemoglobin Release Assay

Assays were performed as previously reported [37]. Defibrinated sheep blood cells were washed and centrifuged several times using buffer A until the supernatant became clear. Homogenized blood cells were incubated with 30 nM of protein (MbxA, Atto488-MbxA^{S9C}, proMbxA, Atto488-proMbxA^{S9C}) for 30 minutes at 37°C. 16% SDS and IMAC buffer were used as positive (100%) and negative (0%) controls. Cells were then centrifuged, supernatants analyzed for hemoglobin release, and quantified via OD on a FLUOstar OPTIMA microplate reader (BMG Labtech) at 544nm. Buffer A: 10 mM Tris–HCl pH 7.5, 155 mM NaCl, 20 mM CaCl2, 5 mM KCl, and 2 mM MgSO4.

4.3. Liposome preparation and leakage assay

Chloroform-dissolved lipids were dried in a rotary evaporator at 40°C for 30 minutes. Lipids were resuspended in 1 mL ANTS buffer (12.5mM ANTS, 45mM DPX, 150mM NaCl, 20mM Tris-HCl pH 7.0). Lipid suspension was sonicated in six cycles (15s on/45s off), 50% duty cycle, and 50% (power) at RT. The resulting small unilamellar vesicles (SUVs) were flash-frozen in liquid nitrogen and thawed at room temperature (~20 min) two times. Liposomes were extruded using a 100nm membrane pore (Extruder: LiposoFast-Basic & Stabilizer, Avestin Inc.), and the liposome size was further confirmed using DLS measurement. Untrapped ANTS+DPX were chromatographically removed through a sephedex G-50 column using 150mM NaCl, and 20mM Tris-HCl pH 7.0 (buffer B). The final lipid concentration of 12 uM

was calculated based on the dilutions from each step. The liposome leakage experiment was performed in buffer B.

4.4. GUV preparation and assay

Two indium tin oxide (ITO)-coated glass slides were cleaned with 70% ethanol and chloroform. Then lipid solution (2*10 µl) was spread on the ITO-coated side, and the lipid area of one slide was fenced by a ring of sigillum wax (Vitrex$_{TM}$). A chamber was prepared by pressing the ITO/lipid-coated sides to each other. The chamber was filled with 300µl of 10% sucrose solution and sealed. Incubated the chamber for 3h at RT, applying an alternating current with 11Hz and 2V. GUVs were harvested using a GELoader® tip (Eppendorf). The chamber was incubated with BSA (1min) before adding GUVs to the observation chamber. The chamber was washed 3 times with PBS. Next, 250µL PBS + 50µL GUVs were added to the chamber. 100nM of (pro)MbxA was added, and time-lapse images were captured for 30min with 30sec time interval.

4.5. Atomic Force Microscopy

AFM was performed in liquid and imaging in intermittent contact mode (AC mode) in a JPK NanoWizard 3 atomic force microscope with NanoWizard Control Software v.5 version 5.0.84 by JPK (JPK, Berlin, Germany), using a non-conductive silicon nitride cantilever (DNP-S10-A, Bruker, Billerica, USA) with a nominal tip radius of 10 nm, a spring constant of 0.35 N/m and a resonance frequency of 65 kHz. Supported lipid bilayers were prepared using POPC or POPC:Cholesterol (1:1) liposomes. For this, 5µl of a 125µM stock was put on muscovite mica surface positioned inside a reservoir for liquid on a glass slide, and incubated with 5µl buffer (20mM Tris-HCl pH 7.0, 650mM NaCl) for 10min. 1ml of 50mM Tris-HCl pH 7.8, 400nM NaCl, and 10mM CaCl2 was added to the reservoir. 100nM of (pro)MbxA was added and incubated for 10min. Next, the mica was washed 3x with buffer. Again, 1ml of buffer was added and imaging was performed. All steps were performed at RT.

4.6. Membrane lipid packing and membrane fluidity analysis

Membrane lipid packing was analyzed by measuring General Polarisation (GP) and membrane fluidity was analyzed by Anisotropy, by using a Horiba Fluorolog-3 fluorometer. 100µM SUVs (see liposome preparation section) were mixed with 0.3µM laurdan to achieve a dye:lipid ratio of 1:333. Samples were incubated at 37°C for 1h in the dark, shaking at 300rpm.

GP measurement: Emission spectra (400-600nm) were measured while exciting at 350nm (Entrance slit: 3.00 nm Bandpass; Exit slit: 3.00 nm Bandpass). GP calculation:

$$(I_{435} - I_{500})/(I_{435} + I_{500})$$

where I is fluorescence intensity.

Anisotropy measurement: Single point anisotropy measurement was performed by excitation at 350nm and an emission monitoring at 435nm. Anisotropy calculation:

$$r = (I_{vv} - GI_{vh})/(I_{vv} + 2GI_{vh})$$

where I is fluorescence intensity; v (vertical), h (horizontal) settings for the excitation/emission polarizers respectively; G is the instrumental correction factor provided by the instrument.

4.7. Flotation assay

SUVs (see liposome preparation section) were mixed with protein to a final volume of 100µL and incubated for 5min at RT. 100µL 60% sucrose solution was added, resulting in 30% sucrose solution with protein and liposomes. The mix was transferred into ultracentrifuge tubes of the AT3 rotor. 250µL of 20% sucrose solution was carefully added on top without disturbing the bottom layer. 50µL of liposome buffer was added on top and centrifuged at 80,000rpm for 1h at 4°C. After ultracentrifugation, samples were carefully taken from the three layers using a gel loading tip like follows: (1) 250µL - Bottom layer (2) 125µL - Middle layer (3) 125µL - Top layer. The same volume of 30% TCA (Trichloroacetic acid) was added to the three fractions. After incubation on ice (15min), samples were centrifuged (17,000xg; 15min; 4°C) and supernatant TCA removed. 500µL of ice-cold acetone was added to the pellet, resuspended, incubated on ice (15min) and centrifuged (17,000xg; 15min; 4°C). Supernatant acetone was removed, pellet dried using a speed vacuum centrifuge (10min). Pellet was resuspended in 30µL and analyzed by SDS PAGE.

4.8. Cell culture and Live-cell imaging

HEp-2 cells were cultivated and passaged in DMEM (Pan Biotech) supplemented with 10% FCS, MEM vitamins, non-essential amino acids, amphotericin B (2.5ug/mL), and gentamicin (50ug/mL). Two days before, HEp-2 cells were seeded in 2mL DMEM in 35mm µ-Dish 1.5 H glass bottom dishes (Ibidi) and grown for 39-48 hours at 37°C under 5% CO_2. Live-cell DMEM

medium with 25mM HEPES in addition to the above-mentioned components is used for all the subsequent steps. Cells were washed with prewarmed DMEM live-cell medium and cell membranes stained using 5µg/mL CellMask Deep Red in DMEM-SG (containing 5µM Sytox Green), for 8min at 37°C and 5% CO_2. Cells were washed with DMEM and replaced with 1 mL DMEM-SG. Images were acquired with Zeiss LSM880 Airyscan. 1mL DMEM-SG and 200nM protein was added into 1mL HEp-2 cells (100nM final). Images were captured every five minutes after incubation and activity was monitored as described before [37].

Atto488-labeled (pro)MbxA^{S9C} was used to visualize HEp-2 cell membrane binding. HEp-2 cells were washed with DMEM medium, replaced with 1mL of fresh DMEM medium, and imaged (Zeiss LSM880 Airyscan). Tile-scan images of 1mL HEp-2 cells were acquired prior to labeled (pro)MbxA and after 10 min incubation (100nM final) Unbound labeled proteins were washed off using DMEM and replaced with 1mL of fresh DMEM medium before image acquisition.

Microscopy settings: Confocal and Airyscan micrographs were recorded using a Zeiss LSM880 Airyscan microscope system (Carl Zeiss Microscopy GmbH) equipped with a Plan-Apochromat 63x/1.4 oil immersion objective lens. For excitation, a 405 nm Laser was used for Hoechst 33342, a 488 nm Argon laser for excitation of Sytox Green and Atto488-labeled MbxA^{S9C}, and a 633 nm laser for excitation of CellMask Deep Red.

4.9. Mass spectrometry analysis of cholesterol removal

Cholesterol was removed from HEp-2 cells by incubation with m- βCD 5mM, 7mM, 10mM, 15mM, or 20mM (1h, 5% CO_2). Prior to GC-MS analysis, 0.5 nanomol (nmol) of internal standard β-sitosterol was added. Lipids were extracted with 0.3mL n-butanol (2 times), solvent evaporated with nitrogen gas. Dried lipid films were resuspended in 100ul MSTFA and incubated (80°C; 30min).

1µl of derivatized compounds was injected and measured on a 5977B GC/MSD (Agilent Technologies) as described [62]. Oven temperature gradient: constant at 70°C for 1min, ramped at 42°C min^{-1} to 280°C, further with 4°C min^{-1} to 320°C, held constant for 3min (total 19min). Electron ionization source: 70eV; source temperature: 200°C, mass range: 60-600m/z, 5 scans per second. Metabolites were identified via MassHunter Qualitative (v b08.00, Agilent Technologies) by NIST14 Mass Spectral Library comparison (https://www.nist.gov/srd/nist-

standard-reference-database-1a-v14). Authentic chemical standards for cholesterol were measured at a concentration of 5,10,50, 100µM and processed in parallel. Peaks were integrated using MassHunter Quantitative (v b08.00, Agilent Technologies). All metabolite peak areas were normalized to the sample amount (24K HEp-2 cells) and internal standard β-sitosterol (Sigma-Aldrich).

5. Acknowledgments

We thank all members of the Institute of Biochemistry for fruitful and stimulating discussions. We are thankful for excellent technical support from Elisabeth Klemp and the CEPLAS Plant Metabolism and Metabolomics Laboratory, which is funded by the DFG under Germany's Excellence Strategy—EXC-2048/1—project ID 390686111. Research was funded by the Jürgen Manchot foundation through a project in the Manchot graduate school 'Molecules of Infections IV' to L.S.

6. References

1. Holland, I.B., et al., *Type I protein secretion—deceptively simple yet with a wide range of mechanistic variability across the family.* EcoSal Plus, 2016. **7**(1): p. 10.1128/ecosalplus. ESP-0019-2015.
2. Benz, R., et al., *Pore formation by the Escherichia coli hemolysin: evidence for an association-dissociation equilibrium of the pore-forming aggregates.* Infection and immunity, 1989. **57**(3): p. 887-895.
3. Ristow, L.C., et al., *The Extracellular Domain of the β(2) Integrin β Subunit (CD18) Is Sufficient for Escherichia coli Hemolysin and Aggregatibacter actinomycetemcomitans Leukotoxin Cytotoxic Activity.* mBio, 2019. **10**(4).
4. Vojtova, J., J. Kamanova, and P. Sebo, *Bordetella adenylate cyclase toxin: a swift saboteur of host defense.* Current opinion in microbiology, 2006. **9**(1): p. 69-75.
5. Brown, A.C., et al., *Membrane localization of the Repeats-in-Toxin (RTX) Leukotoxin (LtxA) produced by Aggregatibacter actinomycetemcomitans.* PLoS One, 2018. **13**(10): p. e0205871.
6. Chacko, F.M. and L. Schmitt, *Interaction of RTX toxins with the host cell plasma membrane.* Biological Chemistry, 2023. **404**(7): p. 663-671.
7. Bakkes, P.J., et al., *The rate of folding dictates substrate secretion by the Escherichia coli hemolysin type 1 secretion system.* Journal of Biological Chemistry, 2010. **285**(52): p. 40573-40580.
8. Koronakis, V., et al., *Crystal structure of the bacterial membrane protein TolC central to multidrug efflux and protein export.* Nature, 2000. **405**(6789): p. 914-919.
9. Nicaud, J.-M., et al., *Characterisation of HlyC and mechanism of activation and secretion of haemolysin from E. coli 2001.* FEBS letters, 1985. **187**(2): p. 339-344.
10. Holland, I.B., L. Schmitt, and J. Young, *Type 1 protein secretion in bacteria, the ABC-transporter dependent pathway.* Molecular membrane biology, 2005. **22**(1-2): p. 29-39.
11. Linhartová, I., et al., *RTX proteins: a highly diverse family secreted by a common mechanism.* FEMS Microbiol Rev, 2010. **34**(6): p. 1076-112.
12. Dassanayake, R.P., S.K. Maheswaran, and S. Srikumaran, *Monomeric expression of bovine beta2-integrin subunits reveals their role in Mannheimia haemolytica leukotoxin-induced biological effects.* Infect Immun, 2007. **75**(10): p. 5004-10.

13. Dileepan, T., et al., *Human CD18 is the functional receptor for Aggregatibacter actinomycetemcomitans leukotoxin.* Infect Immun, 2007. **75**(10): p. 4851-6.
14. Goldsmith, J.A., et al., *Structural basis for non-canonical integrin engagement by Bordetella adenylate cyclase toxin.* Cell Rep, 2022. **40**(7): p. 111196.
15. Guermonprez, P., et al., *The adenylate cyclase toxin of Bordetella pertussis binds to target cells via the alpha(M)beta(2) integrin (CD11b/CD18).* J Exp Med, 2001. **193**(9): p. 1035-44.
16. Jeyaseelan, S., et al., *Lymphocyte function-associated antigen 1 is a receptor for Pasteurella haemolytica leukotoxin in bovine leukocytes.* Infect Immun, 2000. **68**(1): p. 72-9.
17. Lally, E.T., et al., *RTX toxins recognize a β2 integrin on the surface of human target cells.* Journal of Biological Chemistry, 1997. **272**(48): p. 30463-30469.
18. Li, J., K.D. Clinkenbeard, and J.W. Ritchey, *Bovine CD18 identified as a species specific receptor for Pasteurella haemolytica leukotoxin.* Vet Microbiol, 1999. **67**(2): p. 91-7.
19. Reinholdt, J., et al., *Monodisperse and LPS-free Aggregatibacter actinomycetemcomitans leukotoxin: interactions with human β2 integrins and erythrocytes.* Biochim Biophys Acta, 2013. **1834**(2): p. 546-58.
20. Vanden Bergh, P.G., et al., *Porcine CD18 mediates Actinobacillus pleuropneumoniae ApxIII species-specific toxicity.* Vet Res, 2009. **40**(4): p. 33.
21. Wang, J.F., et al., *Molecular and biochemical mechanisms of Pasteurella haemolytica leukotoxin-induced cell death.* Microb Pathog, 1998. **25**(6): p. 317-31.
22. Rahman, W.U., et al., *Binding of Kingella kingae RtxA Toxin Depends on Cell Surface Oligosaccharides, but Not on β(2) Integrins.* Int J Mol Sci, 2020. **21**(23).
23. Balashova, N.V., et al., *Leukotoxin confers beta-hemolytic activity to Actinobacillus actinomycetemcomitans.* Infect Immun, 2006. **74**(4): p. 2015-21.
24. Valeva, A., et al., *Binding of Escherichia coli hemolysin and activation of the target cells is not receptor-dependent.* J Biol Chem, 2005. **280**(44): p. 36657-63.
25. Martín, C., et al., *Membrane restructuring by Bordetella pertussis adenylate cyclase toxin, a member of the RTX toxin family.* J Bacteriol, 2004. **186**(12): p. 3760-5.
26. Osickova, A., et al., *Cytotoxic activity of Kingella kingae RtxA toxin depends on post-translational acylation of lysine residues and cholesterol binding.* Emerg Microbes Infect, 2018. **7**(1): p. 178.

27. Cortajarena, A.L., F.M. Goñi, and H. Ostolaza, *Glycophorin as a receptor for Escherichia coli alpha-hemolysin in erythrocytes.* J Biol Chem, 2001. **276**(16): p. 12513-9.
28. Fong, K.P., et al., *Actinobacillus actinomycetemcomitans leukotoxin requires lipid microdomains for target cell cytotoxicity.* Cell Microbiol, 2006. **8**(11): p. 1753-67.
29. Forman, M.S., et al., *Gangliosides block Aggregatibacter Actinomycetemcomitans leukotoxin (LtxA)-mediated hemolysis.* Toxins (Basel), 2010. **2**(12): p. 2824-36.
30. Gable, P., J. Eaton, and D. Confer. *INTOXICATION OF HUMAN PHAGOCYTES BY BORDETELLA ADENYLATE-CYCLASE TOXIN-IMPLICATION OF A GANGLIOSIDE RECEPTOR*. in *Clinical Research*. 1985. SLACK INC 6900 GROVE RD, THOROFARE, NJ 08086.
31. Gordon, V.M., et al., *Adenylate cyclase toxins from Bacillus anthracis and Bordetella pertussis. Different processes for interaction with and entry into target cells.* J Biol Chem, 1989. **264**(25): p. 14792-6.
32. Herlax, V., et al., *Relevance of fatty acid covalently bound to Escherichia coli alpha-hemolysin and membrane microdomains in the oligomerization process.* J Biol Chem, 2009. **284**(37): p. 25199-210.
33. Morova, J., et al., *RTX cytotoxins recognize beta2 integrin receptors through N-linked oligosaccharides.* Proc Natl Acad Sci U S A, 2008. **105**(14): p. 5355-60.
34. Mrówczyńska, L., et al., *Bordetella Adenylate Cyclase Toxin Can Bind Ganglioside GM1.* BIO, 2011. **1**: p. 67-71.
35. Munksgaard, P.S., et al., *Sialic acid residues are essential for cell lysis mediated by leukotoxin from Aggregatibacter actinomycetemcomitans.* Infect Immun, 2014. **82**(6): p. 2219-28.
36. Vazquez, R.F., et al., *Novel evidence for the specific interaction between cholesterol and α-haemolysin of Escherichia coli.* Biochem J, 2014. **458**(3): p. 481-9.
37. Erenburg, I.N., et al., *Heterologously secreted MbxA from Moraxella bovis induces a membrane blebbing response of the human host cell.* Scientific Reports, 2022. **12**(1): p. 17825.
38. Angelos, J.A., J.F. Hess, and L.W. George, *Cloning and characterization of a Moraxella bovis cytotoxin gene.* Am J Vet Res, 2001. **62**(8): p. 1222-8.
39. Angelos, J.A., J.F. Hess, and L.W. George, *An RTX operon in hemolytic Moraxella bovis is absent from nonhemolytic strains.* Vet Microbiol, 2003. **92**(4): p. 363-77.

40. Baptista, P.J., *Infectious bovine keratoconjunctivitis: a review.* Br Vet J, 1979. **135**(3): p. 225-42.
41. Beard, M.K. and L.J. Moore, *Reproduction of bovine keratoconjunctivitis with a purified haemolytic and cytotoxic fraction of Moraxella bovis.* Vet Microbiol, 1994. **42**(1): p. 15-33.
42. Clinkenbeard, K.D. and A.E. Thiessen, *Mechanism of action of Moraxella bovis hemolysin.* Infect Immun, 1991. **59**(3): p. 1148-52.
43. Henson, J.B. and L.C. Grumbles, *Infectious Bovine Keratoconjunctivitis .1. Etiology.* American Journal of Veterinary Research, 1960. **21**(84): p. 761-766.
44. Hess, J.F. and J.A. Angelos, *The Moraxella bovis RTX toxin locus mbx defines a pathogenicity island.* J Med Microbiol, 2006. **55**(Pt 4): p. 443-9.
45. Lorent, J., et al., *Plasma membranes are asymmetric in lipid unsaturation, packing and protein shape.* Nature chemical biology, 2020. **16**(6): p. 644-652.
46. Harris, F.M., K.B. Best, and J.D. Bell, *Use of laurdan fluorescence intensity and polarization to distinguish between changes in membrane fluidity and phospholipid order.* Biochimica et Biophysica Acta (BBA)-Biomembranes, 2002. **1565**(1): p. 123-128.
47. Sánchez, S.A., et al., *Laurdan generalized polarization: from cuvette to microscope.* Modern research and educational topics in microscopy, 2007. **2**: p. 1007-1014.
48. Kamel, M., et al., *Unsaturated fatty acids augment protein transport via the SecA: SecYEG translocon.* The FEBS journal, 2022. **289**(1): p. 140-162.
49. Wanderlingh, U., et al., *Molecular Dynamics of POPC Phospholipid Bilayers through the Gel to Fluid Phase Transition: An Incoherent Quasi-Elastic Neutron Scattering Study.* Journal of Chemistry, 2017. **2017**(1): p. 3654237.
50. Ulrich, A.S., M. Sami, and A. Watts, *Hydration of DOPC bilayers by differential scanning calorimetry.* Biochimica et Biophysica Acta (BBA)-Biomembranes, 1994. **1191**(1): p. 225-230.
51. Biltonen, R.L. and D. Lichtenberg, *The use of differential scanning calorimetry as a tool to characterize liposome preparations.* Chemistry and physics of lipids, 1993. **64**(1-3): p. 129-142.
52. Baumgart, T., S.T. Hess, and W.W. Webb, *Imaging coexisting fluid domains in biomembrane models coupling curvature and line tension.* Nature, 2003. **425**(6960): p. 821-824.

53. Gu, R.-X., S. Baoukina, and D.P. Tieleman, *Phase separation in atomistic simulations of model membranes.* Journal of the American Chemical Society, 2020. **142**(6): p. 2844-2856.

54. Matsuki, N.T., Masaki Goto, and Hitoshi, *Phase separation in phospholipid bilayers induced by cholesterol.* Encyclopedia of Biocolloid and Biointerface Science 2V Set, 2016: p. 825-840.

55. Coones, R.T., R. Green, and R. Frazier, *Investigating lipid headgroup composition within epithelial membranes: A systematic review.* Soft Matter, 2021. **17**(28): p. 6773-6786.

56. Brown, A.C., et al., *Aggregatibacter actinomycetemcomitans leukotoxin utilizes a cholesterol recognition/amino acid consensus site for membrane association.* Journal of Biological Chemistry, 2013. **288**(32): p. 23607-23621.

57. González Bullón, D., et al., *Cholesterol stimulates the lytic activity of Adenylate Cyclase Toxin on lipid membranes by promoting toxin oligomerization and formation of pores with a greater effective size.* Febs j, 2021.

58. Atapattu, D.N. and C.J. Czuprynski, *Mannheimia haemolytica leukotoxin binds to lipid rafts in bovine lymphoblastoid cells and is internalized in a dynamin-2-and clathrin-dependent manner.* Infection and immunity, 2007. **75**(10): p. 4719-4727.

59. Bumba, L., et al., *Bordetella adenylate cyclase toxin mobilizes its β2 integrin receptor into lipid rafts to accomplish translocation across target cell membrane in two steps.* PLoS pathogens, 2010. **6**(5): p. e1000901.

60. Erenburg, I., *Functional and structural characterization of the RTX proteins MbxA from Moraxella bovis and FrpA from Kingella kingae*. Dissertation, Düsseldorf, Heinrich-Heine-Universität, 2020.

61. Ostolaza, H. and J. Amuategi, *Membrane Interaction Characteristics of the RTX Toxins and the Cholesterol-Dependence of Their Cytolytic/Cytotoxic Activity.* International Journal of Molecular Sciences, 2024. **25**(6): p. 3131.

62. Shim, S.-H., et al., *Loss of function of rice plastidic glycolate/glycerate translocator 1 impairs photorespiration and plant growth.* Frontiers in Plant Science, 2020. **10**: p. 1726.

Supplementary figures

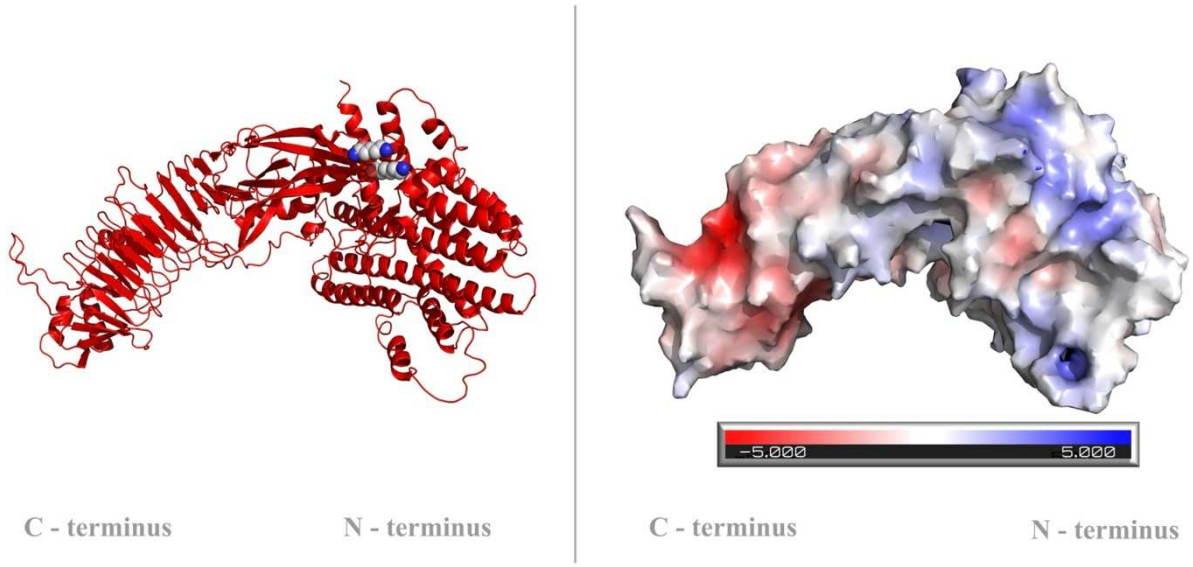

Supplementary Figure 1: *Left: Alpha fold model of proMbxA from a Small-Angle-X-ray-Scattering (SAXS). Right: Surface charge density model using the alpha fold model from SAXS measurement and PyMOL. Blue and red colors refer to positive and negative charges, respectively, as depicted in the figure on the right side.*

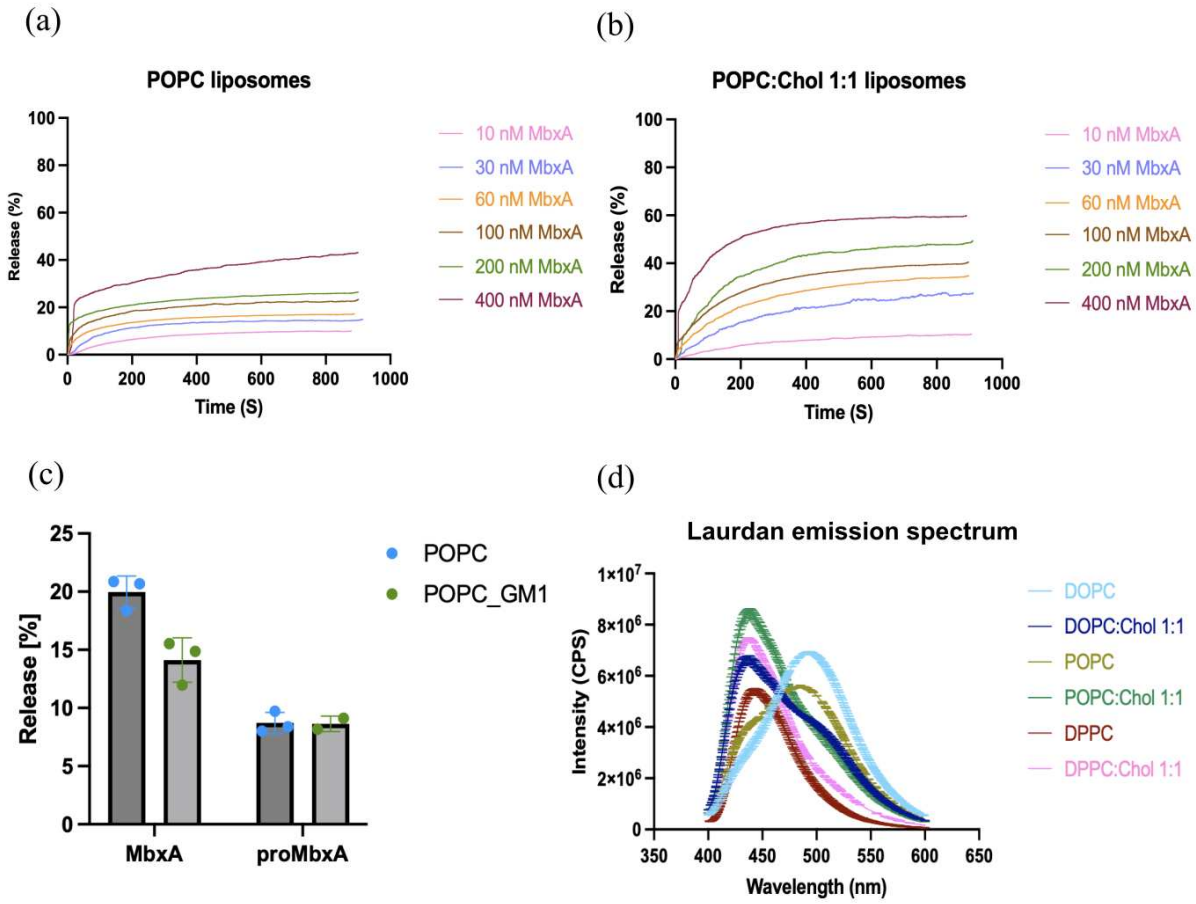

Supplementary Figure 2: *Panels (a&b) depict the time-based percentage release of liposomal content by the lytic activity of different MbxA concentrations of 10 nM, 30 nM, 60 nM, 100 nM, 200 nM & 400 nM on (a)12 μM POPC liposomes and (b) 12 μM POPC:Chol 1:1 liposomes. (c) The percentage of liposomal content released by the lytic activity of MbxA and proMbxA on 30% of GM1-incorporated liposomes. (d) Laurdan emission spectrum of liposomes of different lipid compositions from 400 nm to 600 nm at an excitation wavelength of 350 nm.*

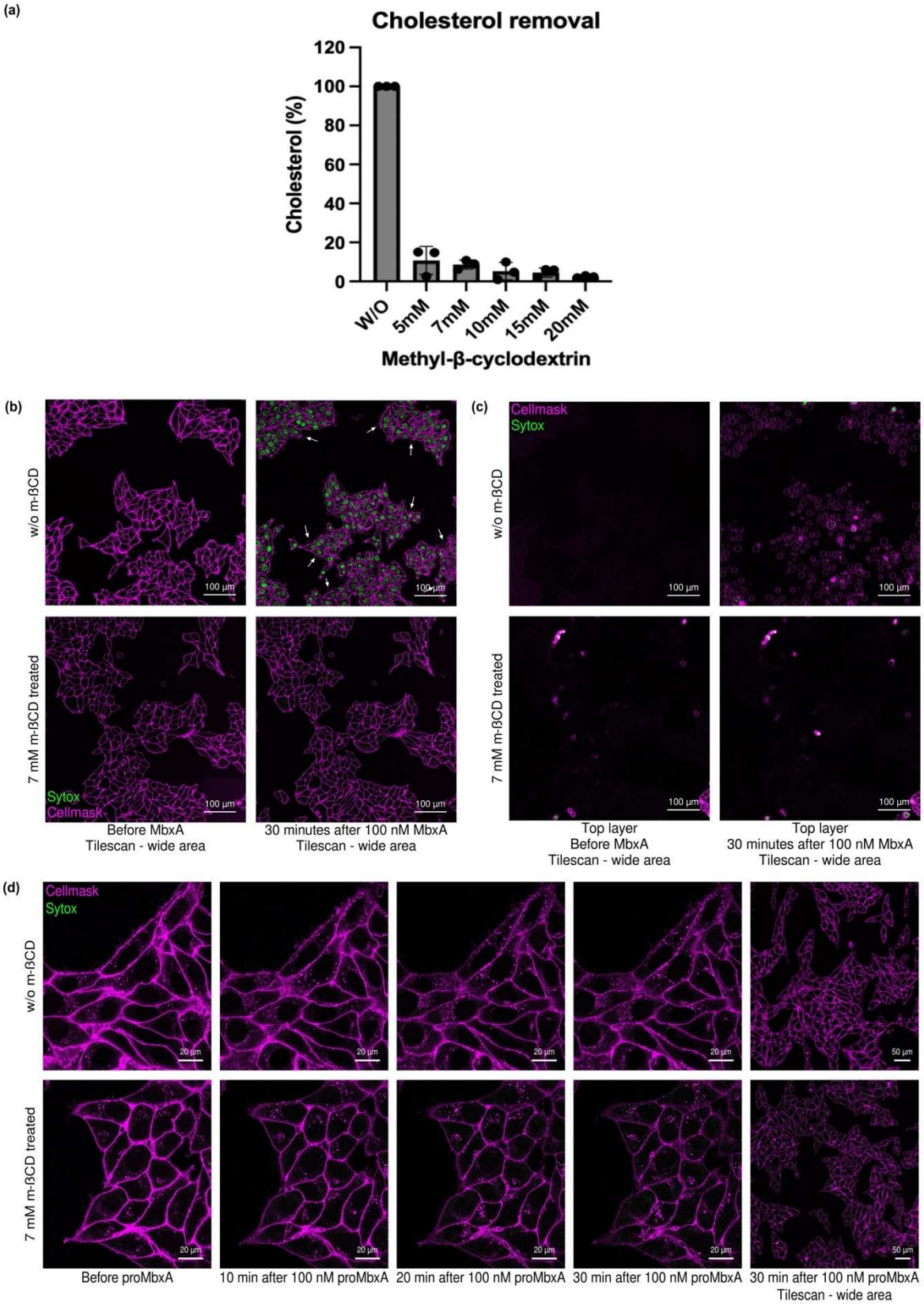

Supplementary Figure 3: *(a) Mass spectrometry data of cholesterol content in the HEp-2 cells when cholesterol was removed from HEp-2 cells using different concentrations of methyl beta-cyclodextrin. At 7mM Methyl-β-cyclodextrin, 8.6 +/- 2.3% of the initial cholesterol content was left. This equals, 2.2-3.9% of the 24.5% cholesterol*

reported in Hep-2 cells. (b) A wider area of HEp-2 cells showing membrane permeabilization and membrane blebbing phenotypes when cholesterol is intact (First row) and the absence of MbxA cytotoxicity when cholesterol is removed from HEp-2 cells; therefore, there is no membrane permeabilization nor membrane blebbing (Second row) when the cells are treated with 100 nM MbxA. (c) A layer above the HEp-2 cells provides a detailed view of the membrane blebs resulting from MbxA cytotoxicity when cholesterol is intact in HEp-2 cells (Upper row). At the same time, cholesterol-removed HEp-2 cells don't show membrane blebs upon MbxA incubation when cholesterol is removed from the HEp-2 cells (Lower row). (d) When HEp-2 cells are incubated with 100 nM proMbxA, both cholesterol-intact (Upper row) and cholesterol-removed (Lower row) HEp-2 cells were unable to induce membrane permeabilization nor membrane blebbing phenotypes.

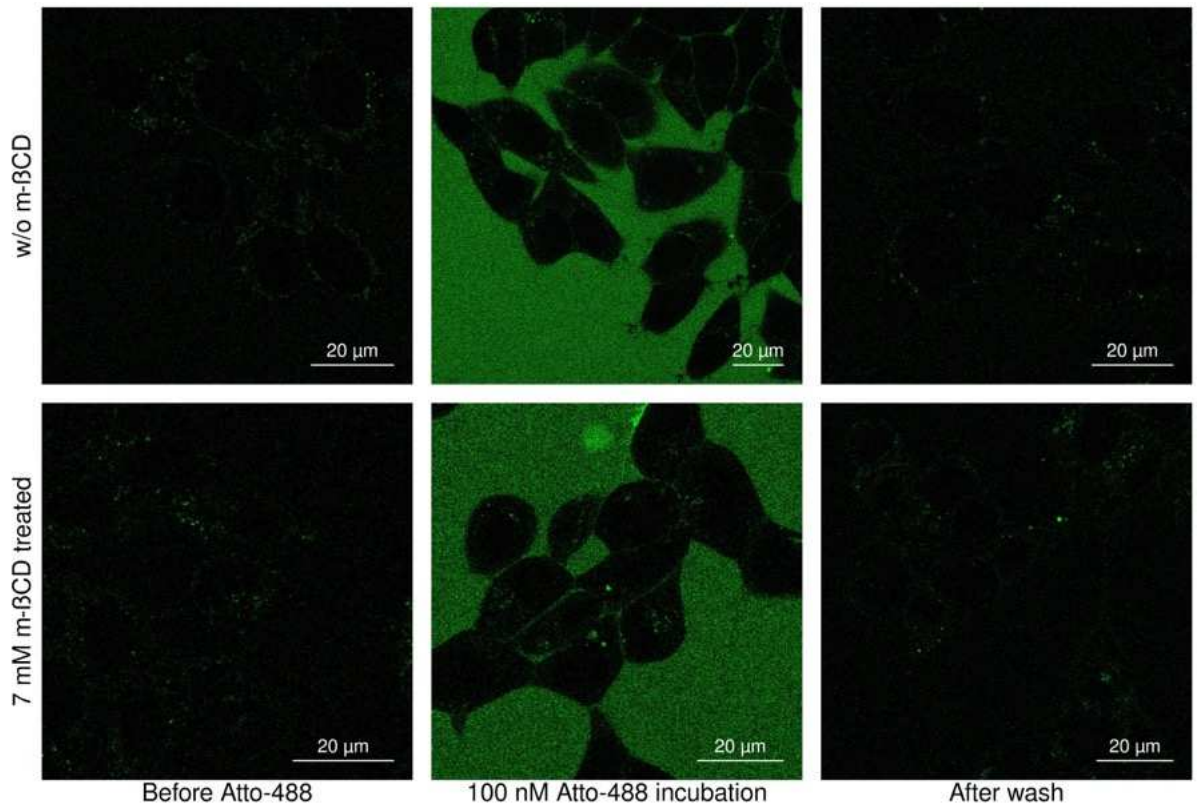

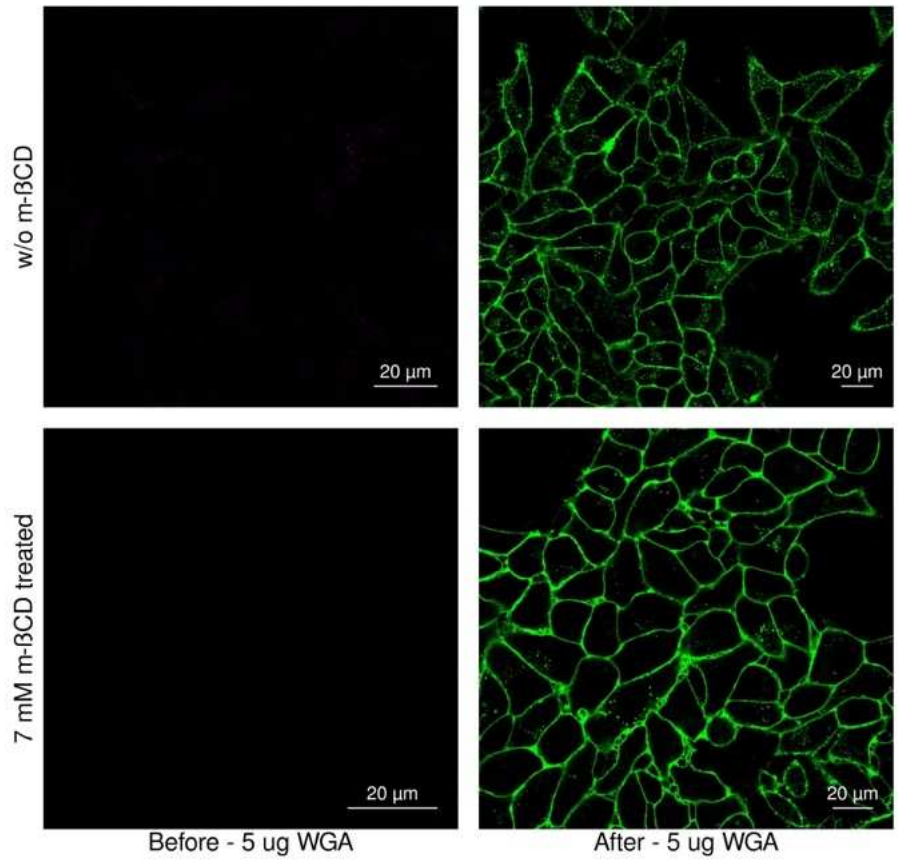

Supplementary Figure 4: *Control experiments by incubating 100 nM Atto-488 dye on (First row) cholesterol intact HEp-2 cells and (Second row) cholesterol removed HEp-2 cells; (left) before incubation, (middle) during incubation, (right) after washing excess dye using buffer. Control experiments by incubating 100 nM Wheat Germ*

Agglutinin (WGA) on (third row) cholesterol intact HEp-2 cells and (fourth row) cholesterol removed HEp-2 cells; (left) before incubation (right) 10 minutes after incubation.

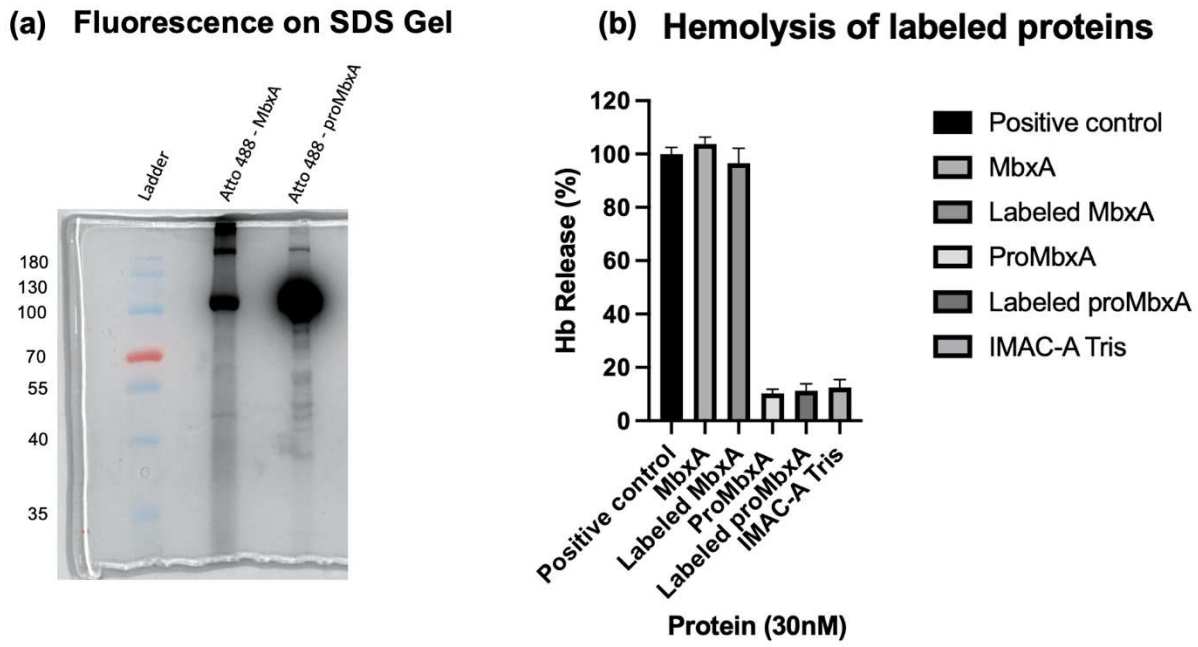

Supplementary Figure 5: *(a) 10% SDS gel showing the fluorescence of Atto-488-labeled MbxA^{S9C} and proMbxA^{S9C}. (b) Hemoglobin release assay showing the activity of proteins.*

Chapter 5

Biophysical and Structural Characterization of MbxA

Authors:	Feby Mariam Chacko, Jens Reiners, Athanasios Papadopoulos, Steven Hardwick, Ben F. Luisi, Sander H. J. Smits & Lutz Schmitt
Published in:	In preparation
Own work:	60%
Contribution:	Optimization of protein expression and secretion Protein purification Hemolytic activity & CD_{50} Analysis Preparation of figures Writing of the manuscript

Biophysical and Structural Characterization of MbxA

Feby Mariam Chacko[1], Jens Reiners[2], Athanasios Papadopoulos[2], Steven Hardwick[3], Ben F. Luisi[3], Sander H. J. Smits[1,2], Lutz Schmitt[1§]

[1] Institute of Biochemistry, Heinrich Heine University Düsseldorf, Universitätsstraße 1, 40225 Düsseldorf, Germany

[2] Center for Structural Studies, Heinrich Heine University Düsseldorf, Universitätsstraße 1, 40225 Düsseldorf, Germany

[3] Department of Biochemistry, University of Cambridge, Tennis Court Road, Cambridge CB21GA, UK

[§] Corresponding author: Lutz Schmitt, Institute of Biochemistry, Heinrich Heine University Düsseldorf, Universitätsstr. 1, 40225 Düsseldorf, Germany, E-Mail: lutz.schmitt@hhu.de

Abstract

This chapter presents a comprehensive biophysical and structural characterization of the RTX toxin MbxA, complementing the main mechanistic studies of this thesis. Functional assays confirmed the potent hemolytic activity of MbxA on sheep red blood cells, with a CD_{50} in the low nanomolar range. Multi-angle light scattering (MALS) analysis revealed that MbxA forms stable pentameric oligomers in solution, even after dilution. Small-angle X-ray scattering (SAXS) of proMbxA further supported a monomeric, elongated conformation with flexibility in the N-terminal region, as revealed by improved fits following SREFLEX refinement of AlphaFold models. Multiple single particle cryo-EM sample preparations, including membrane-associated and detergent-solubilized forms, failed to yield high-resolution reconstructions, and additional stabilization strategies such as chemical crosslinking and nanodisc incorporation were unsuccessful due to loss of activity or membrane lysis. Together, these data define key structural and functional properties of MbxA and document the experimental challenges of capturing its active state, laying the groundwork for future structural studies.

1. Introduction

While the main chapters of this thesis focus on mechanistic and functional insights into MbxA activity, several important datasets generated during this work did not directly fit into the two primary narratives. Nevertheless, these complementary experiments provide valuable context regarding the biophysical, functional, and structural properties of MbxA and its precursor form, proMbxA.

This chapter compiles and presents characterization data obtained through a range of methods, including hemolysis assays, multi-angle light scattering (MALS), single particle cryo-electron microscopy (cryo-EM), and small-angle X-ray scattering (SAXS). Together, these analyses contribute to a broader understanding of MbxA's lytic potential in red blood cells (RBCs), oligomeric behavior, solution structure, and efforts to structurally capture MbxA's interaction with lipid membranes, highlighting both the potential and the experimental limitations encountered.

2. Results

2.1. Functional Characterization of MbxA by Hemolytic Activity

To assess the lytic potential of MbxA on Red Blood Cells (RBCs), the half-maximal cytolytic concentration (CD_{50}) was determined using washed sheep red blood cells. Hemoglobin release into the supernatant serves as a direct indicator of red blood cell lysis, since membrane rupture leads to the rapid efflux of hemoglobin, which can be quantified spectrophotometrically. Serial dilutions of purified MbxA were incubated with RBCs at 37 °C for 30 minutes, and hemolysis was quantified by measuring absorbance at 544 nm. The data were fit to a three-parameter nonlinear regression model to determine the CD_{50} (Figure 1).

MbxA induced robust lysis of RBCs in a concentration-dependent manner, with a plateau in hemoglobin release observed beyond approximately 100 nM. The average CD_{50} value of MbxA was determined to be 5.53 ± 1.34 nM (mean ± SD) across three independent replicates, each fitted individually using nonlinear regression. These results confirm that MbxA is a potent RTX toxin capable of efficiently lysing RBCs at low nanomolar concentrations.

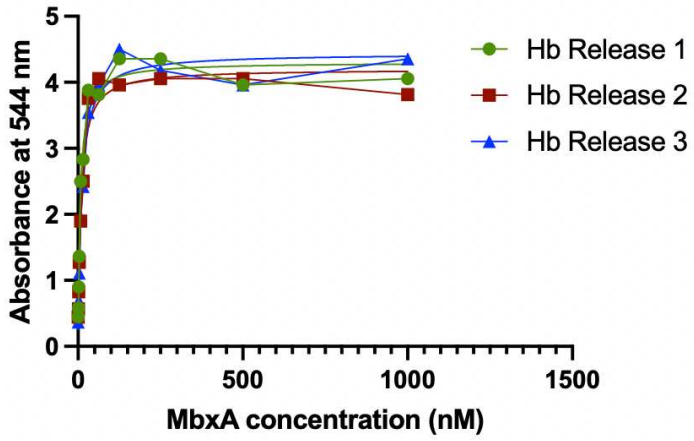

Figure 1. Hemolytic activity of MbxA on sheep RBCs. *Serial dilutions of acylated MbxA were incubated with sheep red blood cells for 30 minutes at 37 °C, and hemoglobin release was measured by absorbance at 544 nm. Each color-coded data set (green circles, red squares, blue triangles) represents an individual replicate, fitted with a nonlinear regression curve (plane curves with corresponding colors for each replicate). The calculated CD_{50} values for the three replicates were 4.28 nM, 5.39 nM, and 6.94 nM, respectively. The average CD_{50} across replicates was 5.53 ± 1.34 nM (mean ± standard deviation). Absorbance values reflect the release of hemoglobin and serve as an indirect indicator of red blood cell lysis.*

2.2. Biophysical Characterization of MbxA by SEC-MALS

To determine the oligomeric state of acylated MbxA in solution, size-exclusion chromatography coupled with multi-angle light scattering (SEC-MALS) was performed using two different protein concentrations. A high-concentration sample (1.31 mg/mL) was analyzed directly, and then diluted to 0.15 mg/mL to test whether oligomeric assembly persists upon dilution. This approach allowed us to assess the stability of oligomer formation under reduced concentration.

At high concentration, the UV chromatogram revealed a major elution peak between ~12-16 mL (Peak 1), with a minor secondary peak around 18 mL (Peak 2) (Figure 2a). Molar mass analysis indicated that Peak 1 corresponds to a molecular weight of approximately 491 kDa, consistent with a pentameric form of MbxA, whereas Peak 2 aligns with the monomeric mass (~99 kDa) (Figure 2a). The dRI signal was relatively low for Peak 1 but increased for Peak 2 (Figure 2b).

Following dilution of the same sample, the UV chromatogram displayed increased heterogeneity with multiple, less-defined peaks spanning ~10-25 mL (Figure 2c). Despite the increased peak overlap, molar mass analysis of Peak 1 yielded a value of approximately 462 kDa (Figure 2c), indicating that the oligomeric form remains largely intact even at lower concentration. Nonetheless, the dRI trace still exhibited a dominant peak near 20 mL (Figure 2d).

SDS-PAGE analysis of both samples confirmed the structural integrity of MbxA, with a prominent band corresponding to the expected monomeric size (~100 kDa) observed in each (Figure 2e). These results demonstrate that MbxA forms stable oligomeric assemblies in solution and that the oligomeric state persists upon dilution.

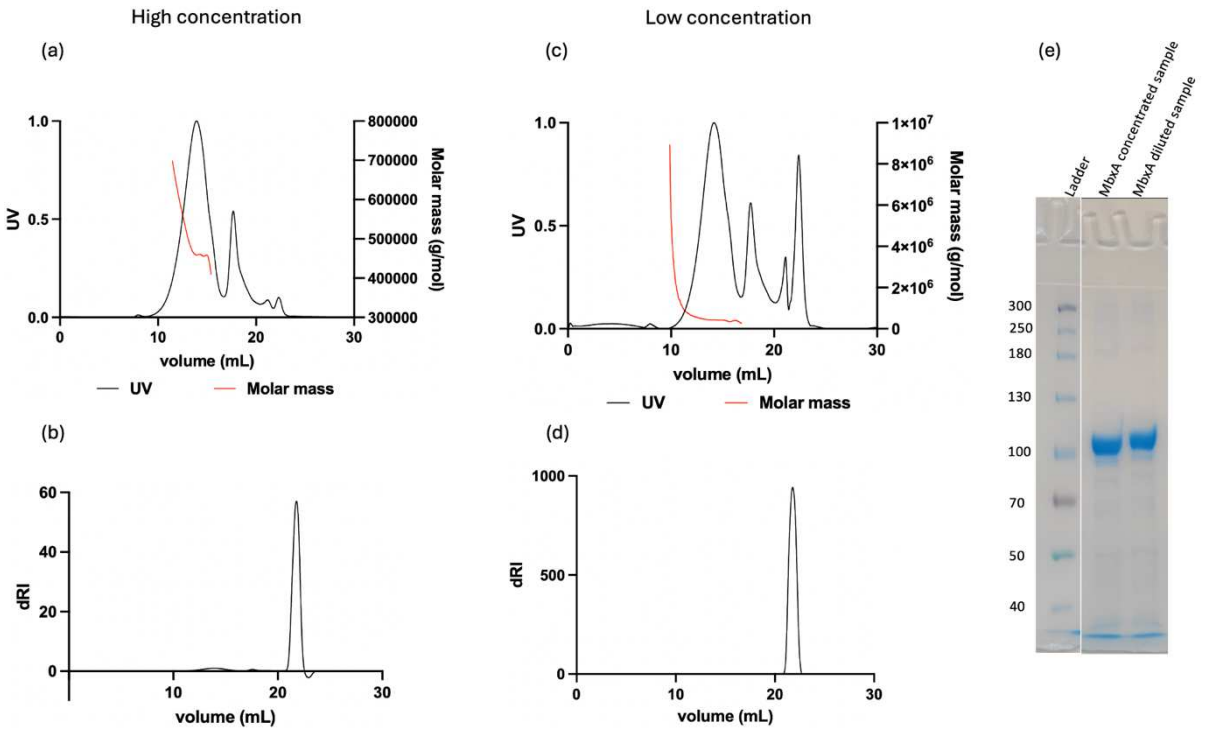

Figure 2. SEC-MALS and SDS-PAGE analysis of MbxA reveals stable oligomeric species. (a,b) *High concentration (1.31 mg/mL):* ***(a)*** *Left Y-axis: UV absorbance trace showing a main elution peak at ~12–16 mL (Peak 1) and a smaller late-eluting peak (Peak 2), Right Y-axis: Molar mass profile of Peak 1 indicates an average molecular weight of ~491 kDa.* ***(b)*** *dRI trace, with a prominent signal at ~20 mL.* ***(c,d)*** *Low concentration (0.15 mg/mL):* ***(c)*** *Left Y-axis: UV trace shows increased heterogeneity across a broader volume range, Right Y-axis: Molar mass of Peak 1 is consistent with ~462 kDa, suggesting preserved oligomeric structure.* ***(d)*** *dRI trace highlights a major peak near ~20 mL.* ***(e)*** *SDS-PAGE analysis of the injected samples confirms the purity of MbxA, with a prominent band corresponding to the monomeric size (~100 kDa) in both concentrated and diluted preparations.*

2.3. Single particle cryo-EM Attempts to Resolve MbxA Structure

Single particle cryo-EM was employed to investigate the structural organization of MbxA under various conditions. Although several different grid and buffer conditions were explored during the project, three representative sample preparations are included here to document the experimental strategy and highlight the limitations encountered.

Sample 1, consisting of proMbxA alone, resulted in heterogeneous particle distributions. The micrographs revealed aggregated particles with poor dispersion and no consistent morphological features (Figure 3a).

Sample 2 included MbxA pre-incubated with POPC:Chol 1:1 liposomes to investigate its pore-forming ability in a lipid environment. Although the micrographs showed large vesicle-like

structures, possibly representing intact or partially disrupted liposomes, no noticeable MbxA-associated densities were resolved (Figure 3b).

Sample 3 involved MbxA solubilized in CHAPSO detergent. While this preparation showed improved dispersion and reduced aggregation in raw micrographs, it did not yield interpretable 2D class averages. Nevertheless, it was the only sample for which 2D classification was performed, and is therefore shown here (Figure 4). The absence of structural features in the resulting classes suggests a high degree of conformational flexibility or insufficient structural homogeneity under the tested conditions.

Taken together, these data illustrate the extensive attempts made to resolve MbxA structure by cryo-EM, and the challenges in stabilizing this protein complex for single-particle analysis.

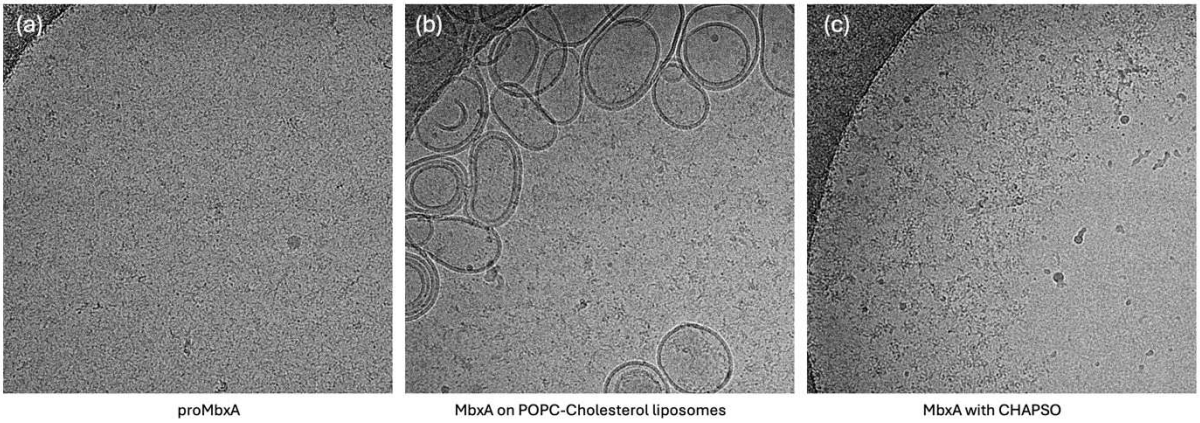

Figure 3. Cryo-EM micrographs of MbxA under three conditions. (a) *proMbxA applied to Quantifoil R1.2/1.3 Cu grids appears aggregated and poorly dispersed, with no consistent particle morphology.* ***(b)*** *MbxA incubated with POPC:Chol liposomes reveals large vesicular structures, but no visible MbxA pore complexes.* ***(d)*** *MbxA prepared with CHAPSO detergent.*

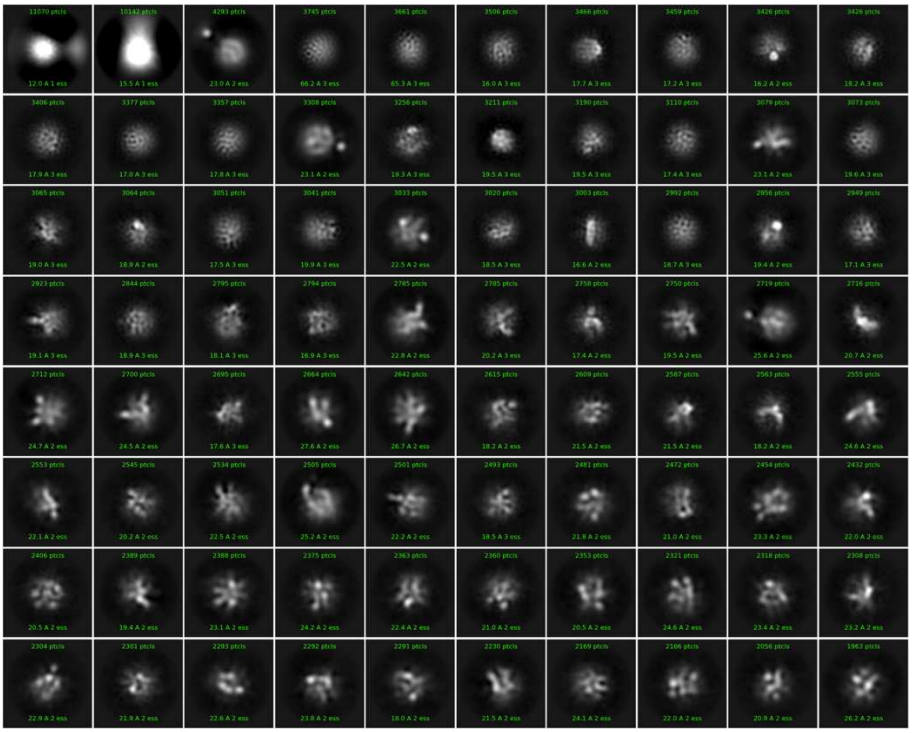

Figure 4. *2D class averages of MbxA prepared with CHAPSO detergent. Micrographs were processed using RELION-3.0. Sample 3, which showed improved particle distribution when prepared in the presence of CHAPSO, was selected for 2D classification as a preliminary structural analysis. Despite extensive particle picking and alignment, no structurally interpretable class averages were obtained, indicating a lack of well-defined orientation or structural homogeneity.*

2.4. Solution Conformation of proMbxA Assessed by SEC-SAXS

SEC-SAXS analysis of proMbxA was performed to investigate its structural properties in solution. The chromatogram revealed distinct elution peaks corresponding to dimeric and monomeric species, with the monomeric fraction used for analysis (Figure 5A). Guinier and *p(r)* analysis yielded an Rg of ~3.9 nm and Dmax of 13.4 nm, indicating an elongated, non-globular particle (Figure 5C–D). The dimensionless Kratky plot showed a bell-shaped curve that deviates from the ideal compact shape, consistent with structural flexibility (Figure 5E).

Molecular mass estimates from Porod volume, MoW2 [1], Bayesian inference [2], and Vc [3] were all in the range of ~87–104 kDa, in agreement with the expected monomeric mass from sequence (99.7 kDa).

Five AlphaFold-predicted models of proMbxA were compared against the experimental data using CRYSOL [4], but all showed poor agreement with χ^2 values between 10.1 and 18.8 (Figure 6, left). The discrepancy was attributed to variability and disorder in the predicted N-

terminal region. To address this, the top-ranking AlphaFold model was refined using SREFLEX, which applies normal mode analysis to introduce flexibility and optimize model fit to SAXS data [5]. The refined model showed significantly improved agreement with the experimental data ($\chi^2 = 1.18$) and a rearranged N-terminal domain (Figure 6, center).

An ab initio envelope was generated using GASBOR [6], and the SREFLEX-refined model fit well within this volume, confirming a consistent overall shape (Figure 7). Superposition of the GASBOR envelope with the refined model using SUPCOMB [7] showed volumetric agreement, supporting the presence of an extended monomer with flexible terminal regions in solution.

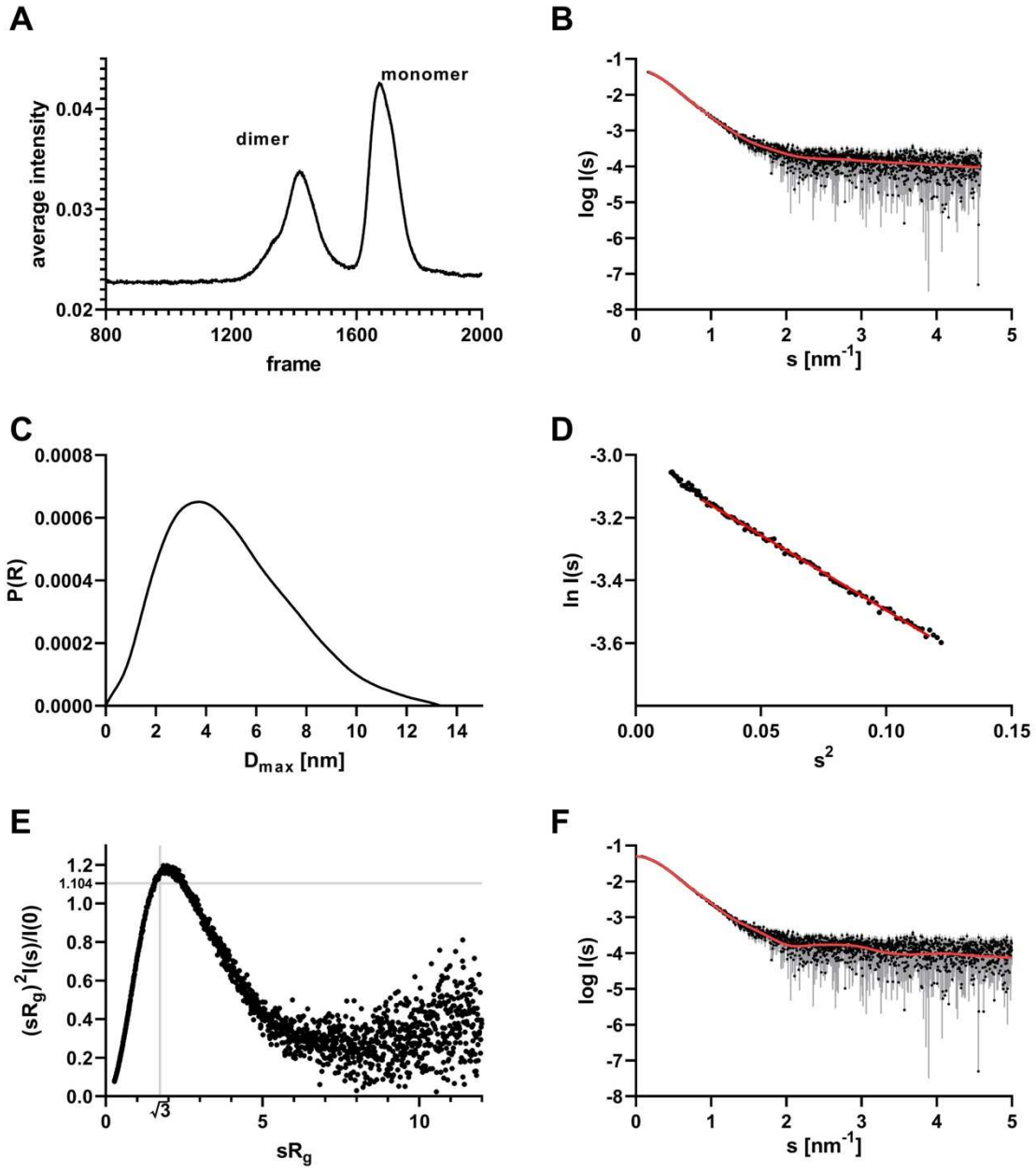

Figure 5. SEC-SAXS analysis of proMbxA reveals an extended monomeric conformation. ***(A)*** *SEC-SAXS intensity trace with dimer and monomer peaks; only the monomer was used for analysis.* ***(B)*** *Experimental scattering curve (black) with GASBOR model fit (red),* $\chi^2 = 1.19$. ***(C)*** *Distance distribution function p(r), indicating a Dmax of 13.4 nm.* ***(D)*** *Guinier plot used to determine Rg (~3.8 nm).* ***(E)*** *Dimensionless Kratky plot suggests partial flexibility.* ***(F)*** *SAXS fit for SREFLEX-refined AlphaFold model,* $\chi^2 = 1.18$.

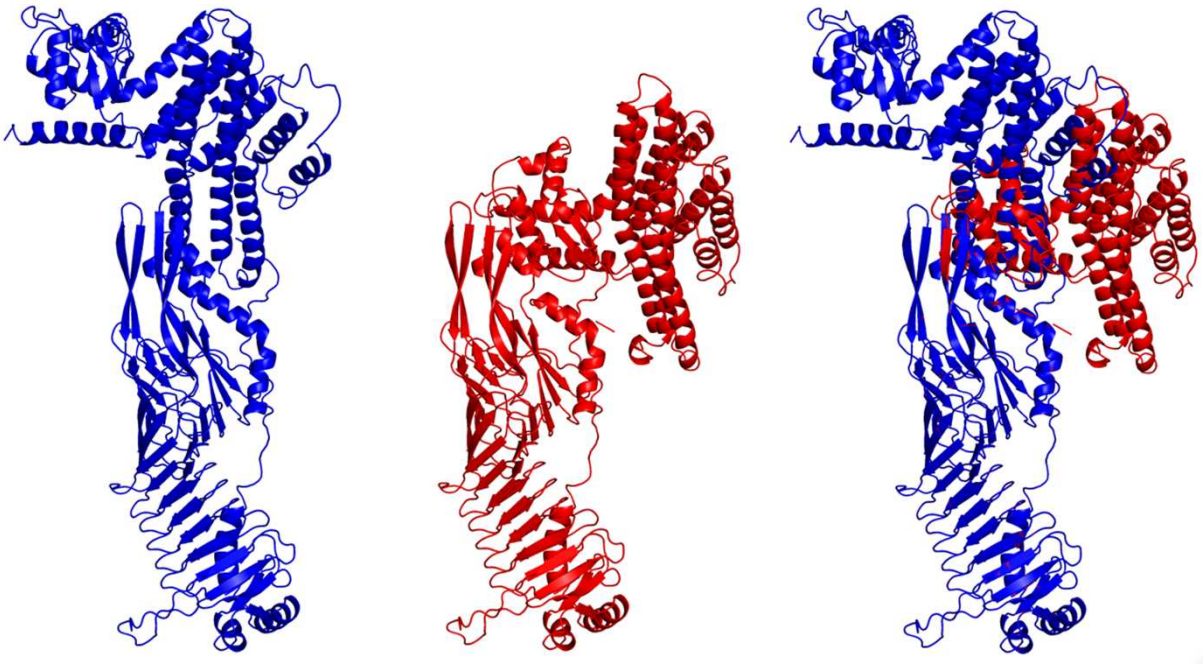

Figure 6. Structural model refinement of proMbxA. *Left: AlphaFold-predicted model of proMbxA (blue) did not fit SAXS data well. Center: SREFLEX-refined model (red) corrected N-terminal flexibility and improved SAXS fit. Right: Overlay of AlphaFold (blue) and SREFLEX (red) models showing structural rearrangement.*

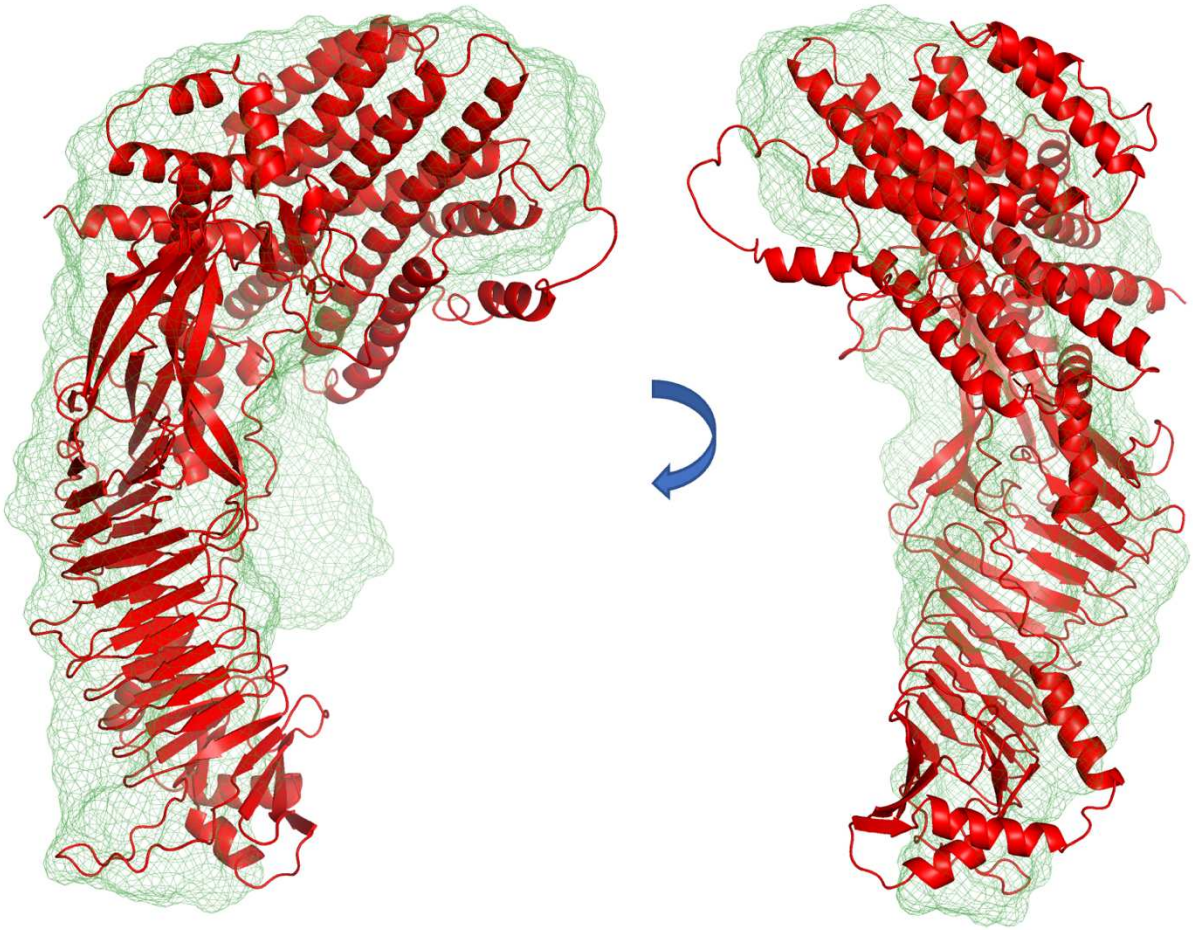

Figure 7. Structural validation of the SREFLEX model using ab initio SAXS envelope. *Superimposition of the SREFLEX-refined proMbxA model (red) with the GASBOR ab initio envelope (green mesh), showing excellent volumetric agreement across multiple orientations.*

3. Discussion

The data presented in this chapter offer a broader biochemical and structural view of MbxA and its precursor form, proMbxA, complementing the main mechanistic stories of this thesis. Functional assays confirmed MbxA's potency in lysing red blood cells, with a CD_{50} in the low nanomolar range.

Biophysical characterization by SEC-MALS revealed the presence of stable oligomeric assemblies, particularly pentamers, that persisted even after dilution, suggesting that oligomerization is not merely concentration-dependent but may represent a stable conformation in solution. SAXS analysis of proMbxA further provided low-resolution insight into its extended, monomeric conformation. While AlphaFold models initially failed to recapitulate the SAXS data due to flexibility in the N-terminal region, refinement using

SREFLEX improved the fit and revealed conformational adjustments consistent with experimental observations.

Despite these successes, efforts to resolve the high-resolution structure of MbxA by cryo-EM faced significant challenges. Multiple sample preparations were screened, including membrane-bound and detergent-solubilized forms, but none yielded suitable datasets for 3D reconstruction. 2D classification of a CHAPSO-containing sample revealed monodisperse but unstructured particles.

Additional strategies were explored to stabilize MbxA for structural studies. Crosslinking was attempted to preserve oligomeric assemblies; however, this approach abolished the protein's lytic activity on sheep red blood cells, likely by interfering with conformational changes necessary for pore formation. Another approach involved reconstitution into MSP2N2 nanodiscs containing different lipid compositions (POPC, POPC:Chol 1:1, POPS). While nanodisc assembly was successful, the addition of MbxA resulted in lipid disruption rather than stable insertion, suggesting that MbxA lysed the nanodisc membranes instead of incorporating into them to form stable pores. These outcomes suggest that MbxA’s membrane interaction is rapid and destructive, complicating its capture in defined structural states for cryo-EM studies. Future work may benefit from strategies that reduce conformational flexibility or stabilize functional intermediates, such as using neutralizing antibodies or receptor mimics to trap MbxA in structurally homogeneous states suitable for single-particle reconstruction. Despite these challenges, the data presented here provide a comprehensive biophysical and functional characterization of MbxA, laying the foundation for future structure-function studies.

4. Materials & Methods

4.1. Hemoglobin Release Assay for CD_{50} Determination

Preparation of Washed Sheep Red Blood Cells (RBCs):

Defibrinated sheep blood (Oxoid) was used as the source of RBCs. One milliliter of whole blood was transferred into 1.5 mL microcentrifuge tubes and centrifuged at 14,000 × *g* for 1 minute at room temperature. The supernatant was discarded, and the cell pellet was resuspended in wash buffer containing 10 mM Tris-HCl (pH 7.5), 155 mM NaCl, 20 mM $CaCl_2$, 5 mM KCl, and 2 mM $MgSO_4$ by brief vortexing (5-10 seconds). This wash step was repeated until the supernatant became colorless, indicating the removal of free hemoglobin. The washed RBCs were pooled into a 50 mL Falcon tube to ensure homogeneous distribution and were used immediately in the hemolysis assay.

Hemolysis Assay Setup:

To assess the hemolytic activity of MbxA, 278 µL of the freshly washed RBC suspension was aliquoted into each well of the first three rows of a deep 96-well plate (Plate A), using a multichannel pipette. All measurements were performed in triplicate. In a separate 96-well plate (Plate B), 50 µL of MbxA stock solution (1.36 mg/mL) was added to wells A1-C1. A two-fold serial dilution of MbxA was carried out across the remaining wells in these rows by sequentially transferring 25 µL of protein solution into 25 µL of Buffer A (50 mM Tris-HCl pH 7.8, 400 mM NaCl, 10 mM $CaCl_2$). Buffer A served as the negative control, and 1 µL of 16% SDS was used in two wells as the positive control for complete lysis (row 4).

Next, 22 µL of each serially diluted MbxA sample from Plate B was transferred into the corresponding wells of Plate A. For the controls, 22 µL of Buffer A (negative control) or SDS (positive control) was added to designated wells. The plates were incubated for 30 minutes at 37 °C. Following incubation, the plates were centrifuged for 3 minutes at 5,200 × *g* to pellet intact cells.

Measurement of Hemolysis:

From each well of Plate A, 20 µL of the supernatant was transferred into 180 µL of wash buffer in a flat-bottom 96-well plate. The release of hemoglobin was quantified by measuring

absorbance at 544 nm using a FLUOstar OPTIMA microplate reader (BMG Labtech). The percentage of hemolysis relative to the SDS control was calculated, and the CD_{50} value was determined by fitting each dataset using nonlinear regression in GraphPad Prism, applying a three-parameter logistic equation:

$$Y = \text{Bottom} + (\text{Top} - \text{Bottom}) / (1 + (X / CD_{50}))$$

where *Y* is the absorbance at 544 nm (indicating hemoglobin release), *X* is the MbxA concentration (in nM), *Bottom* and *Top* represent the minimum and maximum absorbance values, and **CD_{50}** is the concentration of MbxA that results in 50% of the maximal response. The curve assumes a fixed Hill slope of 1.

4.2. Size-Exclusion Chromatography Coupled with Multi-Angle Light Scattering (SEC-MALS)

Protein Preparation:

Recombinant MbxA was expressed and purified by immobilized metal ion affinity chromatography (IMAC). Briefly, solubilized MbxA was refolded by dropwise dilution from 6 M to 400 mM urea in IMAC buffer (50 mM Tris-HCl pH 7.8, 400 mM NaCl, 10 mM $CaCl_2$) under constant stirring at room temperature. The refolded protein was loaded onto a 5 mL Ni^{2+}-charged HiTrap IMAC HP column (Cytiva!) and eluted with a linear imidazole gradient (0-75 mM) in the same buffer. Elution fractions containing MbxA were pooled, concentrated using Amicon Ultra-15 centrifugal filter units (50 kDa MWCO; Merck Millipore), and desalted using a PD-10 column (GE Healthcare) equilibrated with IMAC buffer.

SEC-MALS Analysis:

Two types of samples were analyzed:

- Concentrated sample: MbxA at 1.31 mg/mL
- Diluted sample: The same sample diluted post-concentration to 0.15 mg/mL

Prior to injection, the concentrated sample was centrifuged at 100,000 × *g* for 45 minutes at 4 °C, and the diluted sample was centrifuged at 17,000 × *g* for 10 minutes at 4 °C to remove any aggregates or particulates.

For each run, 220-320 µL of sample was injected into a size-exclusion chromatography system equipped with a Superdex 200 Increase 10/300 GL column (Cytiva), pre-equilibrated with IMAC buffer. The column was connected in line to a miniDAWN TREOS II triple-angle light scattering detector (Wyatt Technologies) and an Optilab T-rEX differential refractive index detector (Wyatt Technologies). The setup was performed using an Agilent 1260 HPLC system with a flow rate of 0.6 mL/min.

Data Processing:

Light scattering and refractive index signals were recorded in real-time, and molar mass calculations were performed using ASTRA software (Wyatt Technology), applying Zimm's model and assuming a dn/dc of 0.185 mL/g for protein [8]. Molecular weight distributions were calculated across the elution peaks and reported as weight-averaged molar masses.

4.3. Single particle cryogenic Electron Microscopy (cryo-EM)

Single particle cryo-EM specimen preparation and data collection were performed at the Department of Biochemistry, University of Cambridge, in the laboratory of Prof. Ben Luisi. All cryo-EM data and images were kindly provided by Dr. Steven Hardwick. Multiple experimental conditions were screened for structure determination of MbxA. Among these, three representative samples are included in this thesis to illustrate the methodological attempts and the challenges encountered. IMAC-purified Pro(MbxA) samples stored at -180 °C were further purified via size-exclusion chromatography using a Superose-6 column, following the protocol described by Erenburg et al. (2022) [9]. Freshly eluted protein was used immediately for grid preparation.

- Sample 1**:** proMbxA at 0.26 mg/mL was applied to glow-discharged Quantifoil R1.2/1.3 Cu 300 mesh grids using a 3-second blot time and blot force -5.
- Sample 2: MbxA (100 nM) was pre-incubated with 12 µM POPC:Chol 1:1 liposomes for 1 minute before application to Quantifoil R1.2/1.3 + 2 nm C Cu 300 mesh grids and flash-frozen to preserve membrane interactions. Blot force was -5.
- Sample 3: MbxA at 1.2 mg/mL was mixed with 200 nM CHAPSO detergent and applied to Ultrafoil R1.2/1.3 Au 300 mesh grids with a blot force of -5.

Cryo-EM grids were glow-discharged using a Quorum Emitech K100X glow discharger. Negative glow discharge was applied using argon gas at 25 mA for 2 minutes to render the grid surface hydrophilic and ensure optimal sample spreading. Subsequently, grids were plunge-frozen in liquid ethane with a Vitrobot Mark IV (FEI). Screening was performed using a Talos Arctica 200 kV transmission electron microscope (ThermoFisher Scientific), and data collection was carried out on a Talos Arctica or Titan Krios instrument (ThermoFisher Scientific). Image processing and 2D classification were performed using RELION-3.0 [10, 11]. Of the three conditions shown, only Sample 3 underwent 2D classification, primarily as a preliminary analysis. No high-resolution structures were obtained from any of the samples.

4.4. Small-Angle X-ray Scattering (SAXS)

SEC-SAXS measurements were carried out at the P12 beamline of the PETRA III synchrotron (DESY, Hamburg, Germany) [12]. ProMbxA was injected at a concentration of 5.3 mg/mL onto a Superose 6 Increase 10/300 column (GE Healthcare) equilibrated in 50 mM Tris-HCl pH 7.8, 100 mM NaCl, and 10 mM $CaCl_2$. The sample was measured at 20 °C with a flow rate of 0.5 mL/min, and scattering data were collected using a PILATUS 6M detector positioned 3.0 m from the sample, covering a momentum transfer range of 0.03–5.8 nm^{-1}.

Frames were recorded continuously (3000 total) with 0.995 s exposure time per frame. Primary data reduction and buffer subtraction were carried out using CHROMIXS [13] and PRIMUS [14], followed by Guinier analysis to determine the radius of gyration (Rg). The distance distribution function *p(r)* and maximum particle dimension (Dmax) were calculated using GNOM [15].

Low-resolution ab initio shape modeling was performed using GASBOR [6]. Structural fits were evaluated by comparing experimental scattering curves to models predicted by AlphaFold [16, 17] using CRYSOL [4]. Due to poor initial agreement, flexible fitting was applied to the AlphaFold model using SREFLEX [5], which performs normal mode analysis to optimize fit to the scattering data. Model superimpositions were visualized and compared using SUPCOMB [7], and structural ambiguity was assessed with AMBIMETER [18].

5. References

1. Fischer, H., et al., *Determination of the molecular weight of proteins in solution from a single small-angle X-ray scattering measurement on a relative scale.* Applied Crystallography, 2010. **43**(1): p. 101-109.
2. Hajizadeh, N.R., et al., *Consensus Bayesian assessment of protein molecular mass from solution X-ray scattering data.* Scientific reports, 2018. **8**(1): p. 7204.
3. Rambo, R.P. and J.A. Tainer, *Accurate assessment of mass, models and resolution by small-angle scattering.* Nature, 2013. **496**(7446): p. 477-481.
4. Svergun, D., C. Barberato, and M.H. Koch, *CRYSOL–a program to evaluate X-ray solution scattering of biological macromolecules from atomic coordinates.* Applied Crystallography, 1995. **28**(6): p. 768-773.
5. Panjkovich, A. and D.I. Svergun, *Deciphering conformational transitions of proteins by small angle X-ray scattering and normal mode analysis.* Physical Chemistry Chemical Physics, 2016. **18**(8): p. 5707-5719.
6. Svergun, D.I., M.V. Petoukhov, and M.H. Koch, *Determination of domain structure of proteins from X-ray solution scattering.* Biophysical journal, 2001. **80**(6): p. 2946-2953.
7. Kozin, M.B. and D.I. Svergun, *Automated matching of high-and low-resolution structural models.* Applied Crystallography, 2001. **34**(1): p. 33-41.
8. Wyatt, P.J., *Light scattering and the absolute characterization of macromolecules.* Analytica chimica acta, 1993. **272**(1): p. 1-40.
9. Erenburg, I.N., et al., *Heterologously secreted MbxA from Moraxella bovis induces a membrane blebbing response of the human host cell.* Scientific Reports, 2022. **12**(1): p. 17825.
10. Scheres, S.H., *RELION: implementation of a Bayesian approach to cryo-EM structure determination.* Journal of structural biology, 2012. **180**(3): p. 519-530.
11. Zivanov, J., et al., *New tools for automated high-resolution cryo-EM structure determination in RELION-3.* elife, 2018. **7**: p. e42166.
12. Blanchet, C.E., et al., *Versatile sample environments and automation for biological solution X-ray scattering experiments at the P12 beamline (PETRA III, DESY).* Applied Crystallography, 2015. **48**(2): p. 431-443.
13. Panjkovich, A. and D.I. Svergun, *CHROMIXS: automatic and interactive analysis of chromatography-coupled small-angle X-ray scattering data.* Bioinformatics, 2018. **34**(11): p. 1944-1946.

14. Konarev, P.V., et al., *PRIMUS: a Windows PC-based system for small-angle scattering data analysis.* Applied crystallography, 2003. **36**(5): p. 1277-1282.
15. Svergun, D., *Determination of the regularization parameter in indirect-transform methods using perceptual criteria.* Applied Crystallography, 1992. **25**(4): p. 495-503.
16. Jumper, J., et al., *Highly accurate protein structure prediction with AlphaFold.* nature, 2021. **596**(7873): p. 583-589.
17. Mirdita, M., et al., *ColabFold: making protein folding accessible to all.* Nature methods, 2022. **19**(6): p. 679-682.
18. Petoukhov, M.V. and D.I. Svergun, *Ambiguity assessment of small-angle scattering curves from monodisperse systems.* Biological Crystallography, 2015. **71**(5): p. 1051-1058.

4. Discussion

4.1. Overview of Key Findings

This thesis investigates the structure, function, and membrane-targeting behavior of the RTX toxin MbxA, an uncharacterized virulence factor encoded by *Moraxella bovis*. Despite its genomic resemblance to the well-studied HlyA from *Escherichia coli*, MbxA had not previously been examined at the molecular level. The work herein establishes a mechanistic framework for understanding how MbxA interacts with host cell membranes, and induces cytotoxicity in mammalian cells. Using a combination of heterologous expression, biophysical analysis, lipid model systems, and cell-based assays, this thesis defines MbxA as a cholesterol-dependent, acylation-activated RTX toxin that disrupts epithelial plasma membranes.

The recombinant expression and purification of MbxA and its inactive precursor, proMbxA, using the HlyA secretion system in *E. coli* was established by Isabelle N Erenburg, which allowed the differential acylation, efficient secretion, protein folding in a Ca^{2+}-rich extracellular environment, and further purification of (pro)MbxA. This strategy enabled subsequent biochemical and molecular characterization of (pro)MbxA and demonstrated that post-translational acylation at two conserved lysine residues is essential for MbxA's cytolytic function, mirroring activation mechanisms described for other RTX toxins [28, 120].

The second objective focused on characterizing the cytotoxic activity of MbxA in epithelial cells. Acylated MbxA induced rapid membrane permeabilization, Ca^{2+} elevation, mitochondrial depolarization, and nuclear shrinkage in HEp-2 cells. Notably, these effects occurred without signs of apoptotic execution, such as PARP cleavage, suggesting a Ca^{2+}-driven necrotic mechanism. Sublytic concentrations of MbxA led to its internalization into intact cells, while higher concentrations caused irreversible membrane damage and blebbing.

In parallel, the role of membrane lipids in MbxA's cytolytic mechanism was examined using artificial liposomes and supported lipid bilayers. These experiments revealed that MbxA activity is strongly enhanced by cholesterol, both in vitro and in live-cell contexts, but that cholesterol is not required for membrane binding. Acylation as well was not required for membrane binding; however, it was essential for membrane insertion and pore formation. Biophysical analyses demonstrated that acylated MbxA assembles into stable oligomeric complexes in solution, while its precursor remains monomeric and flexible.

Collectively, this work shows that MbxA is a potent RTX cytotoxin with distinct functional and mechanistic features. It targets membranes via a cholesterol-facilitated, receptor-independent process (shown by lytic activity in liposomes and ß$_2$ integrin-negative HEp-2 cells and RBCs) and induces non-apoptotic cell death in HEp-2 cells. These findings not only advance our understanding of MbxA's role in *M. bovis* virulence but also expand the broader paradigm of RTX toxin biology by highlighting lipid-based targeting as a central determinant of function.

4.2. MbxA Secretion, Acylation, and Structural Characteristics

The functional activity of RTX toxins depends on a series of precisely coordinated post-translational events that include acylation, secretion, and Ca^{2+}-dependent folding [7, 27]. In this context, the work presented here establishes that MbxA, a putative RTX toxin from *Moraxella bovis*, follows this canonical model exhibited by other prototypical RTX family members such as HlyA, CyaA, and LtxA [7, 27].

MbxA was successfully heterologously expressed in *E. coli* using the hemolysin A (HlyA) type I secretion system (T1SS), and both the acylated (mature) and non-acylated (pro) forms were secreted in an unfolded state into the extracellular medium. As with other RTX proteins, Ca^{2+} in the extracellular environment facilitated folding via the characteristic β-roll structure formed by the C-terminal nonapeptide repeats. While this behavior resembles *E. coli* HlyA and *Bordetella pertusis* CyaA, the functional differentiation between proMbxA and acylated MbxA was particularly interesting in both *in vitro* and cellular assays [40, 64, 121].

The post-translational activation of MbxA was shown to occur by the acylation of two conserved internal lysine residues, K536 and K660, mediated by the acyltransferase HlyC. Mass spectrometry identified myristoylation (C14) and, to a lesser extent, hydroxylated acyl chains on both residues. This is consistent with findings for HlyA, in which K564 and K690 undergo similar modifications catalyzed by HlyC, and where dual acylation is essential for pore-forming activity [20, 49-51, 53]. Likewise, in CyaA, acylation of K860 and K983 enhances membrane insertion and host cell binding [18, 31, 59, 122], and in RtxA and LtxA, the addition of saturated or hydroxylated fatty acids is required for full cytotoxicity [92, 123]. In all cases, the absence of acylation results in a loss of pore-forming activity, underscoring the functional centrality of this lipid modification. For MbxA, this is further reinforced by liposome

and GUV assays, which demonstrated that non-acylated proMbxA could bind to membranes but failed to induce leakage or structural deformation.

The structural features of MbxA were further investigated using a combination of AlphaFold predictions and experimental small-angle X-ray scattering (SAXS) investigations. SAXS analysis of proMbxA revealed an elongated monomeric structure with notable flexibility in the N-terminal region, as confirmed by a poor fit of unrefined AlphaFold models and subsequent improvement using SREFLEX. Such conformational flexibility has also been inferred for other RTX proteins, including HlyA and CyaA, although SAXS-based refinement has been less extensively applied in CyaA [120, 124-126].

An important observation of MbxA was its oligomeric state upon activation. Size-exclusion chromatography coupled with multi-angle light scattering (SEC-MALS) revealed that acylated MbxA forms stable pentameric oligomers in solution, even after dilution. This behavior contrasts with that of proMbxA, which remained monomeric, and suggests that acylation directly induces or stabilizes the oligomeric assembly required for pore formation. For HlyA, oligomerization into heptameric or octameric pores has been demonstrated functionally and biochemically, with acylation being a prerequisite for membrane insertion and assembly [57, 127]. Similarly, CyaA forms oligomeric assemblies upon contact with membranes, and this process is also acylation-dependent [124, 128, 129].

Despite these findings, MbxA exhibited specific challenges for high-resolution structure determination. Cryo-electron microscopy of both liposome and RBC-incubated MbxA samples failed to yield interpretable reconstructions. Similar difficulties have been encountered with other RTX toxins, where pore formation is transient or requires stabilization by lipid bilayers or crosslinking agents, often at the expense of functional activity.

In summary, MbxA follows the classical RTX secretion and activation pattern and contributes several mechanistic insights. Its monomeric, flexible precursor structure and stable oligomeric assembly upon acylation position MbxA as a useful model for dissecting RTX toxin maturation and pore formation.

4.3. Membrane Binding and Pore Formation

4.3.1. Cholesterol Dependency and RTX Toxin Comparison

The pore-forming activity of MbxA exhibits a strong dependence on membrane cholesterol. In lipid leakage assays, the inclusion of cholesterol in liposomes led to a substantial increase in lysis by acylated MbxA, while cholesterol-free membranes showed minimal leakage. This enhancement was acylation-dependent; the non-acylated proMbxA did not cause leakage in either cholesterol-containing or cholesterol-free vesicles, indicating that cholesterol facilitates the insertion and/or stabilization of the toxin, rather than merely promoting binding.

These findings position MbxA alongside several well-characterized RTX toxins, such as *E. coli* hemolysin (HlyA), Bordetella CyaA, and Aggregatibacter LtxA, all of which exhibit similar cholesterol sensitivities [57, 92, 95, 96, 130]. For instance, Herlax et al. and Vázquez et al. demonstrated that HlyA preferentially associates with cholesterol-rich microdomains [57, 95], and that cholesterol is essential for promoting oligomerization and lytic activity. Similarly, González Bullón et al. showed that cholesterol increases the pore size and lytic efficiency of CyaA [96]. In LtxA, a functional CRAC motif was shown to mediate cholesterol-dependent membrane association [130], and similar findings have been reported for Kingella RtxA [92].

Importantly, these cholesterol-dependent RTX toxins often rely on membrane microdomains (lipid rafts) as organizing platforms for insertion. Studies on CyaA [98], LtxA [88], and LktA [97] have shown preferential localization to lipid rafts, even when translocation or receptor engagement is required. MbxA, since it exhibited cytotoxicity towards β_2 integrin-negative HEp-2 cells and RBCs, appears to use cholesterol as a functional surrogate for receptor-like spatial targeting, enabling membrane engagement and lysis in a receptor-independent fashion.

4.3.2. Cholesterol-Recognition Motifs in MbxA

Sequence analysis of MbxA revealed a total of 25 putative cholesterol-recognition motifs, including 13 CRAC (L/V-X_{1-5}-Y-X_{1-5}-R/K) and 12 CARC (R/K-X_{1-5}-Y/F-X_{1-5}-L/V) sequences, distributed across the protein (Table 1). These motifs were identified using ScanProsite and mapped to specific regions of interest based on functional and structural relevance [131].

Notably, four CARC motifs - $CARC_{202-213}$, $CARC_{240-252}$, $CARC_{258-269}$, and $CARC_{317-327}$ - are located within the predicted hydrophobic domain that likely contributes to membrane insertion

and pore formation. An additional four motifs - CRAC/CARC motifs - $CRAC_{22-31}$, $CRAC_{532-542}$, $CRAC_{641-653}$, and $CARC_{542-548}$ - are positioned near the acylation region, suggesting a potential interplay between acylation and cholesterol binding.

These motifs were further mapped onto the SAXS-refined AlphaFold model of proMbxA (Figure 6). The spatial mapping revealed that many of the CRAC/CARC sequences are surface-accessible, especially those located near the acylation region and within the hydrophobic domain. This structural accessibility enhances their likelihood of functional relevance, supporting the hypothesis that MbxA targets cholesterol-rich membrane microdomains through direct lipid-protein interactions. The clustering of cholesterol motifs near the acylation sites suggests a coordinated mechanism whereby acylation not only enables membrane insertion but may also stabilize cholesterol interactions necessary for oligomerization and pore formation.

Predicted Cholesterol Recognition Motifs			
CRAC		CARC	
Localization	Sequence	Localization	Sequence
22-31	LAIPKDYDPQK	202-213	KLQNLNFSKTNL
27-37	LKNLYLAIPK	240-252	KVAAGFELSNQV
326-332	LLAEYQR	258-269	KAISSYVLAQRV
532-542	LTNGKYSYINK	317-327	RKFGYDGDHLL
611-615	VFYSK	387-394	KQAMFESV
641-653	VARGDIYHEVVKR	417-427	KGYDSRYAAYL
824-831	LQNYQSNK	422-431	RYAAYLANNL
		475-487	KAYADAFEDGKKV
		511-522	KTQALHFTSPLL
		531-543	RLTNGKYSYINKL
		542-548	KLKFGRV
		561-567	KLDFSKV
		615-624	KDGGFGNITV
		643-651	RGDIYHEVV
		661-672	RTETIQYRDYEL
		668-675	RDYELRKV
		673-685	RKVGYGYQSTDNL
		817-824	RWYITSNL

Table 1: Putative cholesterol recognition CRAC and CARC motifs identified in the sequence of MbxA. *The motifs were identified with ScanProsite [131] - table adapted from [120].*
Underlined: Surface exposed residues.
Green highlight: CRAC/CARC near the acylation region.
Green highlight & underlined: Surface-exposed CRAC/CARC near the acylation region.
Purple highlight: CRAC/CARC in the hydrophobic domain.
Purple highlight & underlined: Surface-exposed CRAC/CARC in the hydrophobic domain.
Pink highlight: Partially surface-exposed CRAC/CARC.
Blue highlights within pink highlight: Surface-exposed aromatic residues in the partially surface-exposed CRAC/CARC.

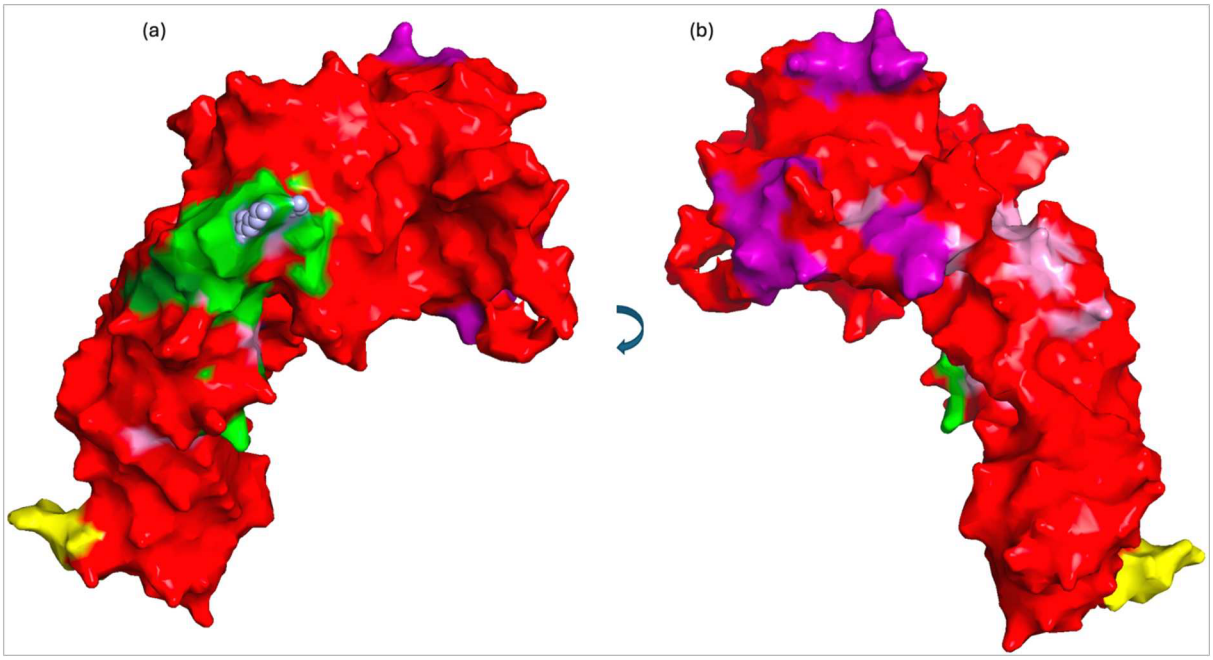

Figure 6. *SAXS-resolved AlphaFold model of proMbxA with CRAC and CARC motifs highlighted. Green indicates motifs near the acylation region; purple denotes those in the predicted hydrophobic domain; pink marks partially surface-exposed motifs. Grey spheres indicate the lysine residues post-translationally modified during activation. Image created in PyMOL [132].*

4.3.3. Liposome-Based Analysis: Ideal Biophysical Platform

The use of synthetic lipid vesicles (liposomes) in this thesis provided a controlled, reductionist system to investigate the membrane activity of MbxA in a receptor-free context. As discussed by Dalla Serra and Menestrina, liposomes are uniquely suited for studying pore-forming toxins (PFTs) because they offer precise control over lipid composition, curvature, charge, and sterol content, enabling direct dissection of lipid-specific effects [133].

In this work, liposome compositions were systematically varied to include:

- Neutral phosphatidylcholine (POPC) vs. charged lipids (POPG, phosphatidylserine)
- Saturated vs. unsaturated lipids
- With or without cholesterol

These combinations revealed that MbxA relies on the net charge and saturation of the lipids and of cholesterol for lysis and is essential for pore formation. Additionally, the absence of proteinaceous components in liposomes confirms that MbxA is capable of receptor-independent membrane disruption, further strengthening its classification as a lipid-targeting RTX toxin.

The experimental flexibility of liposomes also enabled quantitative assessment of toxin-induced leakage using encapsulated dye systems (ANTS/DPX), and correlated well with qualitative observations from GUV rupture and AFM imaging. Together, these data form a basis for the biophysical characterization of MbxA's lytic function.

4.3.4. Pore Kinetics and Leakage Behavior

An important aspect of pore-forming toxin characterization is determining the nature of the leakage: whether vesicles undergo complete (all-or-none) lysis or partial (graded) permeabilization. This distinction informs both pore architecture and membrane interaction dynamics [134-137].

Fluorescence-based dye leakage assays performed in this thesis displayed smooth, dose-dependent increases in fluorescence intensity, with no abrupt transitions or bimodal population behavior. This pattern supports a graded leakage mechanism, wherein individual vesicles lose contents proportionally, rather than rupturing entirely.

This behavior is consistent with theoretical models by Schwarz & Arbuzova and Ladokhin et al., who demonstrated that graded leakage results from dynamic, size-variable pores, typically associated with toroidal or arciform pores rather than rigid, cylindrical β-barrel structures [134, 136]. The liposome data described in this thesis suggest that MbxA forms transient, flexible disruptions, sufficient to allow solute flux but not necessarily full membrane rupture.

Moreover, the requirement for cholesterol and acylation implies that pore formation is a multi-step, regulated process, not an uncontrolled lytic event. The ability to modulate leakage by adjusting cholesterol levels and acylation status further supports a controlled, stepwise pore formation model, typical of several RTX toxins but rarely studied with the biophysical rigor applied here.

4.3.5. Proposed Mechanistic Model for MbxA Pore Formation

RTX toxins belong to the broader class of pore-forming toxins (PFTs), which can be divided into two major structural families based on their membrane-insertion architecture: α-PFTs and β-PFTs [138]. As described in the review by Ostolaza et al., α-PFTs form pores using amphipathic α-helices, while β-PFTs assemble into transmembrane β-barrels composed of extended β-strands contributed by multiple subunits [138]. The two pore types differ not only

in structure but also in pore size, stability, and insertion dynamics, and several PFTs exhibit atypical or hybrid features, including partial toroidal structures or transient arciform lesions. Figure 7 (adapted from Ostolaza et al.) provides a comparative schematic of the pore formation by α- and β-PFT [138].

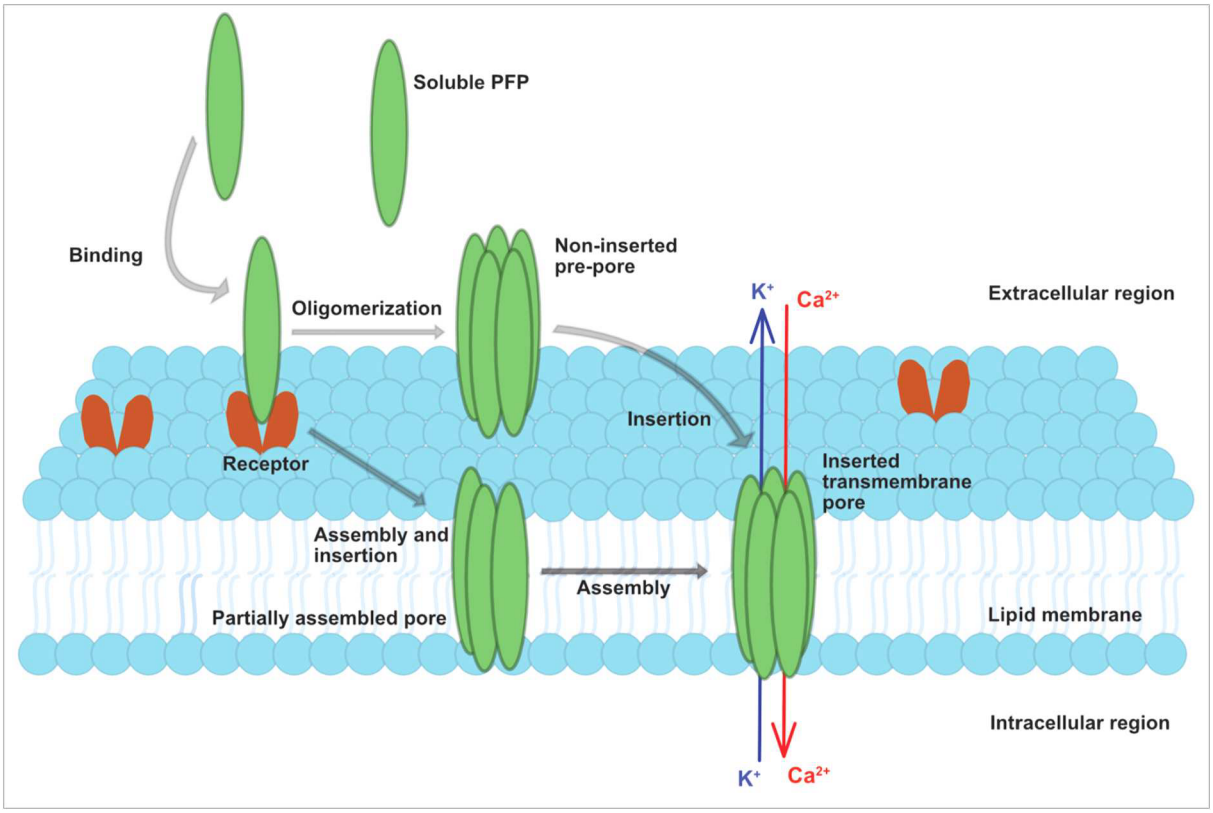

Figure 7. *Schematic model of membrane pore formation by pore-forming proteins (PFPs), adapted from Ostolaza et al. (2019). Soluble PFP monomers interact with target membranes through receptor recognition and/or lipid-specific interactions, leading to concentration-dependent oligomerization. In the β-PFP pathway (top), oligomerization occurs on the membrane surface to form a non-inserted pre-pore, followed by a coordinated insertion step. In contrast, α-PFPs (bottom) typically insert into the membrane concurrently with stepwise oligomerization, which may yield either complete or partially assembled functional pores. The resulting transmembrane structures vary in stoichiometry and architecture but ultimately mediate ionic flux (e.g., Ca^{2+} influx, K^{+} efflux) and membrane permeabilization.*

The SAXS refined alpha fold structure of MbxA was used to gain structural insight into MbxA's pore-forming potential. A key feature was the presence of a surface-exposed α-helical domain, located within the predicted hydrophobic membrane-targeting region, flanked by structured β-sheets that include the acylation sites (K536 and K660). This model is shown in Figure 8 (AlphaFold-SAXS) and provides a molecular basis for understanding MbxA's insertion behavior.

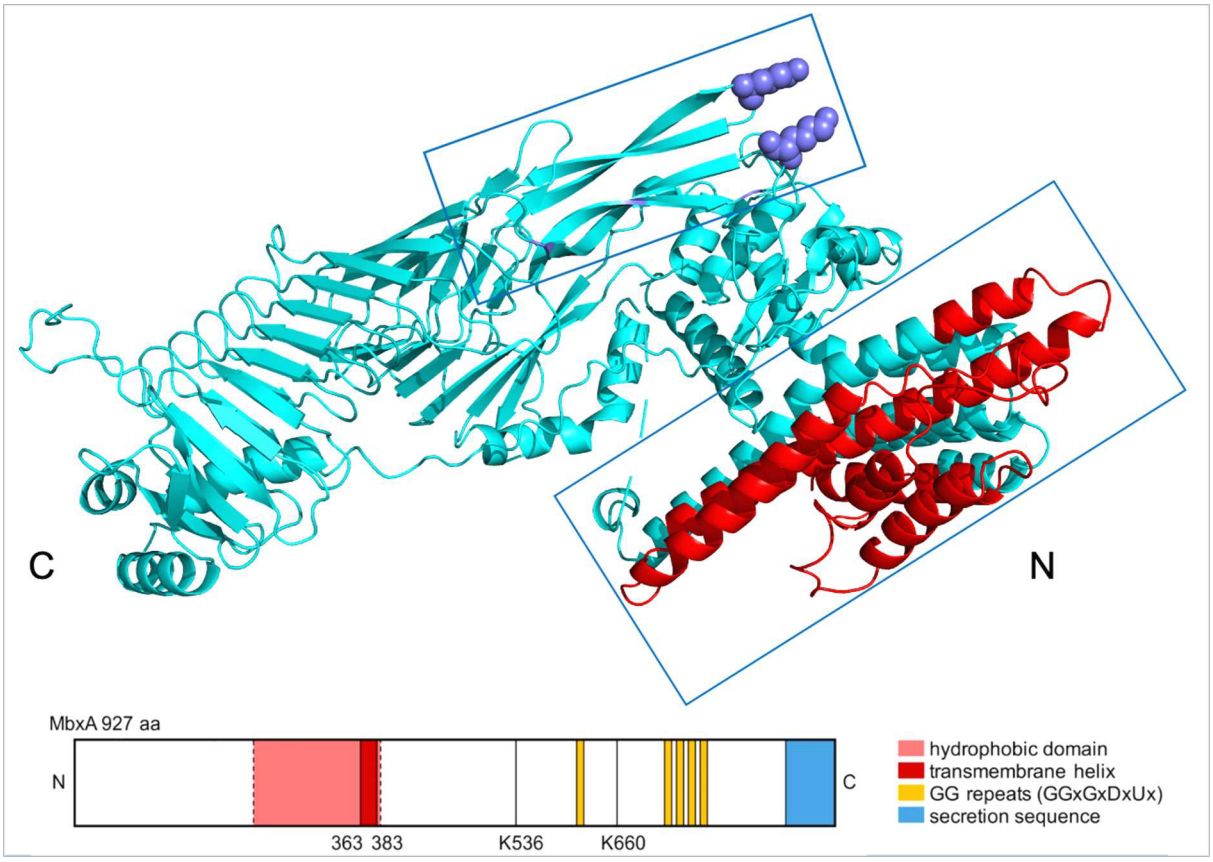

Figure 8. *SAXS-refined AlphaFold model of proMbxA highlighting domain organization relevant to membrane interaction and pore formation. The N-terminal region (red) features a surface-exposed α-helical hydrophobic domain with predicted transmembrane helices, consistent with the behavior of α-pore-forming toxins. The acylation sites (K536 and K660) are located within a β-sheet-rich region (cyan, top box), which characterizes β-pore-forming toxins, and lysine residues are shown as purple spheres. The cartoon below the structure illustrates the primary sequence domain architecture of MbxA, including the hydrophobic region, RTX repeats, and secretion signal. Image created in PyMOL [132].*

Although acylation domains constitute a β-sheet-rich region, the α-helical topology of the membrane-interacting domain aligns more closely with α-PFT behavior and may contribute to the formation of dynamic pores, a conclusion also supported by graded leakage profiles of the liposome leakage assay. The structured acylation region, surrounded by predicted CRAC/CARC motifs, likely serves as a regulatory module that controls insertion depth, stability, or conformational activation upon membrane contact.

These structural insights also coordinate with biophysical models from Bakás et al., who described reversible adsorption and irreversible insertion of HlyA into lipid bilayers [105]. In this model, initial binding is governed by non-covalent interactions (electrostatics,

hydrophobicity), followed by an acylation-dependent conformational switch enabling stable membrane penetration. MbxA appears to follow a similar trajectory.

The findings from liposome leakage, GUV imaging, AFM binding assays, and structural modeling collectively support a multi-step mechanistic model of MbxA pore formation (Figure 9). This model shares features with other RTX toxins, particularly HlyA and CyaA, but also presents unique aspects due to MbxA's receptor-independent membrane targeting.

Step 1: Membrane Binding – Reversible Adsorption?

Initial interaction of MbxA with lipid membranes is acylation-independent, as evidenced by the ability of both MbxA and proMbxA to bind to liposomes and supported bilayers. However, AFM data show that only acylated MbxA remains bound after washing, indicating that membrane association is not sufficient for insertion. Electrostatic and hydrophobic interactions may allow loose surface tethering.

Step 2: Membrane Insertion - Acylation-Dependent Transition

Insertion into the bilayer is dependent on acylation, likely enabling the N-terminal α-helical domain to transition into the bilayer (modeled in Figure 9). The acyl chains, covalently attached at K536 and K660, are hypothesized to anchor the protein in the membrane, allowing the helical regions to penetrate the bilayer.

Step 3: Oligomerization and Pore Formation

SEC-MALS data show that acylated MbxA forms stable pentameric oligomers in solution, while proMbxA remains monomeric. This supports a model where acylation enables or stabilizes toxin-toxin interactions, potentially forming a functional pore complex upon membrane binding. The graded leakage pattern observed in liposome assays implies that the resulting pore is dynamic, transient, and possibly non-ring-like, differing from classical β-barrel pores such as those of α-hemolysin.

Step 4: Cholesterol-Enhanced Activity

Cholesterol, while not essential for membrane binding, dramatically enhances lysis, possibly by facilitating oligomer stabilization or pore opening, through raft localization that

concentrates the toxin or altered bilayer packing. This step is tightly correlated with the spatial distribution of CRAC/CARC motifs, particularly in the hydrophobic domain and near acylation sites.

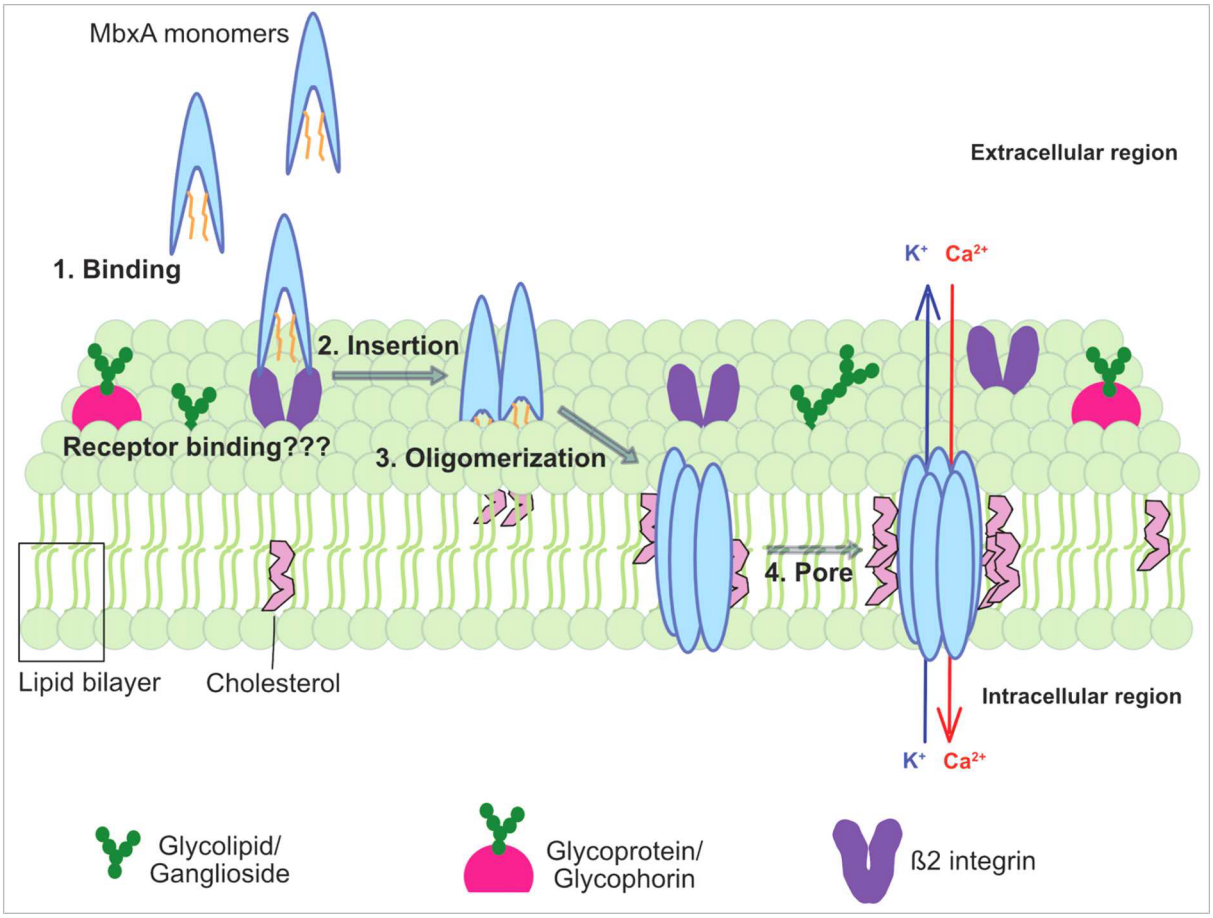

Figure 9. Proposed mechanism of MbxA pore formation on host membranes. *This model illustrates a four-step process of MbxA-induced membrane disruption, supported by the data described in this thesis and RTX literature.* ***(1) Binding:*** *MbxA monomers initially associate with the lipid bilayer in an acylation-independent manner. This binding may trigger a conformational change that exposes the acyl chains.* ***(2) Insertion:*** *Acylated MbxA inserts into the membrane, likely anchoring via acylated lysines and embedding the α-helical domain into the bilayer.* ***(3) Oligomerization:*** *Membrane-inserted MbxA assembles into oligomeric complexes possibly supported by cholesterol, forming dynamic pores that permit graded leakage.* ***(4) Cholesterol-enhanced activity:*** *Cholesterol, while not required for binding, enhances pore formation, possibly through oligomer stabilization or raft localization, consistent with mapped CRAC/CARC motifs. Receptor interaction remains unresolved; potential binding to glycoproteins or integrins, as seen in other RTX toxins, is indicated as hypothetical.*

This four-step model integrates the structural plasticity, lipid-dependence, and acylation sensitivity observed in MbxA, and offers a generalizable framework for understanding receptor-independent RTX toxin behavior. While high-resolution pore structures remain

elusive, the combination of structural modeling and functional assays provides a compelling mechanistic basis for MbxA's cytolytic activity.

4.4. Cell-Type Specificity and Cytotoxicity of RTX Toxins

4.4.1. Biological Activities of RTX Toxins: The Case of HlyA

RTX toxins are classically recognized for their pore-forming cytolytic activity, but emerging models suggest their interactions with host cells are more nuanced, involving complex interplay between toxin-induced damage and host cell responses. A conceptual framework proposed by Wiles and Mulvey (2013) offers a useful perspective for interpreting these dynamics, not exclusively based on HlyA, but rather on the findings across RTX and non-RTX pore-forming toxins (PFTs) [9]. This model highlights two major, sometimes opposing processes: host defensive responses aimed at restoring homeostasis, and toxin-mediated tampering that subverts host functions for bacterial benefit. Although the specific molecular mechanisms of HlyA in this dichotomy are still being investigated, the toxin remains one of the best-characterized RTX proteins and serves as a prototype for understanding general RTX toxin behavior.

Host Defensive Responses to HlyA

PFT-induced lesions, whether caused by RTX toxins or others like streptolysin O or pneumolysin, typically trigger host membrane repair systems. These include:

- Lysosomal exocytosis to patch membrane lesions
- Recruitment of annexins to stabilize membrane curvature
- Actin cytoskeleton remodeling to reinforce the membrane
- Ion channel closure and vesicle shedding to limit cytosolic loss

For HlyA, specific examples of such responses remain limited, but studies like Uhlén et al. have shown that the toxin can induce Ca^{2+} oscillations in renal epithelial cells, possibly contributing to early signaling events or stress adaptation. These oscillations, while initially protective, may also be exploited by bacteria to manipulate host signaling networks [68].

This conceptual view suggests that epithelial and immune cells exposed to PFTs engage in dynamic countermeasures, attempting to survive pore formation through active repair and ionic

re-equilibration. Whether HlyA triggers all such mechanisms remains unclear, but the possibility raises intriguing questions for future investigation.

Pathogen-Driven Host Cell Tampering

In parallel with host defenses, HlyA engages in a second, more insidious role: rewiring host cell behavior in ways that favor bacterial survival and colonization. This includes:

- Cleavage of adhesion molecules (e.g., E-cadherin, integrins) to disrupt epithelial barriers and promote bacterial dissemination [67].
- Endocytosis via LDL receptor pathways to facilitate intracellular trafficking and damage from within [70].
- Activation of inflammatory cascades, including NLRP3 inflammasomes and cytokine secretion in immune cells [69, 71].
- Recruitment of neutrophils and immune modulators, potentially leading to both host damage and bacterial niche formation [73].

Importantly, these processes occur at non-lethal concentrations of HlyA, suggesting that the primary role of the toxin is not always cytolysis, but rather functional manipulation of the host. Nagamatsu et al. demonstrated that the timing and regulation of HlyA expression dramatically influence whether *E. coli* induces acute infection or persistent colonization, emphasizing that RTX toxins operate as finely tuned virulence factors rather than indiscriminate killers [139].

Cell-Type Specificity and Pathophysiological Context

Another critical insight from the literature is that PFT effects vary widely between cell types and exposure conditions. For HlyA, renal epithelial cells [68], bladder epithelial cells [69], macrophages [71], and neutrophils [73] all show different thresholds of susceptibility and distinct downstream effects. Some responses are dominated by rapid necrosis [71], while others involve signaling modulation without immediate lysis [68, 69].

This variability emphasizes that RTX toxins like HlyA and potentially MbxA are highly context-dependent, shaped by both toxin concentration and host cell identity. It also reinforces the importance of studying RTX toxins in physiologically relevant models, as their full range of effects may not manifest in simplified cell lines or short-term assays.

4.4.2. Mechanism and Cell-Type Specificity of LtxA

Another well-characterized member of the RTX toxin family is leukotoxin A (LtxA), produced by *Aggregatibacter actinomycetemcomitans*, a pathogen primarily associated with localized aggressive periodontitis [10]. LtxA is notable for its highly selective toxicity toward immune cells, particularly human and primate leukocytes, due to its ability to bind with high affinity to the β_2 integrin LFA-1 (CD11a/CD18) [76]. This receptor dependence makes LtxA a distinct case within the RTX family, providing a clear contrast to receptor-independent toxins like MbxA.

LtxA's cytotoxic activity is coordinated through a multi-step interaction with the host plasma membrane, as summarized in Figure 10 (adapted from Vega et al.) [10].

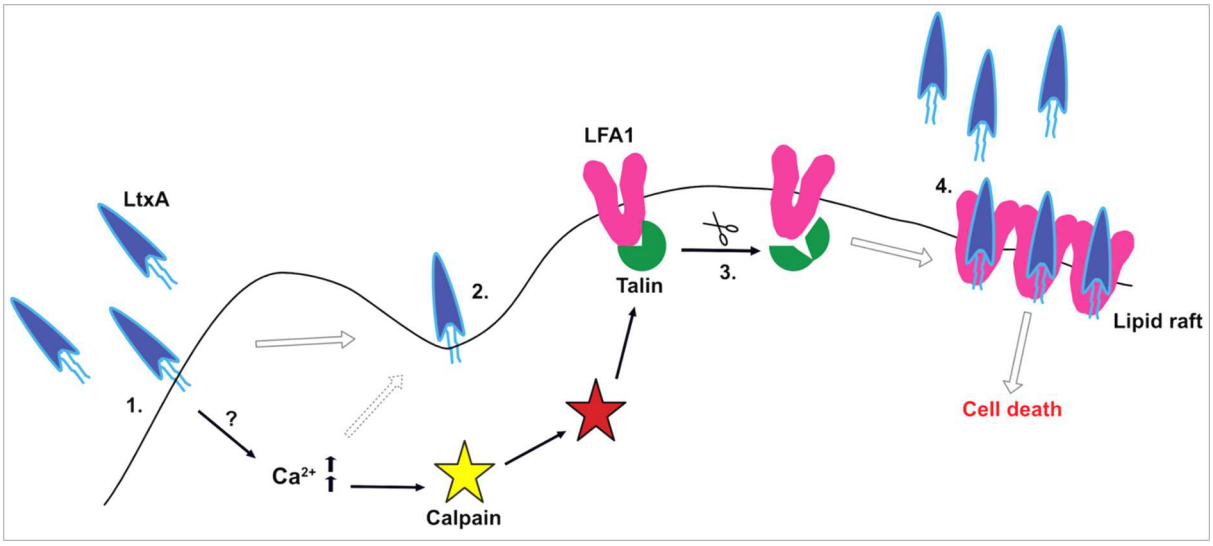

Figure 10. Proposed model of LtxA association with host cell membranes and induction of cell death. *Adapted from Vega et al. (2019), this figure illustrates a multi-step mechanism by which LtxA interacts with the membranes of immune cells.* ***(1)*** *LtxA initially binds to the membrane through passive adsorption and anchors via its fatty acyl chains, potentially triggering an increase in intracellular Ca^{2+} levels.* ***(2)*** *This interaction destabilizes the lipid bilayer, leading to membrane deformation.* ***(3)*** *Elevated Ca^{2+} activates calpain, a Ca^{2+}-dependent protease, which cleaves talin, a cytoskeletal protein anchoring the integrin LFA-1 to the membrane.* ***(4)*** *This allows LFA-1 to cluster in lipid rafts, facilitating further interaction with LtxA and partial membrane insertion. These interactions ultimately result in cell death through membrane disruption and downstream signaling.*

Initially, LtxA adsorbs passively to the membrane and anchors via its fatty acyl chains. This early interaction is sufficient to initiate intracellular Ca^{2+} influx, potentially through early membrane perturbations or pore formation. Once Ca^{2+} levels rise, downstream host responses are activated, including the Ca^{2+}-dependent activation of calpain, a protease that cleaves the

cytoskeletal linker protein talin. This cleavage releases LFA-1 from its anchoring to the actin cytoskeleton, allowing it to cluster within lipid rafts, where LtxA further engages it. This dual interaction, lipid microdomain targeting and receptor binding, enables LtxA to partially insert into the membrane, resulting in cell death via membrane disruption and/or intracellular signaling.

This model reflects the tight interplay between host membrane structure, receptor organization, and RTX toxin function. It also demonstrates how RTX toxins can:

- Exploit host Ca^{2+} signaling for both cytotoxicity and self-positioning
- Use lipid rafts as platforms for membrane insertion and oligomerization
- Induce proteolytic remodeling of host adhesion structures, thereby compromising immune cell function

Importantly, LtxA also exhibits a dose-dependent dual role: at high concentrations, it leads to rapid lysis, while at lower doses, it modulates cytokine production and survival signaling, adding to its complexity as a virulence factor [140-143].

Like HlyA, LtxA is acylation-dependent and cholesterol-sensitive [123]. However, its strict receptor specificity distinguishes it mechanistically. The requirement for LFA-1 explains its narrow host range and cell-type specificity, unlike MbxA, which exhibits toxicity in human epithelial cells without a known receptor, as discussed in Section 4.3.

Taken together, LtxA underscores the functional plasticity of RTX toxins, from receptor-mediated signaling to membrane disruption, and provides a valuable comparative framework for evaluating the receptor-independent yet cholesterol-enhanced activity of MbxA.

4.4.3. Comparative Insights into MbxA Cytotoxicity and RTX Toxin Mechanisms

The data presented in this thesis suggest that MbxA shares key mechanistic features with both HlyA and LtxA, and also diverges in important ways. These comparisons are valuable because, unlike HlyA and LtxA, MbxA has not previously been studied in the context of host cell biology.

Commonalities with HlyA and LtxA

Like HlyA, MbxA displays a clear dependence on post-translational acylation for its cytolytic activity. Only the acylated form (MbxA), not the non-acylated proMbxA, was capable of inducing Ca^{2+} modulation, mitochondrial depolarization, and morphological damage in HEp-2 cells. This aligns with established roles of acylation in enabling membrane insertion and stabilizing RTX toxins in lipid environments, as described for both HlyA and LtxA.

Furthermore, all three toxins exhibit Ca^{2+}-dependent necrosis at high doses and sublethal effects at lower concentrations. When applied to HEp-2 cells, acylated MbxA triggered a cascade of morphological and biochemical changes such as plasma membrane permeabilization and blebbing, nuclear shrinkage, loss of mitochondrial membrane potential, strong and immediate Ca^{2+} modulation, etc., where these effects were rapid and irreversible, hallmarks of necrosis rather than apoptosis. The absence of apoptotic signatures, including caspase-independent PARP cleavage, supports this conclusion. This mode of death closely resembles the high-concentration effects of HlyA, which also causes Ca^{2+} dysregulation, membrane rupture, and necrosis. It reflects the 'overtly cytolytic' face of RTX toxins, as discussed in Wiles & Mulvey's dichotomy [9].

In MbxA-treated HEp-2 cells, subcytolytic doses resulted in toxin internalization without immediate death, a behavior reminiscent of both HlyA-mediated immune tampering and LtxA-driven receptor trafficking and signaling. Although this thesis did not examine downstream signaling, it is plausible, based on the observed mitochondrial stress and MbxA internalisation, that sublytic MbxA exposure could interfere with survival signaling or gene expression. Whether these changes contribute to immune modulation, bacterial colonization, or tissue damage in the context of *M. bovis* infection remains an open question.

Distinctions: Receptor Independence and Host Range

MbxA diverges from LtxA in its lack of receptor specificity. LtxA requires LFA-1 (CD11a/CD18) for cytotoxicity and is thus highly selective for human and primate leukocytes [76]. MbxA, by contrast, exhibits receptor-independent toxicity toward epithelial cells and RBCs.

This independence is more comparable to HlyA, which can act broadly on various epithelial and immune cells via direct membrane targeting. However, HlyA has been recently shown to

engage in LDL receptor-mediated endocytosis [70], while MbxA has not yet been tested for such specific host interactions.

Cell-Type Considerations and Limitations

The ability of acylated MbxA to damage human epithelial cells implies that MbxA acts broadly like HlyA, affecting multiple host species. While HEp-2 cells provided a valuable model to establish the membrane activity and cytotoxic potential of MbxA, this system has several limitations:

- HEp-2 cells are not the natural host target of *M. bovis*, which primarily infects cattle.
- The lack of original host epithelial or immune cells limits the interpretation of in vivo relevance.
- The study did not involve live bacterial infection, so the timing, delivery, and regulation of MbxA in a native infection context remain unknown.

Despite these limitations, the clear membrane-damaging effects of acylated MbxA on epithelial cells align well with known RTX toxin behavior and provide a mechanistic foundation for future studies in host-pathogen systems. In particular, it would be of interest to assess:

- Cytokine responses (e.g., IL-1β, GM-CSF)
- Host signaling pathways (e.g., NF-κB, MAPK)
- Immune cell sensitivity, especially macrophages and neutrophils
- Barrier integrity and adhesion molecule cleavage, as shown for HlyA [67]
- Identifying potential receptors in the native host

Such studies would help determine whether MbxA functions solely as a membrane-disrupting cytotoxin or whether it also engages in non-lethal host modulation to benefit bacterial survival and persistence.

Taken together, the comparative analysis of HlyA and LtxA illustrates the functional adaptability of RTX toxins, which can range from broad-spectrum cytolysins to highly selective immune modulators. MbxA, as characterized in this thesis, aligns with canonical RTX features such as acylation dependency, cholesterol-enhanced activity, and Ca^{2+}-mediated necrosis, but also demonstrates unique attributes, notably, its receptor-independent cytotoxicity in epithelial cells and RBCs. While its precise in vivo role remains to be defined, MbxA functions as a potent pore-forming toxin with the capacity to disrupt membrane integrity, induce ionic

imbalance, and potentially modulate host responses under sublytic conditions. Future studies involving native host systems and live bacterial infections will be essential to determine whether MbxA behaves more like a general membrane disruptor or a refined effector tuned to *M. bovis* pathogenicity. In either case, MbxA expands our understanding of the RTX toxin family and offers a valuable model for studying receptor-independent RTX-mediated cytotoxicity.

4.5. Therapeutic Perspectives from RTX Toxin Research

Beyond their importance in bacterial pathogenesis, RTX toxins are increasingly recognized as promising tools and targets in therapeutic development. Several approaches are being explored to utilize or counteract their activities. For example, synthetic peptides mimicking CRAC/CARC motifs have been proposed as antivirulence agents capable of blocking RTX toxin–cholesterol interactions, thereby preventing pore formation without affecting bacterial viability [103]. Such strategies reflect a broader interest in antivirulence therapies that disarm pathogens by neutralizing toxins rather than relying on traditional antibiotics.

Other efforts have focused on repurposing RTX toxins for therapeutic applications. The best example is LtxA (Leukothera®), which exploits its strict specificity for human leukocytes to selectively eliminate malignant immune cells in leukemias and lymphomas [10]. This highlights how RTX toxins, when appropriately engineered or targeted, can be developed into precision biotherapeutics.

The general RTX pore-forming mechanism itself also holds potential for drug delivery systems. The ability of RTX toxins to form large, dynamic channels in membranes may be adapted for controlled delivery of macromolecules across cell barriers [74, 144]. Understanding the biophysical principles of RTX channel formation, lipid dependence, and oligomerization is therefore central to these translational applications.

The findings presented in this thesis on MbxA contribute to this broader field by advancing knowledge of lipid-mediated, receptor-independent RTX activity. The demonstration of cholesterol sensitivity, the mapping of multiple CRAC/CARC motifs, and the characterization of graded pore leakage provide a new perspective on how RTX toxins can be targeted or engineered at the membrane interface. In particular, MbxA may serve as a model for designing

therapies that exploit or disrupt cholesterol-dependent interactions, expanding strategies currently being tested for other RTX family members.

Thus, while this work primarily advances fundamental understanding of RTX toxin biology, it also underscores the translational potential of RTX studies, bridging basic mechanistic insights with the development of novel therapeutic approaches.

5. Concluding Remarks

This thesis has explored the biochemical and biophysical characterization of the RTX toxin MbxA, investigating its mechanism of membrane interaction, cytotoxic activity, and structural features. The findings presented here establish MbxA as a cholesterol-responsive RTX toxin, whose activity is critically dependent on post-translational acylation. Through a combination of in vitro assays, structural modeling, and cellular analyses, the work concludes a multi-step model of pore formation in which acylation and cholesterol facilitate membrane insertion, and the toxin ultimately induces graded membrane leakage and Ca^{2+}-driven non-apoptotic cell death in epithelial cells.

When positioned alongside other RTX toxins, particularly HlyA, which exhibits broad epithelial toxicity, and LtxA, which targets leukocytes via LFA-1, MbxA appears to follow a distinct but overlapping mechanism. It does not exhibit receptor dependence in *in vitro* assays, but shares with both HlyA and LtxA a reliance on acylation and cholesterol for its cytotoxic activity. These findings suggest that lipid interactions alone may be sufficient to mediate MbxA's cytotoxicity under certain conditions, highlighting the potential for RTX toxins to function through receptor-independent, lipid-targeting mechanisms.

While this study answers several important questions about MbxA, it also opens new directions for future research. The role of specific receptors in MbxA binding has not yet been addressed. While the cholesterol dependence suggests lipid-based targeting, receptor engagement may still play a role in cell-type specificity or internalization. Additionally, mutagenesis of selected CRAC/CARC motifs could clarify their contribution to cholesterol sensitivity and membrane insertion. Furthermore, structural intermediates of MbxA pore formation also remain to be captured. Further development of stabilized constructs or receptor-mimetic complexes may facilitate high-resolution cryo-EM analysis. In addition, the potential immune effects and the role of MbxA in infection are not yet known. Studying MbxA in the context of live bacterial infections and relevant host cell types, such as bovine cells, will be an important next step.

In summary, this work helps to fill a gap in our understanding of RTX toxins by providing a detailed look at MbxA. It shows how this toxin disrupts membranes, how its activity depends on lipid composition and acylation, and how it acts in the absence of a known receptor. These findings lay the groundwork for future studies on MbxA's role in host-pathogen interactions.

6. Bibliography

1. Alouf, J.E., D. Ladant, and M.R. Popoff, *The comprehensive sourcebook of bacterial protein toxins*. 2005: Elsevier.
2. Middlebrook, J.L. and R.B. Dorland, *Bacterial toxins: cellular mechanisms of action*. Microbiological reviews, 1984. **48**(3): p. 199-221.
3. Schmitt, C.K., K.C. Meysick, and A.D. O'Brien, *Bacterial toxins: friends or foes?* Emerging infectious diseases, 1999. **5**(2): p. 224.
4. Sheehan, J., C. Sadlier, and B. O'Brien, *Bacterial endotoxins and exotoxins in intensive care medicine.* BJA education, 2022. **22**(6): p. 224-230.
5. Gonzalez, M., et al., *Bacterial pore-forming toxins: the (w) hole story?* Cellular and Molecular Life Sciences, 2008. **65**(3): p. 493-507.
6. Ulhuq, F.R. and G. Mariano, *Bacterial pore-forming toxins.* Microbiology, 2022. **168**(3): p. 001154.
7. Linhartová, I., et al., *RTX proteins: a highly diverse family secreted by a common mechanism*. FEMS microbiology reviews, 2010. **34**(6): p. 1076-1112.
8. Filipi, K., et al., *Kingella kingae RtxA cytotoxin in the context of other RTX toxins.* Microorganisms, 2022. **10**(3): p. 518.
9. Wiles, T.J. and M.A. Mulvey, *The RTX pore-forming toxin α-hemolysin of uropathogenic Escherichia coli: progress and perspectives.* Future microbiology, 2013. **8**(1): p. 73-84.
10. Vega, B.A., B.A. Belinka Jr, and S.C. Kachlany, *Aggregatibacter actinomycetemcomitans leukotoxin (LtxA; Leukothera®): mechanisms of action and therapeutic applications.* Toxins, 2019. **11**(9): p. 489.
11. Spitz, O., et al., *Type I secretion systems—one mechanism for all?* Microbiology spectrum, 2019. **7**(2): p. 10.1128/microbiolspec. psib-0003-2018.
12. Thomas, S., I.B. Holland, and L. Schmitt, *The type 1 secretion pathway—the hemolysin system and beyond.* Biochimica et Biophysica Acta (BBA)-Molecular Cell Research, 2014. **1843**(8): p. 1629-1641.
13. Collins, A.J., et al., *MapA, a second large RTX adhesin conserved across the pseudomonads, contributes to biofilm formation by Pseudomonas fluorescens.* Journal of Bacteriology, 2020. **202**(18): p. 10.1128/jb. 00277-20.
14. Guo, S., et al., *Structure of a 1.5-MDa adhesin that binds its Antarctic bacterium to diatoms and ice.* Science advances, 2017. **3**(8): p. e1701440.
15. Vance, T.D., et al., *Ca2+-stabilized adhesin helps an Antarctic bacterium reach out and bind ice.* Bioscience Reports, 2014. **34**(4): p. e00121.
16. Lenders, M.H., et al., *Molecular insights into type I secretion systems.* Biological Chemistry, 2013. **394**(11): p. 1371-1384.
17. Kuban, V., et al., *Structural basis of Ca2+-dependent self-processing activity of repeat-in-toxin proteins.* MBio, 2020. **11**(2): p. 10.1128/mbio. 00226-20.
18. O'brien, D.P., et al., *Structural models of intrinsically disordered and calcium-bound folded states of a protein adapted for secretion.* Scientific reports, 2015. **5**(1): p. 14223.
19. Bakás, L., et al., *Calcium-dependent conformation of E. coli α-haemolysin. Implications for the mechanism of membrane insertion and lysis.* Biochimica et Biophysica Acta (BBA)-Biomembranes, 1998. **1368**(2): p. 225-234.

20. Stanley, P., V. Koronakis, and C. Hughes, *Acylation of Escherichia coli hemolysin: a unique protein lipidation mechanism underlying toxin function*. Microbiology and molecular biology reviews, 1998. **62**(2): p. 309-333.
21. Welch, R., *RTX toxin structure and function: a story of numerous anomalies and few analogies in toxin biology*. Pore-forming toxins, 2001: p. 85-111.
22. Bhakdi, S., et al., *Escherichia coli hemolysin may damage target cell membranes by generating transmembrane pores*. Infection and immunity, 1986. **52**(1): p. 63-69.
23. Jeyaseelan, S., et al., *Lymphocyte function-associated antigen 1 is a receptor for Pasteurella haemolytica leukotoxin in bovine leukocytes*. Infect Immun, 2000. **68**(1): p. 72-9.
24. Benz, R., et al., *Adenylate cyclase toxin (CyaA) of Bordetella pertussis. Evidence for the formation of small ion-permeable channels and comparison with HlyA of Escherichia coli*. Journal of Biological Chemistry, 1994. **269**(44): p. 27231-27239.
25. Mock, M. and A. Ullmann, *Calmodulin-activated bacterial adenylate cyclases as virulence factors*. Trends in microbiology, 1993. **1**(5): p. 187-192.
26. Satchell, K.J., *Structure and function of MARTX toxins and other large repetitive RTX proteins*. Annual review of microbiology, 2011. **65**(1): p. 71-90.
27. Linhartova, I., et al., *RTX toxins: a review*. Microbial toxins, 2015: p. 1-29.
28. Erenburg, I.N., et al., *Heterologously secreted MbxA from Moraxella bovis induces a membrane blebbing response of the human host cell*. Scientific Reports, 2022. **12**(1): p. 17825.
29. Gavin, H. and K. Satchell, *MARTX toxins as effector delivery platforms*. *Pathog Dis 73: ftv092*. 2015.
30. Vance, T.D., et al., *Essential role of calcium in extending RTX adhesins to their target*. Journal of Structural Biology: X, 2020. **4**: p. 100036.
31. Boyd, C.D. and G.A. O'Toole, *Second messenger regulation of biofilm formation: breakthroughs in understanding c-di-GMP effector systems*. Annual review of cell and developmental biology, 2012. **28**(1): p. 439-462.
32. Baumann, U., et al., *Three-dimensional structure of the alkaline protease of Pseudomonas aeruginosa: a two-domain protein with a calcium binding parallel beta roll motif*. The EMBO journal, 1993. **12**(9): p. 3357-3364.
33. Boehm, D., R. Welch, and I. Snyder, *Domains of Escherichia coli hemolysin (HlyA) involved in binding of calcium and erythrocyte membranes*. Infection and immunity, 1990. **58**(6): p. 1959-1964.
34. Delepelaire, P., *Type I secretion in gram-negative bacteria*. Biochimica et Biophysica Acta (BBA)-Molecular Cell Research, 2004. **1694**(1-3): p. 149-161.
35. Koronakis, V., et al., *Crystal structure of the bacterial membrane protein TolC central to multidrug efflux and protein export*. Nature, 2000. **405**(6789): p. 914-919.
36. Felmlee, T. and R. Welch, *Alterations of amino acid repeats in the Escherichia coli hemolysin affect cytolytic activity and secretion*. Proceedings of the National Academy of Sciences, 1988. **85**(14): p. 5269-5273.
37. Ludwig, A., et al., *The repeat domain of Escherichia coli haemolysin (HlyA) is responsible for its Ca2+-dependent binding to erythrocytes*. Molecular and General Genetics MGG, 1988. **214**(3): p. 553-561.

38. Rose, T., et al., *Interaction of Calcium with Bordetella pertussis Adenylate Cyclase Toxin: CHARACTERIZATION OF MULTIPLE CALCIUM-BINDING SITES AND CALCIUM-INDUCED CONFORMATIONAL CHANGES (*)*. Journal of Biological Chemistry, 1995. **270**(44): p. 26370-26376.
39. Rhodes, C.R., et al., *Structural consequences of divalent metal binding by the adenylyl cyclase toxin of Bordetella pertussis*. Archives of biochemistry and biophysics, 2001. **395**(2): p. 169-176.
40. Thomas, S., et al., *Equilibrium folding of pro-HlyA from Escherichia coli reveals a stable calcium ion dependent folding intermediate*. Biochimica et Biophysica Acta (BBA)-Proteins and Proteomics, 2014. **1844**(9): p. 1500-1510.
41. Zhang, L., J.F. Conway, and P.H. Thibodeau, *Calcium-induced folding and stabilization of the Pseudomonas aeruginosa alkaline protease*. Journal of Biological Chemistry, 2012. **287**(6): p. 4311-4322.
42. Bhakdi, S., et al., *Potent leukocidal action of Escherichia coli hemolysin mediated by permeabilization of target cell membranes*. The Journal of experimental medicine, 1989. **169**(3): p. 737-754.
43. Gadeberg, O., I. Orskov, and J.M. Rhodes, *Cytotoxic effect of an alpha-hemolytic Escherichia coli strain on human blood monocytes and granulocytes in vitro*. Infection and immunity, 1983. **41**(1): p. 358-364.
44. Jonas, D., et al., *Cytocidal effects of Escherichia coli hemolysin on human T lymphocytes*. Infection and immunity, 1993. **61**(5): p. 1715-1721.
45. Suttorp, N., et al., *Effects of Escherichia coli hemolysin on endothelial cell function*. Infection and immunity, 1990. **58**(11): p. 3796-3801.
46. Keane, W.F., et al., *Mechanism of Escherichia coli alpha-hemolysin-induced injury to isolated renal tubular cells*. The American journal of pathology, 1987. **126**(2): p. 350.
47. Wandersman, C. and P. Delepelaire, *TolC, an Escherichia coli outer membrane protein required for hemolysin secretion*. Proceedings of the National Academy of Sciences, 1990. **87**(12): p. 4776-4780.
48. Ludwig, A., et al., *Mutations affecting pore formation by haemolysin from Escherichia coli*. Molecular and General Genetics MGG, 1991. **226**(1): p. 198-208.
49. Issartel, J.-P., V. Koronakis, and C. Hughes, *Activation of Escherichia coli prohaemolysin to the mature toxin by acyl carrier protein-dependent fatty acylation*. Nature, 1991. **351**(6329): p. 759-761.
50. Stanley, P., et al., *Fatty acylation of two internal lysine residues required for the toxic activity of Escherichia coli hemolysin*. Science, 1994. **266**(5193): p. 1992-1996.
51. Nicaud, J.-M., et al., *Characterisation of HlyC and mechanism of activation and secretion of haemolysin from E. coli 2001*. FEBS letters, 1985. **187**(2): p. 339-344.
52. Trent, M.S., L.M. Worsham, and M.L. Ernst-Fonberg, *The biochemistry of hemolysin toxin activation: characterization of HlyC, an internal protein acyltransferase*. Biochemistry, 1998. **37**(13): p. 4644-4652.
53. Thomas, S., S.H. Smits, and L. Schmitt, *A simple in vitro acylation assay based on optimized HlyA and HlyC purification*. Analytical Biochemistry, 2014. **464**: p. 17-23.

54. Lim, K.B., et al., *Escherichia coli α-hemolysin (HlyA) is heterogeneously acylated in vivo with 14-, 15-, and 17-carbon fatty acids*. Journal of Biological Chemistry, 2000. **275**(47): p. 36698-36702.
55. Osickova, A., et al., *Acyltransferase-mediated selection of the length of the fatty acyl chain and of the acylation site governs activation of bacterial RTX toxins*. Journal of Biological Chemistry, 2020. **295**(28): p. 9268-9280.
56. Herlax, V. and L. Bakas, *Acyl chains are responsible for the irreversibility in the Escherichia coli α-hemolysin binding to membranes*. Chemistry and physics of lipids, 2003. **122**(1-2): p. 185-190.
57. Herlax, V., et al., *Relevance of fatty acid covalently bound to Escherichia coli alpha-hemolysin and membrane microdomains in the oligomerization process*. J Biol Chem, 2009. **284**(37): p. 25199-210.
58. El-Azami-El-Idrissi, M., et al., *Interaction of Bordetella pertussis adenylate cyclase with CD11b/CD18: Role of toxin acylation and identification of the main integrin interaction domain*. Journal of Biological Chemistry, 2003. **278**(40): p. 38514-38521.
59. Masin, J., et al., *Acylation of lysine 860 allows tight binding and cytotoxicity of Bordetella adenylate cyclase on CD11b-expressing cells*. Biochemistry, 2005. **44**(38): p. 12759-12766.
60. Thanabalu, T., et al., *Substrate-induced assembly of a contiguous channel for protein export from E. coli: reversible bridging of an inner-membrane translocase to an outer membrane exit pore*. The EMBO journal, 1998.
61. Balakrishnan, L., C. Hughes, and V. Koronakis, *Substrate-triggered recruitment of the TolC channel-tunnel during type I export of hemolysin by Escherichia coli*. Journal of molecular biology, 2001. **313**(3): p. 501-510.
62. Lenders, M.H., et al., *Directionality of substrate translocation of the hemolysin A Type I secretion system*. Scientific reports, 2015. **5**(1): p. 12470.
63. Lenders, M.H., et al., *In vivo quantification of the secretion rates of the hemolysin A Type I secretion system*. Scientific Reports, 2016. **6**(1): p. 33275.
64. Ostolaza, H., A. Soloaga, and F.M. Goñi, *The binding of divalent cations to Escherichia coliα-haemolysin*. European journal of biochemistry, 1995. **228**(1): p. 39-44.
65. Chenal, A., et al., *RTX calcium binding motifs are intrinsically disordered in the absence of calcium: implication for protein secretion*. Journal of Biological Chemistry, 2009. **284**(3): p. 1781-1789.
66. Bhakdi, S. and E. Martin, *Superoxide generation by human neutrophils induced by low doses of Escherichia coli hemolysin*. Infection and immunity, 1991. **59**(9): p. 2955-2962.
67. Dhakal, B.K. and M.A. Mulvey, *The UPEC pore-forming toxin α-hemolysin triggers proteolysis of host proteins to disrupt cell adhesion, inflammatory, and survival pathways*. Cell host & microbe, 2012. **11**(1): p. 58-69.
68. Uhlén, P., et al., *α-Haemolysin of uropathogenic E. coli induces Ca2+ oscillations in renal epithelial cells*. Nature, 2000. **405**(6787): p. 694-697.
69. Wang, C., et al., *Alpha-hemolysin of uropathogenic Escherichia coli induces GM-CSF-mediated acute kidney injury*. Mucosal immunology, 2020. **13**(1): p. 22-33.

70. Kuhn, H.W., et al., *LDL receptor–mediated endocytosis of Escherichia coli α-hemolysin mediates renal epithelial toxicity.* Proceedings of the National Academy of Sciences, 2025. **122**(24): p. e2505482122.
71. Verma, V., et al., *α-Hemolysin of uropathogenic E. coli regulates NLRP3 inflammasome activation and mitochondrial dysfunction in THP-1 macrophages.* Scientific Reports, 2020. **10**(1): p. 12653.
72. Wiles, T.J., et al., *Inactivation of host Akt/protein kinase B signaling by bacterial pore-forming toxins.* Molecular biology of the cell, 2008. **19**(4): p. 1427-1438.
73. Agace, W.W., et al., *Escherichia coli induces transuroepithelial neutrophil migration by an intercellular adhesion molecule-1-dependent mechanism.* Infection and immunity, 1995. **63**(10): p. 4054-4062.
74. Benz, R., *Channel formation by RTX-toxins of pathogenic bacteria: Basis of their biological activity.* Biochimica et Biophysica Acta (BBA)-Biomembranes, 2016. **1858**(3): p. 526-537.
75. Dassanayake, R.P., S.K. Maheswaran, and S. Srikumaran, *Monomeric expression of bovine β2-integrin subunits reveals their role in Mannheimia haemolytica leukotoxin-induced biological effects.* Infection and Immunity, 2007. **75**(10): p. 5004-5010.
76. Dileepan, T., et al., *Human CD18 is the functional receptor for Aggregatibacter actinomycetemcomitans leukotoxin.* Infection and Immunity, 2007. **75**(10): p. 4851-4856.
77. Goldsmith, J.A., et al., *Structural basis for non-canonical integrin engagement by Bordetella adenylate cyclase toxin.* Cell Rep, 2022. **40**(7): p. 111196.
78. Guermonprez, P., et al., *The adenylate cyclase toxin of Bordetella pertussis binds to target cells via the alpha(M)beta(2) integrin (CD11b/CD18).* J Exp Med, 2001. **193**(9): p. 1035-44.
79. Lally, E.T., et al., *RTX toxins recognize a β2 integrin on the surface of human target cells.* Journal of Biological Chemistry, 1997. **272**(48): p. 30463-30469.
80. Li, J., K.D. Clinkenbeard, and J.W. Ritchey, *Bovine CD18 identified as a species specific receptor for Pasteurella haemolytica leukotoxin.* Vet Microbiol, 1999. **67**(2): p. 91-7.
81. Morova, J., et al., *RTX cytotoxins recognize beta2 integrin receptors through N-linked oligosaccharides.* Proc Natl Acad Sci U S A, 2008. **105**(14): p. 5355-60.
82. Reinholdt, J., et al., *Monodisperse and LPS-free Aggregatibacter actinomycetemcomitans leukotoxin: interactions with human β2 integrins and erythrocytes.* Biochim Biophys Acta, 2013. **1834**(2): p. 546-58.
83. Ristow, L.C., et al., *The extracellular domain of the β2 integrin β subunit (CD18) is sufficient for Escherichia coli hemolysin and Aggregatibacter actinomycetemcomitans leukotoxin cytotoxic activity.* MBio, 2019. **10**(4): p. 10.1128/mbio. 01459-19.
84. Vanden Bergh, P.G., et al., *Porcine CD18 mediates Actinobacillus pleuropneumoniae ApxIII species-specific toxicity.* Vet Res, 2009. **40**(4): p. 33.
85. Wang, J.F., et al., *Molecular and biochemical mechanisms of Pasteurella haemolytica leukotoxin-induced cell death.* Microb Pathog, 1998. **25**(6): p. 317-31.
86. Balashova, N.V., et al., *Leukotoxin confers beta-hemolytic activity to Actinobacillus actinomycetemcomitans.* Infect Immun, 2006. **74**(4): p. 2015-21.

87. Cortajarena, A.L., F.M. Goñi, and H. Ostolaza, *Glycophorin as a receptor for Escherichia coli alpha-hemolysin in erythrocytes*. J Biol Chem, 2001. **276**(16): p. 12513-9.
88. Fong, K.P., et al., *Actinobacillus actinomycetemcomitans leukotoxin requires lipid microdomains for target cell cytotoxicity*. Cell Microbiol, 2006. **8**(11): p. 1753-67.
89. Forman, M.S., et al., *Gangliosides block Aggregatibacter Actinomycetemcomitans leukotoxin (LtxA)-mediated hemolysis*. Toxins (Basel), 2010. **2**(12): p. 2824-36.
90. Mrówczyńska, L., et al., *Bordetella Adenylate Cyclase Toxin Can Bind Ganglioside GM1*. BIO, 2011. **1**: p. 67-71.
91. Munksgaard, P.S., et al., *Sialic acid residues are essential for cell lysis mediated by leukotoxin from Aggregatibacter actinomycetemcomitans*. Infect Immun, 2014. **82**(6): p. 2219-28.
92. Osickova, A., et al., *Cytotoxic activity of Kingella kingae RtxA toxin depends on post-translational acylation of lysine residues and cholesterol binding*. Emerg Microbes Infect, 2018. **7**(1): p. 178.
93. Rahman, W.U., et al., *Binding of Kingella kingae RtxA Toxin Depends on Cell Surface Oligosaccharides, but Not on β(2) Integrins*. Int J Mol Sci, 2020. **21**(23).
94. Valeva, A., et al., *Binding of Escherichia coli hemolysin and activation of the target cells is not receptor-dependent*. J Biol Chem, 2005. **280**(44): p. 36657-63.
95. Vazquez, R.F., et al., *Novel evidence for the specific interaction between cholesterol and α-haemolysin of Escherichia coli*. Biochem J, 2014. **458**(3): p. 481-9.
96. González Bullón, D., et al., *Cholesterol stimulates the lytic activity of Adenylate Cyclase Toxin on lipid membranes by promoting toxin oligomerization and formation of pores with a greater effective size*. The FEBS Journal, 2021. **288**(23): p. 6795-6814.
97. Atapattu, D.N. and C.J. Czuprynski, *Mannheimia haemolytica leukotoxin binds to lipid rafts in bovine lymphoblastoid cells and is internalized in a dynamin-2-and clathrin-dependent manner*. Infection and immunity, 2007. **75**(10): p. 4719-4727.
98. Bumba, L., et al., *Bordetella adenylate cyclase toxin mobilizes its β2 integrin receptor into lipid rafts to accomplish translocation across target cell membrane in two steps*. PLoS pathogens, 2010. **6**(5): p. e1000901.
99. Chacko, F.M. and L. Schmitt, *Interaction of RTX toxins with the host cell plasma membrane*. Biological Chemistry, 2023. **404**(7): p. 663-671.
100. Ostolaza, H. and J. Amuategi, *Membrane Interaction characteristics of the RTX toxins and the cholesterol-dependence of their cytolytic/cytotoxic activity*. International Journal of Molecular Sciences, 2024. **25**(6): p. 3131.
101. Osickova, A., et al., *A conserved tryptophan in the acylated segment of RTX toxins controls their β2 integrin–independent cell penetration*. Journal of Biological Chemistry, 2023. **299**(8).
102. Amuategi, J., R. Alonso, and H. Ostolaza, *Four Cholesterol-Recognition Motifs in the Pore-Forming and Translocation Domains of Adenylate Cyclase Toxin Are Essential for Invasion of Eukaryotic Cells and Lysis of Erythrocytes*. International Journal of Molecular Sciences, 2022. **23**(15): p. 8703.
103. Herlax, V.S., *Potential use of peptides mimicking CRAC/CARC domains as antivirulence therapies to inhibit RTX toxins activities*. 2024.

104. Martín, C., et al., *Adenylate cyclase toxin promotes internalisation of integrins and raft components and decreases macrophage adhesion capacity*. PLoS One, 2011. **6**(2): p. e17383.
105. Bakás, L., et al., *Reversible adsorption and nonreversible insertion of Escherichia coli alpha-hemolysin into lipid bilayers*. Biophysical journal, 1996. **71**(4): p. 1869-1876.
106. Henson, J.B. and L.C. Grumbles, *Infectious Bovine Keratoconjunctivitis .1. Etiology*. American Journal of Veterinary Research, 1960. **21**(84): p. 761-766.
107. Baptista, P.J., *Infectious bovine keratoconjunctivitis: a review*. Br Vet J, 1979. **135**(3): p. 225-42.
108. Bilbao, L., et al., *Genomic characterization of Moraxella bovis and Moraxella bovoculi Uruguayan strains isolated from calves with infectious bovine keratoconjunctivitis*. Revista argentina de microbiología, 2024. **56**(2): p. 165-174.
109. Acquistapace, S., et al., *Outer membrane protein CD of Moraxella bovis as a potential immunogen against infectious bovine keratoconjunctivitis*. Veterinaria (Montevideo), 2021. **57**(216).
110. Wynn, E.L., et al., *Whole genome sequencing of Moraxella bovis strains from North America reveals two genotypes with different genetic determinants*. BMC microbiology, 2022. **22**(1): p. 258.
111. Angelos, J.A., J.F. Hess, and L.W. George, *An RTX operon in hemolytic Moraxella bovis is absent from nonhemolytic strains*. Vet Microbiol, 2003. **92**(4): p. 363-77.
112. Beard, M.K. and L.J. Moore, *Reproduction of bovine keratoconjunctivitis with a purified haemolytic and cytotoxic fraction of Moraxella bovis*. Vet Microbiol, 1994. **42**(1): p. 15-33.
113. Clinkenbeard, K.D. and A. Thiessen, *Mechanism of action of Moraxella bovis hemolysin*. Infection and immunity, 1991. **59**(3): p. 1148-1152.
114. Hoien-Dalen, P.S., R.F. Rosenbusch, and J.A. Roth, *Comparative characterization of the leukocidic and hemolytic activity of Moraxella bovis*. American journal of veterinary research, 1990. **51**(2): p. 191-196.
115. Kagonyera, G.M., L. George, and M. Miller, *Effects of Moraxella bovis and culture filtrates on 51Cr-labeled bovine neutrophils*. American journal of veterinary research, 1989. **50**(1): p. 18-21.
116. Kagonyera, G.M., L.W. George, and R. Munn, *Cytopathic effects of Moraxella bovis on cultured bovine neutrophils and corneal epithelial cells*. American journal of veterinary research, 1989. **50**(1): p. 10-17.
117. Gray, J., P. Fedorka-Cray, and D. Rogers, *Partial characterization of a Moraxella bovis cytolysin*. Veterinary microbiology, 1995. **43**(2-3): p. 183-196.
118. Angelos, J.A., J.F. Hess, and L.W. George, *Cloning and characterization of a Moraxella bovis cytotoxin gene*. American journal of veterinary research, 2001. **62**(8): p. 1222-1228.
119. Hess, J.F. and J.A. Angelos, *The Moraxella bovis RTX toxin locus mbx defines a pathogenicity island*. J Med Microbiol, 2006. **55**(Pt 4): p. 443-9.
120. Erenburg, I., *Functional and structural characterization of the RTX proteins MbxA from Moraxella bovis and FrpA from Kingella kingae*. 2020, Dissertation, Düsseldorf, Heinrich-Heine-Universität, 2020.

121. Karst, J.C., et al., *Calcium, acylation, and molecular confinement favor folding of Bordetella pertussis adenylate cyclase CyaA toxin into a monomeric and cytotoxic form*. Journal of Biological Chemistry, 2014. **289**(44): p. 30702-30716.
122. Meetum, K., et al., *Acylation of the Bordetella pertussis CyaA-hemolysin: Functional implications for efficient membrane insertion and pore formation*. Biochimica et Biophysica Acta (BBA)-Biomembranes, 2017. **1859**(3): p. 312-318.
123. Fong, K., et al., *Aggregatibacter actinomycetemcomitans leukotoxin is post-translationally modified by addition of either saturated or hydroxylated fatty acyl chains*. Molecular oral microbiology, 2011. **26**(4): p. 262-276.
124. Cannella, S.E., et al., *Stability, structural and functional properties of a monomeric, calcium–loaded adenylate cyclase toxin, CyaA, from Bordetella pertussis*. Scientific reports, 2017. **7**(1): p. 42065.
125. Henry, D.A., *Structural Characterization of Aggregatibacter actinomycetemcomitans' Leukotoxin (LtxA), A New Molecular Model and Mechanism for LtxA, and its Implications on LtxA's Behavior as a Leukotoxin*. 2024.
126. Spitz, O., et al., *Identity determinants of the translocation signal for a type 1 secretion system*. Frontiers in Physiology, 2022. **12**: p. 804646.
127. Ludwig, A., R. Benz, and W. Goebel, *Oligomerization of Escherichia coli haemolysin (HlyA) is involved in pore formation*. Molecular and General Genetics MGG, 1993. **241**(1): p. 89-96.
128. Knapp, O. and R. Benz, *Membrane activity and channel formation of the adenylate cyclase toxin (CyaA) of Bordetella pertussis in lipid bilayer membranes*. Toxins, 2020. **12**(3): p. 169.
129. Vojtova-Vodolanova, J., et al., *Oligomerization is involved in pore formation by Bordetella adenylate cyclase toxin*. The FASEB Journal, 2009. **23**(9): p. 2831-2843.
130. Brown, A.C., et al., *Aggregatibacter actinomycetemcomitans leukotoxin utilizes a cholesterol recognition/amino acid consensus site for membrane association*. Journal of Biological Chemistry, 2013. **288**(32): p. 23607-23621.
131. De Castro, E., et al., *ScanProsite: detection of PROSITE signature matches and ProRule-associated functional and structural residues in proteins*. Nucleic acids research, 2006. **34**(suppl_2): p. W362-W365.
132. Schrodinger, L., *The PyMOL molecular graphics system*. Version, 2015. **1**: p. 8.
133. Dalla Serra, M. and G. Menestrina, *Liposomes in the study of pore-forming toxins*, in *Methods in enzymology*. 2003, Elsevier. p. 99-124.
134. Schwarz, G. and A. Arbuzova, *Pore kinetics reflected in the dequenching of a lipid vesicle entrapped fluorescent dye*. Biochimica et Biophysica Acta (BBA)-Biomembranes, 1995. **1239**(1): p. 51-57.
135. Ladokhin, A.S., M.E. Selsted, and S.H. White, *Bilayer interactions of indolicidin, a small antimicrobial peptide rich in tryptophan, proline, and basic amino acids*. Biophysical Journal, 1997. **72**(2): p. 794-805.
136. Ladokhin, A.S., W.C. Wimley, and S.H. White, *Leakage of membrane vesicle contents: determination of mechanism using fluorescence requenching*. Biophysical journal, 1995. **69**(5): p. 1964-1971.
137. Weinstein, J.N., et al., *Phase transition release, a new approach to the interaction of proteins with lipid vesicles Application to lipoproteins*. Biochimica et Biophysica Acta (BBA)-Biomembranes, 1981. **647**(2): p. 270-284.

138. Ostolaza, H., et al., *Membrane permeabilization by pore-forming RTX toxins: what kind of lesions do these toxins form?* Toxins, 2019. **11**(6): p. 354.
139. Nagamatsu, K., et al., *Dysregulation of Escherichia coli α-hemolysin expression alters the course of acute and persistent urinary tract infection*. Proceedings of the National Academy of Sciences, 2015. **112**(8): p. E871-E880.
140. Brown, A.C., et al., *Aggregatibacter actinomycetemcomitans leukotoxin cytotoxicity occurs through bilayer destabilization*. Cellular microbiology, 2012. **14**(6): p. 869-881.
141. Dietmann, A., et al., *Effects of Aggregatibacter actinomycetemcomitans leukotoxin on endothelial cells*. Microbial pathogenesis, 2013. **61**: p. 43-50.
142. Schreiner, H., et al., *A comparison of Aggregatibacter actinomycetemcomitans (Aa) virulence traits in a rat model for periodontal disease*. PloS one, 2013. **8**(7): p. e69382.
143. Vega, B.A., et al., *Aggregatibacter actinomycetemcomitans Leukotoxin (LtxA) requires death receptor Fas, in addition to LFA-1, to trigger cell death in T lymphocytes*. Infection and immunity, 2019. **87**(8): p. 10.1128/iai. 00309-19.
144. Benz, R., *RTX-toxins*. 2020, MDPI. p. 359.

7. Curriculum Vitae

FEBY MARIAM CHACKO

Education

November 2020 – October 2025

Doctoral dissertation

- Heinrich Heine University (HHU), Düsseldorf, Germany.

August 2014 – June 2019

Integrated BS-MS Program in Science

- Indian Institute of Science Education and Research, Thiruvananthapuram (IISER-TVM), India.

May 2013

Higher Secondary School education

- St. Ephrem's Higher Secondary School, Kottayam, India.

Achievements

Fellowships/Awards

November 2020 – October 2024

Manchot Graduate School Scholarship – HHU, Düsseldorf, Germany.

August 2014 – June 2019

Innovation in Science Pursuit for Inspired Research (INSPIRE) Scholarship – Prestigious undergraduate fellowship awarded in India in Science & Technology to the top 1% of students in the country.

Skills

Assay Development & Screening:

- Cell-based and biochemical assay design and troubleshooting
- Experience with membrane integrity assays, toxin-host interaction models
- Expertise in handling confocal microscopy

Molecular & Structural Biology:

- Protein expression & purification (*E. coli*, affinity, SEC, HPLC)
- SDS-PAGE, Native PAGE, Agarose gel electrophoresis
- Molecular cloning, peptide synthesis, nanodisc reconstitution of proteins, protein crosslinking

Software:

- Microsoft Office (Very good), Affinity Designer (Very good), Inkscape (Good), GraphPad Prism (Very good), PyMOL (Good), Omero (Very good), ImageJ/Fiji (Basic).

Languages:

- English (Fluent), German (Advanced Beginner), Hindi (Good), Malayalam (Native)

CONFERENCES & PRESENTATIONS:

- Oral: MOI IV Symposium-1, Cologne (2022) **|** MOI IV Symposium-2, Düsseldorf (2023) **|** MOI IV Symposium-3, Düsseldorf (2024)
- Poster: GBM Conference, Düsseldorf (2022) **|** ETOX Conference, Scotland (2023)
- Attendee: ETOX 2021 (Germany) **|** IISER CBSM 2018 (India)

Publications

- Erenburg, I. N., Hänsch, S., **Chacko, F. M.**, Hamacher, A., Wintgens, S., Stuhldreier, F., ... & Schmitt, L. (2022). Heterologously secreted MbxA from Moraxella bovis induces a membrane blebbing response of the human host cell. *Scientific Reports*, *12*(1), 17825.
- **Chacko, F. M.**, & Schmitt, L. (2023). Interaction of RTX toxins with the host cell plasma membrane. *Biological Chemistry*, *404*(7), 663-671.
- **Chacko, F. M.**, Ganz, S. M., Pfitzer-Bilsing, A., Hänsch, S., Westhoff, P., Weidtkamp-Peters, S., ... & Schmitt, L. (2025). Acylation of the RTX Toxin MbxA stimulates host membrane disruption through a specific interaction with cholesterol. *bioRxiv*, 2025-02.
- Surbhi, Shau, A. K., **Chacko, F. M.**, & Radhakrishnan, S. K. (2025). A starvation-triggered AAA+ ATPase halts chromosome replication progression by disassembling the bacterial DNA sliding clamp. *Current Biology*, 2025-01.

8. Acknowledgements

First and foremost, I would like to express my deepest gratitude to my supervisor, Prof. Dr. Lutz Schmitt. Thank you for this exciting project and for giving me the opportunity to pursue my doctorate. I am especially grateful for your inspiring ideas, your enthusiasm, and the freedom you allowed me throughout this journey. Your constant support, for always being approachable and available whenever I needed guidance, and the chance to participate in different stimulating conferences and collaborations have been invaluable for my scientific growth.

I would also like to sincerely thank my co-supervisor, Prof. Dr. Johannes Hegemann, for the valuable discussions during my yearly presentations and for welcoming me into your lab to carry out experiments. Your feedback and openness have greatly enriched my work.

My heartfelt thanks go to Prof. Dr. Sander Smits, who interviewed and selected me for this PhD position. Your trust gave me the opportunity to embark on this journey, and I will always remain grateful for it.

I am very thankful to Dr. Marten Exterkate for his incredible support and ideas during my laboratory work, as well as for his significant contributions to the writing of the manuscript. I would like to thank Prof. Dr. Stefanie Weidtkamp-Peters, Dr. Sebastian Hänsch, and Anna Hamacher for their support at the advanced imaging facility, and Prof. Dr. Alexej Kedrov for his fruitful discussions and valuable input for my project.

I also remember with gratitude PD Dr. Ulrich Schulte (†) and thank Dr. Jan Stindt for their guidance with formal matters and safety regulations in the institute. A special thanks goes to Dr. Stindt for his particular support during my pregnancy, which was of immense help. I would further like to thank our secretary, Ms. Corinna Franzkowiak, for all her support and assistance during my PhD.

My sincere thanks go to the Jürgen Manchot Foundation and the MOI Graduate School for their financial support and for offering such a diverse and stimulating program. A special thank you to Dr. Stephanie Spelberg for her coordination, organization, and assistance with countless questions. I also thank my MOI colleagues - it was a pleasure to meet you all, and I cherish the

memorable symposium evenings we shared. A very special thanks goes to Fabienne Kocher for her dedicated help with cell culture, for taking the time to support me, and for her contributions to planning our experiments.

I am grateful to Prof. Dr. Ben Luisi for the collaboration, hospitality, and the opportunity to get to know his research group and Cambridge.

A heartfelt thanks goes to Dr. Sigrun Wegener-Feldbrügge, head of the International Researcher Center, who supported me enormously in integrating into the German system. Her exceptional help during a very difficult period in our personal life as foreigners in Germany will always remain unforgettable to me.

I would like to thank our technicians, Martina and Silke, for their constant support. Martina, thank you for being the “lab mom”, for your patience in answering every question, and for creating such a warm and pleasant atmosphere. Silke, thank you for your steady support and willingness to help whenever needed.

A very special acknowledgment goes to Julia Gottstein, who became my pillar of support and my closest friend during the early stages of my time in Germany, both as a foreigner and as a beginner in the lab. You stood by me through ups and downs, and your openness made life in Germany feel comfortable and welcoming. I am deeply thankful also to your family, who welcomed me into their home and made me feel part of it.

Thanks to Sakshi and Zohreh, my dear friends and wonderful office mates, for sharing not only lab life but also life outside of it. You truly made Germany feel like a second home.

I also thank Isabelle, my predecessor in the PhD project, whose work laid the foundation for mine and whose guidance during my initial days helped me to navigate the challenges of working with MbxA. I would also like to thank the Center for Structural Studies (CSS), especially Jens, for the SAXS studies, data analysis, interpretations, and the many fruitful discussions.

Special thanks to Lea for her thoughtful coordination in making every lab member feel valued by remembering important personal occasions, and for the wonderful time we had together in Cambridge. I would also like to acknowledge my colleagues Florestan, Manuel, Hans, Eymen, Vivien, Stefanie, Alexandra, Cigdem, Neele, Kira, Christian, Lars, Gyan, Svenja, Sergiy, and

Philipp for their support and companionship throughout this journey. Additionally, I would like to convey my thanks to my students, Felix, Torben, Simon, and Michelle, for their enthusiasm, dedication, and contributions they provided during this time. My gratitude also extends to the synthetic membrane team, especially Michael, Athanasios, and Mary, who helped me during the early stages of my work. I am equally thankful to Max, Nhi, Tim, and Marius for the many enjoyable times we shared in the lab.

Beyond the lab, I thank my friends Taniya, Tina, and Ashiq, who made Germany feel like a second home. A heartfelt thanks also goes to Senthil and Sreemeenakshi for their kindness in helping me during my initial days and for their continuous support throughout my PhD.

Finally, I am deeply indebted to my family. To my parents (Pappa and Mummy), thank you for making me who I am today, and to my brother, for your unwavering support. To my grandmother (†), who was my greatest emotional support and played a crucial role in shaping me, it is one of the deepest sorrows of my life that you could not witness this achievement.

My heartfelt thanks go to my husband, Dibin, who became part of my life during this PhD. Thank you for your endless patience, love, and encouragement, and for standing by me through the challenges and uncertainties of this journey. Sharing this path with you, as you, too, prepare to defend your doctorate, has been both inspiring and comforting. I am proud of what we have achieved together and grateful for the strength you have given me.

A very special thanks goes to our son, Leonard, the greatest gift at the end of this long journey. Your arrival filled our lives with joy and gave me new strength during the final stages of my PhD. Knowing that you are witnessing Mama’s doctorate, even in your earliest days, makes this achievement even more meaningful. You remind me every day why perseverance and love go hand in hand.

9. Declaration

I hereby declare under oath that I have prepared this dissertation independently and without any inadmissible external assistance, in compliance with the “Principles for Safeguarding Good Scientific Practice at Heinrich Heine University.”

I confirm that I have not previously submitted this dissertation, in this or a similar form, to any other faculty.

I further declare that I have not previously attempted any doctoral studies that were unsuccessful.

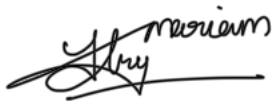

Düsseldorf
03.09.2025

Feby Mariam Chacko